Ca^{2+} signalling between the endoplasmic reticulum and lysosomes

PEACE ATAKPA

University of Cambridge

Department of Pharmacology

A dissertation submitted for the degree of

Doctor of Philosophy

Hughes Hall September 2018

Contents

Preface

The work presented in this dissertation was performed, otherwise stated, solely by the author in the Department of Pharmacology, University of Cambridge between October 2014 and September 2018. This thesis does not exceed the word limit approved by the Biology Degree Committee and is not substantially the same as any other that has been submitted for a degree, diploma or other qualification at any establishment.

Peace Atakpa

3rd September, 2018

Acknowledgements

I would like to sincerely express my gratitude to my supervisor Prof. Colin W Taylor for giving me the opportunity to work as a member of his research group and for his guidance, support, and patience throughout this project.

I thank Dr. David Prole for his helpful support at the start of my PhD and for introducing me to molecular biology. I also thank Dr. Nagendra Babu Thillaiappan and Laura M. van Marrewijk, for their support and collaboration throughout different aspects of this project.

I would like to express my gratitude to other past and present members of the group, for providing a warm and friendly environment. I have to especially mention Dr. Sumita Chakraborty, Stefania Mataragka, Dina Tahboub, Dr. Raul Lagos, Dr. Emily Taylor, Dr. Michael Apta-Smith and Dr. Ana Rossi.

I am sincerely grateful to my parents for giving me the best opportunities in life and for constantly being just a phone call away to provide prayers, support and encouragement. I could not have done this without you. I also thank my siblings Joshua, Caleb and Joy for their constant support.

I thank Pst (Dr). and Pst (Mrs). Joshua Omada for their constant prayers, support and encouragement.

I am grateful to Mr. and Mrs. O.P.S Adaji for their constant encouragement.

I thank my husband, Enemona Emmanuel Adaji for helping me stay sane through very difficult times during this project and being just the absolute best friend throughout this time.

Finally, I would like to thank the Cambridge Commonwealth, European and International Trust for funding my studies.

Summary

Ca^{2+} is a universal and versatile intracellular messenger, regulating a vast array of biological processes due to variations in the frequency, amplitude, spatial and temporal dynamics of Ca^{2+} signals. Increases in cytosolic free Ca^{2+} concentration ($[Ca^{2+}]_c$) are due to influx from either an infinite extracellular Ca^{2+} pool or from the more limited intracellular Ca^{2+} stores. Stimulation of the endogenous muscarinic (M3) receptors of human embryonic kidney (HEK) cells with carbachol results in the activation of phospholipase C (PLC) and formation of inositol 1,4,5-trisphosphate (IP_3), activation of IP_3 receptors (IP_3Rs), release of Ca^{2+} from the endoplasmic reticulum (ER), and activation of store-operated Ca^{2+} entry (SOCE). Lysosomes are the core digestive compartments of the cell, but their importance as signalling organelles is also now widely appreciated. Accumulating evidence indicates that lysosomal Ca^{2+} is important for their physiological functions. Lysosomal Ca^{2+} release triggers fusion during membrane trafficking and, through calmodulin, it regulates lysosome size. Luminal Ca^{2+} is critical for regulation of lysosomal biogenesis and autophagy during starvation through the transcription factor, TFEB. Furthermore, aberrant lysosomal Ca^{2+} is associated with some lysosomal storage diseases.

Lysosomes in mammalian cells have long been suggested to accumulate Ca^{2+} via a low-affinity Ca^{2+}-H^+ exchanger (CAX). This is consistent with evidence that dissipating the lysosomal H^+ gradient increased $[Ca^{2+}]_c$ and decreased lysosomal free $[Ca^{2+}]$, and with the observation that lysosomal Ca^{2+} uptake was followed by an increase in pH_{ly}. Furthermore, heterologous expression of *Xenopus* CAX in mammalian cells attenuated carbachol-evoked Ca^{2+} signals. However, there is no known CAX in mammalian cells, and so the identity of the lysosomal Ca^{2+} uptake pathway in mammalian cells is unresolved. Using mammalian cells loaded with a fluorescent Ca^{2+} indicator, I show that dissipating the pH_{ly} gradient pharmacologically or by siRNA-mediated knockdown of an essential subunit of the H^+ pump, increases the amplitude of IP_3-evoked cytosolic Ca^{2+} signals without affecting those evoked by SOCE. A genetically encoded low-affinity Ca^{2+} sensor expressed on the lysosome surface reports larger increases in $[Ca^{2+}]_c$ than the cytosolic sensor, but only when the Ca^{2+} signals are evoked by IP_3R rather than SOCE. Using cells expressing single IP_3R subtypes, I demonstrate that each of the three IP_3R subtypes can deliver Ca^{2+} to lysosomes. I conclude that IP_3Rs release Ca^{2+} within near-lysosome microdomains that fuel a low-affinity lysosomal Ca^{2+} uptake system. The temporal relationship between the increase in pH_{ly} and reduced Ca^{2+}

sequestration suggests that pH_{ly} affects the organization of the microdomain rather than the Ca^{2+} uptake mechanism. I show that abrogation of the lysosome H^+ gradient does not acutely prevent uptake of Ca^{2+} into lysosomes, but disrupts junctions with the ER where the exchange of Ca^{2+} occurs.

The dipeptide, glycyl-L-phenylalanine 2-naphthylamide (L-GPN), is much used to disrupt lysosomes and release Ca^{2+} from them. The mechanism is widely assumed to require cleavage of GPN by cathepsin C, causing accumulation of amino acid residues, and osmotic lysis of lysosomal membranes. I show, using LysoTracker Red and Oregon Green-dextran to report pH_{ly}, that L-GPN is effective in HEK cells lacking functional cathepsin C, following CRISPR-Cas9-mediated gene disruption. Furthermore, D-GPN, which is resistant to cleavage by cathepsin C, is as effective as L-GPN at increasing pH_{ly}, and it is similarly effective in cells with and without cathepsin C. L-GPN and D-GPN increase cytosolic pH, and the effect is similar when the lysosomal V-ATPase is inhibited with bafilomycin A_1. This is not consistent with GPN releasing the acidic contents of lysosomes. I conclude that the effects of GPN on lysosomes are not mediated by cathepsin C. Both L-GPN and D-GPN evoke Ca^{2+} release, the response is unaffected by inhibition or knock-out of cathepsin C, but it requires Ca^{2+} within the ER. GPN-evoked increases in $[Ca^{2+}]_c$ require Ca^{2+} within the ER, but they are not mediated by ER Ca^{2+} channels amplifying Ca^{2+} release from lysosomes. GPN increases $[Ca^{2+}]_c$ by increasing pH_{cyt}, which then directly stimulates Ca^{2+} release from the ER. I conclude that physiologically relevant increases in pH_{cyt} stimulate Ca^{2+} release from the ER independent of IP_3 and ryanodine receptors, and that GPN does not selectively target lysosomes.

I conclude that all three IP_3R subtypes selectively deliver Ca^{2+} to lysosomes, and that the low pH within lysosomes is required to maintain the junctions between ER and lysosomes, but not for lysosomal Ca^{2+} uptake. I suggest that GPN lacks the specificity required to allow selective release of Ca^{2+} from lysosomes.

Abbreviations

AO	Acridine Orange
AP3	Adaptor protein 3
ARM	Armadillo-repeat domain
ATP	Adenosine triphosphate
βGC	β-glucocerebrosidase
Baf A_1	Bafilomycin A_1
BAPTA	1,2-bis(o-aminophenoxy)ethane-N,N,N',N'-tetraacetic acid
BK channel	Ca^{2+}-activated K^+ channel
BTF	β -trefoil
cADPR	Cyclic adenosine diphosphate ribose
cAMP	Cyclic adenosine monophosphate
$[Ca^{2+}]_c$	Intracellular free Ca^{2+} concentration
$[Ca^{2+}]_e$	Extracellular free Ca^{2+} concentration
CcA	Concanamycin A
CCh	Carbachol
CICR	Ca^{2+}-induced Ca^{2+} release
CLC	Chloride channel
CLD	Central linker domain
CLM	Cytosol-like media
CLN	Neuronal ceroid lipofuscinosis
CPA	Cyclopiazonic acid

CRAC	calcium release-activated channels
CRISPR	Clustered regularly interspaced short palindromic repeats
Cy-GG	Cytosolic green modified Ca^{2+} indicator for optical imaging 1.2
$\Delta\psi$	Lysosome membrane potential
DAG	Diacylglycerol
Dx	Dextran
D-GPN	Glycyl-D-phenylalanine-β-naphthylamide
DMEM	Dulbecco's Modified Eagle's Medium
DMSO	Dimethyl sulfoxide
DTT	Dithiothreitol
EC_{50}	Half-maximally effective concentration
EDTA	Ethylene diamine tetraacetic acid
EE	Early endosome
EGFR	Epidermal growth factor receptor
EGTA	ethylene glycol-bis(β-aminoethyl ether)-N,N,N',N'-tetraacetic acid
ER	Endoplasmic reticulum
FBS	Foetal bovine serum
GDP	Guanosine diphosphate
Gly-Arg-AMC	Glycyl-arginine-diazomethylketone
Gly-Phe-DMK	Glycyl-L-phenylalanine-diazomethylketone
JD	Juxtamembrane domain
L-GPN	Glycyl-L-phenylalanine-β-naphthylamide

GTP	Guanosine triphosphate
HBS	HEPES-buffered saline
HEK	Human embryonic kidney
IBC	IP_3-binding core
IC_{50}	half-maximally inhibitory concentration
IP_3	Inositol 1,4,5-trisphosphate
IP_3R	IP_3 receptor
KO	Knock-out
LAMP1	Lysosome-associated membrane protein 1
LAMP2	Lysosome-associated membrane protein 2
LE	Late endosome
LeuLeuOME	L-leucyl-L-leucine methyl ester
LIMP2	Lysosomal integral membrane protein 2
LMP	Lysosomal membrane permeabilization
LRO	Lysosome-related organelle
LSD	Lysosomal storage disease
M3R	M3 muscarinic receptor
M6P	Mannose-6-phosphate
M6PR	Mannose-6-phosphate receptor
MAM	Membrane-associated membranes
MCS	Membrane contact site
MCU	Mitochondrial Ca^{2+} uniporter

Mfn2	Mitofusin 2
MSDH	O-methyl-serine dodecylaminehydrochloride
NAADP	Nicotinic acid adenine dinucleotide phosphate
NCL	Neuronal ceroid lipofuscionosis
NCX	Na^+-Ca^{2+} exchanger
NHE	Na^+/H^+-exchanger
NKA	Na^+-K^+-ATPase
OG	Oregon Green
ORP1L	Oxysterol-binding protein-1
PCR	Polymerase chain reaction
pEC_{50}	-log EC_{50}
pIC_{50}	-log IC_{50}
pH_{cyt}	Cytosolic pH
pH_{ly}	Lysosomal luminal pH
PIP_2	Phosphatidylinositol 4,5-bisphosphate
PLA	Proximity ligation assay
PLC	Phospholipase C
PM	Plasma membrane
PMCA	Plasma membrane Ca^{2+}-ATPase
PPA 2	Pyrophosphatase 2
PTP1B	Protein tyrosine phosphatase 1B
PTPIP51	Protein tyrosine phosphatase-interacting protein 51

RIPA	Radio immuno precipitation assay
RNF26	Ring finger protein 26
R_{coloc}	Pearson's correlation coefficient
RNAi	Ribonucleic acid interference
ROC	Receptor-operated Ca^{2+} channel
ROI	Region of interest
RyR	Ryanodine receptor
SDS-PAGE	Sodium dodecyl sulfate-polyacrylamide gel electrophoresis
SERCA	Sarco/endoplasmic reticulum Ca^{2+}-ATPase
sgRNA	Single guide RNA
siRNA	Small interfering ribonucleic acid
SLC36	Solute carrier 36
SMOC	Second messenger-operated Ca^{2+} channel
SOAR/CAD	STIM1 Orai-activating region/CRAC-activation domain (the region of STIM1 that activates Orai 1)
SOC	Store-operated Ca^{2+} channel
SOCE	Store-operated Ca^{2+} entry
SR	Sarcoplasmic reticulum
STARD3	StAR-related lipid transfer domain-3
STARD3NL	StAR- related lipid transfer domain-3 N-terminal like
STIM1	Stromal interaction molecule-1
TAE	Tris-acetate-EDTA
TBS	Tris-buffered saline

TE	Tris-EDTA
TFEB	Transcription factor E-Box
TG	Thapsigargin
TGN	Trans-Golgi network
TIRF	Total internal reflection fluorescence
TMD	Transmembrane domain
TPC	Two pore channel
TRPC	Transient receptor potential canonical subtype
TRPML1	Transient receptor potential mucolopin 1
VAMP	Vesicle-associated membrane protein
VAPA	VAMP-associated protein A
VAPB	VAMP-associated protein B
VOC	Voltage-operated Ca^{2+} channel
WT	Wild-type

1. Introduction

1.1 An overview of Ca^{2+} signalling

In physiological conditions, intracellular messengers are critical to the transduction of the diverse extracellular stimuli that cells encounter into intricately regulated and specialised intracellular responses. Ca^{2+} is a universal and versatile intracellular messenger regulating a vast array of biological processes due to variations in the frequency, amplitude, and spatial and temporal dynamics of Ca^{2+} signals (Berridge *et al.*, 2000; Taylor & Dale, 2012). A plethora of signalling machinery underlies the versatility of Ca^{2+} signalling and allows the independent regulation of seemingly unrelated processes such as fertilization, proliferation, muscle contraction and apoptosis (Berridge *et al.*, 2000; Bootman *et al.*, 2001; Whitaker, 2006). Unlike most intracellular messengers, whose signalling is finely tuned by a balance between synthesis and degradation, Ca^{2+} homeostasis is regulated by its transport across membranes and binding to specialised proteins (Bootman & Berridge, 1995). The intracellular free Ca^{2+} concentration ($[Ca^{2+}]_c$) can increase due to influx from an infinite extracellular Ca^{2+} pool or from the more limited intracellular Ca^{2+} stores. Ca^{2+} reaching the cytosol is rapidly transported into juxta-apposed organelles or out of the cell into the extracellular medium. This protects cells from prolonged elevations of $[Ca^{2+}]_c$, which are cytotoxic.

1.1.1 Ca^{2+} release from intracellular stores

Cells in physiological conditions are bathed in a high concentration of Ca^{2+} (~1 mM) in the extracellular medium. In resting conditions, the $[Ca^{2+}]_c$ is maintained at 10 -100 nM, which is 10,000 times lower than the extracellular free Ca^{2+} concentration ($[Ca^{2+}]_e$) and considerably lower than the $[Ca^{2+}]$ within intracellular Ca^{2+} stores (typically 100s of µM). This gradient is supported by cellular machineries that are constantly pumping Ca^{2+} back into the extracellular medium or into specialised organelles. The endoplasmic reticulum (ER) in non-excitable cells and the sarcoplasmic reticulum (SR) in muscle are the best characterised Ca^{2+} stores. They contain free $[Ca^{2+}]$ of up to 100-700 µM (Hogan & Rao, 2007), with the majority of the ER Ca^{2+} load bound to characteristic Ca^{2+} buffers with low affinity and high capacity, such as calsequestrin, calreticulin or calnexin (Prins & Michalak, 2011). However, other organelles have also been reported to sequester Ca^{2+}. These include lysosomes (luminal free $[Ca^{2+}]$ ~500 µM) (Christensen *et al.*, 2002; Lloyd-Evans *et al.*, 2008), mitochondria (1-

10 µM) (Baughman *et al.*, 2011) and the Golgi apparatus (~300 µM) (Dolman & Tepikin, 2006) (see Figure 1.1).

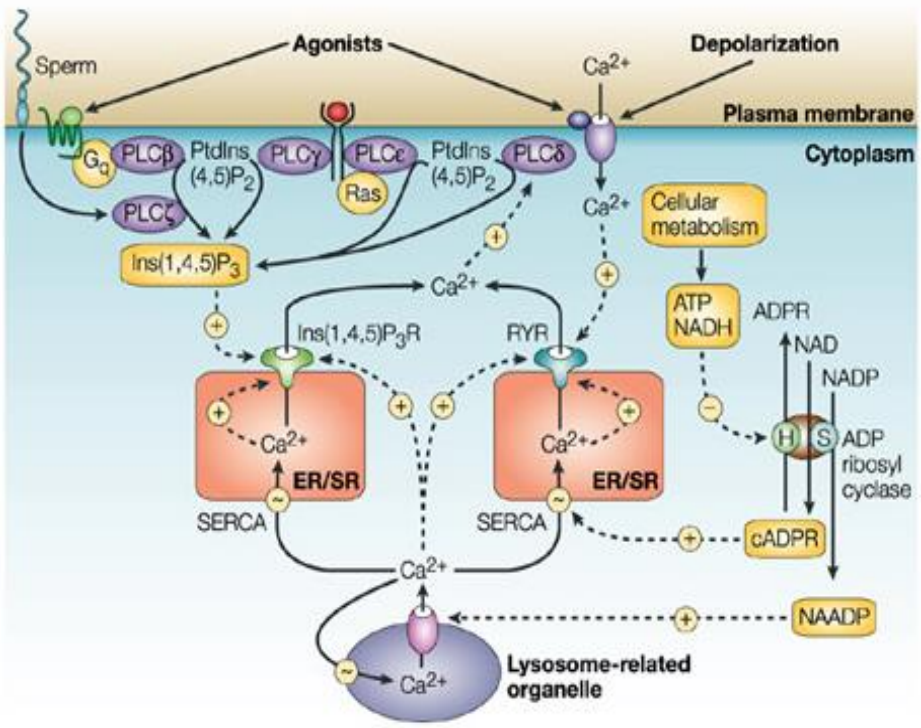

Figure 1.1 **Overview of intracellular Ca^{2+} stores.** Ca^{2+} can be mobilised from intracellular stores by IP_3R (ER/SR), RyR (ER/SR) or NAADP (lysosomes), upon stimulation of extracellular receptors by agonists or by depolarisation. Upon binding of agonists to receptors, such as Gq-coupled muscarinic M3 receptors, phospholipase C (PLC) is activated leading to cleavage of PIP_2 and production of IP_3, which along with Ca^{2+} regulates IP_3R. cADPR and NAADP are each synthesised by the same enzyme. NAADP probably stimulates Ca^{2+} release from lysosomes, while cADPR may regulate either the SERCA or RyR. There is also cross-talk between different stores, as Ca^{2+} from ER can be sequestered by lysosomes, and Ca^{2+} released from lysosomes can modulate IP_3R and RyR activity. Image is reproduced from Berridge *et al*. (2003).

Coordinated regulation of Ca^{2+} release and Ca^{2+} extrusion from the cytosol is essential to maintain a low $[Ca^{2+}]_c$ and circumvent the toxic effects of prolonged exposure to high $[Ca^{2+}]_c$ (Orrenius *et al.*, 2003). A common mechanism for the generation of Ca^{2+} signals in response to extracellular stimuli is the release of Ca^{2+} from intracellular stores via second messengers (Berridge *et al.*, 2000). Inositol 1,4,5-trisphosphate (IP_3) (Berridge *et al.*, 1983) and cyclic adenosine diphosphate ribose (cADPR) (Fill & Copello, 2002) are the most studied and well characterized Ca^{2+}-releasing messengers. However, a third potent and ubiquitous messenger, nicotinic acid adenine nucleotide diphosphate (NAADP), has also been described (Lee *et al.*, 1995) (Figure 1.1). NAADP remains the most controversial of the three Ca^{2+}-mobilising agents. This would be discussed in more detail in **Section 1.2.3.**

The sensing of extracellular stimuli, such as growth factors, drugs or hormones, results in the activation of receptors such as Gq-coupled receptors (GPCR) or receptor tyrosine kinases (RTK) on the plasma membrane (PM). Gq-coupled receptors activate the trimeric Gq protein, which is made up of α, β and γ subunits. Upon binding of an agonist, such as acetylcholine or histamine, the active receptor promotes dissociation of GDP and binding of GTP to Gαq. This allows dissociation of the α subunit from the βγ complex. These subunits then activate different isoforms of phospholipase C (PLC) (Figure 1.1). PLC hydrolyses a PM lipid, phosphatidylinositol 4,5-bisphosphate (PIP_2), into signalling molecules, diacylglycerol (DAG) and IP_3. DAG remains in the PM, as it is a lipophilic molecule, where it may stimulate protein kinase C or the activity of second-messenger-operated channels (SMOCs), including some members of the canonical transient receptor potential channel (TRPC) family, resulting in Ca^{2+} influx (Hofmann *et al.*, 1999). The water-soluble IP_3 molecule diffuses into the cytoplasm to the ER, where it binds to the IP_3-binding core (IBC) of the IP_3 receptor (IP_3R). Although IP_3 was thought to diffuse freely in the cytosol (Allbritton *et al.*, 1992), it is now clear that there are sufficient IP_3-binding sites in most cells to slow its diffusion (Dickson *et al.*, 2016; Taylor & Konieczny, 2016). Binding of IP_3 to the IBC triggers a conformational change resulting in the efflux of Ca^{2+} from the ER through the IP_3R. Recovery from IP_3R-mediated Ca^{2+} signals is dependent on the inactivation of IP_3 and clearance of Ca^{2+} from the cytosol. IP_3 is inactivated by phosphorylation, which is mediated by IP_3-3-kinase converting IP_3 to inositol 1,3,4,5-tetrakisphosphate (IP_4), or by dephosphorylation, which converts IP_3 to inositol 1,4-bisphosphate (IP_2). It is unlikely that physiological concentrations of either metabolite bind to IP_3R (Saleem *et al.*, 2013). It has,

however, been suggested that IP_4 might regulate Ca^{2+} entry (Irvine, 2007; Miller *et al.*, 2007). The role of IP_4 in physiological conditions remains controversial.

IP_3 receptors

IP_3Rs are ubiquitously expressed in eukaryotic cells and predominately occur in the ER membrane. IP_3R can also be found on the nuclear envelope (Malviya *et al.*, 1990), PM (Dellis *et al.*, 2006; Foskett *et al.*, 2007) as well as in the Golgi (Pinton *et al.*, 1998) and secretory vesicles (Yoo & Albanesi, 1990) of animal cells. IP_3Rs are also present in protozoans (Prole & Taylor, 2011). However, no similar protein has been found in plants (Wheeler & Brownlee, 2008) or fungi (Prole & Taylor, 2012). There are three subtypes of IP_3R and their splice variants encoded in the genomes of vertebrates (Furuichi *et al.*, 1989; Mignery *et al.*, 1989; Taylor *et al.*, 1999). Different cell types express the different subtype to different degrees. For example, the IP_3R2 isoform is predominately expressed in cardiac myocytes (Vervloessem *et al.*, 2015), IP_3R1 is predominately expressed in Purkinje cell neurons (Maeda *et al.*, 1989; Nakanishi *et al.*, 1991), and IP_3R3 in pancreatic β cells (Blondel *et al.*, 1994). Although all three IP_3R subtypes have ~ 65% sequence homology, they also exhibit different biophysical and regulatory properties (Foskett *et al.*, 2007). IP_3R2 is the most sensitive subtype to IP_3 and mediates robust and regular Ca^{2+} oscillations, whilst IP_3R1 mediates less regular Ca^{2+} oscillations (Zhang *et al.*, 2011). IP_3R3 is the least sensitive of the three subtypes and is reported to only mediate monophasic Ca^{2+} transients (Tu *et al.*, 2002; Iwai *et al.*, 2005). Although results are cell-type and stimulus-specific, a theme in the field is that IP_3R2 is pro-oscillatory and IP_3R3 is anti-oscillatory, whilst IP_3R1 can mediate both Ca^{2+} transients and oscillations (Zhang *et al.*, 2011).

The structure of rat IP_3R has been resolved to ~4.7 Å through cryo-electron microscopy (cryo-EM) (Fan *et al.*, 2015). Very recently, a similar structure of human IP_3R was resolved with and without IP_3 up to ~3.5 Å (Paknejad & Hite, 2018). A single IP_3R subunit consists of cytosolic N- and C- termini as well as 6 transmembrane domains (TMDs), towards the C-terminus which form the ion-conducting pore of the functional receptor (Foskett *et al.*, 2007; Seo *et al.*, 2012). A functional IP_3R is a tetrameric channel. This can be homomeric or heteromeric. Activation of IP_3R occurs following the binding of IP_3 to the IP_3-binding core (IBC), which sits close to the N-terminus (residues 224-604) of each subunit in an IP_3R (Bosanac *et al.*, 2002). The number of IP_3 molecules required to bind for receptor activation has been a long-standing question in the field. However, recent structure-activity studies

using concatenated tetrameric IP_3R proposed that all 4 subunits of the IP_3R need to be bound to IP_3 for activation to occur (Alzayady *et al.*, 2016; Taylor & Konieczny, 2016). Furthermore, IP_3R gating requires binding of both IP_3 and Ca^{2+} (Foskett *et al.*, 2007). Two binding sites for Ca^{2+} have been reported to occur in IP_3R3, one at the central linker domain (CLD) and armadillo-repeat domain 2 (ARM2) inteface and the other is thought to occupy a pocket between juxtamembrane domain (JD) and ARM3 recently (Figure 1.2) (Paknejad & Hite, 2018). The Ca^{2+}-dependent regulation of IP_3R activity is biphasic depending on the presence or absence of IP_3 (Taylor & Tovey, 2010). Therefore, a co-regulation of IP_3R by IP_3 and Ca^{2+} is thought to occur, where the presence of low concentrations of Ca^{2+} in the presence of IP_3 activates the channel (Mak & Foskett, 1998) and high Ca^{2+} concentrations in the absence of IP_3 are inhibitory (Kaftan *et al.*, 1997; Mak & Foskett, 1998).

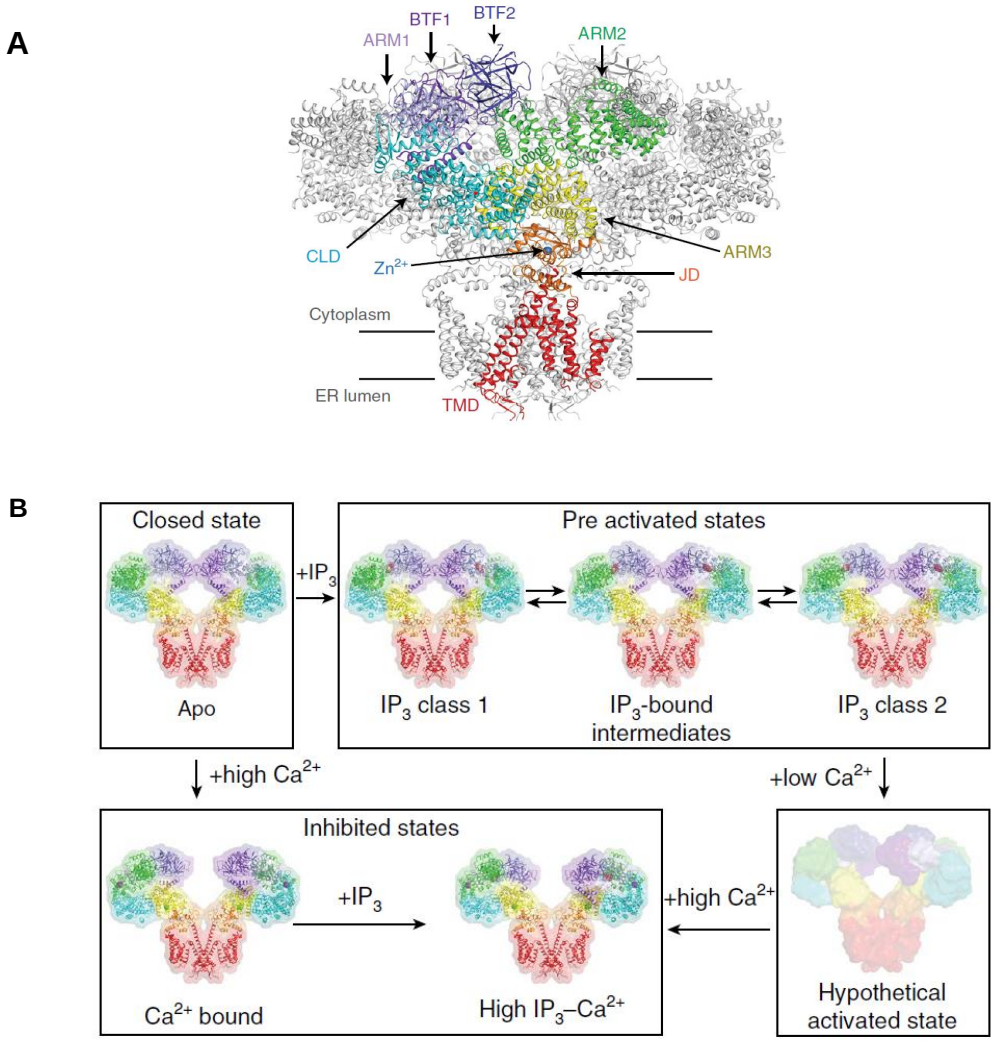

Figure 1.2 **Model of human IP$_3$R and regulation by IP$_3$ and Ca^{2+}.** (A) Structure of tetrameric human IP$_3$R3. Side view is in the plane of the membrane with the cytoplasmic domain at the top. The key domains of a single subunit are shown in colour. The N-terminal cytoplasmic domain which contains two β-trefoil-containing domains (BTF1, shown in purple and BTF2, shown in blue), the first segment of the central linker domain (CLD, shown in cyan), three armadillo-repeat domain (ARM1 (violet), ARM2 (green) and ARM3 (yellow) and the second segment of the CLD, is followed by a juxtamembrane domain (JD) (orange) and a transmembrane domain (TMD) (red). (B) In the absences of both IP$_3$ and Ca^{2+}, IP$_3$R3 exists in a closed state. Binding of IP$_3$, promotes a conformational change to one of the pre-activated states. Following this, binding of Ca^{2+} causes a conformational change to what is thought to be the activated state. IP$_3$R bound to IP$_3$ in high Ca^{2+} conditions causes the receptor to exist in an inhibited state. Images are reproduced from Paknejad *et al* (2018).

Other regulators of IP_3R have also been reported. These can be broadly categorised into proteins that bind to enhance the functions of IP_3R, inhibit the functions of IP_3Rs or modulate the spatial distribution of IP_3R (Prole & Taylor, 2016). Proteins that have been reported to enhance or inhibit the activity of IP_3R work largely by modulating the IP_3 and Ca^{2+}-mediated regulation of IP_3R (Prole & Taylor, 2016). For example, IP_3R in some settings are preferentially arranged in microdomains with GPCRs, βγ subunits, and some PLC isoforms (Tu *et al.*, 1998). This arrangement is thought to facilitate effective delivery of IP_3 to IP_3R, thereby enhancing activation (Prole & Taylor, 2016) Also, in single-channel recordings, chromogranin B, an ER-resident protein binds to IP_3R enhancing its activity in response to IP_3 (Thrower *et al.*, 2003). Conversely, calmodulin (CaM), CaBP1 and calcineurin have been reported to be involved in a Ca^{2+}-dependent inhibition of IP_3R (Michikawa *et al.*, 1999; Prole & Taylor, 2016). Furthermore, IP_3R-binding protein released with IP_3 (IRBIT), has been shown to inhibit all IP_3R subtypes (Ando *et al.*, 2003). In mouse cerebellum, IRBIT has been reported to occur in the cytosol and to compete with IP_3 for binding at the IBC of the IP_3R, therefore modulating the sensitivity of IP_3R to IP_3 (Ando *et al.*, 2014). Other regulators include cytosolic ATP (Tu *et al.*, 2005), luminal Ca^{2+} (Irvine, 1990; Berridge, 2007) and phosphorylation and dephosphorylation (Vanderheyden *et al.*, 2009). Furthermore, cAMP-dependent protein kinase (PKA) phosphorylates all IP_3R subtypes, potentiating IP_3R1- and IP_3R2-mediated Ca^{2+} signals (Bruce *et al.*, 2002; Wagner *et al.*, 2003; Wagner *et al.*, 2004). The effect of phosphorylation of IP_3R by PKA appears to be cell-type specific. IP_3R3-mediated Ca^{2+} signals have been reported to be attenuated following PKA-mediated phosphorylation in pancreatic cells (Giovannucci *et al.*, 2000), whilst PKA has been reported to activate IP_3R3 in insulinoma cells (Chaloux *et al.*, 2007). High concentrations of cAMP, independent of PKA, can also increase the sensitivities of all IP_3R subtypes (Short & Taylor, 2000; Tovey *et al.*, 2003; Tovey & Taylor, 2013). This highlights how tightly regulated the activities of IP_3R are in cells.

IP_3R and the ryanodine receptor (RyR) are closely related and are the most characterised Ca^{2+}-release channels that populate the ER and SR. IP_3R and RyR are large-conductance channels that show poor selectivity for Ca^{2+} over other cations. Both IP_3R and RyR have three different subtypes. IP_3R and RyR are both tetrameric proteins with structural similarities reported in the N and C terminus of each subunit (Lai *et al.*, 1988; Shah & Sawhamini, 2001; Seo *et al.*, 2012). However, a single subunit of RyR is bigger at ~550 kDa (Lai *et al.*, 1988) than a single IP_3R subunit at 250 kDa (Foskett *et al.*, 2007). Furthermore,

the stimulus for the activation of both receptors is distinct. The opening of RyR is regulated by the plant alkaloid ryanodine, in a concentration-dependent manner, where low concentrations increase the open probability (Buck *et al.*, 1992), and high concentrations are inhibitory (Zimanyi *et al.*, 1992). RyR1, in skeletal muscles is regulated by $Ca_v1.1$ during excitation-contraction coupling (des Georges *et al.*, 2016). RyR2 in cardiac muscles is activated by Ca^{2+} influx through $Ca_V1.2$ via Ca^{2+}-induced Ca^{2+}-release (CICR) (Fabiato, 1983). Other regulators of RyR include ATP (Kushmerick *et al.*, 1992), calmodulin (Hamilton & Reid, 2000) and FK506-binding protein (FKBP) (Marx *et al.*, 1998). Furthermore, cADPR, formed by the enzyme ADP ribosyl cyclase (Lee, 1999) is also reported as an activator of RyR (Lee, 1997; Ogunbayo *et al.*, 2011). However, this remains controversial (see **Section 1.2.3**).

1.1.2 Ca^{2+} entry from the extracellular space

The main Ca^{2+}-permeable channels in the PM can be classified based on their mode of activation into voltage-operated channels (VOC), ligand-operated channels (LOC) and store-operated channels (SOC) (Berridge, 1997). However other Ca^{2+}-permeable channels located on the PM have been reported to allow Ca^{2+} influx into the cell, including mechanosensitive Ca^{2+} channels (Welsh *et al.*, 2002; Yin & Kuebler, 2010) and temperature-sensitive Ca^{2+} channels (Togashi *et al.*, 2006; Bautista *et al.*, 2007).

VOCs on the PM are triggered to open by membrane depolarisation, particularly in excitable cells such as neurones, leading to L, P/Q, R or T-type Ca^{2+} currents (Lacinova, 2005). The classification is based on their pharmacological properties and voltage sensitivities. In muscle, the influx of Ca^{2+} following activation of VOCs is coupled with RyR to regulate contraction (Catterall, 1991; Bers, 2000; Bers, 2002). Ca^{2+} influx, following the activation of VOCs in neuronal cells, regulates neurotransmitter release (Catterall, 2000; Stephens *et al.*, 2001; Nanou & Catterall, 2018).

LOCs are PM-resident Ca^{2+} channels that are activated by ligand binding to allow Ca^{2+} influx into cells. Examples of LOCs include NMDA and AMPA receptors present in neuronal synapses and activated by the neurotransmitter glutamate (Burnashev *et al.*, 1995). Nicotinic acetylcholine receptors (Burnashev, 1998) and P2X receptors activated by binding of extracellular ATP are further examples of LOCs (Virginio *et al.*, 1998). In all the examples of LOCs described above, the binding of the agonist occurs on the extracellular side. However, in a subgroup of LOCs the activating agonist binds on the cytosolic side of the PM to allow

Ca^{2+} influx. This subgroup is called SMOC. DAG produced following PLC activation has been reported to activate PM Ca^{2+}-permeable channels in this way (Hofmann *et al.*, 1999; Okada *et al.*, 1999; Birnbaumer, 2009). Other examples of SMOCs include arachidonate-regulated Ca^{2+} channels (Shuttleworth, 1996), cyclic nucleotide-gated Ca^{2+} channels (Biel & Michalakis, 2009), as well as the TRPC (transient receptor potential, type C) family of receptors (Plant & Schaefer, 2005)

SOC are PM-resident Ca^{2+}-permeable channels, activated following the depletion of intracellular stores to allow SOC rapid and sustained influx of Ca^{2+} which can contribute to the refilling of intracellular stores (Putney, 2004). This Ca^{2+} influx, previously called capacitative Ca^{2+} entry, is now widely called store-operated Ca^{2+} entry (SOCE). The phenomenon of Ca^{2+} entry regulated by the state of the intracellular stress has been long described (Putney, 1986), but it was only in 2005 that the proteins regulating it were described. The molecular sensor of ER Ca^{2+} concentration is now known to be stromal interaction molecule 1 (STIM1), and the Ca^{2+} channel in the PM is Orai1 (Liou *et al.*, 2005; Roos *et al.*, 2005; Feske *et al.*, 2006; Cahalan, 2009). There are two isoforms of STIM (STIM1-2), which share ~60 % sequence homology (McNally *et al.*, 2012). STIM1 consists of an N-terminal domain containing the EF-hand Ca^{2+}-sensing motif in the ER lumen, a single membrane-spanning TMD, and C-terminus (Stathopulos *et al.*, 2008). The C-terminal, as well as the coiled-coil domains (CC1-3), a serine/proline region and a polybasic domain, are cytosolic (Hogan & Rao, 2015). STIM1 is distributed in the ER in resting conditions. Following depletion of ER Ca^{2+} content, such as following Ca^{2+} release or in stress conditions, STIM1, via its luminal EF-hand domain senses the drop in ER [Ca^{2+}], oligomerises from dimers into tetramers and redistributes to ER-PM junctions to activate Orai1 (Liou *et al.*, 2005; Lewis, 2007; Smyth *et al.*, 2008; Tamarina *et al.*, 2008). There are three isoforms of Orai in mammalian cells (Orai1-3). Orai1 has four TMD, an intracellular N domain and a pore-forming C-terminal domain (Yeromin *et al.*, 2006). The Orai1 channel is a hexamer (Hou *et al.*, 2012). The oligomerization of STIM1 leads to a conformational change that extends its polybasic domain and exposes the Orai1-activating motif called the SOAR/CAD domain (Park *et al.*, 2009; Yuan *et al.*, 2009; Prakriya & Lewis, 2015). The extended polybasic domain of STIM1 is known to interact with PIP_2 and other phospholipids at the PM, in a manner that traps STIM1 at ER-PM junctions facilitating the STIM1 gating of Orai1 channels (Liou *et al.*, 2007; Korzeniowski *et al.*, 2009). Binding of the SOAR/CAD domain allows opening of the Orai channel to allow Ca^{2+} influx into the cell. The

physiological role of STIM2 is not well understood. Downregulation of STIM2 has a minimal effect on SOCE in multiple cell lines (Liou *et al.*, 2005; Roos *et al.*, 2005; Soboloff *et al.*, 2006). However, STIM2 could be involved in the regulation of basal cytosolic and ER Ca^{2+} concentrations (Brandman *et al.*, 2007; Lu *et al.*, 2009), and it may influence the effectiveness of STIM1 in activating Orai1 (Miederer *et al.*, 2015).

The STIM-Orai pathway is not the only reported mechanism for Ca^{2+} entry. Other channels such as TRPCs after store depletion have also been reported to act as SOC to drive Ca^{2+} influx (Lee *et al.*, 2010). There are seven isoforms of TRPC (TRPC1-7) (Vazquez *et al.*, 2004). The evidence for TRPC channels as SOCE-mediators has largely come from knockdown studies, where downregulation of TRPC1 results in a reduction of SOCE signals in diverse cell types (Liu *et al.*, 2003; Mehta *et al.*, 2003; Tiruppathi *et al.*, 2006). Knockdown of TRPC4 has also been shown to downregulate EGF-induced SOCE activation in epithelial cells (Yang *et al.*, 2005). Furthermore, TRPC4 has been reported to be part of an essential component of the SOCE machinery in adrenal cells (Philipp *et al.*, 2000), endothelial cells (Sundivakkam *et al.*, 2012) and in smooth muscle cells (Zhang *et al.*, 2004). TRPC has been reported to form complexes with STIM1 and Orai1 to mediate Ca^{2+} influx (Liao *et al.*, 2008; Birnbaumer, 2009). However, TRPC is less Ca^{2+} selective than most SOC currents (Lopez *et al.*, 2016). Therefore, whilst TRPC could be a regulator of SOCE, it now seems clear that STIM1/Orai1 interaction are the key players in SOCE.

Since the identification of the core machinery for SOCE in most cells, there is now a growing list of regulators of SOCE. Most of the modulators of SOCE channels have been reported to strengthen the interaction between STIM1 and Orai1. CRACR2A (Ca^{2+} release-activated channel-regulator 2A), is a 45-kDa protein, that has been reported to form a ternary complex with STIM1 and Orai1 to stabilise their interaction. CRACR2A therefore promotes SOCE (Srikanth *et al.*, 2010). The translocation of STIM to ER-PM junctions following Ca^{2+} store depletion is thought to be an important rate-limiting step in the activation of Ca^{2+} entry (Liou *et al.*, 2007). There are classes of SOCE modulators that work by promoting STIM translocation to ER-PM junctions. These include, STIM-activating enhancer (STIMATE), which populates the ER membrane and is reported to enhance the translocation of STIM1 to ER-PM junctions (Jing *et al.*, 2015) and septins (Sharma *et al.*, 2013). Whilst EB1 binding from STIM1 is thought to restrict STIM1 translocation to ER-PM junctions (Chang *et al.*, 2018). Other regulators include SOCE-associated regulatory factor (SARAF), proposed to prevent spontaneous activation of SOCE by interacting with the C-terminal inhibitor domain

of STIM1 (Palty *et al.*, 2012; Albarran *et al.*, 2016). Furthermore, intracellular Ca^{2+} release channels, particularly immobile IP_3R, have been shown populate ER-PM junctions where STIM1 occurs (Thillaiappan *et al.*, 2017). The IP_3R may therefore both directly and indirectly regulate SOCE (Chakraborty *et al.*, 2016).

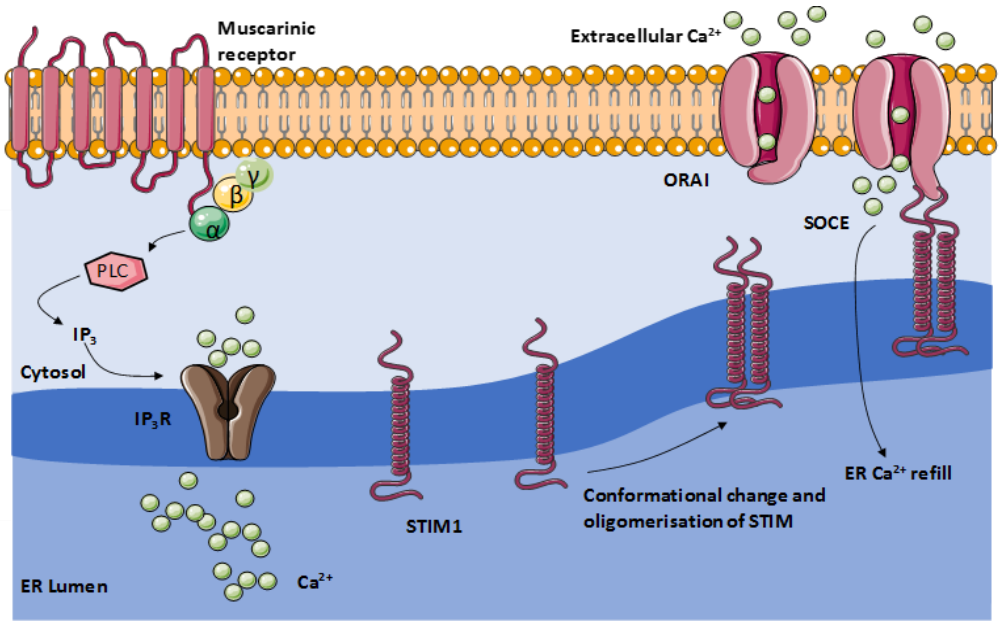

Figure 1.3 **Activation of SOCE.** ER Ca^{2+} depletion such as following mobilisation of Ca^{2+} form the ER following IP_3R release of Ca^{2+} leads to oligomerisation and translocation of STIM1 towards the PM, where it regulates Orai1 gating and activates SOCE.

As understanding of the SOCE machinery has increased, so has the understanding of the downstream function of SOCE Ca^{2+} signals. SOCE regulates gene expression via nuclear factor of activated T cells (NFAT) (Kar *et al.*, 2011), lymphocyte activation (Kerschbaum & Cahalan, 1999) and regulation of adenylyl cyclase (Fagan *et al.*, 2000). SOCE is also thought to be critical for the immune system, as mutations in STIM 1 and STIM2 result in autoimmune diseases in mice (Oh-Hora *et al.*, 2008). Orai1-deficient mice have defects in T and B cell functioning (Gwack *et al.*, 2008). Mutations in Orai1 and STIM1 cause severe immunodeficiencies, myopathy and ectodermal dysplasia (McCarl *et al.*, 2009). SOCE has been widely believed to be critical for acute ER Ca^{2+} refilling, but the ER still contains Ca^{2+} in cells devoid of known SOCE mechanisms (Zheng *et al.*, 2018). This shows that SOCE is not critical for long-term ER Ca^{2+} homeostasis. Nonetheless, SOCE-mediated Ca^{2+} signals are important physiological and pathological effectors.

1.1.3 Ca^{2+} extrusion mechanisms

To maintain cellular homeostasis, increases in $[Ca^{2+}]_c$ are rapidly cleared to protect the cells from the effects of prolonged elevated $[Ca^{2+}]_c$, such as apoptosis and necrosis. The clearance of Ca^{2+} from the cytosol is mediated by proteins that use either energy from ATP hydrolysis or the membrane electrochemical gradient. For example, the PM Ca^{2+} ATPases (PMCA) move Ca^{2+} out of the cytosol to the extracellular space hydrolysing ATP in the process (Carafoli, 1991). The sarco/endoplasmic reticulum Ca^{2+} ATPases (SERCA) likewise use ATP hydrolysis to actively pump Ca^{2+} back into the ER/SR (Periasamy & Kalyanasundaram, 2007). For one molecule of ATP hydrolysed, two Ca^{2+} ions are pumped into the ER by SERCA (Inesi & Tadini-Buoninsegni, 2014). For PMCA, the ratio is one molecule of ATP hydrolysis to one Ca^{2+} ion extruded to the extracellular space (Brini & Carafoli, 2011). The Na^+/Ca^{2+} exchanger (NCX) in the PM extrudes Ca^{2+} from the cell in exchange for Na^+ moving down its gradient in a ratio of three Na^+ ions to one Ca^{2+} ion (Hilge, 2012). NCX acts in both a 'forward' and 'reverse' mode. In the forward mode, the Na^+ influx is coupled to Ca^{2+} extrusion, whilst in the reverse mode, Na^+ extrusion is coupled to Ca^{2+} influx (Blaustein & Lederer, 1999).

In recent years, mitochondria and lysosomes have also been found to contribute to sequestering Ca^{2+} following an increase in $[Ca^{2+}]_c$. NCLX in the inner mitochondrial membrane also moves Ca^{2+} up its gradient from the mitochondrial matrix to the cytosol (Palty *et al.*, 2010; O-Uchi *et al.*, 2012). A membrane potential also drives Ca^{2+} accumulation by mitochondria through a channel (the mitochondrial uniporter, MCU) expressed in the inner mitochondrial membrane (O-Uchi *et al.*, 2012). The role of mitochondria in shaping cytosolic Ca^{2+} signals has been well documented as mitochondria are reported to possess a substantial Ca^{2+} uptake capacity through a low affinity uptake system to allow clearing of Ca^{2+} from microdomains. However, the free $[Ca^{2+}]$ in the mitochondria is ~1-10 µM (Collins *et al.*, 2001; Baughman *et al.*, 2011; De Stefani *et al.*, 2011), which is low compared to the other intracellular Ca^{2+} stores such as the ER. Lysosomes have also been reported to selectively sequester Ca^{2+} released via IP_3R (Lopez-Sanjurjo *et al.*, 2013). Lysosomes are discussed further in chapter 3 and in section **1.2**.

The rates and sensitivities of the various Ca^{2+}-clearing pathways either into intracellular stores or extracellular space are different. Whilst the PMCA and SERCA are high-affinity Ca^{2+}-clearing systems, NCX and MCU are low-affinity Ca^{2+}-clearing systems (Rizzuto *et al.*,

1993; Pozzan *et al.*, 1994; Collins *et al.*, 2001). The high affinity of SERCA and PMCA means they can detect and respond to modest changes in $[Ca^{2+}]_c$. The low affinity of the MCU matches observations that mitochondrial uptake of Ca^{2+} released from the ER occurs at specialised microdomains at membrane contact sites between the ER and mitochondria (see **Section 1.3**). Understanding the mechanisms of lysosomal sequestration of Ca^{2+} released from the ER is not well characterised (see **Chapter 3**).

1.1.4 Spatial and temporal organisation of Ca^{2+} signalling

Intracellular Ca^{2+} signals are not homogenous, but they are instead characterized by diverse patterns regulated in part by the nature and intensity of the extracellular stimulation. This diversity in the temporal and spatial dynamics of Ca^{2+} signals contributes to the versatility of Ca^{2+} signalling. Ca^{2+} signals are usually generated from localised regions in the cell. For Ca^{2+} signals evoked by IP_3Rs, low-level stimulation allows the localised opening of a single IP_3R resulting in a Ca^{2+} 'blip'. These stochastic openings of single Ca^{2+} channels are rapidly terminated unless the Ca^{2+} they release can reach nearby IP_3Rs with IP_3 bound (Dickinson *et al.*, 2012; Ruckl *et al.*, 2015). They then trigger a Ca^{2+} puff' (or 'spark' for RyR) (Berridge *et al.*, 2000), when a small cluster of IP_3Rs open together. With more intense stimulation, a puff can activate a neighbouring puff site resulting in a regenerative Ca^{2+} wave that can spread across a cell or into neighbouring cells through gap junctions. Studies in chicken DT40 cells using patch-clamp recordings of the outer nuclear membrane suggest that IP_3 stimulates clustering of IP_3Rs into small clusters of about five receptors (Taufiq *et al.*, 2009). This requires that IP_3Rs are mobile within the ER and nuclear envelope. However, previous optical analyses of Ca^{2+} signals suggested that Ca^{2+} blips and puffs originate from static points (Thomas *et al.*, 2000; Tovey *et al.*, 2001; Smith *et al.*, 2014). A more recent study using endogenously tagged IP_3R1 show ~74% of IP_3R are mobile within the ER and only the immobile IP_3R respond to IP_3 (Thillaiappan *et al.*, 2017). This result shows that IP_3R are already clustered into functional units and only the immobile IP_3R are licensed to respond to IP_3 (Thillaiappan *et al.*, 2017). An emerging theme is that IP_3R are spatially organised into functional clusters and only a sub-population of immobilised IP_3R are licensed to respond to IP_3. The mechanisms by which these IP_3Rs are immobilised are still not known. These results show the importance of understanding the spatial arrangement of IP_3R or RyR on the ER as single channels or clusters, and of how that relates to the resulting Ca^{2+} responses (blip, puff or a regenerative wave).

Ca^{2+} signals generated in response to extracellular stimuli can be spatially organised at a confined space such as Ca^{2+} oscillations at extremities of secretory cells (microdomains) or amplified and propagated throughout the cell as global events (Ca^{2+} waves) (Petersen, 2004). The existence of Ca^{2+} microdomains is facilitated by the slow diffusion of Ca^{2+}, due to Ca^{2+} buffers in the cytosol such as parvalbumin, calbindin and calretinin (Schwaller, 2010). Spatially organised Ca^{2+} microdomains have been implicated in various physiological processes, such as neurotransmitter release at presynaptic junctions. Here, a localised pulse of Ca^{2+} released by P/Q type voltage-gated Ca^{2+} channels on the PM can mediate exocytosis of neurotransmitters at presynaptic junctions (Berridge, 2006). Ca^{2+} released from internal stores has also been reported to mediate exocytosis of glutamate at synaptic junctions (Grosche *et al.*, 1999; Volterra & Meldolesi, 2005). The occurrence of effective Ca^{2+} microdomains is reliant on the close apposition of effector proteins, organelles and Ca^{2+} transporters. Ca^{2+} signals also display complex temporal dynamics that contribute to the final cellular response (Slavov *et al.*, 2013). For example, oscillatory Ca^{2+} signals, but not sustained signals, control the pulsatile secretion of insulin (Bertram *et al.*, 2010). Ca^{2+} oscillations can also affect the regulation of signalling protein such as ras (Cullen & Lockyer, 2002) and transcription factors like NFAT (Hogan *et al.*, 2003) and NFkB (Kupzig *et al.*, 2005; Tabary *et al.*, 2006). The oscillatory nature of Ca^{2+} signals requires feedback loops that provide both positive and negative feedback control of Ca^{2+} release from intracellular stores, but the details are not yet fully resolved (Thurley *et al.*, 2014). Nevertheless, this intricate control is important in protecting cells from prolonged increases in $[Ca^{2+}]_c$ as well as in transducing the Ca^{2+} signals into different downstream processes. Ca^{2+} oscillations present as repetitive transient Ca^{2+} elevations in $[Ca^{2+}]_c$ that encodes a myriad of cellular responses. The versatility and universality of Ca^{2+} signals are notably due to the intricate decoding of complex Ca^{2+} oscillations.

1.2 Lysosomes as signalling organelles

Lysosomes are the digestive compartments of the cell that degrade endocytosed or obsolete intracellular material (Cooper & Hausman, 2000). Extracellular materials destined for degradation are funnelled to lysosomes via the endocytic pathway, whilst intracellular components are delivered to lysosomes via the autophagic pathway. In the last few years, lysosomes have come to be appreciated as important components of physiological processes rather than just catabolic units in the cell. Lysosomes are tuned to sensing both extracellular and intracellular cues and are important for maintaining cellular homeostasis, energy metabolism and organelle biogenesis (Settembre *et al.*, 2011; Roczniak-Ferguson *et al.*, 2012). Lysosomes are membrane-bound vesicular organelles with a luminal pH of ~4.5 in animal cells and they contain many hydrolytic enzymes (Saftig & Klumperman, 2009). The acidity is important for the activity of the lysosomal enzymes. The lysosomes membrane is protected from degradation by a thick layer of glycocalyx formed from the heavy glycosylation of the membrane proteins (Settembre *et al.*, 2013). The lysosomal membrane protects the cytosol from the enzymatic activities of lysosomes. However, even after rupture of lysosomes, the cytosol is partially protected because most lysosomal enzymes are optimally active at the acidic pH of the lysosome (Mellman *et al.*, 1986), although disruption of lysosomal membranes and leakage of lysosomal enzymes have been reported to induce cell death (Guicciardi *et al.*, 2004). The total number of proteins in lysosomes has been estimated to be approximately 130 (Gao *et al.*, 2017), however, not all of these have been functionally characterised largely, due to their low abundance and hydrophobic properties which hinders isolation and purification (Schroder *et al.*, 2010). Of the 130 proteins, there are believed to be 60 diverse soluble catalytic enzymes in the lysosomal lumen.

Dysfunction in lysosomal activity is an important mediator of lysosomal storage diseases (LSDs), which refer to a class of genetic diseases involving mutations in lysosomal enzymes or altered lysosomal signalling. LSDs are usually characterised by the accumulation of undegraded substrates in lysosomes. For example, Gaucher disease, which is the most common LSD, is due to a mutation in glucocerebrosidase leading to accumulation of toxic undegraded metabolites in the cell (Morgan *et al.*, 2011; Sardi *et al.*, 2015). Impaired lysosomal homeostasis has also been implicated in Parkinson's disease, a common neurodegenerative disease (Neudorfer *et al.*, 1996; Aharon-Peretz *et al.*, 2004). Batten disease, a fatal childhood neurodegenerative condition, is another common LSD,

characterized also by the accumulation of storage material in lysosomes. This disease is highly associated with mutations in neuronal ceroid lipofuscinoses (NCLs) (Cárcel-Trullols *et al.*, 2015). Defective NCL expression leads to the faulty production of important lysosomal proteins, such as battenin (Golabek *et al.*, 1999).

1.2.1 Biogenesis of lysosomes

The biogenesis of lysosomes is a process that involves both endocytic and biosynthetic pathways (Saftig & Klumperman, 2009). The biosynthesis of lysosomal proteins occurs in the ER and they are processed in the Golgi, where most hydrolases are targeted to the lysosomes largely by the addition of mannose-6-phosphate (M6P) within the trans-Golgi network (TGN). The M6P receptor (M6PR) mediates transport of these proteins from the Golgi either directly to lysosomes or via the PM and endocytic trafficking to lysosomes (Braulke & Bonifacino, 2009; Saftig & Klumperman, 2009). Endocytosis allows cells to take up materials from the extracellular space. The internalised 'cargo' is either recycled or reaches lysosomes for degradation (Saftig & Klumperman, 2009). Endocytosed vesicles from the PM first encounter early endosomes (EE); this allows either recycling of the endocytosed vesicles back to the PM or progression to late endosomes (LE). Although, the movement of cargo from EE to LE might require some transport vesicles (Aniento, 1993), a more widely accepted view is that EE progress to LE via a maturation process (Stoorvogel *et al.*, 1991). The pH of the lumen of EE is ~6. This allows dissociation of newly synthesised hydrolases from M6PR arriving from the TGN, and recycling of M6PR back to the TGN (Saftig & Klumperman, 2009). Because M6PRs are absent from lysosomes, the absence of M6PRs is a widely accepted means of distinguishing lysosomes from other compartments in the endocytic pathway (Morgan *et al.*, 2011). Various theories exist for the progression of endocytosed cargo from LE (pH 5-6) to lysosomes. Firstly, movement of the endocytosed cargo from LE to lysosomes may be mediated by vesicular transport, suggesting a role for carriers in moving cargo between the two organelles. A second proposition is the 'kiss and run' hypothesis, where transient fusion and mixing of contents is followed by a splitting process (Storrie & Desjardins, 1996). The third hypothesis suggests that the LE and lysosomes completely fuse, followed by budding of a reformed lysosome for reuse (Bright *et al.*, 2005; Pryor & Luzio, 2009). A fourth hypothesis is that LE progressively mature into lysosomes, losing markers like the M6PR and taking up the characteristics of lysosomes such as lower pH (Saftig & Klumperman, 2009). Some evidence now supports the complete fusion

of LE and lysosomes. A hybrid organelle with a size matching a combination of the two organelles containing markers of LE (such as M6PR) and lysosomes (cathepsin L) has been observed in vitro (Mullock *et al.*, 1998) and in optical studies of intact cells (Futter, 1996). However, transient 'kissing' events are also observed to precede complete fusion of the two organelles (Mullock *et al.*, 1998; Bright *et al.*, 2005). Therefore, the biogenesis of lysosomes may arise via a combination of the different processes described.

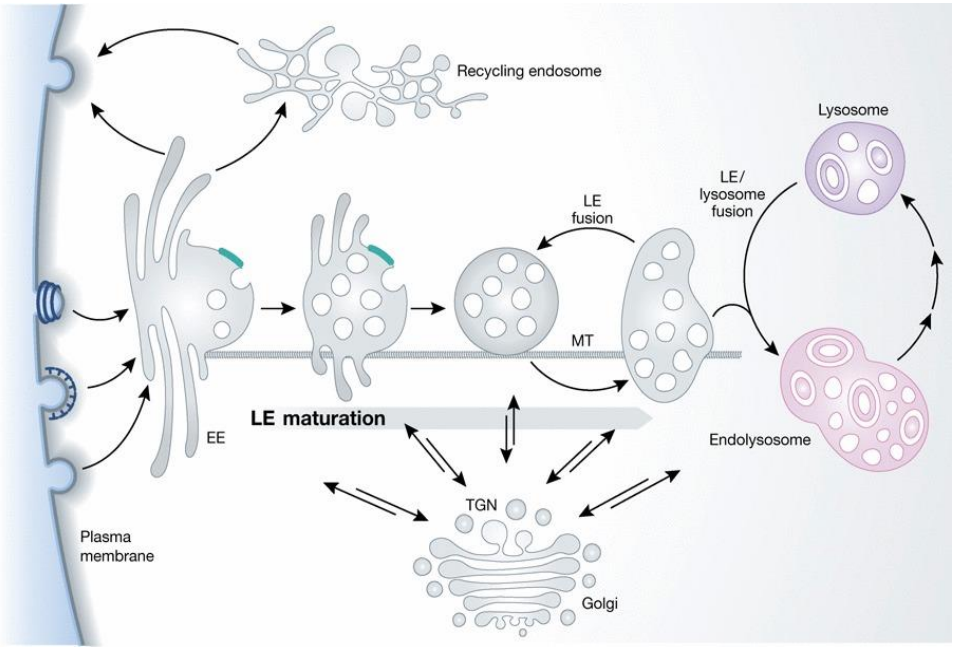

Figure 1.4 **Biogenesis of lysosomes**. The biogenesis of lysosomes begins with endocytosis at the PM, resulting in the first compartment, the early endosome (EE), which acts as a sorting centre for endocytosed cargo. Parts of the EE can be recycled back to the PM or progress through the endocytic pathway. EE mature to form late endosomes (LE). Formation of lysosomes from LE is proposed to occur either by maturation or a fusion event. As the endocytic pathway progresses, the luminal pH decreases. Lysosomal proteins are produced in the ER and proceed via the TGN for targeting to lysosomes directly or via the endocytic pathway. Image is reproduced from Huotari and Helenius (2011).

There are also M6P-independent routes for trafficking of proteins to lysosomes, for example targeting of β-glucocerebrosidase (βGC) to lysosomes via lysosomal integral membrane protein 2 (LIMP2) (Saftig & Klumperman, 2009). Binding of βGC and LIMP2 is pH-dependent, such that the proteins associate in the ER and dissociate in the acidic lumen of lysosomes (Reczek *et al.*, 2007). LIMP2 knock-out mice show a deficiency in βGC translocation to lysosomes (Reczek *et al.*, 2007). The lysosomal targeting of lysosomal membrane proteins (LMPS) is less understood. The most studied route for the translocation of LMPs is via the adaptor protein 3 (AP3) through the indirect translocation pathway (Ihrke *et al.*, 2004; Peden *et al.*, 2004). It has also been suggested that LAMP-1 and LAMP-2 are delivered to lysosomes by a pathway independent of M6PR and AP3. Evidence from this study shows that LAMP1 and LAMP2 may be directly delivered to lysosomes via VAMP7 and hVps41 (Pols et al 2013). Understanding the molecular mediators in the biogenesis of lysosomes remains a very active area of research.

Other organelles similar to lysosomes but with specialised functions have been described. These are called lysosome-related organelles (LROs) and are thought to share the same mechanisms of biogenesis, enzyme targeting and basic hallmarks, but have acquired additional specialist functions. For example, secretory lysosomes which show combined properties of lysosomes and secretory granules (Morgan, 2011a). Secretory lysosomes undergo secretion at the PM to possibly contribute to PM repair and other cellular defence mechanisms (Luzio *et al.*, 2014). Other LROs include melanosomes and lytic granules (Morgan *et al.*, 2011). The biogenesis of LROs is thought to utilise the same machineries as lysosomes but they contain additional proteins such as Rab27a in secretory organelles that is otherwise absent in lysosomes (Morgan *et al.*, 2011).

1.2.2 Lysosomal acidification mechanism

Lysosomal pH (pH_{ly}) is maintained by the V-ATPase, which is found ubiquitously in animal cells and continuously drives H^+ into the lumen of endo-lysosomal organelles against the electrochemical gradient. V-ATPase is also found in the Golgi apparatus, PM of certain cells (e.g. osteoclasts) (Voronov *et al.*, 2013) and in synaptic vesicles (Bodzeta *et al.*, 2017). H^+ translocation via the V-ATPase is driven by energy from ATP hydrolysis (1 ATP is hydrolysed for each 2-4 H^+ transported) (Morgan, 2011a). The V-ATPase is a large complex comprising up to 14 polypeptides arranged to form the ATP-, ADP- and Pi-interacting cytoplasmic region (V_1 domain), and the transmembrane domain that allows H^+ translocation

(V_0) (Beyenbach and Wieczorek, 2006). The V_1 domain contains a peripheral stalk, where ATP hydrolysis occurs leading to rotation of the central stalk, which transfers the energy to the V_0 domain allowing a conformational change that allows movement of H^+ into the lumen (Beyenbach and Wieczorek, 2006). The pH values of the different endocytic compartments are different; therefore, the activity of V-ATPase has to be tightly regulated. Although it is not entirely known how this regulation occurs, the varying density of V-ATPase across different compartments of the endocytic pathway (Huotari & Helenius, 2011) and differential rates of association and dissociation of the V_1 and V_0 domains (Maxson & Grinstein, 2014), have been proposed as regulators of the V-ATPase activity. Furthermore, the pH of lysosomes varies depending on their position in the cell, with lysosomes in the perinuclear region being more acidic than lysosomes in the peripheral region (Johnson *et al.*, 2016). Peripheral lysosomes exhibit decreased V-ATPase activity and increased passive leak of protons (Johnson *et al.*, 2016).

The activity of the V-ATPase is electrogenic, generating a positive membrane potential ($\Delta\psi$) in the lumen of the lysosome as well as establishing a H^+ gradient. The lysosomal membrane potential ($\Delta\psi$) is a difference of V_{lumen} from $V_{cytosol}$ ($\Delta\psi = V_{cytosol} - V_{lumen}$) (Xu and Ren, 2015). It is a function of a balance between H^+ pumps and ionic homeostasis by a plethora of pumps, exchangers and leak channels. Na^+ and K^+ gradients between lysosomal lumen and cytosol are important in maintaining resting lysosomal $\Delta\psi$ and the acidification rate of lysosomes (Ishida *et al.*, 2013). The $[Na^+]$ is greater in the lumen compared to the cytosol, whereas the $[K^+]$ is lower in the lumen relative to the cytosol (Xu and Ren, 2015). There is a wide variation in reported values of $\Delta\psi$ in the literature, which range from +10 to +100 mV (Morgan *et al.*, 2011). The protonmotive force generated from the activity of V-ATPase is coupled to transport of amino acids via solute carrier 36 (SLC36) (Thwaites & Anderson, 2011) and anions such as chloride, via chloride channel-7 (CLC-7) (Scott & Gruenberg, 2011). Acidification of the lysosome lumen is critical for the core functions of lysosomes. Alkalinisation of lysosomes results in mistargeting of proteases and ligands in multiple cell types (Gonzalez-Noriega *et al.*, 1980; Basu *et al.*, 1981; Reaves & Banting, 1994; Presley *et al.*, 1997). A functional V-ATPase is also required for the appropriate budding of carrier vesicles in the endocytic pathway as this is attenuated by alkalinising agents (Clague *et al.*, 1994; van Weert *et al.*, 1995; Aniento *et al.*, 1996). Also, The V-ATPase is structurally required for homotypic vesicle fusion either directly (Baars *et al.*, 2007; Takeda *et al.*, 2008), or indirectly by interaction with SNARE proteins (Strasser *et al.*, 2011).

Furthermore, the V-ATPase is important for lysosomal nutrient sensing, providing a critical sensor for metabolic switching from anabolic to catabolic states (Zhang *et al.*, 2014). The mammalian target of rapamycin complex 1 (mTORC1) is a serine/threonine kinase mediator of anabolic processes for energy balance in times of nutrient scarcity (Zoncu *et al.*, 2011). During starvation, mTORC1 occurs diffusely in the cytosol, however in the presence of nutrients/amino acids, there is a rapid translocation of mTORC1 to the lysosome surface. Lysosomal recruitment of mTORC1 involves multiple proteins in a tightly regulated complex. In the presence of amino acids, Rag GTPase complex becomes active by adopting a Rag-A/B GTP bound conformation and Rag-C/D GDP bound conformation and this facilitates the lysosomal attachment of mTORC1 by directly interacting with Raptor (Sancak *et al.*, 2010). The translocation of mTORC1 to the lysosomal surface is important, because mTORC1 is usually inhibited due to its phosphorylation, but upon reaching the lysosome surface, it encounters Rheb (Ras homolog enriched in brain). Rheb is a small GTPase that activates mTORC1 kinase activity (Saucedo *et al.*, 2003). Once activated, mTORC1 can phosphorylate downstream effectors which collectively work to promote anabolic processes and inhibit catabolic processes. The V-ATPase regulates recruitment and activation of mTORC1 in a mechanism independent of lysosomal acidification (Zoncu *et al.*, 2011). Association of the V_0 and V_1 subunit is increased upon amino acid starvation, and dissociation increases in the presence of amino acids (Stransky & Forgac, 2015). The activity of the V-ATPase is important in maintaining lysosomal homeostasis and optimal functioning. The V-ATPase can be selectively inhibited by bafilomycin A_1 and concanamycin A, two macrolide antibiotics (Yoshimori *et al.*, 1991; Drose & Altendorf, 1997). The effects of bafilomycin A_1 and concanamycin A are explored further in chapter 3.

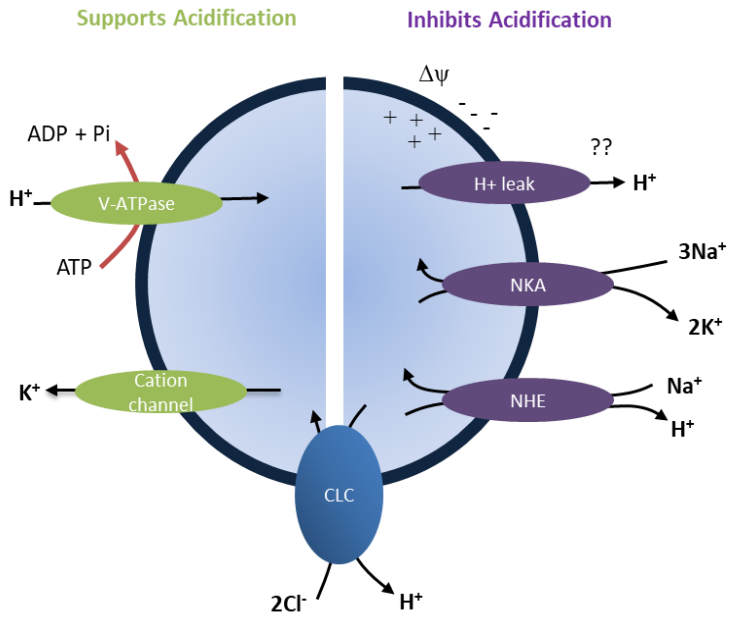

Figure 1.5 **Overview of proteins affecting the pH of acidic organelles**. The activity of the V-ATPase provides H^+ that maintain the acidic pH_{ly} and a luminal positive $\Delta\psi$. This requires proteins (e.g. chloride channels (CLC), cation channels) that allow charge-compensation to sustain H^+ pumping. Possible H^+ leak channels such as Na^+/H^+ exchanger (NHE) also contribute to maintaining the pH_{ly} set point. The Na^+-K^+-ATPase (NKA) is also thought to support the luminal-positive $\Delta\psi$. The activity of CLC is believed to both support (uptake of negatively charged Cl^- ions) and inhibit (H^+ extrusion) acidification of lysosomes.

1.2.3 Overview of lysosomal Ca^{2+}

The recognition of lysosomes as a significant Ca^{2+} store rather than solely as degradative organelles has only occurred in recent years. Due to the difficulty in deciphering the effect of pH vs Ca^{2+} on indicators, there have been limited studies with pH-adjusted luminal Ca^{2+} measurements in lysosomes. However, in macrophages, using Ca^{2+}-sensitive dextran (Dx) and readjusting for pH, the estimated free [Ca^{2+}] in the lysosomes was reported to be 400-600 µM (Christensen *et al.*, 2002), substantially higher than basal $[Ca^{2+}]_c$, suggesting the presence of lysosomal Ca^{2+} uptake and storage mechanisms. Similar results were obtained in human B lymphoblasts (Lloyd-Evans *et al.*, 2008). Following this, lysosomes have been shown to accumulate Ca^{2+} in HEK cells, COS-7 cells and HeLa cells (Lopez-Sanjurjo *et al.*, 2013; Garrity *et al.*, 2016). Furthermore, accumulating evidence supports the presence of an unidentified low-affinity, Ca^{2+} uptake system in lysosomes (Lopez-Sanjurjo *et al.*, 2013;

Garrity *et al.*, 2016). This is proposed to drive substantial accumulation of Ca^{2+}, which might then be mobilized by NAADP or other activators of lysosomal Ca^{2+} release channels (Churchill *et al.*, 2002).

There is growing evidence for the importance of lysosomal Ca^{2+} for the physiological functions of lysosomes. Lysosomal Ca^{2+} release is a critical trigger to allow fusion in membrane trafficking (Pryor *et al.*, 2000). Furthermore, luminal Ca^{2+} is critical for transcription factor E box (TFEB)-mediated regulation of lysosomal biogenesis and autophagy during starvation (Medina *et al.*, 2015). Lysosomal Ca^{2+} release is also reported to regulate lysosomal size in a calmodulin-dependent manner (Cao *et al.*, 2017). Additionally, aberrant lysosomal Ca^{2+} has been reported in some LSDs (Kiselyov *et al.*, 2010).

Ca^{2+} release by lysosomes

The role of acidic organelles as signalling compartments is rapidly emerging, but our understanding of Ca^{2+} handling by lysosomes is not as well understood as it is for the ER. The most recently discovered Ca^{2+}-mobilising messenger is NAADP. It was first reported in 1987, when it was observed to release Ca^{2+} in sea urchin eggs independent of IP_3- and cADPR-sensitive stores (Clapper *et al.*, 1987; Lee *et al.*, 1995). Thapsigargin, an irreversible inhibitor of SERCA that unmasks a Ca^{2+} leak in ER leading to depletion of its Ca^{2+} content, had no effect on NAADP-mediated Ca^{2+} release (Chini *et al.*, 1995; Lee *et al.*, 1995). NAADP-mediated Ca^{2+} release has been reported in invertebrates (Albrieux *et al.*, 1998), vertebrates (Cancela *et al.*, 1999) and plants (Navazio *et al.*, 2000). It is thought to be the most potent agent capable of mobilising intracellular Ca^{2+} stores with effective concentrations in the pM - nM range (Ronco *et al.*, 2015). There is now substantial evidence that the intracellular targets of NAADP are lysosomes and related acidic organelles. Bafilomycin A_1, a selective inhibitor of lysosome vacuolar-type H^+ ATPase (V-ATPase) (Yoshimori *et al.*, 1991), selectively abrogated NAADP-mediated Ca^{2+} release (Churchill *et al.*, 2002; Yamasaki *et al.*, 2004). These studies have strengthened the proposition that NAADP acts by mobilising Ca^{2+} from acidic organelles.

There still remains some controversy in the field, as there are reports of NAADP mobilising Ca^{2+} by activating RyR on the nuclear envelope of acinar cells (Gerasimenko *et al.*, 2003). Considerable effort has been invested in identifying the molecular target of NAADP. NAADP has been proposed to activate RyR on ER and on acidic organelles (Mojzisová *et al.*, 2001; Hohenegger *et al.*, 2002). The Ca^{2+}-mobilising effect of NAADP was blocked by

inhibitors of RyR in T-lymphocytes (Dammermann and Guse, 2005) and pancreatic acinar cells (Gerasimenko, 2006). This observation, however, has not been replicated in other cells. For example, over-expression of RyR in HEK 293 cells potentiated cADPR-mediated Ca^{2+} release, without a corresponding potentiation of NAADP-induced Ca^{2+} release (Calcraft *et al.*, 2009). Also, arguing against RyR as a selective target of NAADP is the observation that NAADP retains its ability to mobilise Ca^{2+} in cells devoid of RyRs (Calcraft *et al.*, 2009; Ogunbayo *et al.*, 2011). It is unclear whether acidic stores like lysosomes express RyR or the observed responses are a result of the close apposition of lysosomes to ER allowing an initial NAADP-evoked Ca^{2+} release to be amplified by CICR mediated by RyR. TRPML1 has also been proposed to mediate responses to NAADP (Bargal *et al.*, 2000). It belongs to the mucolipin family of ion channels, and it is implicated in mucolipidosis type IV, a neurodegenerative disease in children. TRPML1 is a Ca^{2+}-permeable channel localised to LE (Kilpatrick *et al.*, 2016). NAADP has been reported to activate TRPML1 to cause Ca^{2+} release that is unaffected by inhibition of IP_3R and RyR (Zhang & Li, 2007). However, others have failed to detect a functional link between TRPML1 and NAADP. For example, TRPML1 knockout mice show unperturbed NAADP-induced Ca^{2+} release (Yamaguchi *et al.*, 2011). But an interesting observation is that TRPML1 co-immunoprecipitates with two-pore channels (TPC), and this might have implications for the NAADP-evoked Ca^{2+} signals observed (Yamaguchi *et al.*, 2011). These conflicting observations mean that the exact interplay between TRPML1 and NAADP remains unresolved.

The most convincing candidate for the molecular target of NAADP is TPCs. TPCs are highly glycosylated proteins localised to LE and lysosomes. The high glycosylation of the protein protects it from the acidic lumen of the lysosome (Morgan, 2014). There are three isoforms of TPCs; TPC1 and TPC2 are the more common isoforms in animal cells. TPC1 is more localised to EE, whilst TPC2 is more localised to lysosomes (Zhu *et al.*, 2010; Morgan, 2011a). There is no TPC3 in primate and rodent genomes (Cai & Patel, 2010). TPC/NAADP-mediated Ca^{2+} signalling has been associated with various physiological and pathological processes such as muscle differentiation (Aley *et al.*, 2010), homeostasis of liver cells (Grimm *et al.*, 2014), contraction in smooth muscle (Tugba Durlu-Kandilci, 2010), neo-angiogenesis (Favia *et al.*, 2014) and Ebola infection (Sakurai, 2015). NAADP activates TPCs in a bell-shaped concentration-dependent manner (Calcraft *et al.*, 2009; Brailoiu *et al.*, 2010; Pitt *et al.*, 2010; Schieder *et al.*, 2010b). NAADP-dependent Ca^{2+} release via TPC is inhibited by Ned-19, which is a cell-permeant NAADP antagonist (Brailoiu *et al.*, 2010; Pitt

et al., 2010). Over-expression of TPC and its RNAi-mediated knockdown caused corresponding changes in NAADP-induced Ca^{2+} release (Morgan, 2014). Re-expression of TPC into $TPC1^{-/-}$ and $TPC2^{-/-}$ cells re-sensitised the cells to NAADP-mediated Ca^{2+} release (Ruas *et al.*, 2015). Additional evidence has come from electrophysiology studies showing that TPC gating is NAADP-regulated (Brailoiu *et al.*, 2010; Pitt *et al.*, 2010; Schieder *et al.*, 2010b). Different strategies have been used here, such as redirecting TPC to the PM, which results in bafilomycin A_1-insensitive NAADP-regulated Ca^{2+} influx independent of acidic organelles (Brailoiu *et al.*, 2010). Secondly, direct patch-clamp measurements from enlarged single lysosomes with over-expressed TPC2 also showed that TPCs are NAADP-sensitive Ca^{2+}-permeable channels (Schieder *et al.*, 2010b).. A third approach was the incorporation of TPC2 into artificial lipid bilayers (Pitt *et al.*, 2010; Rybalchenko *et al.*, 2012; Pitt *et al.*, 2014).

Some recent contradictory evidence has reported that TPCs are neither gated by NAADP nor permeant to Ca^{2+}. TPC was reported to be activated by $PI(3,5)P_2$ resulting in Na^+ conduction in endo-lysosomal compartments (Wang *et al.*, 2012; Cang *et al.*, 2013). Patch-clamp recording from cells isolated from wild type and TPC knockout mice suggested that TPCs were Na^+-selective channels (Wang *et al.*, 2012). Here, TPC mainly conducted Na^+ in a $PI(3,5)P_2$-sensitive, NAADP-insensitive manner (Wang *et al.*, 2012). The TPC knockdown status of these cells has been questioned as they may still retain an ability to express functional variants of TPC proteins (Ruas *et al.*, 2015). There is also evidence that NAADP does not directly bind to TPC, but binds to accessory proteins which facilitate its binding to TPC (Walseth *et al.*, 2011; Lin-Moshier *et al.*, 2012; Walseth *et al.*, 2012). There is, however, no known candidate for this accessory protein. Although the evidence that TPC2 contributes to a NAADP-regulated Ca^{2+} channel in lysosomes is substantial, it remains a controversial area.

Other Ca^{2+} release channels identified on lysosomes include P2X4 (Qureshi *et al.*, 2007) and TRPM2 (Figure 1.6) (Lange *et al.*, 2009). P2X4 as other purinoceptors were known to be at the cell surface, however it is has been reported to also be present on the lysosomal membrane with a luminal nucleotide binding domain (Qureshi *et al.*, 2007). Similarly, TRPM2, largely thought to be on the PM as been reported to localize to lysosomes with some reports of sensitivity to NAADP. Although requiring concentrations orders of magnitude higher than what is known for other NAADP-sensitive channels such as TPC2 (Morgan, 2011a).

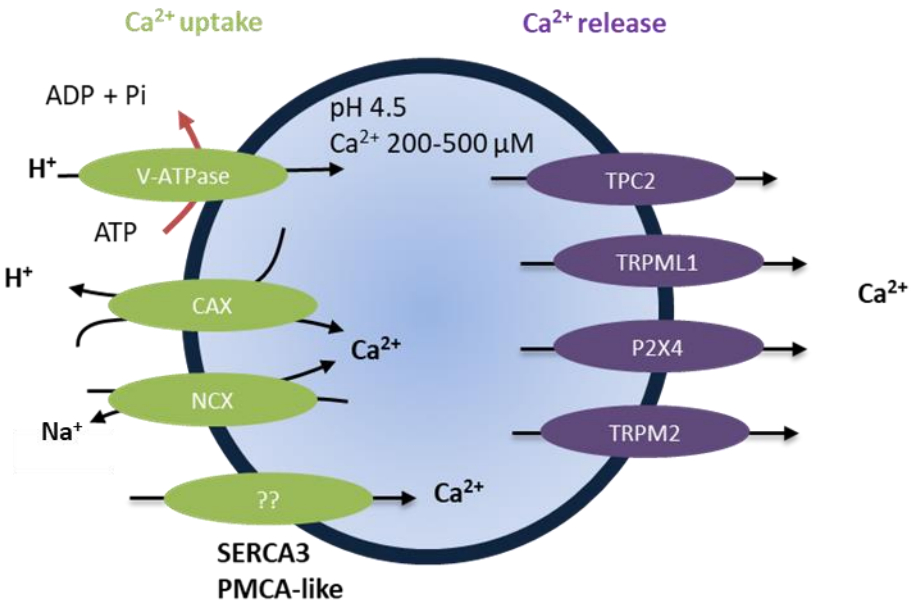

Figure 1.6 **Ca^{2+} filling and release mechanisms of lysosomes.** The specific Ca^{2+} uptake protein into lysosomes is not known. However, mechanisms involving a Ca^{2+}/H^+ exchanger (CAX) have been suggested, although there is no known CAX in mammalian cells. A coupled transport system involving Na^+/Ca^{2+} exchange (NCX), coupled to Na^+/H^+ exchange has also been proposed. Other Ca^{2+} uptake mechanisms involving SERCA3 and PMCA-like Ca^{2+} pumps have also been proposed. Ca^{2+} release channels proposed include TRPML1, TPC2, P2X4 receptors and TRPM2.

Lysosomal Ca^{2+} uptake

Lysosomes can undergo cycles of Ca^{2+} emptying and refilling (Garrity *et al.*, 2016). ML-SA1, a synthetic compound identified as a potent activator of TRPML channels on lysosomes, was shown to mediate robust Ca^{2+} release from lysosomes (Garrity *et al.*, 2016). Early re-challenge with ML-SA1 lead to decreased responses, however, after sufficient time in Ca^{2+}-containing medium, the responses to ML-SA1 recovered (Garrity *et al.*, 2016). These results provide evidence that lysosomes can continuously support a Ca^{2+} uptake process, albeit via an unknown mechanism.

The identity of the mechanism mediating endo-lysosomal Ca^{2+} uptake is unknown. In plants, Ca^{2+} uptake by the vacuole (function of which is similar to that of lysosomes in animal cells) against its electrochemical gradient occurs via P-type Ca^{2+}-ATPases or Ca^{2+}/H^+ exchangers

(CAX) that use energy provided by the H^+ gradient (Schönknecht, 2013). The vacuolar CAX shares some sequence and topological homology with PMCA, however the CAX uptake system is a low-affinity Ca^{2+} uptake system, compared to the high-affinity PMCA (Rooney & Gross, 1992; Brini & Carafoli, 2009; Morgan, 2011a). A similar Ca^{2+}/H^+ exchange is proposed to occur in animal cells. This is thought to occur directly via a CAX-like protein or indirectly via a two-way mechanism involving a Na^+/H^+ exchanger in parallel with a Ca^{2+}/Na^+ exchanger (Klemper, 1985; Patel & Docampo, 2010) (Figure 1.6). In mammalian cells, the luminal pH has been long thought to be critical for lysosomal Ca^{2+} handling (Morgan *et al.*, 2011). In sea urchin oocytes, flooding the peri-vesicular regions of the acidic vesicles with high [Ca^{2+}] resulted in a concomitant increase in the luminal pH (Morgan & Galione, 2007). A loss of function mutation in mucolipin-3, a pH-regulated Ca^{2+} channel, leads to extensive Ca^{2+} accumulation and an accompanying alkalinisation of endo-lysosomal organelles (Lelouvier & Puertollano, 2011). Also, abolishing the lysosomal H^+ gradient with bafilomycin A_1 or NH_4Cl leads to a decrease in the free [Ca^{2+}] in lysosomes (Christensen *et al.*, 2002). A study suggests that lysosomes express a BK_{ca}-like channel, called $LysoK_{VCa}$ (Wang *et al.*, 2017) . $LysoK_{VCa}$ is proposed to be a Ca^{2+}-activated K^+-conducting channel, analogous to PM Ca^{2+}-activated K^+ channels (Wang *et al.*, 2017). $LysoK_{VCa}$ currents were blocked by the BK_{Ca} inhibitors, paxilline and quinidine. Increasing $[Ca^{2+}]_c$ induced large amplitude single-channel openings of $LysoK_{VCa}$ and resulted in a more negative lysosomal $\Delta\psi$ in patched lysosomes (Wang *et al.*, 2017). Lysosomal Ca^{2+} filling was attenuated by dissipating the K^+ gradient in lysosomal preparations using valinomycin and abolished by pre-treatment with paxilline and quinidine (Wang *et al.*, 2017). Co-stimulation of lysosomal preparations with NS1619 (BK_{Ca} channel activator) and ML-SA1 (TRPLM1 activator) potentiated lysosomal Ca^{2+} release (Wang *et al.*, 2017). The BK-like channel in lysosomes has been implicated in the regulation of Ca^{2+} via TRPML-1 as inhibition by paxilline attenuated Ca^{2+} release from lysosomes promoting the accumulation of Ca^{2+} in lysosomes (Cao *et al.*, 2015). Although Wang *et al.*, (2017) show that the regulation of lysosomal Ca^{2+} uptake does not require the lysosome pH gradient, but is dependent on $\Delta\psi$, they note that lysosomal H^+ release may activate $LysoK_{VCa}$ by simultaneously raising luminal pH. Therefore these observations may not be completely independent of the pH_{ly}. One concern is that proteomic analyses have not detected BK_{Ca}-like channels in lysosomes, suggesting that the observation might be an artefact of random fusion events of lysosomes with other cellular structures induced by vacuolin. Juxta-lysosomal Ca^{2+} was measured using TRPML-GCamP3, which has a high affinity for Ca^{2+}, thus may not reliably detect only local Ca^{2+} changes.

Nevertheless, novel mechanisms for lysosomal Ca^{2+} are emerging and require careful interrogation.

A further class of proteins proposed to mediate Ca^{2+} uptake into lysosomes are endolysosomal Ca^{2+} pumps. These are suggested to be thapsigargin-insensitive ATP-hydrolysing Ca^{2+} pumps that actively drive Ca^{2+} into vacuolar-type organelles (Morgan, 2011a). Evidence for this has come largely from the observations that vanadate, an inhibitor of P-type Ca^{2+}-ATPases inhibits Ca^{2+} uptake in vacuoles (Rooney & Gross, 1992; Rooney *et al.*, 1994), protist acidocalcisomes (Vercesi *et al.*, 1994), rabbit reticulocyte endosomes (Nunez *et al.*, 1990) and the Golgi (Pinton *et al.*, 1998). The presence of Ca^{2+}-ATPases does not appear to be widespread across all acidic Ca^{2+} stores, as the vanadate-mediated inhibition of Ca^{2+} uptake was not observed in fungal acidic Ca^{2+} stores (Milani *et al.*, 2001), human neutrophil endocytic organelles (Krause & Lew, 1987) nor in oocytes (Churchill *et al.*, 2002). This suggests that the contribution of Ca^{2+}-ATPases to Ca^{2+} uptake in acidic Ca^{2+} stores occurs only in specialised cells. SERCA3 has been suggested as a specific candidate for Ca^{2+} uptake into NAADP-sensitive acidic Ca^{2+} stores in platelets (Lopez *et al.*, 2005). However, the expression of SERCA3 is limited to specific tissues (Prasad *et al.*, 2004). Our understanding of the mechanisms important in maintaining ionic gradients in the lysosomes is still limited. More research is required to elucidate the mechanism governing uptake of Ca^{2+} into lysosomes.

The most well characterised Ca^{2+} store in the cell is the ER. Ca^{2+} release and Ca^{2+} entry into the ER is highly regulated. The distance between the ER and lysosomes is as narrow as 8.3 nm, which would favour crosstalk between the organelles (Alpy *et al.*, 2013). One of the long-standing controversies in the field is resolving the interdependence between the ER and lysosomal Ca^{2+} release. Nonetheless, lysosomal Ca^{2+} uptake systems have been shown to preferentially sequester Ca^{2+} released from the ER, without accumulating Ca^{2+} which entered the cell via SOCE (Lopez-Sanjurjo *et al.*, 2013). The Ca^{2+} signals resulting from CCh-evoked Ca^{2+} release were exaggerated by bafilomycin A_1, whereas SOCE evoked by thapsigargin or cyclopiazonic acid (CPA) was insensitive to bafilomycin A_1 (Lopez-Sanjurjo *et al*., 2013). The relationship between ER and lysosomes is consistent with their close association, as demonstrated by various optical studies (Jaiswal *et al.*, 2002; Kilpatrick *et al.*, 2013; Lopez-Sanjurjo *et al.*, 2013). The release of Ca^{2+} from the ER is spatially and temporally regulated, where possibly only a subset of the Ca^{2+} released is detected in the cytosol and an undetected

subset is channelled via highly specialised microdomains to organelles such as lysosomes. There is a growing consensus suggesting the presence of an ER-lysosome Ca^{2+} interface, through which an exchange could occur albeit through an unknown uptake system. In summary, it is not known how lysosomes sequester Ca^{2+}, and even the most long-standing suggestion that it requires the lysosomal H^+ gradient has recently been challenged (discussed further in Chapter 3). More research is required to elucidate the mechanism regulating lysosomal Ca^{2+} uptake.

1.3 Structure and function of membrane contact sites

The organisation of organelles into membrane-bound structures allows for spatial separation of biochemical processes, but it also creates a need for a means of transferring metabolites and signalling molecules between organelles. One solution to this is the presence of membrane contact sites (MCSs), where the membranes of two organelles are held 10-50 nm apart by specific tether proteins without the direct association of the membranes (Figure 1.7) (Prinz, 2014; Quon & Beh, 2015). The ER consists of a complex reticular network that extends throughout the cell from the nuclear envelope to the cell periphery. It is widely viewed as a central connector forming contact sites with diverse organelles in the cell. A characteristic feature of contact sites between the ER and other organelles is the exclusion of ribosomes at this interface, suggesting specialised organisation of the ER at these junctions (Csordas *et al.*, 2006; Eden *et al.*, 2010; Friedman *et al.*, 2011; Alpy *et al.*, 2013; Friedman *et al.*, 2013). Furthermore, at contact sites, tethering occurs without complete fusion of the two membranes (Phillips & Voeltz, 2016). The structure and dynamics of ER MCSs is better resolved now with electron microscopy and more recently with high-resolution optical microscopy (Valm *et al.*, 2017). The distances between ER and endosomes are now resolved to 3-15 nm (Alpy *et al.*, 2013) and the distance between the ER and mitochondria resolved to less than 15 nm (Csordas *et al.*, 2006; Friedman *et al.*, 2011). Cumulative analysis of interactions with the ER suggests that 2-5% of the surface area of mitochondria forms an MCS with the ER (Cosson *et al.*, 2012; Murley *et al.*, 2013) and similarly 3-5% of the surface area of an endosome forms an MCS with the ER (Eden *et al.*, 2010; Alpy *et al.*, 2013; Friedman *et al.*, 2013). The functional consequence of MCS is the provision of microenvironments for specialised biochemical processes such as organelle trafficking, intracellular Ca^{2+} signalling, cell survival and lipid exchange.

One of the known functions of MCS is to regulate organelle biogenesis, particularly mitochondria and endosomes. The mitochondrial network is constantly undergoing remodelling due to fission and fusion events. In mammalian cells, mitochondrial fission is the controlled by dynamin-related protein 1 (DRP1). DRP1 oligomerises into spirals that surround the mitochondria to mediate breakage in both the inner and outer membranes (Ingerman *et al.*, 2005; Mears *et al.*, 2011). The assembly point of DRP1 or Dnm1 (the yeast homologue) on mitochondria is regulated by ER MCS, thereby regulating the point of mitochondrial fission (Friedman *et al.*, 2011; Murley *et al.*, 2013). Parts of the mitochondria in contact with the ER have been shown to be constricted and this marks the point of DRP1 or Dnm1 assembly (Friedman *et al.*, 2011). Similarly, ER-endosome MCS has also been shown to regulate the fission of late endosomes from early endosomes during lysosomal biogenesis. During cargo sorting, the ER-endosome MCS arranges around the budding domain, colocalising with the WASH complex-associated FAM21 (Rowland *et al.*, 2014). This interaction is followed by a dynamic rearrangement of an ER tubule around the budding domain leading to a complete fission of the bud (Rowland *et al.*, 2014). The composition of the tethering complexes in this setting are not clearly defined, however, a member of the cargo recognition complex consisting of vacuolar protein sorting-associated protein-26 (VPS35) has been suggested as a possible tether recruiting the ER to these sites (Rowland *et al.*, 2014). Nonetheless, this shows the ER-endosome MCS regulates the position and timing of endosome fission. ER-endosome MCS have also been reported to regulate the sorting and degradation of epidermal growth factor receptor (EGFR) by providing a microenvironment for its dephosphorylation by protein-Tyr phosphatase 1B (PTP1B) localised to the ER (Eden *et al.*, 2010). The dephosphorylation of EGFR by PTP1B is critical for its internalisation and degradation.

ER MCS also regulates the dynamics of endosomes. The ER itself is very dynamic and constantly undergoing remodelling along the microtubule cytoskeleton. During endosome-to-lysosome maturation, endosomes traffic along microtubules maintaining contacts with the ER as they progress through the endocytic pathway. The composition of the ER contact sites with endosomes changes though the maturation process. Notably, about 90% of late endosomes have been reported to show some contact with the ER during organelle trafficking (Friedman *et al.*, 2013). Furthermore, changes in intracellular cholesterol levels affect lysosomal trafficking and distribution by modulating the ER-lysosome MCS (Rocha *et al.*, 2009). During cholesterol depletion, lysosomes accumulate at the cell periphery. Conversely in the

presence of cholesterol, lysosomes accumulate at the perinuclear region via a mechanism that requires oxysterol-binding-related protein 1L (ORPIL) (Rocha *et al.*, 2009). ORP1L senses cholesterol in the lysosomal membrane via its ΔORD domain. This induces a conformational change in ORP1L allowing it to interact with the Rab7-RILP- (Rab-interacting lysosomal protein) $p150^{Glued}$ dynein complex resulting in the trafficking of lysosomes to the perinuclear region (Rocha *et al.*, 2009). In cholesterol-depleted conditions, ORP1L binds to ER VAP protein instead of the Rab7–RILP complex interfering with $p150^{Glued}$ binding and causing a more peripheral positioning of lysosomes. A major hallmark of Niemann-Pick type C and other lysosomal storage diseases is a marked accumulation of lysosome in the perinuclear region (Mukherjee & Maxfield, 2004; Neufeld *et al.*, 2004) accompanied with an overload of lysosomal cholesterol (Frolov *et al.*, 2003). This could occur as a result of a defect in the cholesterol sensing and/or lysosomal trafficking via the ORP1L and Rab7–RILP–p150 complex.

Another candidate protein for the ER-lysosome MCS that can sense lysosomal cholesterol levels, altering MCS to regulate lysosomal trafficking, is steroidogenic acute regulatory protein (STARD3) and STARD3 N-terminal like protein (STARD3NL). These are expressed on lysosomes (Aley *et al.*, 2010; Alpy, 2013). Like ORP1L, STARD3 is able to bind to cholesterol in vitro through its START domain (Tsujishita & Hurley, 2000). STARD3 and STARD3NL were shown to create MCSs with ER by recruiting and binding to ER-resident VAMP-associated proteins A (VAP-A) and B (VAP-B) (Alpy *et al.*, 2013). STARD3 and STARD3NL contain a transmembrane MENTAL domain connected to FFAT motifs exposed on the cytoplasmic face of the lysosomes (Alpy *et al.*, 2013). The interaction of STARD3/STARD3NL with VAP is facilitated by the presence of the FFAT-like motif, which is conserved in both STARD3 and STARD3NL (Alpy *et al.*, 2013). Although the cytoskeletal mediators of STARD3 modulation of lysosome positioning are not yet characterised, heterologous expression of STARD3 has been shown to result in perinuclear enrichment of lysosomes. Conversely knockdown of STARD3 results in the redistribution of lysosomes to the cell periphery (Holtta-Vuori *et al.*, 2005). These tethering proteins are independent of each other as knockdown of ORP1L and PTP1B did not affect MCS formation by STARD3 and STARD3NL with VAP (Alpy *et al.*, 2013).

Protrudin is an ER-resident protein that can also contribute to ER lysosome MCS (Chang *et al.*, 2013; Raiborg *et al.*, 2015). Protrudin is a VAP-interacting protein that also binds to Rab7

on lysosomal membranes as well as to phosphatidylinositol-3-phosphate (PtdIns(3)P (enriched in endosomal membranes) via its FYVE domain (Raiborg *et al.*, 2015). This promotes movement of lysosome to the cell periphery, particularly neurite outgrowths (Raiborg *et al.*, 2015). Knockdown of protrudin leads to accumulation of lysosomes in the perinuclear region (Raiborg *et al.*, 2015). Furthermore, ubiquitin ligase Ring finger protein 26 (RNF26) located on the ER is reported to regulate endosomal movement between the perinuclear and peripheral regions of the cell in a ubiquitination-dependent manner (Jongsma *et al.*, 2016). Therefore, there is rapidly growing evidence for the role of ER-lysosome MCS in regulating lysosomal trafficking and positioning.

MCS are likely to regulate Ca^{2+} signals by providing microdomains for the efficient delivery of Ca^{2+} to effector proteins or organelles at synapse-like interfaces. A classic example of a MCS regulating Ca^{2+} signals is at the ER-PM junction where SOCE occurs. Here, the close apposition of both membranes, allow the drop in ER $[Ca^{2+}]$ to activate a PM channel through a direct interaction between proteins in the two membranes (see Figure 1.2).

Ca^{2+} uptake by mitochondria is facilitated by close apposition of ER and the outer mitochondrial membrane stabilized by MCS. For example, Ca^{2+} sequestration by the mitochondrial Ca^{2+} uniporter (MCU) is dependent on an optimum distance between the organelles (Qi *et al.*, 2015). The MCU is a low-affinity Ca^{2+}-permeable channel, requiring $[Ca^{2+}]$ orders of magnitude higher than in the bulk cytosol for its activation (Marchi & Pinton, 2014). Due to slow rates of Ca^{2+} diffusion in cytosol, IP_3-mediated increases in $[Ca^{2+}]_c$ are higher around IP_3R than globally. There is evidence of a high $[Ca^{2+}]_c$ exceeding 10 µM around ER-mitochondria MCS (Csordas *et al.*, 2010). This suggests the presence of high Ca^{2+} microdomains occurring transiently after IP_3R-mediated Ca^{2+} release (Rizzuto *et al.*, 1993; Rizzuto *et al.*, 1998; Szabadkai *et al.*, 2006). GRP75, a cytosolic chaperone protein, forms a tether between VDAC (voltage-dependent anion channel) present on the outer mitochondrial membrane and IP_3R on the ER (Szabadkai *et al.*, 2006). Mitochondria are well situated to shape Ca^{2+} signals released from the ER (Rizzuto *et al.*, 2004). Increasing the gap between both organelles using artificial tethers attenuates the Ca^{2+} transfer from ER to mitochondria (Csordas *et al.*, 2006; Csordas *et al.*, 2010). The finding that Ca^{2+} exchange occurs between ER and mitochondria at MCS populated by IP_3R revolutionised our understanding of Ca^{2+} signalling by demonstrating that the ER could deliver its Ca^{2+} signals to the cytosol and other organelles. Apart from contributing to the cytosolic Ca^{2+} clearing

mechanism, uptake of Ca^{2+} by mitochondria is important for mitochondrial function. Constitutive IP_3R activity regulates mitochondrial bioenergetics as well as macro-autophagy in cells (Cardenas *et al.*, 2010). Key mitochondrial enzymes important for energy production such as pyruvate dehydrogenase, NAD^+-isocitrate dehydrogenase and 2-oxoglutarate dehydrogenase are Ca^{2+}-regulated (Denton, 2009). Intricate regulation of mitochondrial Ca^{2+} uptake is required because mitochondrial Ca^{2+} overload triggers apoptotic signals (Pinton *et al.*, 2008).

There is growing research into regulators of ER-mitochondria MCS. Depletion of Mitofusin 2 (MFN2), a GTPase found in the outer membrane of mitochondria, was shown to disrupt ER-mitochondria MCS and attenuate Ca^{2+} transfer (de Brito & Scorrano, 2008). However, this is controversial as others have shown that depletion of MFN2 strengths ER-mitochondria MCS (Cosson *et al.*, 2012; Filadi *et al.*, 2015). Other reported regulators of ER-mitochondria MCS include promyelocytic leukaemia tumour suppressor (PML) (Giorgi *et al.*, 2010). PML forms a complex with Akt and PP2A at mitochondria-associated membranes (MAMs) to regulate IP_3R-mediated Ca^{2+} release, fine-tuning the amount of Ca^{2+} transferred to mitochondria and the response to pro-apoptotic stimuli (Giorgi *et al.*, 2010). Understanding the physiological regulation of ER-Mitochondria MCS and Ca^{2+} signalling remains an exciting area of research.

Like mitochondria, most lysosomes are closely apposed to the ER (Friedman *et al.*, 2013; Kilpatrick *et al.*, 2013; Lopez-Sanjurjo *et al.*, 2013). The distance between the ER and lysosomes is as narrow as 8.3 nm, which would favour crosstalk between the organelles (Alpy, 2013). High-resolution studies show that lysosomes are also intimately associated with SR to form discrete microdomains in ventricular myocytes (Aston *et al.*, 2017). The cross talk between lysosomes and ER is bidirectional. Ca^{2+} released from ER is sequestered by lysosomes (Lopez-Sanjurjo *et al.*, 2013), and Ca^{2+} released upon GPN-mediated rupture of lysosomes has been reported to induce IP_3R-mediated Ca^{2+} spikes (Kilpatrick *et al.*, 2013). The interaction between lysosomes and ER is reminiscent of the interaction between the ER and mitochondria. For example, lysosomes sequester Ca^{2+} released by IP_3R (Lopez-Sanjurjo *et al.*, 2013; Garrity *et al.*, 2016), lysosomes are proposed to buffer cytosolic Ca^{2+} following release from the ER (Lopez Sanjurjo *et al.*, 2013), and lysosomes form extensive tethers with the ER (Eden *et al.*, 2010; Helle *et al.*, 2013; Prinz, 2014). However, whereas high local $[Ca^{2+}]$ at the surface of mitochondria have been directly determined by tethered Ca^{2+} sensors,

this has yet to be demonstrated for lysosomes (Montero *et al.*, 2000). Hence, many questions remain to be answered concerning the identity and functions of MCS tethering proteins in relation to Ca^{2+} exchange between ER and lysosomes.

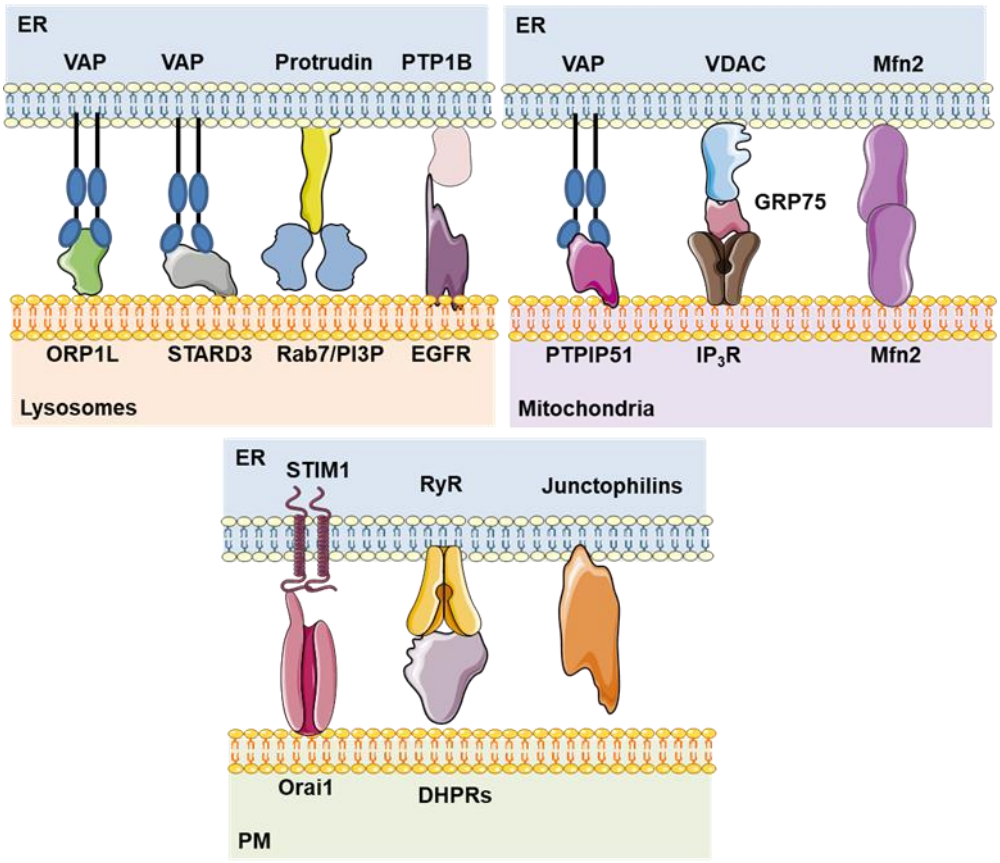

Figure 1.7 **Selected tethering proteins reported to populate ER MCS in mammalian cells involved in regulating Ca^{2+} signalling**. Multiple tethering proteins populate specialised MCS between the ER and multiple organelles. Tethering proteins not described in the text include VAPB (ER) interaction with protein tyrosine phosphatase-interacting protein 51 (PTPIP51) on the outer mitochondria membrane to regulate Ca^{2+} homeostasis (De vos *et al.*, 2012). Junctophilins have a single TMD spanning the SR membrane, and a protruding cytosolic domain that interacts with the PM to also regulate Ca^{2+} signalling (Takeshima *et al.*, 2000; Hirata *et al.*, 2006). Although overexpression of junctophilins strengthens SR/PM interactions (Takeshima *et al.*, 2000), it is not required for assembly of SR/PM junctions (Prinz, 2014). The voltage-sensing dihydropyridine receptor (DHPR) activates RyR1 in the SR in the closely apposed SR/PM junctions of skeletal muscles (Rebbeck *et al.*, 2011).

1.4 Practical limitations to studying lysosomal Ca^{2+} release

The accurate measurement of pH_{ly} is now optimised and readily achievable (Johnson *et al.*, 2016). However, quantitatively measuring the lysosomal Ca^{2+} content is more difficult. Using electron microbe analysis (Morgan *et al.*, 2011) and plasma mass spectrometry (Wang *et al.*, 2012), the total [Ca^{2+}] of lysosomes has been estimated to be 14 mM and ~2 mM respectively. These approaches either rely on fixed cells where organelles are identified by morphology or following cell fractionation methods which are usually contaminated with other organelles. Therefore, it has so far been difficult to reproducibly quantify the total and free [Ca^{2+}] in the lysosomal lumen.

Measuring the free luminal [Ca^{2+}] in lysosomes is challenging. Only two studies have quantitatively reported an estimated free [Ca^{2+}], they suggest it to be ~500 µM (Christensen *et al.*, 2002; Lloyd-Evans *et al.*, 2008). The very acidic pH of lysosomes alongside their cocktail of proteolytic enzymes are major limitations for luminal measurements of Ca^{2+}. The pH can alter the dye by quenching the chromophore or altering the Ca^{2+} binding kinetics, both of which are deleterious to meaningful luminal Ca^{2+} measurements (Morgan *et al.*, 2015). One strategy used in directing materials to lysosomes is by hijacking the endocytic machinery to direct probes to lysosomes. Usually, this involves the co-endocytosis of dextran tagged pH- and Ca^{2+}-sensitive probes to allow ratiometric reporting of pH and Ca^{2+} changes in lysosomes using a pulse-chase protocol (Gerasimenko *et al.*, 1998; Lloyd-Evans *et al.*, 2008). The chase component is used to allow movement of the dextran-conjugated probes to lysosomes, which are the terminal compartments of the endocytic pathway. For example, Rhod-2, when loaded at 37^{o}C, has been used in reporting lysosomal Ca^{2+} (Mirnikjoo *et al.*, 2009), however, Rhod-2 is also reported to accumulate in the mitochondria due to its cationic nature (Trollinger *et al.*, 1997). The selectivity of Rhod-2 in measuring lysosomal Ca^{2+}, therefore, requires careful consideration. However, more selectivity has been achieved using dextran conjugates to direct probes to lysosomes. Nevertheless, to successfully obtain meaningful results, it is important to use pH-resistant probes. The rhodamine dyes are more stable than fluorescein dyes. However, limitations exist, such as the difficulty in directing even dextran conjugates to lysosomes consistently. The effect of pH_{ly} on Ca^{2+} indicators is confounded by the dynamic changes in pH_{ly} that occurs during lysosomal Ca^{2+} modulations (Morgan & Galione, 2007; Cosker *et al.*, 2010; Collins *et al.*, 2011; Morgan, 2011b; Lopez Sanjurjo *et al.*, 2013).

The problems with luminal Ca^{2+} measurements remain unsolved. However, one strategy is the use of genetically-modified fluorescent proteins appended to lysosomal proteins on the cytosolic side of the membrane to allow measurement of peri-lysosomal Ca^{2+} changes. An advantage of this approach is an insight into local Ca^{2+} changes around lysosomes that can otherwise be missed in global Ca^{2+} measurements, whilst avoiding problems with luminal degradation of proteins. This approach has been used for secretory vesicles (Pouli *et al.*, 1998; Emmanouilidou *et al.*, 1999) and LE/lysosomes. In the lysosomal studies, GCaMP3 was fused to the N-terminus of TRPML1 (Shen *et al.*, 2012) or YCaM3.6 cameleon was fused to the C-terminus of LAMP1 (McCue *et al.*, 2013). However, the Ca^{2+} indicators used have high-affinity for Ca^{2+}, which limited the ability to selectively report juxta-lysosomal Ca^{2+} dynamics. Therefore, the need for a low-affinity fluorescent sensor to detect peri-lysosomal Ca^{2+} changes remains.

Another approach used in studying lysosomal Ca^{2+} signalling is by releasing lysosomal Ca^{2+} and assessing changes in $[Ca^{2+}]_c$. The most common pharmacological tools used are NAADP, ML-SA1 and GPN. The target and organelle selectively of NADDP remains controversial (see **Section 1.2.3**). The use of NAADP has also been limited because it is not cell-permeant and the AM ester form is highly unstable and not readily available. NAADP is also reported to have a lag time (up to minutes) to attain a peak change in $[Ca^{2+}]_c$ (Morgan *et al.*, 2015). The TRPML agonist, ML-SA1, is widely used to release lysosomal Ca^{2+} (Morgan *et al.*, 2015; Kilpatrick *et al.*, 2016). However, there is a suggestion that the action of TRPML1 is not limited to local lysosomal Ca^{2+} signalling and involves ER Ca^{2+} and extracellular Ca^{2+} influx as well (Kilpatrick 2016). This remains a useful tool, but, caution is required in interpreting results obtained using ML-SA1 as a selective reporter of lysosomal Ca^{2+} release. GPN is most widely used as a selective disruptor of lysosomes. GPN is proposed to be cleaved by cathepsin C in the lysosomal lumen, leading to lysosomal permeabilization and leakage of Ca^{2+} (Jadot *et al.*, 1984; Turk *et al.*, 2001). Although widely believed and cited, the evidence for this model is minimal. I return to explore the action of GPN in Chapter 4. And even seemingly straightforward tools such as NAADP and Ml-SA1 that has offered insight into lysosomal activity, have difficulties, such as complexity arising from interactions between different organelles. It is, for example, difficult to disentangle Ca^{2+} signals arising directly from lysosomal Ca^{2+} release from those that have been amplified by Ca^{2+} release from the ER. Disrupting lysosomes pharmacologically or via siRNA might also lead to compensatory off-target effects. In conclusion, there is still no reliable means to measure

[Ca^{2+}] within the lysosomal lumen, and these tools are urgently needed to investigate the mechanism of Ca^{2+} uptake by lysosomes.

1.5 Aims of this project

Lysosomes have come to be appreciated as Ca^{2+} signalling hubs, capable of sequestering and releasing Ca^{2+} in highly regulated processes. The release of lysosomal Ca^{2+} via TRPML1 is reported to regulate lysosomal size in a calmodulin-dependent manner (Cao *et al.*, 2017), regulate lysosomal biogenesis in nutrient sensing, and autophagy in starvation (Medina *et al.*, 2015), and precede lysosomal fusion in membrane trafficking (Pryor *et al.*, 2000). Also, aberrant lysosomal Ca^{2+} is implicated in some LSDs (Kiselyov *et al.*, 2010).

Lysosomes selectively sequester Ca^{2+} released from IP_3Rs, unmasked following inhibition of lysosomal V-ATPase with bafilomycin A_1 (Lopez Sanjurjo *et al.*, 2013). However, this has been challenged by evidence that refilling of lysosomes with Ca^{2+} is independent of the V-ATPase (Garrity *et al.*, 2016). There is, therefore, a need to investigate the exchange of Ca^{2+} between ER and lysosomes and the contribution of the V-ATPase to it. I address these issues in chapter 3.

In interrogating lysosomal Ca^{2+} uptake and release, one of the most widely used tools to selectively release lysosomal Ca^{2+} is GPN. About a hundred publications report the use of GPN (Berg *et al.*, 1994; Haller *et al.*, 1996; Churchill *et al.*, 2002; Morgan & Galione, 2007; Dionisio *et al.*, 2011; Coen *et al.*, 2012; Davis *et al.*, 2012; Kilpatrick *et al.*, 2013; Ruas *et al.*, 2015; Garrity *et al.*, 2016; Melchionda *et al.*, 2016). In chapter 4, I examine the mechanism of action of GPN.

2. Materials and Methods

2.1 Materials

Bovine serum albumin (BSA) was from Europa Bio-Products (Ely, UK). Bafilomycin A_1 was from Fluorochem (Hadfield, UK) and Alfa Aeser (Massachusetts, USA). Concanamycin A was from Insight Biotechnology (Middlesex, UK). Thapsigargin and cyclopiazonic acid (CPA) were from Bio-Techne (Minnesota, USA). Fluo 8-AM was from Stratech Scientific (Suffolk, UK). 1,2-bis(O-aminophenoxy)ethane-N,N,N',N'-tetraacetic acid (BAPTA) was from Phion (Dorset, UK). Agarose and α-select gold efficiency competent *Escherichia coli* were from Bioline Ltd (London, UK). Platinum Pfx DNA polymerase, custom primers, Rapid DNA ligation kit, DMEM/F-12 GlutaMAX, TrypLE express, Iscove's Modified Dulbecco's Medium (IMDM), Tris-acetate SDS (sodium dodecyl sulphate) running buffer, 3-8% Tris-acetate PAGE (polyacrylamide gel electrophoresis) gel, EDTA-free Pierce protease inhibitor mini-tablets, Spectra multicolour broad range protein ladder, iBLOT transfer kit, NucBlue Live ReadyProbes Reagent, SNARF-5F, Dextran (Dx) conjugates of Oregon Green™ 488 (10 kDa), Fluorescein (3 &10 kDa), and LysoTracker Red DND-99 were from ThermoFisher (Paisley, UK). TransIT-LT1 transfection reagent was from GeneFlow (Lichfield, UK). HiPerFect transfection reagent, siRNA against ATP6V0C or a non-silencing control siRNA (catalogue numbers s79 and AM4611), QIAquick gel extraction kit, QIAprep spin miniprep kit and QIAprep endofree maxi kit were from Qiagen (Crawley, West Sussex). Cell culture plastics and 96-well assay plates were from Greiner (Stonehouse, Gloucestershire, UK). Imaging dishes (35-mm diameter with a 7-mm No. 0 glass insert) were from MatTek Corporation (Ashland, USA) or IBL (Baustoff+Labor GmbH, Austria). Ionomycin was from Merck Eurolab (Nottingham, UK). Poly-L-lysine, Triton X-100, carbamylcholine chloride (carbachol), dimethyl sulfoxide (DMSO), Pluronic F-127, foetal bovine serum (FBS), Duolink proximity ligation kit, Tween-20, dithiothreitol (DTT), Triton X-100, nigericin, monensin, MES, ethylenediaminetetraacetic acid (EDTA) and Tris base were from Sigma-Aldrich (Poole, Dorset, UK). Human plasma fibronectin was from Merck Millipore (Watford, UK). Caged cell-permeant IP_3 (ci-IP_3/PM) was from SiChem (Bremen, Germany). Glycyl-L-phenylalanine 2-naphthylamide (GPN) and Gly-Arg-AMC were from Bachem (St. Helens, UK) and Santa Cruz Biotechnology (Texas, USA), respectively. Glycyl-D-phenylalanine 2-naphthylamide (D-GPN) was custom-synthesised by LifeTein (Somerset, USA). Gly-Phe-DMK was from MP Bio (Derby, UK). ECL prime Western blotting detection reagent was

from GE Life Sciences (Little Chalfont, UK). Vector px458 was from Addgene (plasmid#48138). Antibodies used for protein expression analysis were mouse anti-cathepsin C (Santa Cruz Inc.,1:500), rabbit anti-TMCO1 (Sigma, 1:1000), mouse anti-β-actin (Cell Signaling, 1:1000), donkey anti-mouse IgG-HRP (1:2000) and donkey anti-rabbit IgG-HRP (1:5000) from Santa Cruz, Inc. (California, USA). Antibodies used for PLA were: VAP-A (mouse, Santa Cruz Biotechnology, sc-293278), Rab7 (rabbit, Cell Signaling Technology, D95F2) and GFP (mouse, ThermoFisher, A-11120). Other reagents, unless otherwise specified, were from Sigma-Aldrich (Dorset, UK).

2.2 Cell culture and transfection

Human embryonic kidney (HEK) cells, in which CRISPR/Cas9 was used to delete one or more IP_3R subtypes, were from Kerafast (Boston, MA, USA) (Alzayady *et al.*, 2016). HAP1 cells, genetically engineered using CRISPR/Cas9 to disrupt genes for all three IP_3R subtypes, were developed with Horizon Discovery (Cambridge, UK). Hereafter, HEK and HAP1 cells with no functional IP_3R are referred to as HEK-3KO and HAP1-3KO cells respectively. HeLa and HEK-293 cell lines were cultured in Dulbecco's Modified Eagles Medium (DMEM)/F-12 with GlutaMAX supplemented with FBS (10%). HAP1 cells were cultured in Iscove's Modified Dulbecco's Medium (IMDM) GlutaMAX with 10% FBS. The cells were maintained at 37°C in humidified air with 5% CO_2 and passaged every 3-4 days using GibcoTrypLE Express. All cell lines were confirmed to be free of mycoplasma. For cell population assays, cells were seeded on poly-L-lysine (10% v/v)-coated 96-well plates. For imaging, cells were grown on 35-mm glass-bottomed dishes coated with human fibronectin (10 µg/ml).

For plasmid DNA transfection, HEK and HeLa cells were seeded on fibronectin-coated 35-mm glass-bottomed dishes in serum-containing medium and grown for 24 h at 37ºC with 5% CO_2. Cells were transfected with plasmids encoding Ca^{2+} indicators or tagged proteins according to the manufacturer's instructions using TransIT-LT1 reagent (1 µg DNA/2.5 µl reagent). TransIT-LT1 reagent was added to the plasmid in serum-free medium and incubated at 22°C for 15 min to allow the formation of complexes. The complexes were then added drop-wise to the cells, ensuring a uniform distribution within the plate. The cells were incubated for 24 h before imaging.

For siRNA transfection, the ThermoFisher high-throughput transfection procedure was used. siRNA directed against ATP6V0C or a non-silencing control siRNA (catalogue numbers 79 and AM4611, ThermoFisher) was spotted onto empty wells of a 96-well plate. The siRNA was overlaid with siPORT NeoFX Transfection Agent (220 ng siRNA/µl reagent) diluted in serum-free medium and incubated for 10 min at 22ºC to allow the formation of complexes. The complexes were then overlaid with cells in suspension (30,000 cells/well) to a final volume of 200 µl (40 nM/well). Experiments were performed 48 - 72 h after transfection.

2.3 Measurements of $[Ca^{2+}]_c$ in cell populations

Confluent monolayers of cells grown in a 96-well plate were loaded with fluo-8 by incubation for 1 h at 20°C in HEPES-buffered saline (HBS, 100 µl) containing fluo 8-AM (2 µM) and 0.02% Pluronic F-127. Cells were then washed and incubated in HBS for 1 h at 20°C to allow de-esterification of fluo 8-AM. HBS had the following composition: 135 mM NaCl, 5.9 mM KCl, 1.2 mM $MgCl_2$, 1.5 mM $CaCl_2$, 11.5 mM D-glucose, 11.6 mM HEPES, pH 7.3. $CaCl_2$ was omitted from nominally Ca^{2+}-free HBS, and in some experiments, (see figure legends) BAPTA (final concentration 2.5 mM) was added to the HBS immediately before stimulation to reduce the free $[Ca^{2+}]$ of the HBS to < 20 nM. Fluorescence was recorded using a FlexStation III fluorescence plate-reader that allows automated fluid additions while recording fluorescence (Molecular Devices, Sunnyvale, CA, USA). Fluorescence was recorded at 1.44-s intervals, with excitation at 485 nm and emission at 525 nm. Data were collected and analyzed using SoftMax Pro (Molecular Devices). Maximal (F_{max}) and minimal (F_{min}) fluorescence values were determined from parallel wells after addition of Triton X-100 (0.1%) to lyze cells with either 10 mM $CaCl_2$ (F_{max}) or 10 mM BAPTA (F_{min}). The fluorescence values (F) were calibrated to $[Ca^{2+}]_c$ using a K_D = 389 nM (fluo 8) from:

$$[Ca^{2+}]_c = K_D \times \frac{(F - F_{min})}{(F_{max} - F)}$$

2.4 *In vitro* calibration of fluo 8

Since the K_D of BAPTA for Ca^{2+} (160 nM in the absence of Mg^{2+}) (Pethiget al., 1989) is unaffected by pH changes between 7 and 8 (Tsien, 1980), standard Ca^{2+} solutions were prepared in modified cytosol-like medium (MCLM). MCLM had the following composition: 140 mM KCl, 20 mM NaCl, 20 mM HEPES and 10 mM BAPTA. Solutions containing the

free acid form of fluo-8 were placed in 96-well plates and fluorescence was recorded at intervals of 1.44 s using a fluorescence plate reader (FlexStation), with excitation at 485 nm and emission at 525 nm. Calculation of free [Ca^{2+}] were computed using http://maxchelator.stanford.edu/webmaxc/webmaxcS.htm.

2.5 Measurements of pH_{cyt} in cell populations

Confluent cultures of cells grown in 96-well plates were loaded with the ratiometric pH indicator, SNARF-5F (Liu et al., 2001), by incubation (30 min, 20°C) with SNARF-5F AM (2 μM) in HBS containing Pluronic F-127 (0.02%). Cells were washed in HBS, and fluorescence was recorded from cells in HBS (20°C) at intervals of 3.8-s (excitation, 543 nm; emission, 580 and 640 nm) using a FlexStation 3 fluorescence plate-reader with SoftMaxPro software. Fluorescence was calibrated to pH_{cyt} from:

$$pH_{cyt} = pK_a - \log\left[\frac{(R - R_b)}{(R_a - R)} \times \frac{F_b}{F_a}\right]$$

Where, p*Ka* is the negative log of the acid-base dissociation constant (K_a); R is the fluorescence emission ratio (F580/F640); R_a (F_a) and R_b (F_b) are the fluorescence ratios (or fluorescence intensities at 640 nm) for the fully protonated and de-protonated forms of the indicator. For calibration, cells loaded with SNARF-5F were treated for 30 min in Ca^{2+}-free cytosol-like medium (CLM, pH 7.4) with nigericin (50 μM), which is a H^+/K^+ antiporter. CLM was then replaced by CLM supplemented with nigericin (50 μM) and buffered at different pH values (pH 5.0 - 8.5), and SNARF-5F fluorescence was measured. Ca^{2+}-free CLM had the following composition: KCl 140 mM, NaCl 4 mM, $MgCl_2$ 1.4 mM, HEPES 10 mM, EGTA 1 mM.

2.6 Cloning of LAMP1-G-GECO1.2

The initial templates for cloning of the low-affinity Ca^{2+} sensor, LAMP1-G-GECO1.2 (Ly-GG) targeted to the lysosomal membrane were LAMP1-mCherry (Lopez-Sanjurjo *et al.*, 2013) and cytosolic G-GECO1.2 (Zhao *et al.*, 2011). A HindIII restriction site was inserted at the 5' end of LAMP1-mCherry using primer LAMP1F. LAMP1-mCherry contained a pre-existing BamHI site. Primers LAMP1F and LAMP1R were used to amplify the LAMP1 sequence from LAMP1-mCherry using PCR. The PCR conditions are described in Table 2.1

Table 2.1 **Thermocycling parameters for PCR reactions used to construct Ly-GG**

	Temperature (˚C)	**Time**	**Number of cycles**
Preliminary denaturation	94	3 min	1
Denaturation	94	15 s	25
Annealing	55	30 s	
Extension	68	105 s	
Final extension	68	2 min	1

The LAMP1 PCR product was digested with HindIII and BamHI. The digested PCR products were analysed by agarose gel electrophoresis. A 1% agarose gel containing Midori Green DNA stain (4 µl/100 ml) was used. 6x DNA loading dye was mixed with the PCR product prior to loading onto the agarose gel. Tris-acetate-EDTA (TAE) buffer comprises 40 mM Tris, 20 mM acetic acid and 1 mM EDTA. The electrophoresis was run at 115 V for 45 min. A Fastgene LED transilluminator was used to detect the bands, which were then purified using a Qiagen gel extraction kit. The product at this point was LAMP1 with flanking sticky ends derived from the HindIII and BamHI sites. A BamHI site was introduced in frame with the 5′ end of G-GECO1.2 via PCR, using the conditions shown in Table 2.1 and primer G-GECO1.2F (Table 2.2). An EcoRI site was introduced at the 3′ end of G-GECO1.2 using the primer GGECO1.2R (Table 2.2). The product was then digested with BamHI and EcoRI, run on a 1% agarose gel, and the DNA contained within the band was purified using the Qiagen gel extraction kit.

The Ly-GG construct was then assembled in pcDNA3.1(+) (ThermoFisher), a mammalian expression vector. pcDNA3.1(+) was digested with HindIII and EcoRI overnight to create sticky ends suitable for ligation with the LAMP1 and G-GECO1.2 fragments. The digested LAMP1, G-GECO 1.2 and pcDNA3.1(+) were ligated using T4 DNA ligase according to the manufacturer's protocol.

Table 2.2 **Primers used for PCR amplification and sequencing of plasmids**

Primer name	Sequence
GGECO1.2F	CATGGATCCATGGTCGACTCATCACGTCGTAAG
GGECO1.2R	GTAGAATTCCTACTTCGCTGTCATCATTTG TACAAACTCTTC
LAMP1F	TACAAGCTT GCTTCGAATTCTCGCCACCAT
LAMP1R	GGTGGATCCTCCTGAACCTCCGATGGTCTG ATAGCCCGCG
LAMP1SeqF1	ACGTTCAGCACCTCCAACTA
LAMP1SeqF2	ATCGGCAGGAAGAGGAGTCA
T7 promoter (F)	TAATACGACTCACTATAGGG
BGH Reverse	TAGAAGGCACAGTCGAGG
GGECO1.2SeqM	CAAACCCCAGTGTGTCCAAG
GGECO1.2SeqE	GCCTACCACTACCAGCAGAA

The ligated DNA was transformed in gold efficiency *E. coli* α-select competent cells according to the manufacturer's protocol and inoculated on carbenicillin-containing (100 µl/ml) agar plates. The agar plates were incubated for 16 h at 37°C. Single colonies were picked into sterile lysogeny broth (LB) Miller medium containing 100 µg/µl carbenicillin. The bacterial culture was grown for 16 h at 37°C in a shaking incubator at 260 rpm. The cells were harvested, and the plasmid was purified using a QIAprep spin miniprep kit according to the manufacturer's protocol. Following sequence verification, the plasmid DNA was amplified and purified using a Qiagen endofree plasmid maxi kit according to the manufacturer's protocol. The DNA was eluted in Tris-EDTA (TE) buffer, and the concentration was determined using BioDrop µLITE (BioDrop, UK). TE buffer is composed of 10 mM Tris-Cl, pH 8.0, and 1 mM EDTA.

The sequence of LAMP1-R-GECO1.2 was verified using primers: LAMP1SeqF1, LAMP1SeqF2, T7 promoter (F) and BGH Reverse using the Sanger sequencing service (Table 2.2) (Source BioSciences, UK). The sequence of LAMP1-G-GECO1.2 was verified using primers: LAMP1SeqF1, LAMP1SeqF2, T7 promoter (F), GGECO1.2SeqM and GGECO1.2SeqE (Table 2.2). Sequencing data were analysed using BioEdit software (Ibis Biosciences) and alignments were carried out using Clustal Omega (http://www.ebi.ac.uk/Tools/msa/clustalo/).

2.7 Quantitative PCR

QPCR was carried out as previously described (Tovey *et al.*, 2008). cDNA was synthesized in a final volume of 20 µl directly from a lysate prepared from confluent cells in one well of a 96-well plate, using a FastLane cell cDNA kit (QIAGEN, Crawley, UK). For QPCR, each reaction included primers specific for ATP6V0C and for calibration, primers for a housekeeping gene (glyceraldehyde phosphate dehydrogenase, GAPDH). Each reaction (20 µl) included Rotor-Gene SYBR Green PCR master mix (10 µl), cDNA (5 µl), Quantitect primer assay (2 µl) and RNAase-free water (3 µl). In two negative controls, the primers were omitted during QPCR, or the reverse transcriptase was omitted during cDNA synthesis. For QPCR (Rotor-Gene 6000; Corbett Life Sciences), an initial denaturation at 95°C for 5 min was followed by 40 cycles of amplification (93°C for 5 s, 60°C for 10 s) and then a melting curve (72°C to 95°C). Expression of mRNA relative to that for GAPDH was calculated from:

$$\text{Expression} = \frac{E^{-C_T^{ATP6VOC}}}{E^{-C_T^{GAPDH}}},$$

Where, E is the amplification efficiency, calculated as 10^m, where m is the average fluorescence increase for four cycles increase after the cycle threshold (C_T) for the indicated PCR product. Results are reported as mean ± SD for cDNA samples independently isolated from 6 different experiments.

2.8 Proximity ligation assay and analysis

A Duolink proximity ligation assay (PLA, Sigma) was used to quantify interactions between proteins less than ~40 nm apart, according to the manufacturer's instructions. The method uses antibodies from two species (mouse and rabbit) to recognize two candidate proteins *in situ* (Figure 2.1). The antibodies are then recognized by secondary antibodies conjugated to complementary oligonucleotides, which are amplified to incorporate a fluorescent nucleotide (Texas Red) only if the pair of secondary antibodies are less than ~40 nm apart (Fredriksson *et al.*, 2002; Koos *et al.*, 2013). Cells gown on fibronectin-coated 35-mm glass-bottom dishes were fixed at 20°C (4% paraformaldehyde, 30 min), washed with PBS, permeabilized (0.25% Triton X-100, 5 min), and incubated with primary antibodies (12-16 h, 4°C). Cells were washed 3 x 5 min in PBS with constant agitation, before addition of PLA probes. The Duolink® In Situ PLA probe anti-Rabbit PLUS and anti-Mouse MINUS (Sigma) were used. Equal volumes of both PLA probes were mixed in the antibody diluent provided in the kit (1:5 dilution, 12 µl PLUS, 12 µl MINUS and 36 µl diluent). Incubation with PLA probes (1 h,

37°C) was performed in a preheated humidity chamber to ensure that the cells do not dry out. Cells were washed for 2 x 5 min with wash buffer A, at 20°C with shaking and then incubated with ligase in a preheated humidity chamber (1:40 dilution in ligation buffer, 30 min, 37°C). Next, following 2 x 5 min wash with wash buffer A, amplification was performed by incubating cells with polymerase (1:80 dilution in amplification buffer, 30 min, 37°C) in the dark. Following this, cells were washed (2 x 10 min) in wash buffer B, and further 1-min wash in 0.01x wash buffer B. Cells were then mounted in Duolink II mounting medium containing DAPI to label the nucleus (Sigma) and imaged the next day. For imaging, cells were stored at 4°C overnight. For ER-lysosome interactions, the primary antibodies were against VAP-A (1:100) and Rab7 (1:100), and for EFGP-IP_3R1-lysosome interactions they were against GFP (1:500) and Rab7 (1:100). The specificity of the PLA reactions was confirmed by the omission of either primary antibody (VAP-A or Rab7) and, for EGFP-IP_3R1-lysosome measurements by using cells without EGFP-IP_3R1.

PLA products were visualized using an Olympus microscope with x100 objective, and spots were quantified using CellProfiler software (http://cellprofiler.org/). The pipeline for analysis (Figure 2.2) was constructed by me based on previously published methods (Carpenter *et al.*, 2006).

An overlay RGB image of the maximum projection of PLA dots and nucleus staining was exported into Cell profiler, and then split into individual channels. Primary objects (nucleus) were defined based on the differences between DAPI-stained nuclei and the background fluorescence. Next, secondary objects were defined by extending out from the nucleus up to 80 pixels using the Distance-N method. The total number of PLA dots in the field was then identified, and sorted into the different cell objects identified (secondary objects). Dots outside the cell mask drawn were rejected as outliers.

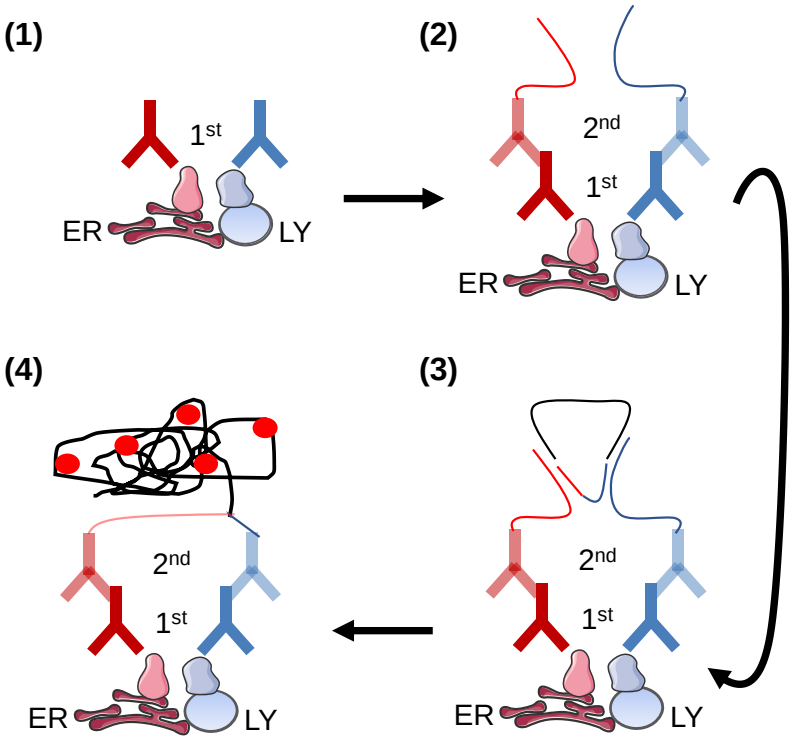

Figure 2.1 **In situ PLA to detect protein-protein interactions in fixed cells**. (1) Two proteins of interest are recognised by two specific primary antibodies (1st) raised in two different species (e.g. mouse and rabbit). (2) Two oligonucleotide-conjugated secondary antibodies (2nd) recognising either mouse or rabbit antibodies are then added. (3) If the target proteins are in close proximity (~40 nm), the PLA probes hybridizes to connector oligonucleotides and ligated to form a circular DNA. (4) The circular DNA is then a template for rolling circle amplification (RCA) catalysed by a polymerase. During amplification, the RCA products incorporate a fluorescent tag (Texas red). The resulting red dots are detected by fluorescence microscopy.

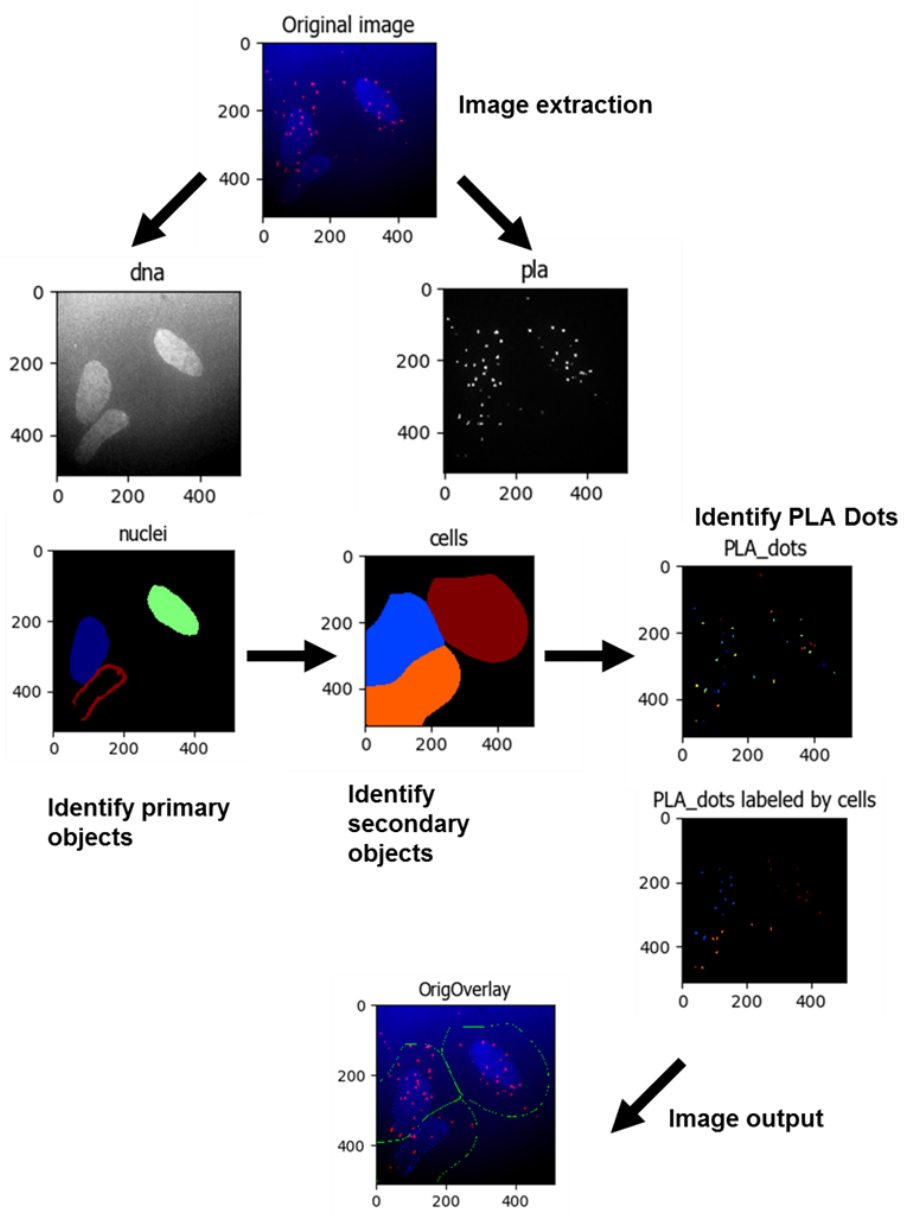

Figure 2.2 **Schematic representation of the PLA analysis conducted with Cell Profiler**. Nucleus stained with DAPI was defined as a primary object. Secondary objects were identified by making extensions from the centroid of the nucleus. Finally, PLA dots within each cell was counted and assigned to the parental cell.

2.9 Generation of a cathepsin C KO HEK cell line

CRISPR/Cas9 was used to disrupt the gene encoding cathepsin C (CTSC). Guide sequences were chosen based on two web-based tools, E-crispr.org (Heigwer *et al.*, 2014) and zitfit.partners.org (Sander *et al.*, 2010). Oligonucleotides encoding four different guide RNAs (sgRNA) were used to target the first, second and third exons of CTSC (Exon 1: GCTGGGCACCTGGGTCTTCC; Exon 1: GCCCTCCTGCTGCTTCTCTC; Exon 2: GATACAGCATATGATGACCT; Exon 3: GTTGACATACACATTCTCAG). Each guide and its complementary sequence had a sticky end (5´-CACC or 5´-AAAC) to allow ligation into the Px458 vector, which also encodes Cas9 nuclease and GFP (Addgene #48138) (Ran et al., 2013). Vectors were digested with BbsI, which cuts after the hU6 promotor in the px458 vector and analysed by agarose gel electrophoresis. Following gel extraction, the product at this point was a digested vector with sticky ends. Guide RNA oligos were made double-stranded by PCR. Samples were first incubated for 30 min at 37°C to anneal the oligos, then for 5 min at 95°C, then ramped down to 25 °C at 5°C/min. Then, the annealed guide RNAs oligos were ligated into the digested px458 vector using T4 DNA ligase (ThermoScientific) according to the manufacturer's protocol. The coding sequence of the final plasmid was verified by sequencing using the Hu6 primer, which binds to the promoter in front of the insert. The coding sequences of the four final plasmids were verified. HEK cells were transfected with pX458-sgRNAs using Trans LT1 (4 µg DNA per 6-well plate). After 48 h, EGFP-expressing cells were sorted as single cells into 96-well plates by fluorescence-activated cell sorting (FACS). After 8 weeks, clones were screened by Western blotting and validated using a functional assay. CRISPR/Cas9 experiments were done by Laura van Marrewijk.

2.10 Generation of HEK cells deficient in TMCO1

The methods used to generate cells deficient in Transmembrane and Coiled-Coil Domains 1 (TMCO1) were the same as those used to generate HEK-CTSC-KO cells. The only effective sgRNA (GAAGCGGAAGTGCGATCTTC) targeted exon 1. Neither different sgRNAs, targeting exon 1 (GTGCACGGCTCTGCTCGCAG) or exon 3 (GAAACAATAACAGAGTCAGC and GTTTACAGTGGAAAAGAAGA), nor repeated transfections with multiple sgRNAs succeeded in achieving cells with both TMCO1 alleles disrupted. CRISPR/Cas9 experiments were done by Laura van Marrewijk.

2.11 Protein isolation

Whole cell lysates for Western blotting and cathepsin C activity assay were obtained as follows. Cells in 6-well plates were washed twice with 1.5 ml PBS. 30 µl of pre-chilled Radio Immuno Precipitation Assay (RIPA) buffer was added to each well of the 6-well plate. The RIPA buffer composition was 150 mM NaCl, 1% Triton X-100, 0.5% sodium deoxycholate, 0.1% SDS and 50 mM Tris at pH 8.0. Cells from each well were scraped into a pre-chilled Eppendorf tube. The samples were syringed 5 times using a blunt needle. The samples were sonicated for 3 × 10 s on iced water. The samples were maintained at 4 °C for 1 h with constant agitation. Supernatants were obtained after centrifugation (~14,000 ×g, 15 min, 4°C).

2.12 Western blotting

The protein-loading sample was made up to 20 µl (13 µl lysate supernatant, 5 µl LDS (lithium dodecyl sulphate) sample buffer 4x, and 2 µl of 1M DTT (dithiothreitol). The sample was heated for 10 min at 85°C and loaded onto a 3-8% Tris-acetate PAGE gel. Electrophoresis was achieved by applying 160 V for 1 h in Tris-acetate SDS running buffer. Following electrophoresis, separated proteins on the SDS-PAGE gel were transferred onto a polyvinyl difluoride (PVDF) membrane using the iBLOT gel transfer system. Membrane blocking was carried out in Tris-buffered saline (TBS) supplemented with 0.1% Tween-20 (TBST) and 5% BSA (bovine serum albumin) for 1 h with gentle shaking at 22°C. TBS was composed of 50 mM Tris-HCl, 150 mM NaCl, adjusted to pH 7.5 using HCl. The membrane was washed with TBST and incubated with the primary antibody at 40°C for 16 h with gentle shaking. Following this, the membrane was washed 3 times (5 min each) with 15 ml TBST at 22°C. The membrane was then incubated with secondary antibody solution (1:5000 dilution of IgG-HRP) in TBST with 1% BSA for 1 h at 22°C with gentle shaking. Following this, the membrane was washed 3 times (5 min each) with 15 ml TBST. Enhanced chemiluminescence (ECL) primer Western blotting detection reagent (Amersham, UK) and a Syngene PXi chemiluminescence detection system were used to detect HRP. The antibodies used were mouse anti-cathepsin C (Santa Cruz Inc.,1:500), rabbit anti-TMCO1 (Sigma, 1:1000), mouse anti β-actin (Cell Signaling, 1:1000), donkey anti-mouse IgG-HRP (1:2000) and donkey anti-rabbit IgG-HRP (1:5000).

2.13 Measurement of cathepsin C activity

Cathepsin C activity was measured according to a protocol modified from previously described methods (Hamilton *et al.*, 2008; Eick *et al.*, 2014). Whole cell lysates were extracted from HEK WT and HEK-CTSC-KO cells as described (**Section 2.11**). HEK cell lysates were diluted in assay buffer (25 mM MES, 50 mM NaCl, 5 mM DTT, pH 6) to provide a protein concentration of 200 μg/ml, and distributed into 96-well plates (50 μl/well). Cleavage of Gly-Arg-AMC (50 μM) was monitored at 0.2-min intervals (excitation, 380 nm; emission 460 nm) using a FlexStation 3 plate-reader and SoftMax Pro software. A substrate blank was included as a control.

2.14 Fluorescence microscopy

Fluorescence microscopy used an inverted Olympus IX83 microscope equipped with a 100x objective (numerical aperture, NA, 1.49), a multi-line laser bank (395, 405, 425, 488, 561 and 647 nm) and an iLas^2 targeted laser illumination system (Cairn, Faversham, UK). Excitation light was transmitted through either a quad dichroic beam-splitter (TRF89902-QUAD) or a dichroic mirror (for 425 nm; ZT442rdc-UF2, Chroma, Germany). Emitted light was passed through appropriate filters (Cairn Optospin; peak/bandwidth: 480/40 nm, 525/50 nm, 630/75 nm and 700/75 nm) and detected with either an iXon Ultra 897 electron multiplied charge-coupled device (EMCCD) camera (512×512 pixels, Andor, Belfast, Northern Ireland). For all multi-colour imaging, I confirmed that there was no bleedthrough between channels. For TIRFM, the penetration depth was 90-140 nm. The iLas^2 illumination system was used for TIRFM and wide-field imaging. Bright-field images were acquired using a Cairn MonoLED illuminator.

All fluorescence images were corrected for background by subtraction of fluorescence from a region outside the cell. Image capture and processing were done using MetaMorph Microscopy Automation and Image Analysis Software (Molecular Devices).

2.15 Measurement of near-lysosome Ca^{2+} signals

HeLa cells transfected with Ly-GG were washed three times in HBS, and Ly-GG fluorescence (excitation at 488 nm, emission at 525 nm) was imaged using wide-field fluorescence microscopy (50 frames/min) at 20ºC. After background correction, the Ly-GG fluorescence associated with single lysosomes was measured using single-particle tracking with the MetaMorph Track Objects plugin (Meijering *et al.*, 2012). A template-match algorithm was used to connect tracks between successive frames. Tracks that terminated before completion of the recording (240 s for cells stimulated with histamine; 1330 s for analyses of SOCE) were excluded from the analysis. In parallel analyses of HeLa cells expressing Cy-GG, ROIs similar in dimensions to tracked lysosomes (radius ~1.6 µm) were manually selected for analysis.

2.16 Flash photolysis of caged IP_3

HeLa cells grown on fibronectin-coated glass-bottomed dishes were first transfected with Ly-GG or Cy-GG, then loaded with ci-IP_3/PM (1 µM, 50 min) (Dakin & Li, 2007). After washing and incubation in HBS for a further 45 min, cells were imaged (20°C) using an inverted Olympus IX83 microscope equipped with a 100x objective. Ly-GG fluorescence was recorded in wide-field (488 nm excitation, 525/50 nm emission). Cells were imaged for 50 s before photolysis of ci-IP_3 using a SPECTRA X-light engine (Lumencor, 395/20 excitation, exposure time 50 ms/frame for 10 frames). Images were acquired at 50-ms intervals with an iXon Ultra 897 EMCCD camera. Images were collected, corrected for background fluorescence and analyzed using MetaMorph. Ly-GG was tracked to determine Ca^{2+} signals around single lysosomes. It is worth noting that photolysis of ci-IP_3 releases an active, but more metabolically stable, analogue of IP_3 (i-IP_3, in which the 2- and 3-hydroxyls are linked by an isopropylidene group) (Dakin & Li, 2007).

2.17 Loading lysosomes with luminal fluorescent indicators

To load lysosomes by endocytosis with fluorescent dyes, cells grown on poly-L-lysine-coated, glass-bottomed 35-mm dishes were incubated (16 h, 37°C) in culture medium supplemented with either a dextran-conjugated indicator (0.1 mg/ml) or Lucifer Yellow (0.2 mg/ml). After a further 4-6 h in the same medium without indicator, to chase along the

indicator along the endocytic pathway into lysosomes, cells were used for experiments (Figure 2.3).

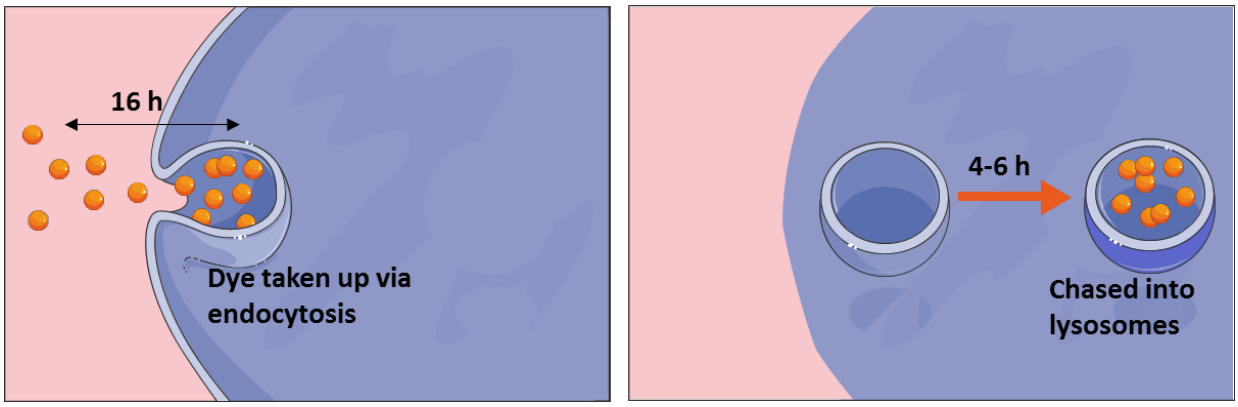

Figure 2.3 **Chasing indicators into the lysosomal lumen by endocytosis.** Dextran in the extracellular medium is taken up into endosomes via endocytosis and then chased into lysosomes by incubating cells in a medium without the dextran.

For labelling with LysoTracker Red, cells were incubated in HBS with LysoTracker Red DND-99 (100 nM, 20°C). After 20 min, cells were washed three-times with HBS and used immediately. Oregon Green-Dx and fluorescein-Dx were excited at 488 nm and emitted fluorescence was captured using a 525/50 nm filter (peak/bandwidth). LysoTracker Red was excited at 561 nm and emitted fluorescence was captured using a 630/75 nm filter (peak/bandwidth).

2.18 Measurement of pH_{ly}

Cells were incubated with the ratiometric pH indicator, fluorescein-Dx (10-kDa, 0.2 mg/ml), for 16 h followed by a 4-h chase in DMEM F12 at 37ºC. The cells were then washed 3 times with HBS and imaged immediately with alternating excitation/emission (F_{425}: λ_{ex} = 425 nm, λ_{em} = 480 nm. F_{488}: λ_{ex} = 488 nm, λ_{em} = 525 nm). Images were collected for 100 ms, with 5-min between each round of data acquisition. After background subtraction, regions of interest (ROIs) were drawn around lysosome clusters and fluorescence ratios (R, which increases with increased pH) were calculated from F_{488}/F_{425} at each time point. Results are presented as R/R_0, where R_0 is the fluorescence ratio recorded before stimulation.

For experiments where LysoTracker Red was used qualitatively to report the timeframe of pH_{ly} changes following addition of concanamycin A (Figure 3.20), cells were loaded with 50 nM LysoTracker Red DND-99 for 1 h, washed 3 times with HBS, and imaged immediately.

2.19 Measurement of lysosomal size

Lysosome size was measured in HEK cells expressing LAMP1-mCherry. After application of a threshold (ImageJ Threshold), particles were accepted for analysis if they had a circulatory value ($4.\pi.\text{area/circumference}^2$) of 0.6-1.0. The circularity criterion ensured that only roughly circular particles were selected for analysis (Lai *et al.*, 1988). Visual inspection of images before and after application of the selection criteria confirmed that most lysosomes were included in the final analysis. The Feret diameter is used to report lysosome size, which is the maximum distance between two points on the perimeter of the particle (ImageJ Analyze Particles).

2.20 Other image analysis

Time-lapse recordings of cells loaded with Dx-conjugated indicators were analysed by taking randomly selected ROI large enough for each to include several lysosomes (ROI, 3.2 μm x 3.2 μm). Fluorescence changes were then expressed as F/F_0, where F_0 and F denote the average fluorescence within the ROI at the start of the experiment (F_0) and at each subsequent time point (F).

To analyse the number of lysosomes in cells before and after GPN treatment, the Fiji TrackMate plugin (Tinevez *et al*., 2017) was used to identify lysosomes as spots in background-corrected wide-field images.

For colocalisation analysis, R_{coloc} was calculated from all pixels within the ROI that exceeded a threshold value (ImageJ Colocalisation Analysis/Colocalisation Threshold):

$$R_{coloc} = \frac{\sum(Ri - Rm)(Gi - Gm)}{\sqrt{\Sigma(Ri - Rm)^2 \Sigma(Gi - Gm)^2}}$$

where, Gi and Ri are the intensities of individual green and red pixels respectively, and Gm and Rm are the mean intensities of green and red pixels. After quantifying colocalization of fluorophores using Pearson's correlation coefficient (R_{coloc}), Costes randomization method

with 100 iterations (Costes *et al.*, 2004), was used to confirm that any colocalization was more than expected from randomly distributed fluorophores (ImageJ Colocalisation Analysis/Colocalisation Test).

2.21 Statistical analysis

All analyses were done using GraphPad Prism (version 5, La Jolla, CA, USA). For each experiment, concentration-effect relationships were fitted using non-linear curve-fitting to a Hill equation. From each experiment, pEC_{50} and the maximal response were obtained and used in statistical analyses. A Student's *t*-test (2 variables) one-way or two-way ANOVA (more than 2 variables) was used for statistical analyses. Dunnett's, Tukey's multiple comparison tests and Bonferroni post hoc tests were conducted where stated. A *P*-value < 0.05 was considered significant.

3. IP_3R selectively deliver Ca^{2+} to lysosomes at ER-Lysosomes contact sites

3.1 Introduction

There is some evidence that the ER is required for lysosomes to fill with Ca^{2+}, but the intricate details are unclear. Previous work from this laboratory suggested that Ca^{2+} released from the ER is selectively accumulated by lysosomes. That conclusion derives substantially from the evidence that bafilomycin A_1 selectively increased the amplitude of the cytosolic Ca^{2+} signals evoked by IP_3R. For example, muscarinic M3 receptors in HEK cells, activated by carbachol (CCh) that stimulate the formation of IP_3 (Lopez-Sanjurjo *et al.*, 2013). This potentiation is not due to NAADP, because inhibition of NAADP-mediated Ca^{2+} release by NED-19 affected neither the CCh-induced alkalinisation of lysosomes (assumed to reflect the increased activity of a Ca^{2+}-H^+ exchange mechanism) nor the amplitude of the cytosolic Ca^{2+} signals evoked by CCh (Lopez-Sanjurjo *et al.*, 2013). These results suggest that lysosomes continuously sequester Ca^{2+} released via IP_3Rs. Disruption of lysosomes unmasks this sequestration of Ca^{2+} and leads to greater increases in $[Ca^{2+}]_c$ after stimulation with CCh. This evidence agrees with others in the field suggesting that the pH_{ly} is important for lysosomal Ca^{2+} uptake (**Section 1.2.3**). However, CAX genes have been found in protostomes, deuterostomes, amphibians, reptiles and birds, but not in placental mammals (Melchionda *et al.*, 2016). Furthermore, it has been reported that inhibition of the V-ATPase does not affect the acute refilling of lysosomes in mammalian cells (Garrity *et al.*, 2016). Together, these results suggest that the almost universally accepted view that lysosomal Ca^{2+} uptake requires an H^+ gradient requires closer examination.

The primary effect of the V-ATPase on the lysosomal membrane is to maintain the characteristic low pH of lysosomes (Figure 3.1A). However, there are also secondary effects arising from changes in pH_{ly}, as low pH_{ly} is important in maintaining ionic balance, cargo sorting and maintenance of proper functioning of lysosomal hydrolytic enzymes. For example, a chronic increase in pH_{ly} affects the expression of key lysosomal proteins such as lysosomal/autophagy master transcription factor TFEB and of the V-ATPase itself (Guha *et al.*, 2014). Knockdown of V-ATPase induces accumulation of non-functional lysosomes abrogating autophagic pathway (Mauvezin *et al.*, 2015). Furthermore, yeast vacuoles expressing mutant V-ATPase are enlarged because the balance between fusion and fission is disrupted (Baars *et al.*, 2007; Peri & Nusslein-Volhard, 2008). Acute increases in pH_{ly}

following treatment with methylamine (MA) or bafilomycin A_1 promote lysosomal fusion in a calmodulin-dependent manner (Cao *et al.*, 2015). Furthermore, inhibition of V-ATPase with concanamycin A or bafilomycin A_1 decreases the total lysosome volume in HEK cells (Figure 3.1B) (Abu-Remaileh *et al.*, 2017). Other means of increasing pH_{ly} in single cells such as following heterologous expression of Arl8b promotes a distinct redistribution of lysosomes to peripheral regions (Johnson *et al.*, 2016).

Treatment with pharmacological agents known to increase pH_{ly}, such as chloroquine, has been repeatedly reported to induce clinical manifestations of retinopathy (Bernstein & Ginsberg, 1964; Araiza-Casillas *et al.*, 2004). This has been linked to the effect of chloroquine on lysosomes in a number of ways. Firstly, in whole-animal models, chronic increase in pH_{ly} following treatment with chloroquine show an increase in retinopathy, characterised by increased enzyme accumulation in lysosomes (Bernstein & Ginsberg, 1964; Meier-Ruge, 1965; Guha *et al.*, 2014). Notably, chronic alkalinisation of lysosomes results in impaired degradation of outer segments in retinal pigment epithelial (RPE) cells isolated from patients, and this was rescued by reacidification of lysosomes (Liu *et al.*, 2008; Guha *et al.*, 2012). Hence, increasing the pH of lysosomes can have a plethora of secondary effects that remain unexplored in relation to lysosomal Ca^{2+} homeostasis.

Lysosome enlargement can also be induced by small molecules such as brefeldin A (Wood & Brown, 1992) and chloroquine (Yoon *et al.*, 2010). But, these are not selective to lysosomes (Lippincott-Schwartz *et al.*, 1991) and they perturb Ca^{2+} signalling (Dickinson *et al.*, 2010). Vacuolin, a triazine-based molecule, reversibly enlarges lysosomes (Cerny *et al.*, 2004; Huynh & Andrews, 2005; Durchfort *et al.*, 2012), but the mechanisms are not well characterised. However, vacuolin is routinely used to provide fused organelles large enough to patch-clamp (Dong *et al.*, 2010; Schieder *et al.*, 2010a; Wang *et al.*, 2012; Cang *et al.*, 2013). Enlargement of lysosomes with vacuolin increased the amplitude of the cytosolic Ca^{2+} signals evoked by IP_3R in HEK cells (Lopez-Sanjurjo *et al.*, 2013). This provides evidence that altering lysosomal size and morphology can disrupt lysosomal Ca^{2+} homeostasis.

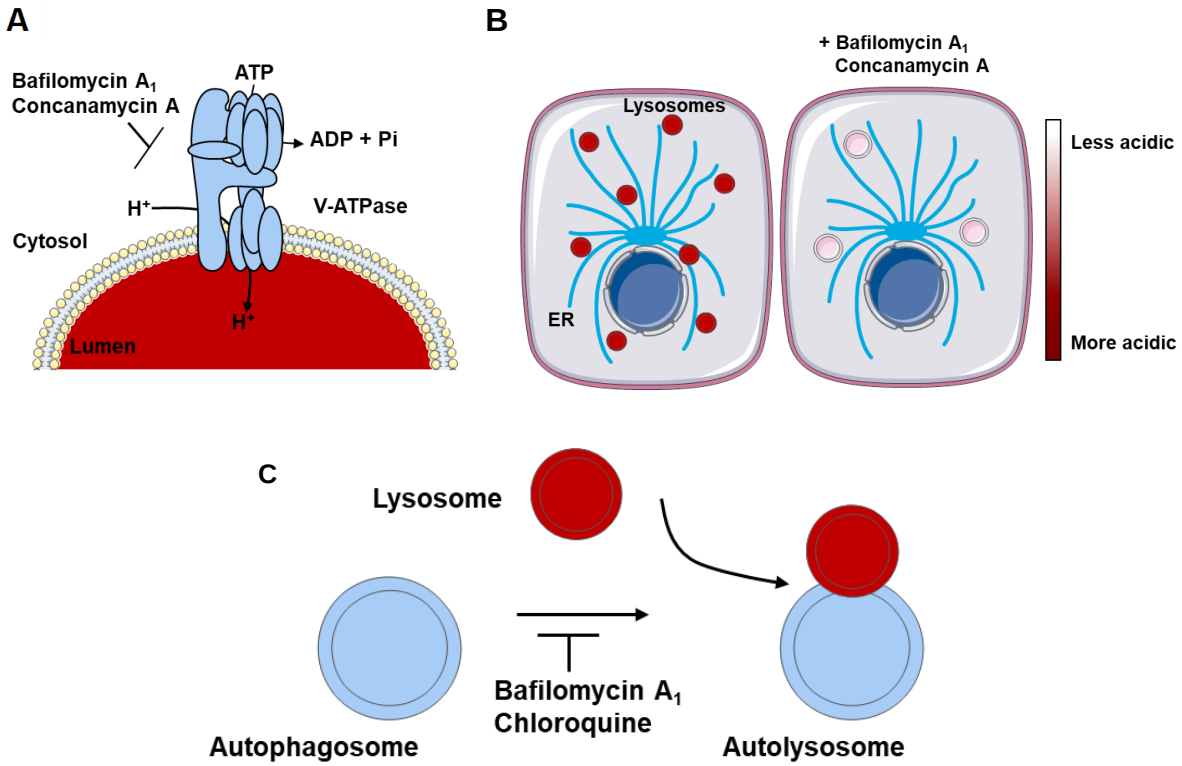

Figure 3.1 **Inhibition of the V-ATPase affects the distribution and functions of lysosomes.** (A) Bafilomycin A_1 and concanamycin A inhibit the V-ATPase, blocking the pumping of H^+ into the lysosomal lumen. This leads to an increase in pH_{ly}. (B) Inhibition of the V-ATPase causes lysosomes to redistribute and increase in size (Cao *et al.*, 2015), and there is an overall decrease in total cellular lysosomal volume (Abu-Remaileh *et al.*, 2017). (C) During autophagy, autophagosomes fuse with lysosomes to allow transfer of materials destined for degradation by autolysosomes. Lysosome alkalinising agents such as bafilomycin A_1 and chloroquine, inhibit this fusion, thereby inhibiting autophagy (Redmann *et al.*, 2017).

Pharmacological inhibition of IP_3R has been shown to inhibit the refilling of lysosomes with Ca^{2+} (Garrity *et al.*, 2016). Ca^{2+} refilling of lysosomes was completely blocked by Xestospongin C, used to inhibit IP_3R, but unaffected in DT40 cells lacking IP_3R. However, Xestospongin C has been shown to have off-target effects such as emptying the ER (Solovyova *et al.*, 2002) and it does not universally inhibit IP_3Rs (Saleem *et al.*, 2013). There is a poorly defined relationship between pH_{ly}, lysosomal morphology and the impact of these on the exchange of Ca^{2+} between ER and lysosomes. These relationship are explored in this chapter.

3.2 Materials and Methods

All materials and methods have been described in chapter 2.

3.3 Results and Discussion

3.3.1 Dissipating the lysosomal H^+ gradient potentiates Ca^{2+} signals evoked by IP_3R

Stimulation of endogenous muscarinic receptors (M3R) in HEK cells by cholinomimetics such as CCh results in the activation of PLC and formation of IP_3 (**Section 1.1.1**). This has been previously shown to result in a biphasic Ca^{2+} signal (Tovey *et al.*, 2008), comprising an initial Ca^{2+} transient due to Ca^{2+} release from intracellular stores mediated by IP_3R (Tovey *et al.*, 2008; Lopez-Sanjurjo *et al.*, 2013) and a more sustained increase in $[Ca^{2+}]_c$ resulting from SOCE. Experiments described here were carried out in Ca^{2+}-free HBS to allow the effects of CCh on Ca^{2+} release from intracellular stores to be specifically addressed. This was achieved by addition of the Ca^{2+}-chelating agent BAPTA 30 s prior to stimulation with CCh. The results, which are consistent with previous observations (Lopez-Sanjurjo *et al.*, 2013), show that CCh causes a concentration-dependent increase in $[Ca^{2+}]_c$, reflecting the IP_3-mediated release of Ca^{2+} from intracellular stores ($pEC_{50} = 4.8 \pm 0.2$, $n = 6$, where pEC_{50} is the negative logarithm of the molar concentration of CCh required to cause a half-maximal response) (Figure 3.2).

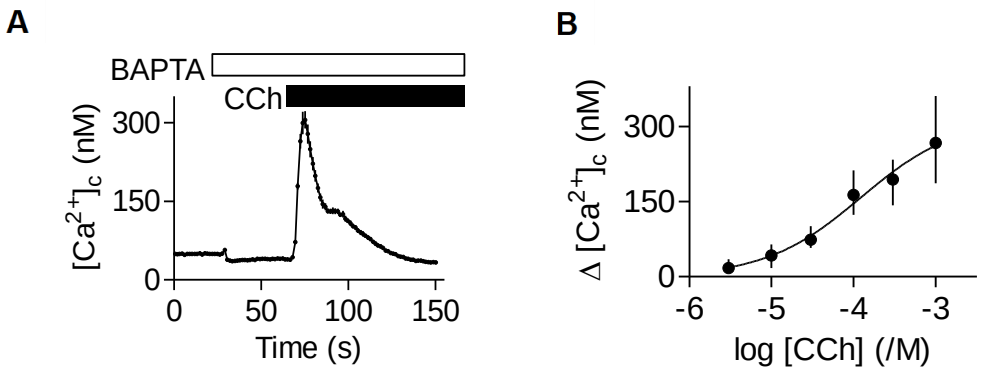

Figure 3.2 **CCh stimulates Ca^{2+} release from intracellular stores in HEK cells** (A) Typical increases in $[Ca^{2+}]_c$ obtained from populations of HEK cells stimulated with a maximal concentration of CCh (1 mM) in Ca^{2+}-free HBS. Results are means ± SD for 3 wells from a single experiment. (B) Concentration-dependent effects of CCh on peak Ca^{2+} signals ($\Delta[Ca^{2+}]_c$) recorded from populations of HEK cells in Ca^{2+}-free HBS. Results are means ± SEM from 6 experiments, each with 3 replicates.

The CCh-induced increase in $[Ca^{2+}]_c$ in HEK cells is selectively mediated by IP_3R as it is abolished by inhibition of PLC, but unaffected by inhibition of RyR or TPC2 (Lopez Sanjurjo *et al.*, 2013). Therefore, CCh mobilises Ca^{2+} selectively from intracellular stores via IP_3R.

LysoTracker is a lipophilic amine conjugated to the probe Red DND-99 (Duvvuri *et al.*, 2004). Therefore, it accumulates in the most acidic parts of the cell. LysoTracker Red colocalises with LAMP1 in HEK cells (R_{coloc} of 0.80 ± 0.1, n = 4) (Figure 3.3), therefore it efficiently labels lysosomes in these cells. R_{coloc} is the Pearson's correlation coefficient; 1 denotes perfect colocalization. To allow dissipation of the lysosomal H^+ gradient, HEK cells were treated with bafilomycin A_1 or concanamycin A, which inhibit the V-ATPase. Treatment with concanamycin A, a more selective inhibitor of the V-ATPase than bafilomycin A_1 (Drose & Altendorf, 1997; Huss & Helmut, 2009), results in loss of LysoTracker accumulation in HEK cells (Figure 3.4A). Similar results were obtained following treatment with bafilomycin A_1 (Figure 3.4B).

Treatment of HEK cells with concanamycin A (1 μM, 1 h), under conditions that dissipate the lysosome H^+ gradient, caused a significant increase in the basal $[Ca^{2+}]_c$ (Figure 3.5B, C). Furthermore, the peak increase in $[Ca^{2+}]_c$ evoked by CCh, which stimulates IP_3 formation via

endogenous M_3 muscarinic receptors in HEK cells, was significantly increased by concanamycin A (Figure 3.5B, D).

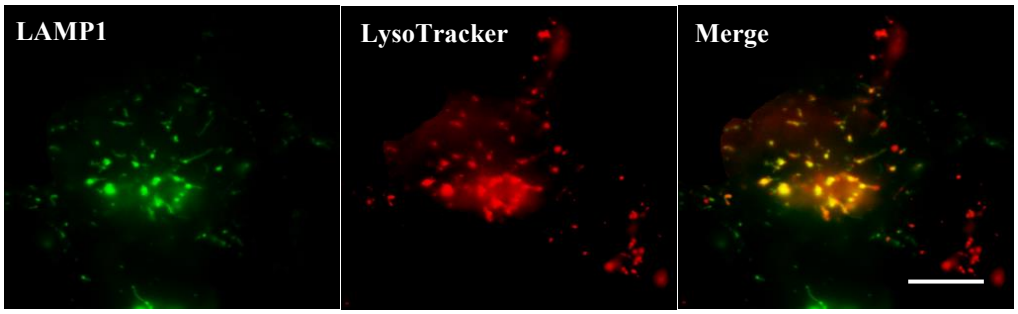

Figure 3.3 **LysoTracker colocalises with LAMP1 in HEK cells.** Wide-field images of HEK cells transiently transfected with LAMP1-GFP and loaded with LysoTracker Red (100 nM, 10 min). Scale bar is 10 µm. Image is typical of 4 independent dishes.

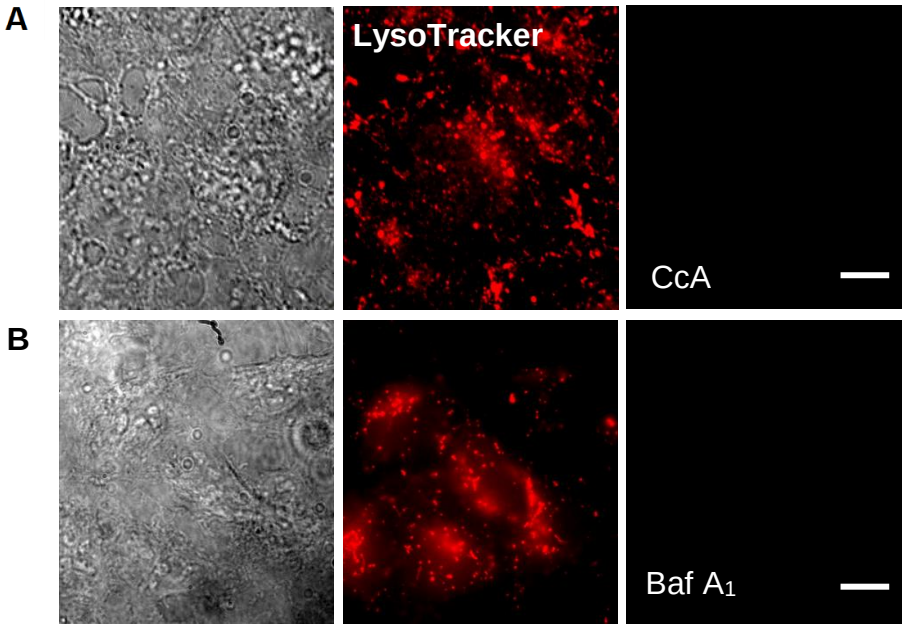

Figure 3.4 **Bafilomycin A_1 and concanamycin A abolish LysoTracker accumulation in lysosomes.** Brightfield (left) and wide-field images of HEK cells loaded with LysoTracker Red (100 nM, 10 min) with or without concanamycin A (CcA, 1 µM, 1 h) (A) or bafilomycin A_1 (Baf A_1, 1 µM, 1 h) (B). The images are typical of 3 independent experiments.

Similar results were obtained following treatment of HEK cells with bafilomycin A_1, which caused a significant increase in basal $[Ca^{2+}]_c$ (Figure 3.6A). Furthermore, bafilomycin A_1 significantly potentiated the CCh-evoked increase in $[Ca^{2+}]_c$ (Figure 3.6A, C).

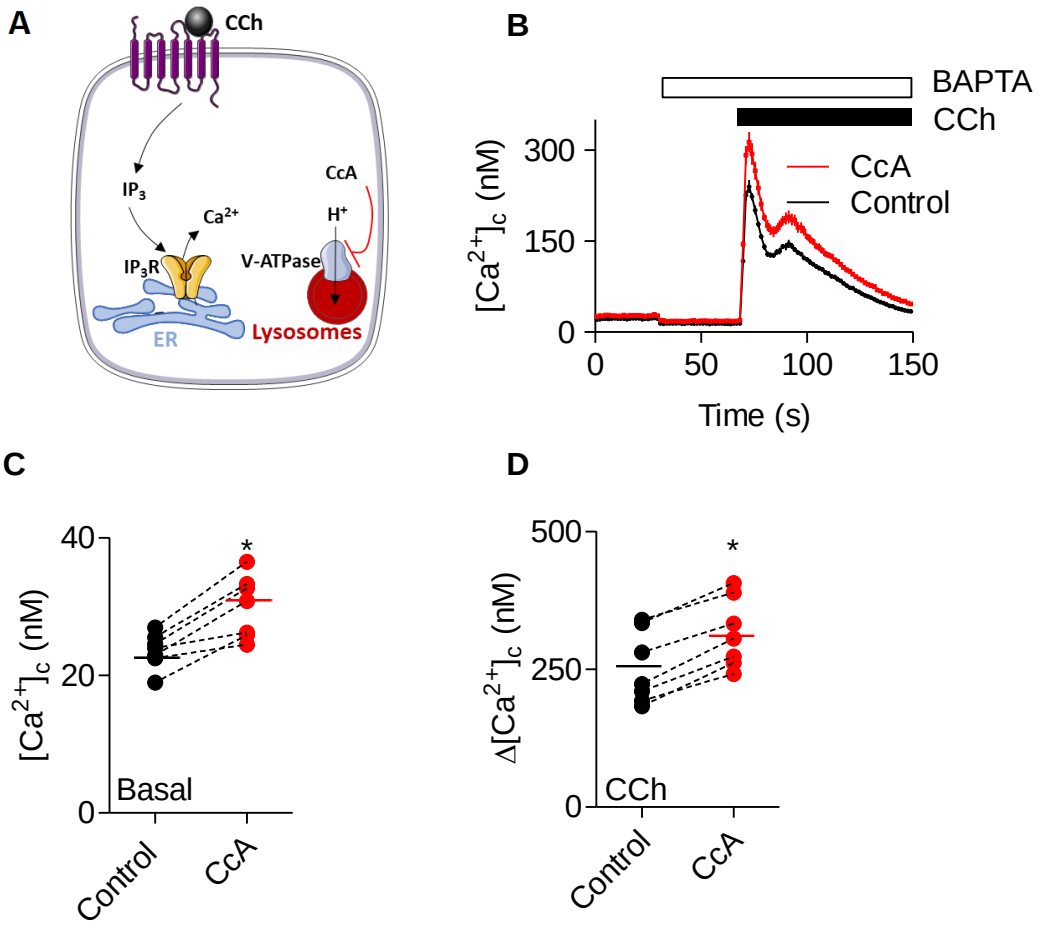

Figure 3.5 **Inhibition of lysosomal acidification potentiates CCh-evoked Ca^{2+} signals in HEK cells.** (A) Bafilomycin A_1 and concanamycin A inhibit the lysosomal V-ATPase and so prevent H^+ accumulation by lysosomes. (B) Fluo-8-loaded HEK cells were treated with concanamycin A (CcA, 1 μM, 1 h) in HBS before addition of BAPTA (2.5 mM) to chelate extracellular Ca^{2+} and then CCh (1 mM) to stimulate IP_3 formation. Typical results show means ± SD from 3 wells in a single experiment. (C, D) Summary results show effects of CcA on basal $[Ca^{2+}]_c$ (C) and peak increase in $[Ca^{2+}]_c$ ($\Delta[Ca^{2+}]_c$) evoked by CCh (D). Results show paired individual values (each from 3 determinations) and the mean (n = 7, line). $^*P <$ 0.05, paired Student's t-test.

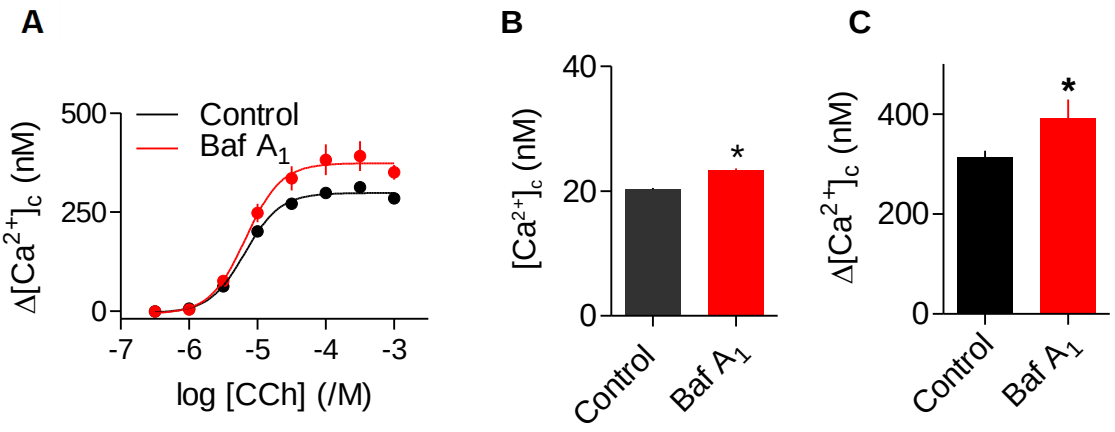

Figure 3.6 **Inhibition of lysosomal acidification potentiates CCh-evoked Ca^{2+} signals in HEK cells.** (A) Concentration-dependent effects of CCh on peak Ca^{2+} signals ($\Delta[Ca^{2+}]_c$) with and without pre-incubation with bafilomycin A_1 (Baf A_1, 1 µM, 1 h). Results are means ± SEM from 5 independent experiments. (B) Basal $[Ca^{2+}]_c$ in HEK cells treated with Baf A_1. $^*P < 0.05$, Student's *t*-test. (C) Peak increases in $[Ca^{2+}]_c$ ($\Delta[Ca^{2+}]_c$) evoked by CCh alone or after incubation with Baf A_1. Results are means ± SEM, $n = 5$, with triplicate determinations in each. $^*P < 0.05$, Student's *t*-test.

Similar results were obtained in HeLa cells, where treatment with bafilomycin A_1 resulted in an increase in basal $[Ca^{2+}]_c$ from 65 ± 6 nM to 73 ± 7 nM ($P < 0.05$, paired Student's *t*-test, $n = 5$). The IP_3R-mediated increase in $[Ca^{2+}]_c$ following stimulation with a maximal concentration of histamine was also potentiated by bafilomycin A_1 (Figure 3.7A, B).

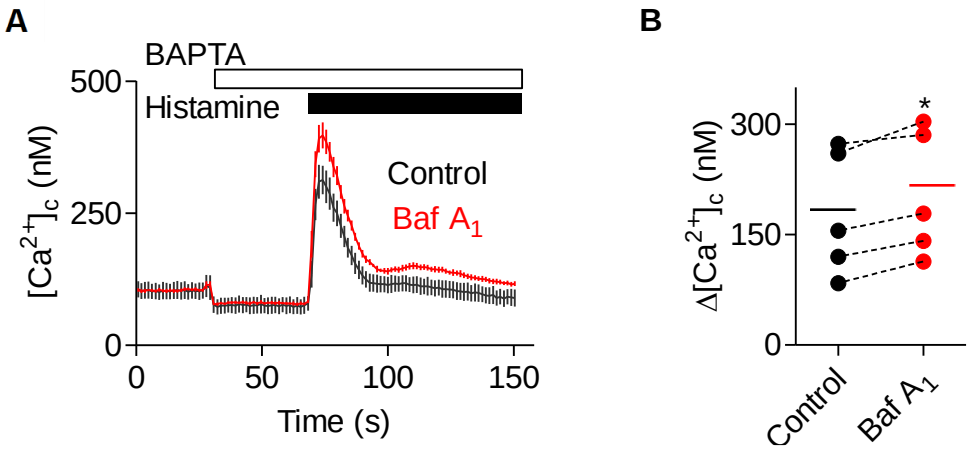

Figure 3.7 **Inhibition of lysosomal acidification potentiates histamine-evoked Ca^{2+} signals in HeLa cells.** (A) Fluo-8-loaded HeLa cells were treated with Baf A_1 (1 μM, 1 h) in HBS before addition of BAPTA (2.5 mM) to chelate extracellular Ca^{2+}, and then histamine (100 μM) to stimulate IP_3 formation. Typical results show means ± SD from 3 wells in a single experiment. (B) Summary results show $\Delta[Ca^{2+}]_c$ as paired comparisons of peak histamine responses (each with 3 replicates) and the mean value (n = 5, line). $^*P < 0.05$, paired Student's t-test.

A small interfering RNA (siRNA) to an essential pore-forming subunit of the V-ATPase (ATP6V0C) (Figure 3.8A) (Forgac, 2007) reduced expression of its mRNA by 55 ± 4% (n = 6) (Figure 3.8B). There are no reliable antibodies to determine expression of the ATP6V0C protein (Mangieri *et al.*, 2014). Following knockdown of ATP6V0C, the accumulation of LysoTracker Red in lysosomes was attenuated, indicating an increase in pH_{ly} (Figure 3.8C). This agrees with a previous report that siRNA to ATP6V0C is sufficient to dissipate the pH_{ly} gradient (Mangieri *et al.*, 2014).

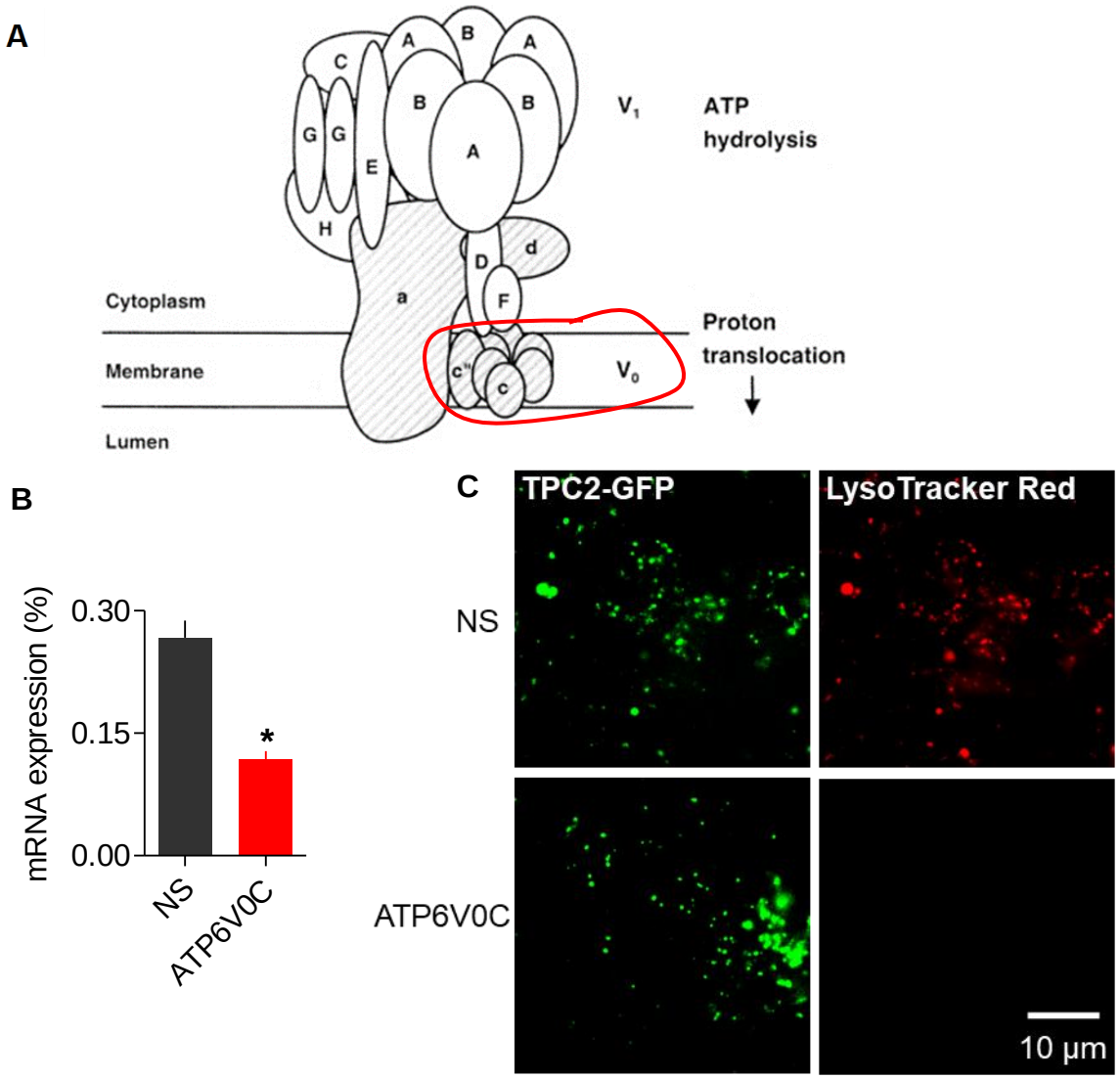

Figure 3.8 **Knockdown of ATP6V0C dissipates the lysosomal H^+ gradient** (A) ATP6V0C (circled in red) is a key subunit of the V-ATPase involved in the translocation of H^+ into the lysosomal lumen to drive lysosomal acidification. Image is modified from Smith *et al* (2003). (B) Expression of mRNA for ATP6V0C relative to that for GAPDH in cells treated with non-silencing siRNA (NS) or siRNA for ATP6V0C. Results are means ± SEM from 6 experiments. $^*P < 0.05$, paired Student's *t*-test. (C) TIRFM images show the effects of the indicated siRNAs in HEK cells expressing TPC2-GFP or stained with LysoTracker Red (100 nM, 10 min). Scale bar applies to all images. Images are typical of 3 independent experiments.

Unlike bafilomycin A_1 and concanamycin A, siRNA to ATP6V0C did not significantly affect the basal $[Ca^{2+}]_c$, but the siRNA significantly increased the amplitude of the CCh-evoked Ca^{2+} signals to the same extent as concanamycin A (Figure 3.9). The different effect of siRNA and pharmacological inhibition of the V-ATPase on basal $[Ca^{2+}]_c$ might arise from an adaptive response to the more prolonged siRNA treatment. Furthermore, there was no further effect of concanamycin A on the CCh-evoked increase in $[Ca^{2+}]_c$ after knockdown of the V-ATPase (Figure 3.9B). These results confirm that the effects of concanamycin A on CCh-evoked Ca^{2+} signals are mediated by inhibition of the V-ATPase. The results are important because bafilomycin A_1 and concanamycin A have additional effects, which at higher concentrations include inhibition of the P-ATPases that transport Ca^{2+} across the PM and ER membranes.

Inhibition of V-ATPase does not affect the production of IP_3 nor the sensitivity of the IP_3R to IP_3 (Lopez Sanjurjo *et al.*, 2013). Furthermore, the Ca^{2+} content of the ER is unaffected by pre-treatment with bafilomycin A_1 (Lopez Sanjurjo *et al.*, 2013). Hence, inhibition of V-ATPase potentiates the IP_3R-mediated increase in $[Ca^{2+}]_c$, not by increasing Ca^{2+} released from the ER, but by unmasking the ability of lysosomes to sequester Ca^{2+} released from the ER via IP_3R.

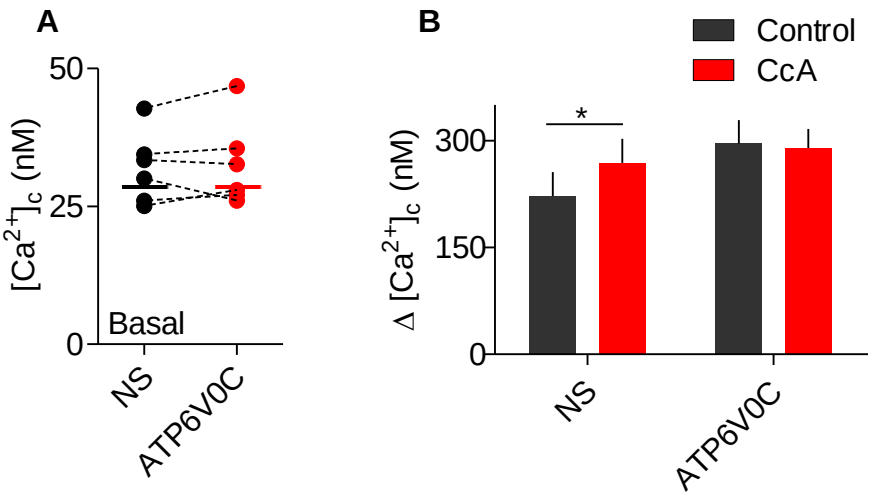

Figure 3.9 **Knockdown of ATP6V0C potentiates CCh-evoked Ca^{2+} signals in HEK cells** (A) Summary results show effects of siRNA treatments on basal $[Ca^{2+}]_c$. Results show paired individual values (each from 3 determinations) and the mean (n = 6, line). (P = 0.56, paired Student's t-test). (B) Summary results show the effect of siRNA treatments on CCh-evoked Ca^{2+} signals with or without CcA pre-incubation (1 µM, 1 h). Results are means ± SEM, n = 3-5, with triplicate determinations in each. $^{*}P < 0.05$, two-way Anova, Bonferroni post hoc test.

3.3.2 Dissipating the lysosomal H^+ gradient does not affect SOCE

The sustained response to CCh, and to most stimuli that activate PLC, requires Ca^{2+} entry across the PM through the SOCE pathway, which is stimulated by loss of Ca^{2+} from the ER (Parekh & Putney, 2005; Lopez-Sanjurjo *et al.*, 2013). In cells pre-treated with thapsigargin in Ca^{2+}-free HBS to deplete the ER of Ca^{2+}, restoration of extracellular Ca^{2+} caused a sustained increase in $[Ca^{2+}]_c$ reflecting the activity of SOCE (Figure 3.10A). Although the global increase in $[Ca^{2+}]_c$ resulting from thapsigargin-evoked SOCE was comparable to the increase after CCh-evoked Ca^{2+} release, the SOCE signals were not significantly affected by concanamycin A (Figure 3.10A, B).

Bafilomycin A_1 also had no effect on the Ca^{2+} signals evoked by SOCE in HEK cells, even when the amplitudes of the SOCE exceeded the Ca^{2+} signals evoked by IP_3Rs (Figure 3.11A). Similar results were obtained in HeLa cells, where thapsigargin evoked SOCE was unaffected by bafilomycin A_1 (Figure 3.11B).

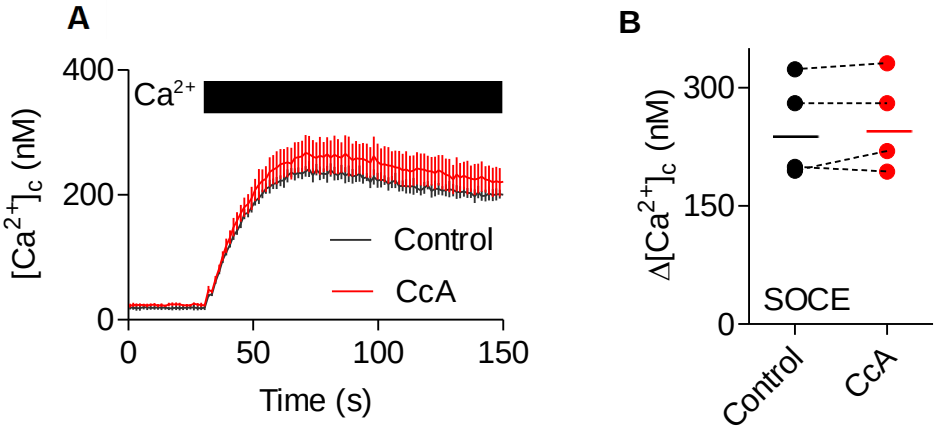

Figure 3.10 **Inhibition of lysosomal V-ATPase with concanamycin A does not affect the Ca^{2+} signals evoked by SOCE.** (A) HEK cells were treated with thapsigargin (1 µM, 15 min) in Ca^{2+}-free HBS to activate SOCE before restoration of extracellular Ca^{2+} (10 mM) alone or after treatment with CcA (1 µM, 1 h). Typical results show means ± SD from 3 wells in a single experiment. (B) SOCE after the restoration of extracellular Ca^{2+} (10 mM) to cells pre-treated with thapsigargin in nominally Ca^{2+}-free HBS is shown for control or CcA-treated cells. Results are from 4 independent experiments.

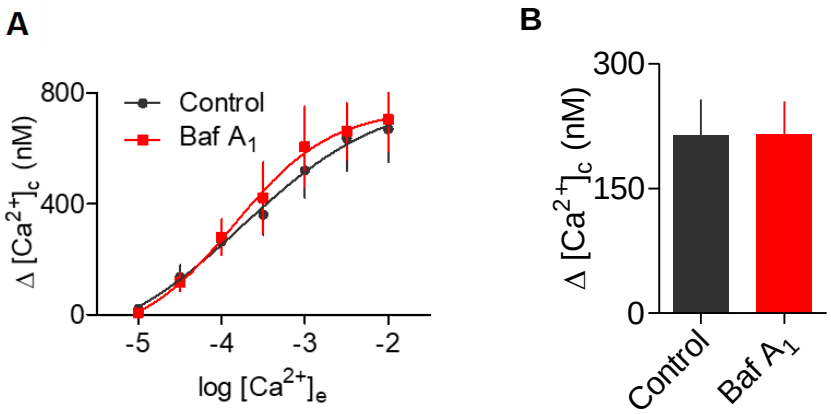

Figure 3.11 **Inhibition of lysosomal V-ATPase with bafilomycin A_1 does not affect the Ca^{2+} signals evoked by SOCE**. (A) HEK cells preincubated with Baf A_1 (1 µM, 1 h) were treated with thapsigargin (1 µM, 15 min) in Ca^{2+}-free HBS before restoration of extracellular Ca^{2+}. Summary results show means ± SEM, n = 3, with triplicate determinations in each. (B) SOCE after the restoration of extracellular Ca^{2+} (10 mM) to HeLa cells pre-treated with thapsigargin in nominally Ca^{2+}-free HBS is shown for control or Baf A_1-treated cells (1 µM, 15 min). Results are means ± SEM from 4 independent experiments (P = 0.81, paired Student's t-test).

Furthermore, following the knockdown of ATP6VOC, the thapsigargin-induced SOCE was not significantly different compared to cells treated with scrambled siRNA (n = 7, P = 0.18) (Figure 3.12). These results extend previous observations (Lopez-Sanjurjo *et al.*, 2013) by demonstrating that disruption of the pH_{ly} gradient, using siRNA to the V-ATPase or pharmacological inhibitors, exaggerates the cytosolic Ca^{2+} signals evoked by IP_3-evoked Ca^{2+} release without affecting those evoked by SOCE (Figure 3.13).

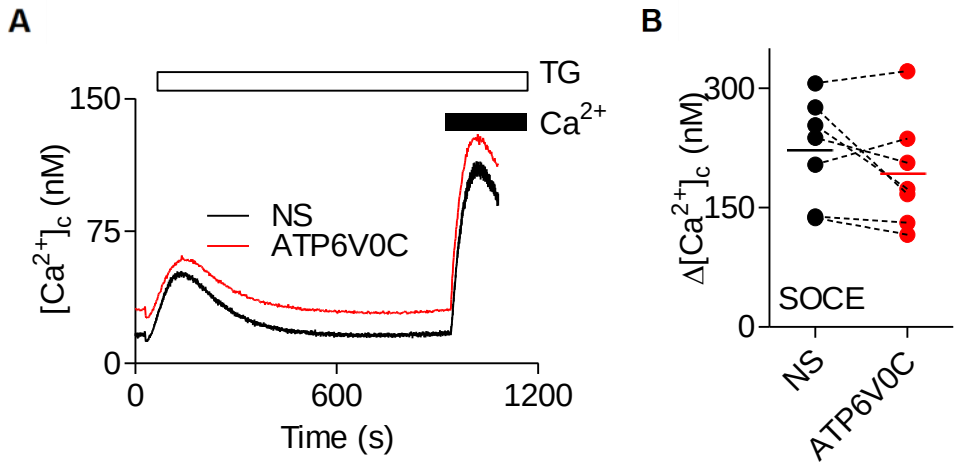

Figure 3.12 **Knockdown of ATP6VOC has no effect on thapsigargin-induced SOCE signals**. (A) HEK cells were treated with thapsigargin (1 μM, 15 min) in Ca^{2+}-free HBS to activate SOCE before restoration of extracellular Ca^{2+} (10 mM) in cells treated with the indicated siRNA. (B) Summary results show $\Delta[Ca^{2+}]_c$ after restoration of extracellular Ca^{2+} to cells treated with the indicated siRNA. P = 0.18, Student's t-test. Results are mean values from 7 independent experiments, with triplicate determinations in each.

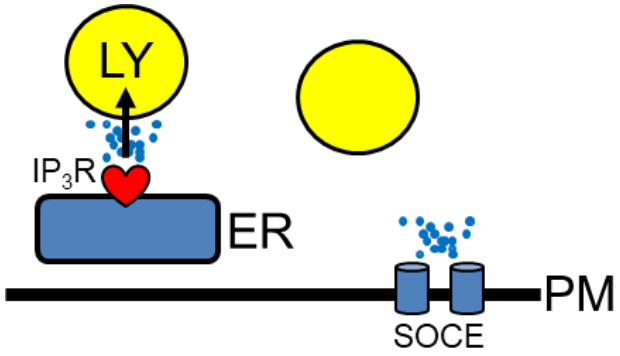

Figure 3.13 **Lysosomes selectively shape IP_3R-mediated Ca^{2+} signals.** Lysosomes (LY) selectively sequester Ca^{2+} released from ER through IP_3Rs, but not Ca^{2+} entering the cell through SOCE.

3.3.3 IP_3Rs selectively deliver Ca^{2+} to lysosomes

Results described so far establish a selective communication between IP_3R and lysosomes. The next strategy was to use a minimally perturbing assay to investigate the selective coupling between lysosomes and IP_3R. There is a need for Ca^{2+} indicators that directly report free [Ca^{2+}] within the lysosome lumen, but their development presents considerable challenges (**Section 1.4**). An improvement on present measurements of global $[Ca^{2+}]_c$ with conventional Ca^{2+} indicators would be to use a low-affinity Ca^{2+} indicator tethered to the cytosolic surface of the lysosome membrane to measure juxta-lysosomal [Ca^{2+}]. Previously, lysosomal proteins have been tethered to high-affinity Ca^{2+} sensors, thus making it difficult to selectively measure juxta-lysosomal Ca^{2+} (Shen *et al.*, 2012; McCue *et al.*, 2013; Garrity *et al.*, 2016). My first attempt to generate a low-affinity fluorescent protein tethered to a lysosomal protein was done by attaching R-GECO1.2 (Wu *et al.*, 2014) to the C-terminus of LAMP1. However, this protein did not localise to lysosomes, but instead formed aggregates within HEK cells (results not shown). I thus have tethered the C-terminus of LAMP1 to the low-affinity Ca^{2+} sensor (G-GECO1.2, $K_D^{Ca} = 1.2$ μM) (Zhao *et al.*, 2011). G-GECO1.2 was initially produced by random mutagenesis of GCaMP (Zhao *et al.*, 2011), which comprises a circularly permuted green fluorescent protein (cpGFP), CaM-binding M13 peptide and calmodulin (CaM) (Zhao *et al.*, 2011). Binding of Ca^{2+} to the modified CaM, allows the Ca^{2+}-CaM to bind to M13 and that causes an increase in the GFP fluorescence intensity.

HeLa cells, in which histamine stimulates IP_3 formation and Ca^{2+} release from the ER (Thillaiappan *et al.*, 2017), were used for these experiments because they are better suited for imaging organelles. In HeLa cells, just as in HEK cells, IP_3-evoked increases in $[Ca^{2+}]_c$ were potentiated by bafilomycin A_1, whereas SOCE-evoked Ca^{2+} signals were not (Figure 3.7 and Figure 3.11B). For comparison with these local measurements of [Ca^{2+}] at lysosome membranes, I used the same low-affinity sensor expressed in the cytosol (Cy-GG) to record global increases in $[Ca^{2+}]_c$. Since the peak $[Ca^{2+}]_c$ after histamine stimulation does not exceed ~360 nM (Figure 3.7), Ly-GG and Cy-GG selectively report local increases in $[Ca^{2+}]_c$ in HeLa cells. In HeLa cells, Ly-GG co-localized with LAMP1-mCh ($R_{coloc} = 0.93 \pm 0.02$, $n = 3$) and with the lysosomal cation channel, TPC2-RFP ($R_{coloc} = 0.86 \pm 0.09$, $n = 3$) (Figure 3.14). All colocalization analyses were done from wide-field images.

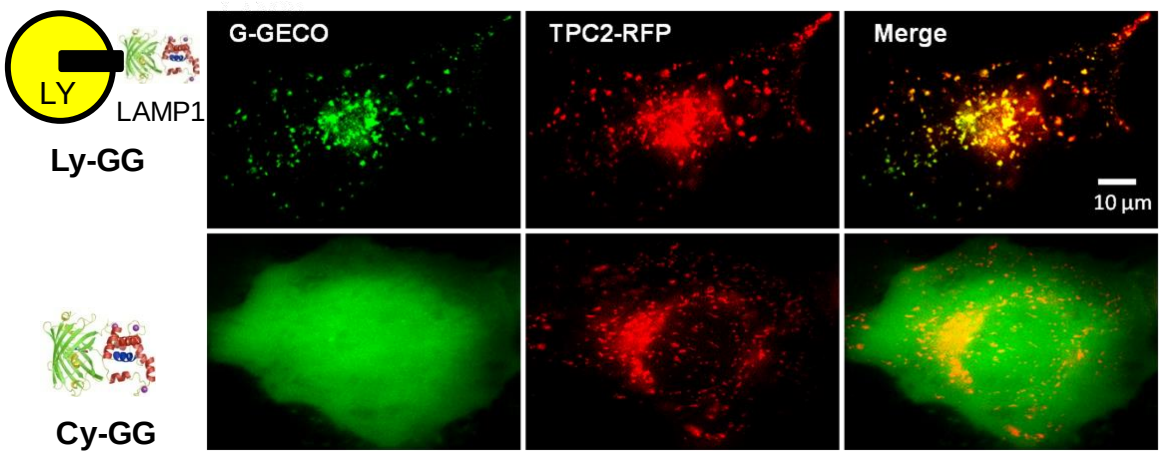

Figure 3.14 **Ly-GG is specifically targeted to lysosomes.** Wide-field fluorescence images of HeLa cells expressing TPC2-RFP with either Ly-GG (top) or Cy-GG (bottom). Scale bar = 10 µm.

In unstimulated cells, $[Ca^{2+}]_c$ (reported as F/F_{max}) was similar when detected with Ly-GG (F/F_{max} = 0.25 ± 0.01, n = 3) and Cy-GG (0.23 ± 0.01, n = 3, P = 0.33, Student's t-test) (Figure 3.15D), suggesting that the Ca^{2+} affinity of the sensor was unaffected by differential targeting. HeLa cells in Ca^{2+}-free HBS were stimulated with histamine, which evokes IP_3 formation, and fluorescence was recorded from single tracked lysosomes (Ly-GG) or from comparable areas of cytosol (Cy-GG) (see **Section 2.15**). Histamine caused a transient increase in Cy-GG fluorescence and a larger transient increase in Ly-GG fluorescence that came close to saturating the indicator (Figure 3.15A-C). The change in fluorescence (F/F_{max}) for Ly-GG was 0.73 ± 0.08 (n = 4) and for Cy-GG it was 0.44 ± 0.04 (n = 3, $P < 0.05$, Student's t-test).

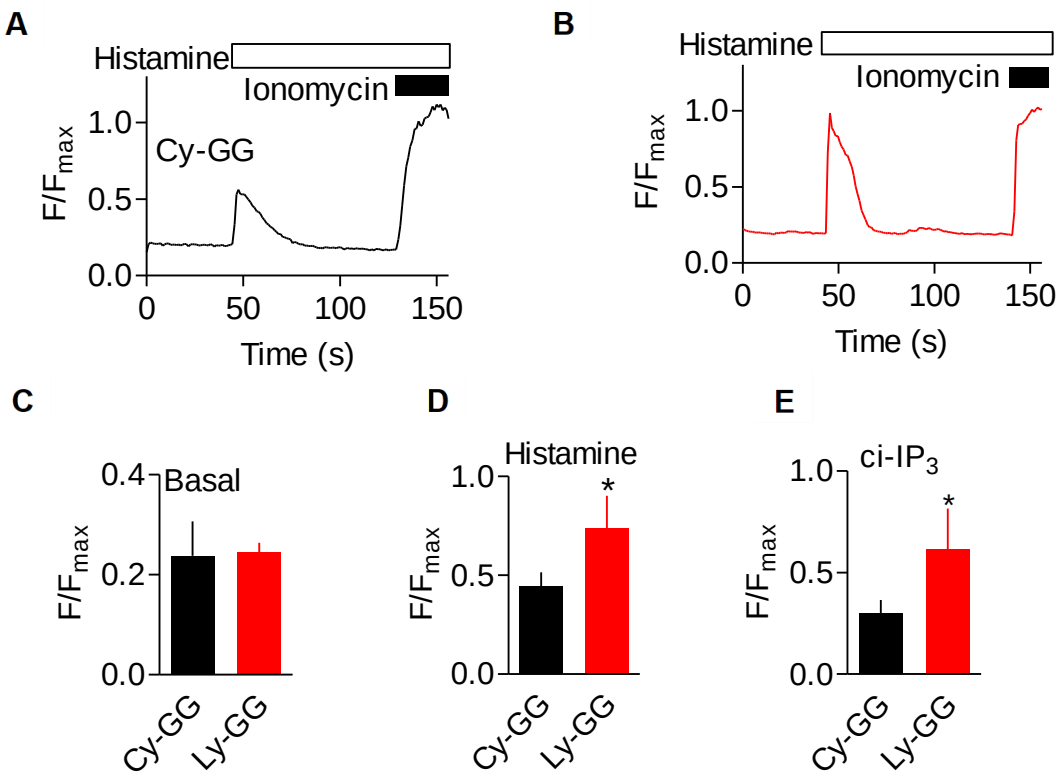

Figure 3.15 **Lysosomes are exposed to local large [Ca^{2+}] after Ca^{2+} release via IP_3R.** (A, B) Recordings from HeLa cells expressing Cy-GG (A) or Ly-GG (B) showing responses to histamine (100 μM) in Ca^{2+}-free HBS, and then ionomycin (10 μM) with 2 mM $CaCl_2$ (to saturate sensor). Results (F/F_{max}, where F_{max} is response after ionomycin) show responses of a single tracked lysosome (B) or a similarly sized cytosolic ROI (A). (C,D) Summary results (mean ± SEM) show basal fluorescence (C) (3 experiments with 198 ROI for Cy-GG, and 83 tracks for Ly-GG), and peak fluorescence signals (D) evoked by histamine for Cy-GG (3 experiments with 198 ROI) and Ly-GG (4 experiments with 83 lysosome tracks). (E) Summary results show peak fluorescence signals following uncaging of ci-IP_3 (mean ± SEM). $^{*}P < 0.05$, Student's *t*-test.

The distribution of the fluorescence intensity changes of Ly-GG from 83 tracked lysosomes showed a 41% overlap with those from Cy-GG, but the remaining 59% responded with much larger changes (Figure 3.16). There was no difference in the average speed of lysosomes responding to histamine with large ($F/F_{max} > 0.6$; speed = 0.45 ± 0.17 μm/s, $n = 51$) or cytosol-like responses ($F/F_{max} < 0.6$; 0.34 ± 0.22 μm/s, $n = 32$; $P = 0.60$).

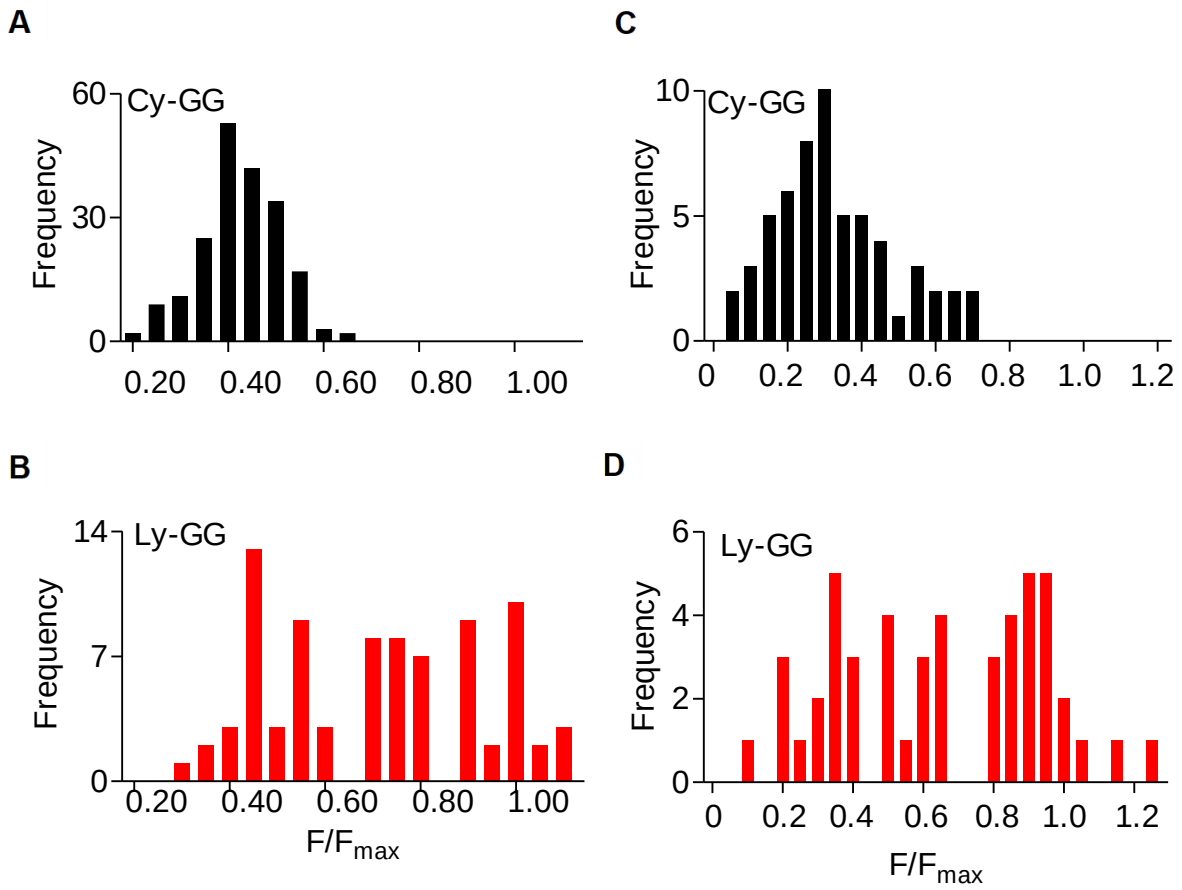

Figure 3.16 **IP$_3$Rs selectively deliver Ca^{2+} to a subset of lysosomes.** (A, B) Summary results from the experiments in Figure 3.15, show the distribution of F/F_{max} values for Ly-GG and Cy-GG for tracks (Ly-GG) or ROIs obtained from cells stimulated with histamine. The distribution of values for Cy-GG is consistent with a normal distribution (Kolmogorov-Smirnov normality test, $P = 0.0018$), whereas the distribution of values for Ly-GG appears multi-modal ($P > 0.1$). (C,D) Distribution of peak F/F_{max} values for Cy-GG (C) and Ly-GG (D) after photolysis of ci-IP$_3$ in Ca^{2+}-free HBS (n = 59 ROIs from 4 dishes for Cy-GG, and 49 tracks from 3 dishes for Ly-GG).

Activation of histamine (H_1) receptors has been previously reported to cause the production of NAADP, which can trigger release of Ca^{2+} from acidic stores (Esposito *et al.*, 2011). The consequence of this would be that the Ca^{2+} detected by Ly-GG upon histamine stimulation could be due to release of Ca^{2+} directly from lysosomes and not from the ER via IP$_3$R. However, HeLa cells have been reported to respond to NAADP only after overexpression of TPC2, since they do not express TPC2 endogenously (Lu *et al.*, 2013). In Hela cell populations, U73122, an inhibitor of PLC (Bleasdale *et al.*, 1990), caused a concentration-

dependent inhibition (pIC_{50} (negative log of the half-maximally inhibitory concentration) = 6.6 ± 0.07, n = 3) of the Ca^{2+} signals evoked by a maximally effective concentration histamine (100 μM), while the inactive analogue, U73343 (≤10 μM), had no effect (Figure 3.17A). Furthermore, in single cells, the histamine-mediated increase in Ly-GG fluorescence was abolished by treatment with U73122 (10 μM, 20 min). This establishes that the histamine-induced increase in $[Ca^{2+}]_c$ is dependent on IP_3 production and consequently dependent on IP_3R-mediated release of Ca^{2+} from the ER.

Another approach was direct activation of IP_3Rs by photolysis of caged IP_3 (ci-IP_3). Photolysis of ci-IP_3 also caused increases in $[Ca^{2+}]_c$ that were larger at the lysosome surface than in the bulk cytosol (Figure 3.15E). Furthermore, whereas U73122 abolished Ly-GG responses to histamine, it had no effect on responses to photolysis of ci-IP_3 (Figure 3.17D), consistent with the effects of U73122 on histamine-evoked Ca^{2+} signals arising from inhibition of PLC. My results establish that Ca^{2+} release through IP_3Rs is required for the near-lysosome Ca^{2+} signals.

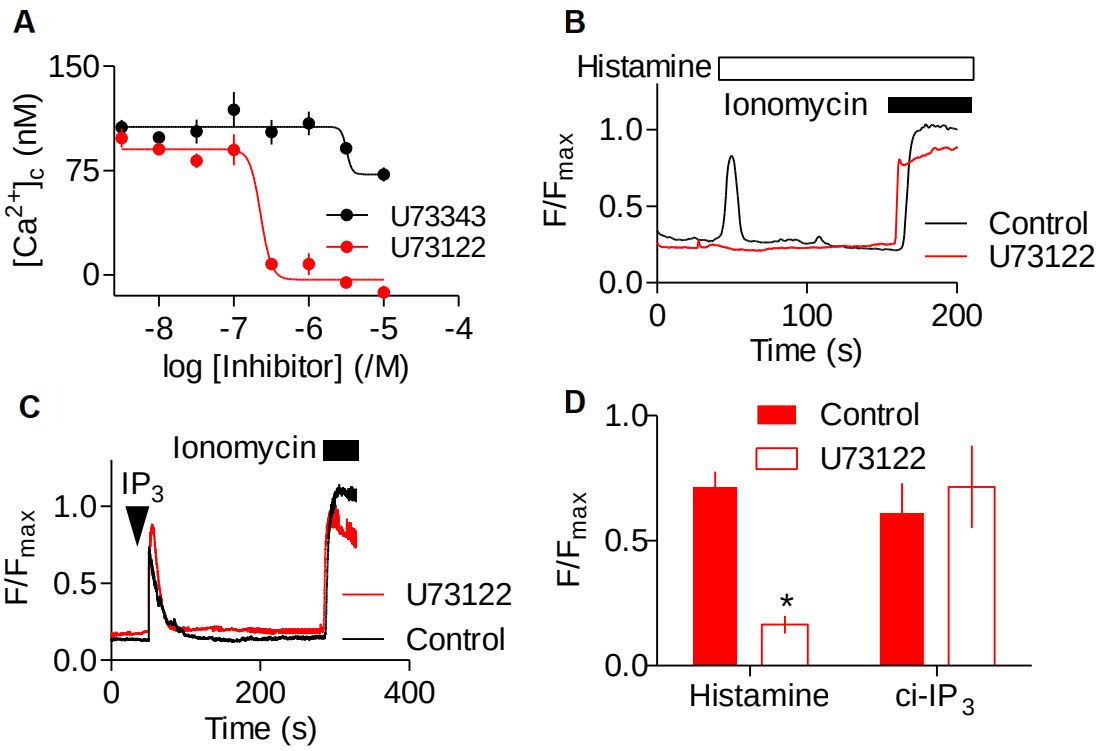

Figure 3.17 **Histamine-mediated increase in $[Ca^{2+}]_c$ requires PLC in HeLa cells.** (A) Effects of the indicated concentrations of U73122 or U73343 (20 min) on the peak increase in $[Ca^{2+}]_c$ evoked by histamine (100 μM). Results are means ± SEM from 3 experiments, each with 3 determinations. (B, C) Typical traces from HeLa cells expressing Ly-GG show responses to histamine (100 μM) (B) or photolysis of ci-IP_3 (C) in Ca^{2+}-free HBS with or without U73122 (10 μM, 20 min), and then ionomycin (10 μM) with 2 mM $CaCl_2$. Results show responses of a single tracked lysosome. (D) Summary results show the effects of U73122 (10 μM, 20 min) on peak Ly-GG signals evoked by histamine (100 μM) or photolysis of ci-IP_3. Mean ± SEM, n = 3-4. $^*P < 0.05$, Student's t-test, relative to control.

Cells were incubated in Ca^{2+}-free HBS with thapsigargin to empty the stores, followed by restoration of Ca^{2+} to allow SOCE. There was no difference in the signal reported by Ly-GG and Cy-GG during Ca^{2+} release from the ER in response to thapsigargin (Figure 3.18A, B). There was no significant difference between the signal detected by Cy-GG and Ly-GG following SOCE signals after restoration of extracellular Ca^{2+} to thapsigargin-treated cells (Figure 3.18C). These results suggest that during histamine-evoked Ca^{2+} release through IP_3Rs about 60% of lysosomes experience a much larger increase in $[Ca^{2+}]_c$ than the global increase in $[Ca^{2+}]_c$. SOCE, by contrast, does not selectively deliver Ca^{2+} to lysosomes.

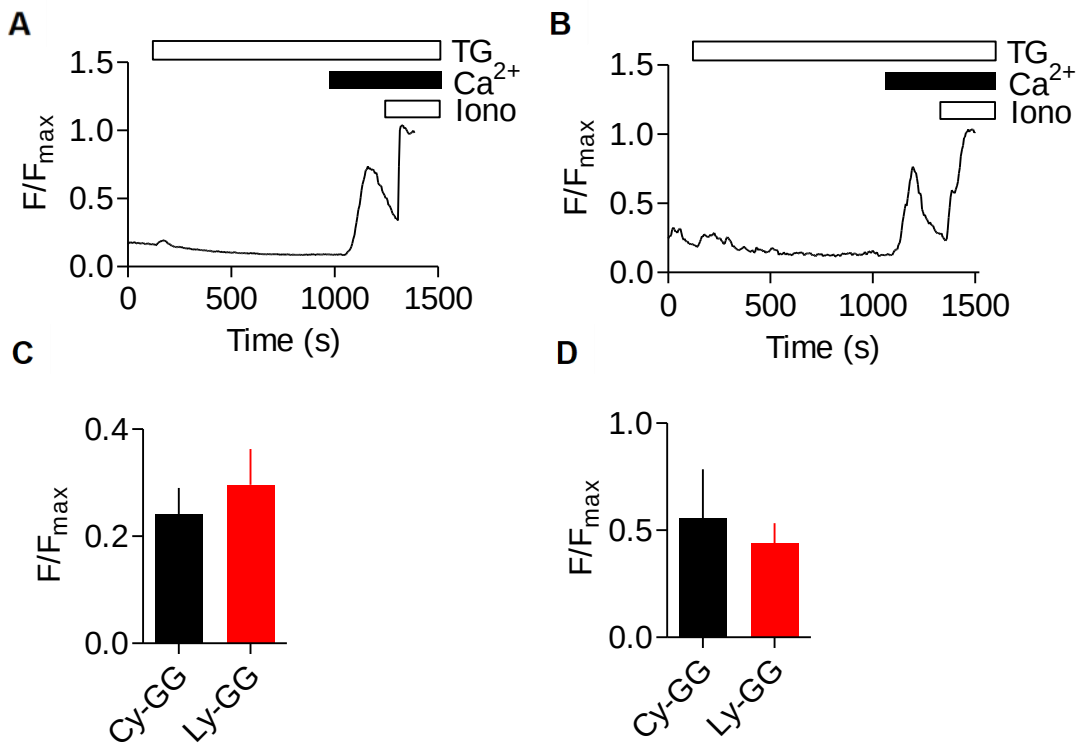

Figure 3.18 **There is no difference between the Ca^{2+} signals detected by lysosomes and in the cytosol following SOCE.** (A, B) Typical recordings from HeLa cells expressing Cy-GG (A) or Ly-GG (B) show responses in Ca^{2+}-free HBS to TG (1 µM), restoration of extracellular Ca^{2+} (2 mM), and then ionomycin (10 µM). (C) Summary results (mean ± SEM) show peak responses to TG (1 µM) in Ca^{2+}-free HBS (30 tracks for Ly-GG and 45 ROI for Cy-GG). (D) Summary results for the peak signal evoked during SOCE following restoration of extracellular Ca^{2+}. Results are means ± SEM (30 tracks for Ly-GG and 45 ROI for Cy-GG) from at least 3 independent experiments.

Others have previously used a Ca^{2+} sensor targeted to lysosome membranes (LAMP1-yellow cameleon3.60) to detect Ca^{2+} signals evoked by histamine in HeLa cells (McCue *et al.*, 2013), but this sensor with its high affinity (K_D^{Ca} = 250 nM) (Nagai *et al.*, 2004) cannot distinguish local from global increases in $[Ca^{2+}]_c$. My use of a targeted low-affinity sensor to lysosome membranes (Ly-GG, K_D^{Ca} = 1.2 µM) has shown that IP_3Rs, but not SOCE, selectively deliver Ca^{2+} to about 60% of lysosomes. A similar situation prevails for mitochondria, where the release of Ca^{2+} from IP_3Rs adjacent to mitochondria generates a high local $[Ca^{2+}]$, sufficient to allow Ca^{2+} uptake through the low-affinity mitochondrial uniporter complex (MCU) (Rizzuto *et al.*, 2012). For both lysosomes and mitochondria, the ER

through its SERCA and IP_3Rs, provides a route through which Ca^{2+} can be accumulated from the low $[Ca^{2+}]_c$ of resting cells by a high-affinity uptake system (SERCA) and then delivered locally (through IP_3Rs) at a high concentration to a low-affinity uptake system (MCU or lysosomes).

IP_3Rs provide a link between extracellular stimuli and delivery of Ca^{2+} to lysosomes, but additional unidentified ER Ca^{2+} channels may also deliver Ca^{2+} to lysosomes in unstimulated cells. Therefore, in agreement with a recent report (Garrity *et al.*, 2016), these results suggest that microdomains of high local $[Ca^{2+}]$ presented to lysosomes by IP_3Rs may facilitate lysosomal Ca^{2+} uptake.

3.3.4 Lysosomes sequester Ca^{2+} released by all IP_3Rs

The Ca^{2+} signals evoked by histamine in HeLa cells or by CCh in HEK cells are initiated by activation of IP_3Rs. The former is confirmed by the lack of response to histamine following inhibition of PLC and the latter by the lack of response to CCh in HEK cells without IP_3Rs (**Section 3.3.6**). Western blot analysis show that the HEK cells from which the HEK-IP_3RKO cells were generated, express all three IP_3R subtypes, with $IP_3R3 \geq IP_3R1 > IP_3R2$ (Mataragka & Taylor, 2018). Differential regulation of Ca^{2+} signalling by different IP_3R subtypes is an emerging theme in cell signalling. For example, siRNA against IP_3R1 and IP_3R3, but not IP_3R2, attenuated the activation of calcium release-activated channels (CRAC) in liver cells (Jones *et al.*, 2011). Interactions between the ER and mitochondria, which appear similar to the cross talk between ER and lysosomes, have been reported to require specific IP_3R subtypes. In astrocytes, IP_3R2 has been reported to colocalise with mitochondria, while in HEK cells and Chinese Hamster Ovary (CHO) cells, IP_3R3 has been reported to colocalise with mitochondria (Mendes *et al.*, 2005). To investigate the subtype-selectivity in communication between IP_3R and lysosomes, HEK cells in which the genes for one or two of the three IP_3R subtypes had been disrupted were used (Alzayady *et al.*, 2016). There was no significant difference in the basal $[Ca^{2+}]_c$ between the seven cell lines examined and nor did bafilomycin A_1 affect the basal $[Ca^{2+}]_c$ in any of the cell lines (Figure 3.19).

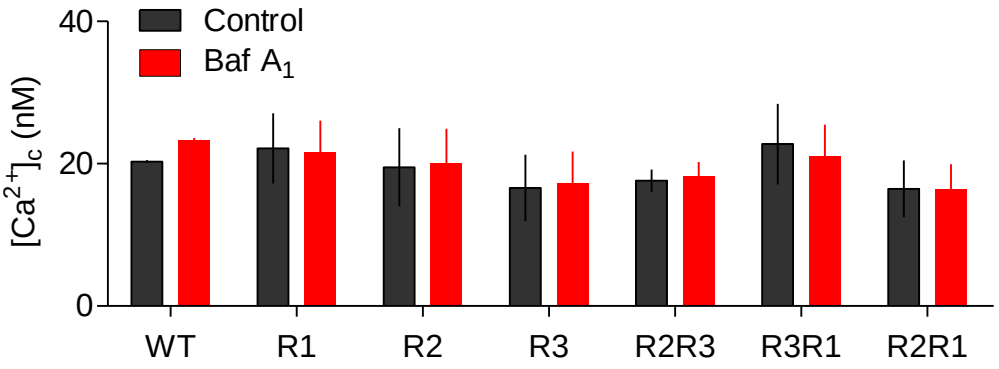

Figure 3.19 **Basal $[Ca^{2+}]_c$ is unaffected by bafilomycin A_1 in cells expressing one or more IP_3R subtype.** Summary results show the basal $[Ca^{2+}]_c$ in HEK cells treated with or without Baf A_1 (1 µM, 1 h). Results are means ± SEM, *n* = 3, with triplicate determinations in each experiment. WT, wild-type and for others R denotes the native IP_3R subtypes exposed in each cell line.

There were some unexpected differences in the amplitudes of the increase in $[Ca^{2+}]_c$ evoked by a maximal concentration of CCh (1 mM) between wild-type cells and the cell lines lacking one or more IP_3R subtypes, with some of the latter giving larger signals (Figure 3.20). This has not been explored further, but it probably arises from changes in the expression of M3 receptors or downstream signalling proteins during the selection of cell lines. However, the effects of bafilomycin A_1 were similar in wild-type HEK cells and in cells lacking any one or two of the native IP_3R subtypes, irrespective of the amplitude of the CCh-evoked Ca^{2+} signals (Figure 3.20, Table 3.1). In each case, bafilomycin A_1 caused the increase in $[Ca^{2+}]_c$ evoked by 1 mM CCh to be increased by about 20-30%. These results demonstrate that all three IP_3R subtypes can deliver Ca^{2+} to lysosomes.

Table 3.1 **Response to CCh in control and bafilomycin A_1-treated populations of HEK cells expressing different combinations of IP_3Rs subtypes.** The IP_3R subtype expressed in each cell line is listed under 'cell type'. From the results shown in Figure 3.20. Results (means ± SEM from 6 independent experiments) show pEC_{50} values for CCh, peak increase in $[Ca^{2+}]_c$ and basal $[Ca^{2+}]_c$. $^*P < 0.05$, paired Student's *t*-test, relative to control in each.

Cell type	**Treatment**	**Basal $[Ca^{2+}]_c$ (nM)**	**Peak $[Ca^{2+}]_c$ (nM)**	**pEC_{50} (/M)**
HEK WT	Control	20 ± 0.2	298 ± 6	5.18 ± 0.04
	Bafilomycin A_1	23 ± 0.3	373 ± 14*	5.17 ± 0.07
IP_3R1	Control	22 ± 9	175 ± 20	5.10 ± 0.20
	Bafilomycin A_1	21 ± 9	212 ± 23*	5.11 ± 0.26
IP_3R2	Control	19 ± 8	497 ± 11	5.81 ± 0.06
	Bafilomycin A_1	19 ± 8	624 ± 14*	5.78 ± 0.07
IP_3R3	Control	19 ± 8	413 ± 32	5.05 ± 0.17
	Bafilomycin A_1	20 ± 9	471 ± 34*	5.03 ± 0.16
IP_3R1 and IP_3R2	Control	18 ± 8	518 ± 9	5.75 ± 0.06
	Bafilomycin A_1	19 ± 8	625 ±16*	5.72 ± 0.09
IP_3R1 and IP_3R3	Control	22 ± 10	451 ± 35	5.58 ± 0.35
	Bafilomycin A_1	21 ± 9	552 ± 43*	5.58 ± 0.38
IP_3R2 and IP_3R3	Control	17 ± 7	491 ± 18	5.57 ± 0.09
	Bafilomycin A_1	18 ± 8	631 ± 22*	5.54 ± 0.08

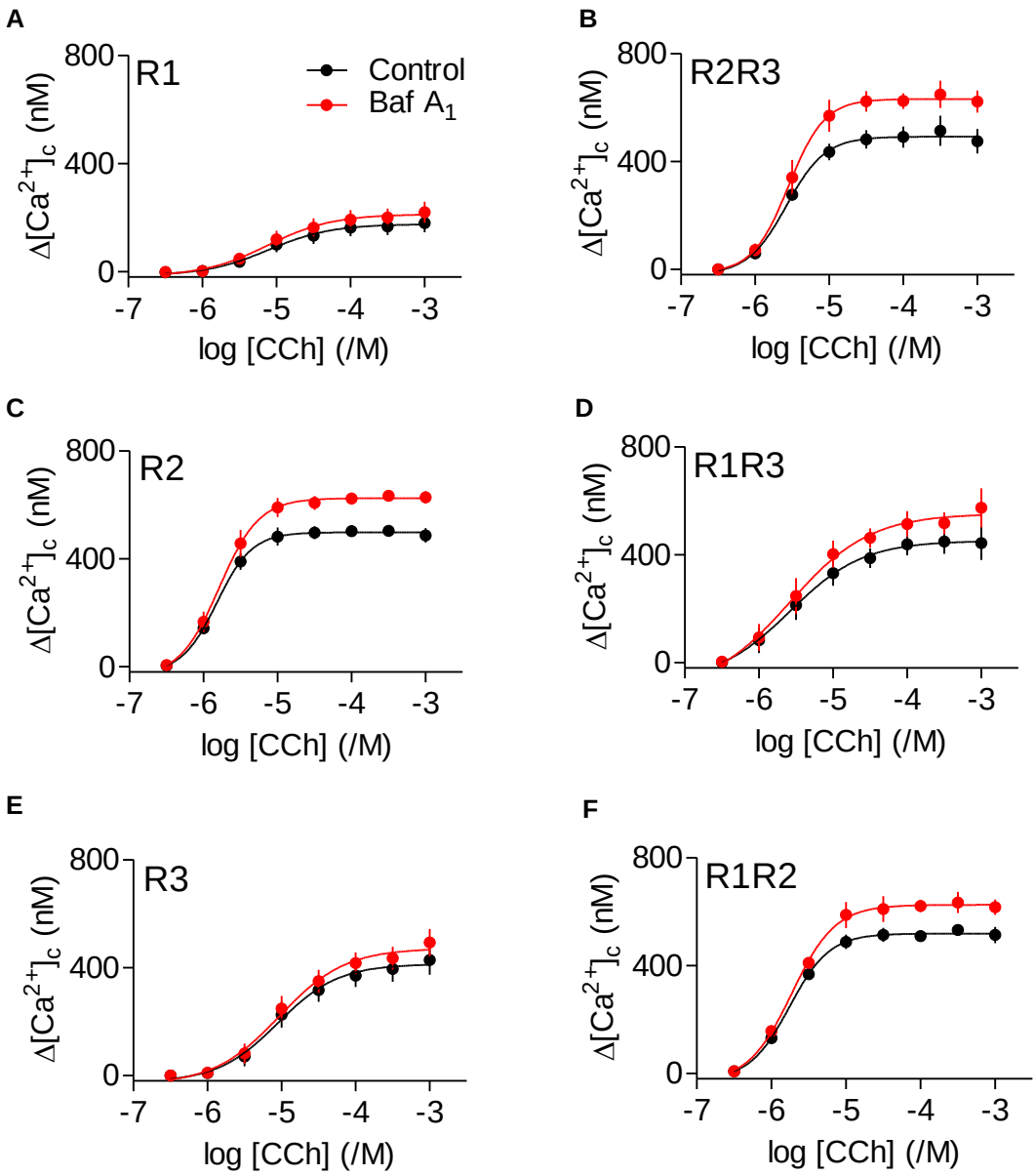

Figure 3.20 **Lysosomes sequester Ca^{2+} released by all IP_3R subtypes.** (A-F) Concentration-dependent effects of CCh on Ca^{2+} release with and without pre-incubation with bafilomycin A_1 shown in HEK cells expressing only IP_3R1 (A), IP_3R2 and IP_3R3 (B), IP_3R2 (C), IP_3R3 and IP_3R1 (D), IP_3R3 (E) and IP_3R2 and IP_3R1 (F) in Ca^{2+}-free HBS. Results show means ± SEM, n=6 independent experiments. Summary results and statistics are shown in Table 3.1.

3.3.5 A sustained increase in pH_{ly} disrupts lysosomal distribution and Ca^{2+} handling

Fluorescein-Dx (10-kDa) directed to lysosomes of HEK cells by endocytosis, allows the ratiometric imaging of pH_{ly}: excitation at 488 nm is pH-sensitive, whilst it is relatively insensitive to pH following excitation at 425 nm (Canton & Grinstein, 2015; Johnson *et al.*, 2016). CcA caused a time-dependent increase in the fluorescence ratio indicating a dissipation of the lysosomal H^+ gradient (Figure 3.21A, B). This increase reached a plateau after approximately 40 min (Figure 3.21B). Similarly, there was a significant loss of LysoTracker Red in lysosomes after a 30-min treatment with CcA, indicative of lysosomal alkalinisation (Figure 3.21D). Hence, both a quantitative (fluorescein-Dx) and qualitative (LysoTracker) means of assessing the time course for loss of the lysosomal H^+ gradient, provide evidence that the lysosomal H^+ gradient is significantly lost 30-40 mins after treatment with concanamycin A.

In parallel analyses, the effects of concanamycin A on the Ca^{2+} signals evoked by CCh were determined. As expected, prolonged incubation with concanamycin A caused the amplitude of the CCh-evoked increase in $[Ca^{2+}]_c$ to increase (Figure 3.21C), consistent with normal lysosomes sequestering Ca^{2+} released through IP_3Rs. However, the effect of concanamycin A on CCh-evoked Ca^{2+} signals was much slower to develop than its effect on pH_{ly}. There was no evident effect of concanamycin A on Ca^{2+} signals within 40 min, and a statistically significant potentiation of CCh-evoked Ca^{2+} signals required a 60-min incubation with concanamycin A (Figure 3.21C). These results suggest that Ca^{2+} sequestration by lysosomes persists after dissipation of the H^+ gradient, suggesting that compromised sequestration of the Ca^{2+} released through IP_3Rs may be a secondary consequence of the increase in pH_{ly}.

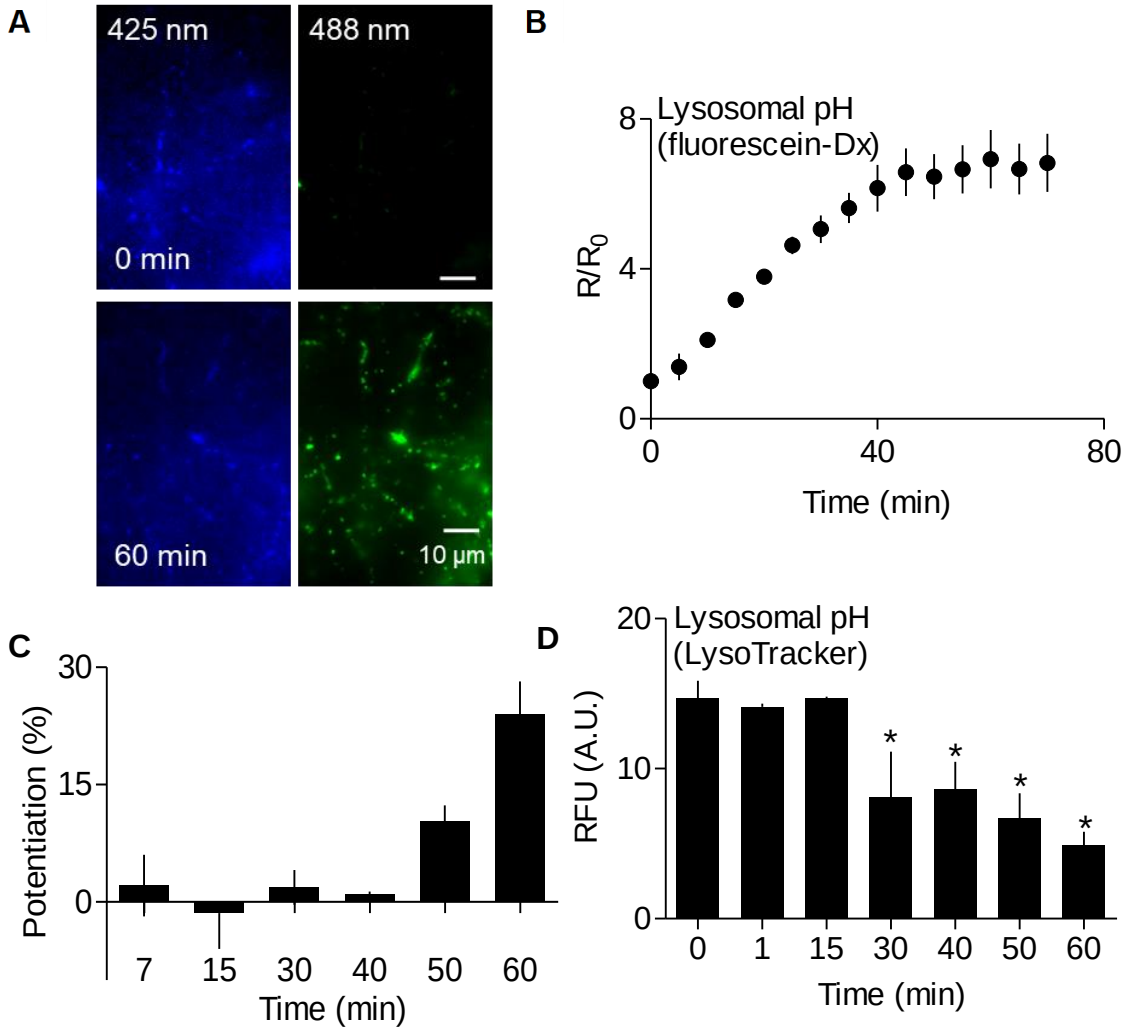

Figure 3.21 **Concanamycin A dissipates the lysosomal H^+ gradient more rapidly that it dissipates lysosomal Ca^{2+} uptake.** (A) Lysosomes of HEK cells were loaded with fluorescein-Dx (pK_a = 6.4). Wide-field images show fluorescence recorded at pH-sensitive (λ_{ex} = 488 nm) and insensitive (λ_{ex} = 425 nm) wavelengths before (0 min) and after CcA (1 µM, 1 h). Images typical of 3 experiments. (B) Summary results (mean ± SEM, *n* = 3) show time course of pH_{ly} changes after CcA as fluorescence ratios ($R = F_{488}/F_{425}$), which increase as pH increases. R_0 is R determined before CcA. (C) Parallel analysis of CcA (1 µM) effects on peak increase in $[Ca^{2+}]_c$ evoked by CCh (1 mM) in Ca^{2+}-free HBS. Results (mean ± SEM, *n* = 4-9, with 3 determinations) show increase in peak Ca^{2+} signal in presence of CcA relative to that in its absence, as percentage of response evoked by CCh alone. (D) Effects of CcA (1 µM) using LysoTracker Red (50 nM, 1 h) fluorescence, which declines as pH_{ly} increases. Mean ± SEM, *n* = 4-10. $^*P < 0.05$, one-way ANOVA with Dunnett's *post hoc* test, relative to t = 0.

Lysosomes have been previously reported to fuse when their pH increases (Cao *et al.*, 2015), and the least acidic lysosomes are more peripherally located (Johnson *et al.*, 2016). I therefore considered whether the delayed effects of concanamycin A on CCh-evoked Ca^{2+} signals might be due to redistribution of lysosomes. In control conditions, lysosomes are densely packed in the perinuclear region. However, following prolonged treatment with concanamycin A, there was in increase in the number of enlarged lysosomes and they were more peripherally located (Figure 3.22A). Prolonged treatment with concanamycin A caused a small, but statistically insignificant, decrease in the number of small lysosomes and a significant increase in the number of large lysosomes (Figure 3.22B). These changes, perhaps suggesting fusion of lysosomes, are similar to those evoked by knockdown of a core subunit of the V-ATPase (Figure 3.8C). Hence, prolonged dissipation of the lysosomal H^+ gradient causes lysosomes to enlarge and accumulate peripherally. These changes could thereby disrupt their interactions with ER. Vacuolin, which is routinely used to enlarge lysosomes (Dong *et al.*, 2010; Schieder *et al.*, 2010a; Wang *et al.*, 2012; Cang *et al.*, 2013), has also been shown to prevent the sequestration of Ca^{2+} released from the ER by lysosomes (Lopez Sanjurjo *et al.*, 2013). Therefore, both my results and those with vacuolin suggest that the effect of inhibition of V-ATPase on lysosomal Ca^{2+} uptake could be a secondary consequence of perturbing lysosomal morphology and/or distribution rather than a primary consequence of the dissipation of the pH_{ly} gradient.

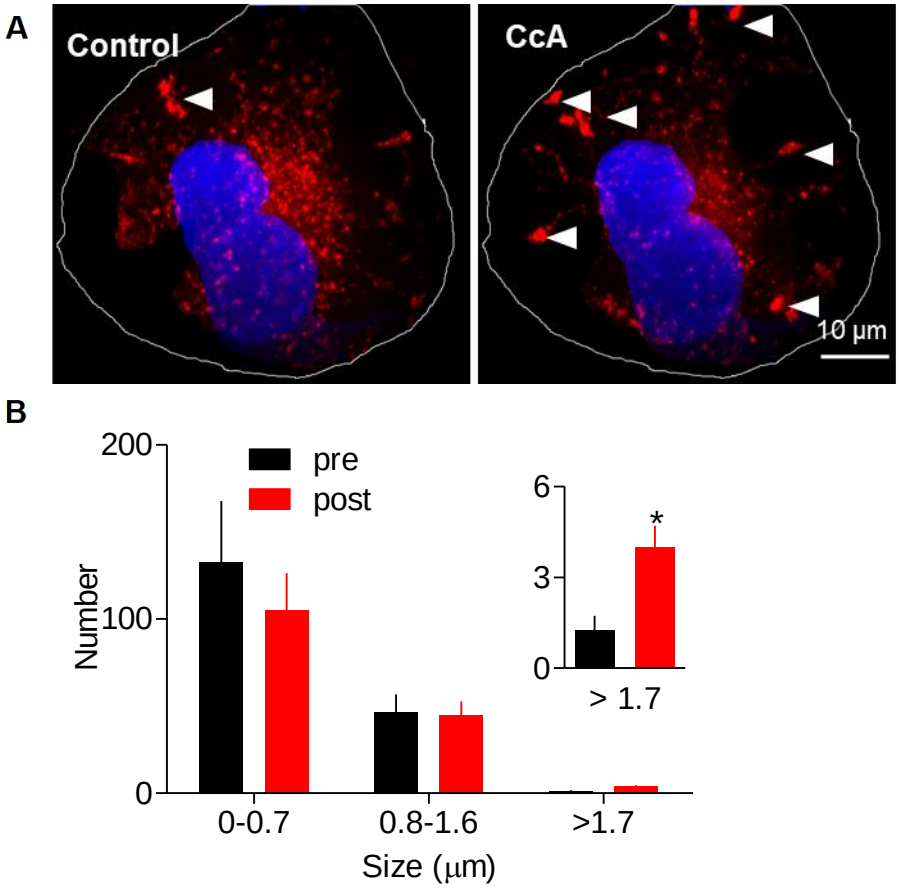

Figure 3.22 **Treatment with concanamycin A enlarges lysosomes.** (A) Confocal z-stack of HEK cells expressing LAMP1-mCherry before and after CcA (1 µM, 1 h). Nuclei stained with NucBlue. The appearance of larger lysosomes in the cell periphery (white arrows) following CcA (1 µM, 1 h) was clearly observed in 4 of 6 cells. (B) Effect of CcA (1 µM, 1 h) on distribution of lysosome sizes (reported as Feret diameter, see **Section 2.19**). Results are from 721 (control) and 617 lysosomes (CcA-treated) from 4 experiments. Inset shows enlargement of largest size category. $^{*}P < 0.05$, Student's *t*-test.

3.3.6 Association of lysosomes and ER does not require IP_3R

Lysosomes traffic and form contact sites with the ER (Kilpatrick *et al.*, 2013; Lopez-Sanjurjo *et al.*, 2013; Garrity *et al.*, 2016). I investigated the role of IP_3R in the formation of ER lysosome junctions.

Previously, abrogation of the lysosomal H^+ gradient was shown to increase the $[Ca^{2+}]_c$ evoked by inhibition of SERCA with thapsigargin (Lopez-Sanjurjo *et al.*, 2013). In that report, IP_3R was proposed to mediate the Ca^{2+} leak from the ER. However, in HEK cells lacking IP_3Rs (IP_3RKO), where the CCh-mediated increase in $[Ca^{2+}]_c$ was abolished (

Figure 3.23A), the thapsigargin-mediated Ca^{2+} signals persisted (

Figure 3.23B-D). Furthermore, bafilomycin A_1 potentiated the peak increase in $[Ca^{2+}]_c$ evoked by thapsigargin by 45 ± 14 % in HEK WT and by 48 ± 4 % in HEK cells lacking IP_3Rs respectively (n = 4) (

Figure 3.23).

Similar results were obtained in HAP1 cells, which are a near-haploid mammalian cell line routinely used for gene-editing (Essletzbichler *et al.*, 2014). Stimulation of permeabilised HAP1 cells with IP_3 releases Ca^{2+} from the ER in WT cells, but not in cells genetically engineered to lack all IP_3R (HAP1-KO) (Figure 3.24A, B) (Atakpa *et al*., 2018). This establishes that HAP1 cells contain functional IP_3R that are lost in the HAP1-KO cells. Inhibition of SERCA with thapsigargin released Ca^{2+} in WT HAP1 cells and the increase in $[Ca^{2+}]_c$ was potentiated by bafilomycin A_1 (Figure 3.24C, D). This suggests that in HAP1 cells, thapsigargin also unmasks a Ca^{2+} leak from the ER and the Ca^{2+} released is then sequestered by lysosomes. Similar results were obtained in HAP1 cells without IP_3R (Figure 3.24D). This confirms that IP_3R neither mediate the passive leak of Ca^{2+} from the ER nor form an essential part of the junctions between ER and lysosomes.

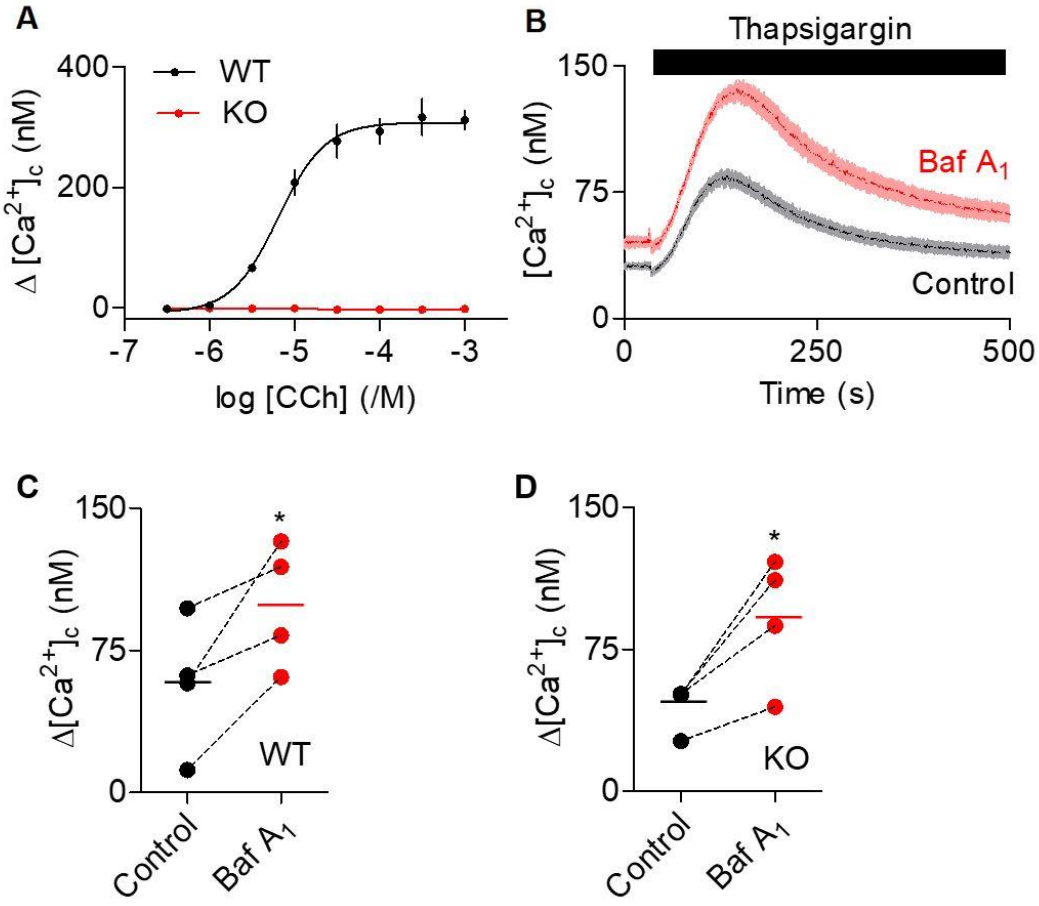

Figure 3.23 **Bafilomycin A_1 exaggerates thapsigargin-evoked increases in $[Ca^{2+}]_c$ in HEK cells lacking IP_3Rs.** (A) Concentration-dependent effects of CCh on Ca^{2+} release in wild-type (WT) HEK cells and HEK cells without IP_3Rs (KO) cells (means ± SEM, n = 3 independent experiments). (B) HEK cells were treated with Baf A_1 (1 μM, 1 h) in HBS before addition of BAPTA (2.5 mM) and thapsigargin (1 μM). Typical results show means ± SD from 3 wells in a single experiment. (C-D) Summary results of experiments described in B show thapsigargin-evoked release in WT cells (C) and KO cells (D) with or without Baf A_1. Results (C and D) are mean values from 4 experiments, with triplicate determinations in each. $^*P < 0.05$, paired Student's t test.

To assess the role of IP_3R in the physical affiliation of ER and lysosomes, firstly, I used fluorescent markers to label ER and lysosome membranes and secondly *in situ* proximity ligation assay (PLA). In mammalian cells, fluorescently labelling the ER and lysosomes has been used to report an intimate interaction between the two organelles (Lopez Sanjurjo *et al.*, 2013; Rowland *et al.*, 2014; Garrity *et al.*, 2016).

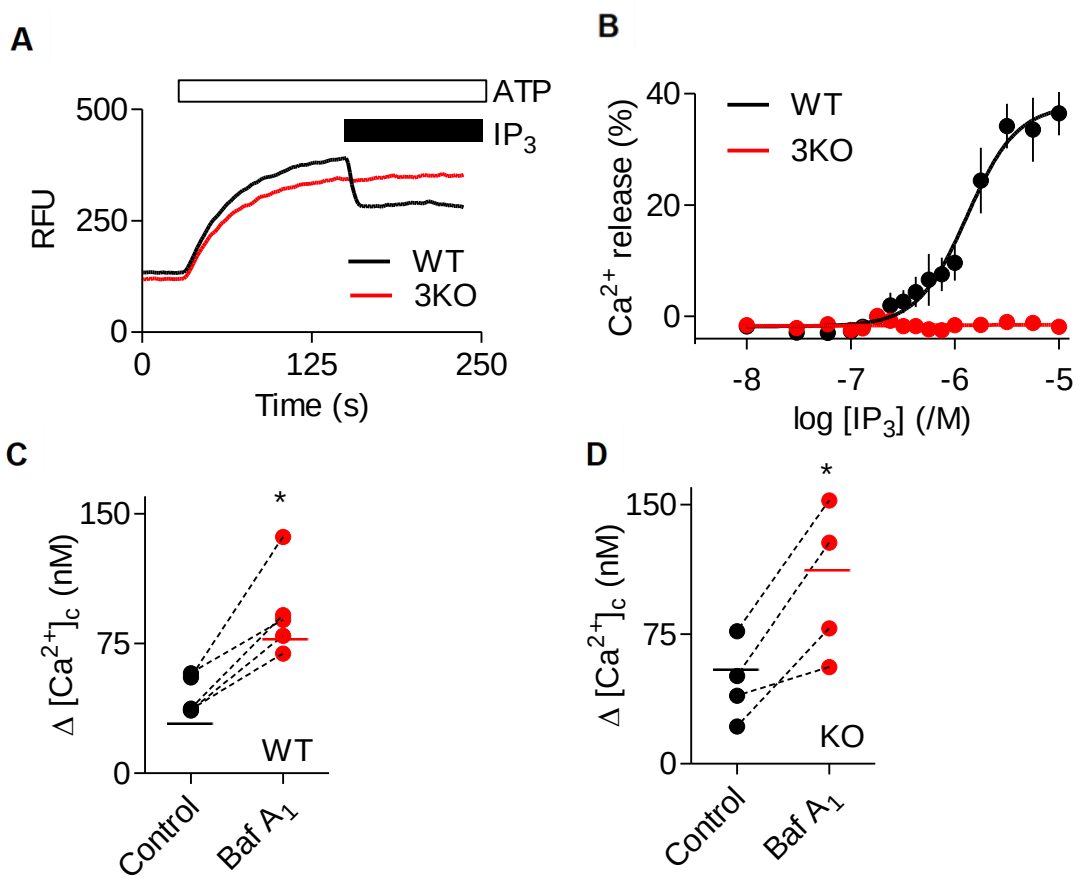

Figure 3.24 **Bafilomycin A_1 exaggerates thapsigargin-evoked increases in $[Ca^{2+}]_c$ in the HAP1 cells lacking IP_3Rs.** (A) Effect of IP_3 on Ca^{2+} release from the ER in HAP1-WT and HAP1-KO cells. Typical results show means ± SD from 3 wells in a single experiment. (B) HAP1 cells were treated with Baf A_1 (1 µM, 1 h) in HBS before addition of BAPTA (2.5 mM) and then thapsigargin (1 µM). Typical results show means ± SD from 3 wells in a single experiment. (C, D) Summary results (n = 4-5, with triplicate determinations in each) show the peak thapsigargin-evoked Ca^{2+} release in WT (C) and KO cells (D). $^{*}P < 0.05$ paired Student's *t*-test. Results in A and B were obtained by Stefania Matargka.

Using TIRF microscopy, there was a clear affiliation between lysosomes and the ER, with the majority of lysosomes residing close to the ER for prolonged periods (Figure 3.25). In HEK WT cells, lysosomes reside on ER tubules for up to 100s (Figure 3.26). Analogous interactions have been reported previously (Lopez Sanjurjo *et al.*, 2013; Garrity *et al.*, 2016). Similar results were obtained in HEK KO cells which lack IP_3R, where lysosomes also sit at ER tubules for prolonged periods (Figure 3.26B). This result also suggest that the affiliations between the ER and lysosomes remain in the absence of IP_3R.

The intimate relationship between lysosomes and IP_3R has been previously described (Lopez-Sanjurjo *et al.*, 2013). In HeLa cells, in which IP_3R1 was endogenously tagged with EGFP, (EGFP-IP_3R1-Hela cells) (Thillaiappan *et al.*, 2017), most lysosomes were mobile, but they often paused, sometimes for tens of seconds, at IP_3R puncta. Lysosomes were also observed to park at IP_3R puncta for a prolonged period and jump from one IP_3R cluster to another These features have been described by Dr. Thillaiappan in a recent publication (Atakpa *et al.*, 2018).

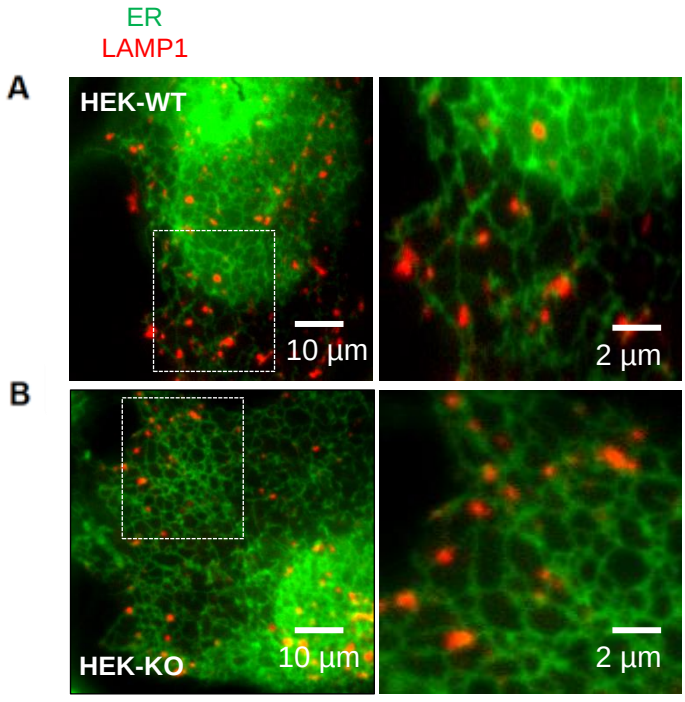

Figure 3.25 **IP_3Rs are not required to sustain ER-lysosome contacts.** TIRFM images of wild-type HEK cells (WT) (A) and HEK cells lacking IP_3Rs (KO) (B), expressing mCherry-LAMP1 and EGFP-ER. Enlargements of the boxed region (right) show intimate interactions between lysosomes and the ER in WT and KO cells.

Although, TIRF microscopy is useful in showing the trafficking of lysosomes and ER, one limitation is that because it is diffraction-limited, it does not provide accurate information about junctions between organelles (< 50 nm apart). Therefore, I used PLA to investigate ER-lysosome MCS in HEK WT and HEK-IP_3RKO cells (see **Section 2.8**). This assay reveals the proximity (<40 nm) between two proteins by fluorescent dots. PLA has been used previously to investigate ER-mitochondria junctions, where they revealed IP_3R-VDAC interactions (Honrath *et al.*, 2017; Thivolet *et al.*, 2017).

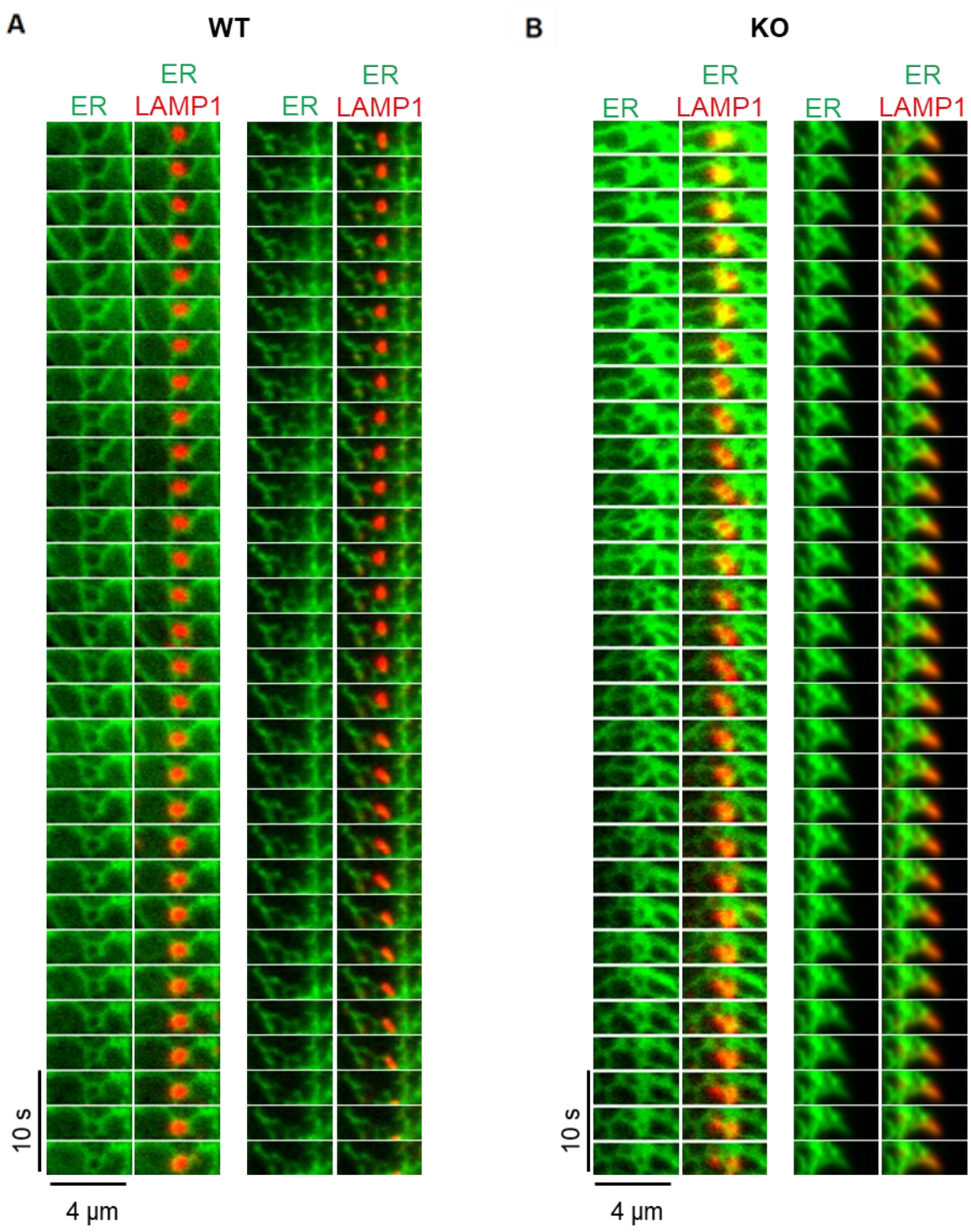

Figure 3.26 **Lysosomes reside for long periods on ER tubules in HEK cells**. (A-B) Time series from experiments similar to those described in Figure 3.25 (shown at 3-s intervals) show the dynamics of ER-lysosomes interactions. Lysosomes remain in stable contact with the ER for prolonged periods in WT (A) and KO (B) cells. Brightness and contrast were auto-adjusted to mitigate the effects of bleaching.

To investigate ER-lysosome junctions, antibodies to VAP-A (ER) and Rab7 (lysosomes) were used, as they have been reported to occur at multiple ER-lysosome junctions (Rocha *et al.*, 2009; Alpy *et al.*, 2013; Raiborg *et al.*, 2015). PLA utilising antibodies to endogenous VAP-A and Rab7, detected many spots in HEK cells indicative of VAP-A/Rab7 proximity (MCS) (Figure 3.27). When either primary antibody was omitted, the PLA dots were almost abolished confirming the specificity of the PLA (Figure 3.27). The number of PLA dots per cell was reduced following treatment with concanamycin A, but the number was not different in HEK cells with and without IP_3Rs (Figure 3.27C). This suggests that endogenous VAPA and Rab7 occur at MCS in HEK cells. This MCS is not affected by loss of IP_3R, but disrupted following treatment with concanamycin A.

The PLA technique was also used by Dr. Thillaiappan (described in Atakpa *et al*., 2018), to investigate whether IP_3R reside in close proximity to lysosomes using antibodies to Rab7 and GFP to identify endogenously tagged EGFP-IP_3R1. PLA detected many spots in EGFP-IP_3R1-Hela cells indicating IP_3R/Rab7 proximity, but not in WT cells with no EGFP tags. This confirms the specificity of the PLA (Atakpa *et al*., 2018). The number of PLA spots detected was significantly reduced following treatment with concanamycin A for 1 h (Atakpa *et al*., 2018). Furthermore, in these cells, EGFP-IP_3R puncta and the PLA spots indicative of VAP-A/Rab7 proximity were significantly colocalized (Mander's colocalization coefficient, 0.62 ± 0.16, $n = 10$ cells, Coste's *P*-value, 100%) (Atakpa et al 2018). This shows that the MCS between ER and lysosomes (revealed by the proximity of VAP-A and Rab7) are populated by IP_3R puncta. This indicates that lysosomes associate with regions of ER where there are IP_3R puncta.

Collectively, the results show that IP_3Rs associate with stable ER-lysosome MCS, but they are not required for their assembly. Increasing pH_{ly} causes a redistribution of lysosomes and disrupts these junctions thereby affecting lysosome Ca^{2+} uptake (Figure 3.28).

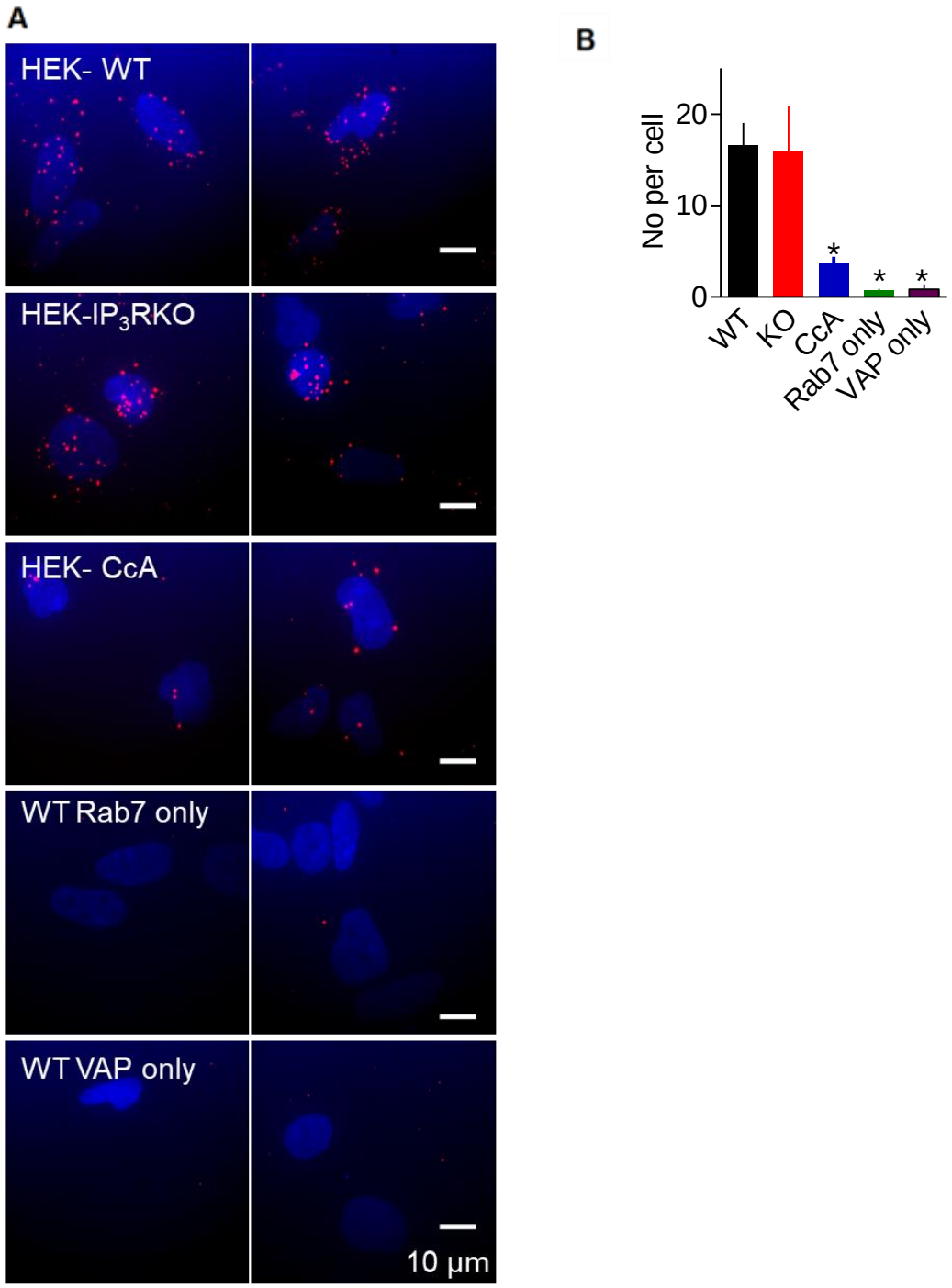

Figure 3.27 **PLA Analyses show IP$_3$Rs at ER-Lysosome MCS.** (A) Images of HEK cells with (WT) and without (KO) IP$_3$Rs from PLA analyses of VAP-A proximity to Rab7. Confocal maximum intensity Z-projections show PLA spots (red) and nuclei (blue). Effects of CcA (1 µM, 1 h) and omission of either primary antibody (Ab) are shown. (B) Summary results (mean ± SD, *n* = 15-25 cells from 3 experiments (2 experiments for single-antibody) controls) show number of PLA spots/cell. $P < 0.05$, one-way ANOVA with Dunnett's test, relative to WT control.

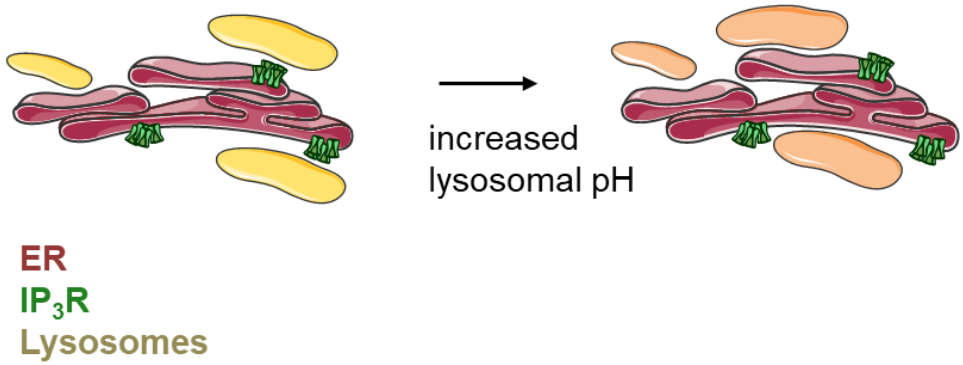

Figure 3.28 **Dissipating pH_{ly} gradient does not immediately prevent lysosomal Ca^{2+} uptake, but slowly disrupts junctions within which it occurs.** Most lysosomes are closely associated, probably by tethers, with ER at MCS populated by small clusters of IP_3Rs. Increasing the pH_{ly} affects the distribution of lysosomes, thereby disrupting ER-lysosome junctions.

3.4 Conclusions

I have shown that dissipating the pH_{ly} gradient pharmacologically or genetically unmasks the selective sequestration by lysosomes of Ca^{2+} released from the ER by IP_3R (**Section 3.3.1**), but not Ca^{2+} entering the cell via SOCE (**Section 3.3.2**). This corresponds with previous observations (Lopez-Sanjurjo *et al.*, 2013). In addition, the use of a low-affinity Ca^{2+} sensor tuned to detect peri-lysosomal Ca^{2+} reported that IP_3Rs, but not SOCE, delivers Ca^{2+} selectively to the surface of a large subset of lysosomes (**Section 3.3.3**). This suggests that lysosomes are preferentially situated in specialised areas of the cells to allow the occurrence of Ca^{2+} microdomains to fuel a low-affinity Ca^{2+} uptake system into lysosomes.

My results also suggest that all IP_3R subtypes can deliver their Ca^{2+} to lysosomes (**Section 3.3.4**). Although it is established that dissipating the lysosomal H^+ gradient inhibits Ca^{2+} uptake, there is a large temporal mismatch between the effects of concanamycin A on pH_{ly} and attenuated Ca^{2+} uptake, with the latter developing much more slowly (**Section 3.3.5**). I conclude that lysosomes can, at least acutely, accumulate Ca^{2+} in the absence of a pH gradient.

IP_3Rs associate with stable ER-lysosome MCS, but they are not required for their assembly since exchange of Ca^{2+} between the ER and lysosomes persists in the absence of IP_3R (**Section 3.3.6**). I suggest that the inability of lysosomes to sequester Ca^{2+} released from the

ER after sustained inhibition of the V-ATPase results from a disruption of the MCS between lysosomes and ER at which the Ca^{2+} transfer occurs. The ER, with its high-affinity SERCA and large-conductance Ca^{2+} channels, behaves like a compressor or piston linking a low $[Ca^{2+}]_c$ to the low-affinity uptake systems of organelles at specialised junctions (Figure 3.29).

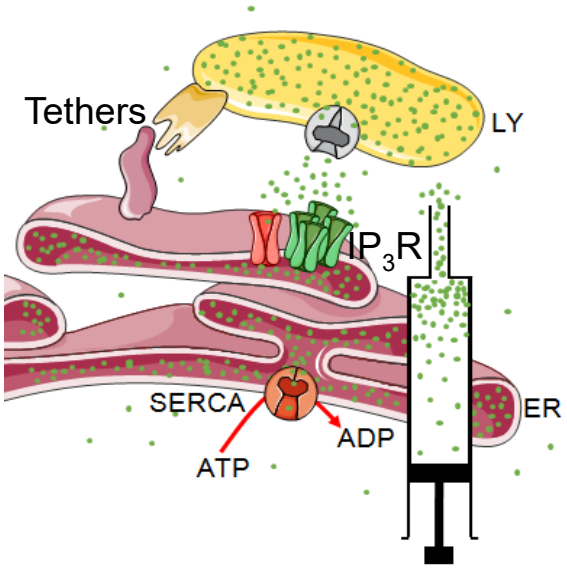

Figure 3.29 **The ER delivers Ca^{2+} to lysosomes in a piston-like manner at junctions populated by IP_3R**. Delivery of Ca^{2+} through IP_3Rs or unidentified 'leak channels' into MCS provides a low-affinity Ca^{2+} uptake system in lysosomes with the high local $[Ca^{2+}]$ required for its activity. The ER, with its high-affinity Ca^{2+} pump (SERCA) accumulates Ca^{2+} from cytosol, and delivers it at high local concentration to the surface of lysosomes through large-conductance IP_3Rs. ER behaves as an ATP-powered piston to concentrate Ca^{2+} around the lysosomal uptake system.

4. GPN evokes Ca^{2+} release from the ER by increasing cytosolic pH independent of lysosomes and cathepsin C

4.1. Introduction

4.1.1 Glycyl-L-phenylalanine-2-naphthylamide as a cathepsin C substrate used to study lysosomal biology

Glycyl-L-phenylalanine 2-naphthylamide (GPN) (see Figure 4.1A for its structure) is a frequently used lysosome-perturbing treatment. A search on PubMed Central on GPN returns ~100 articles. GPN has been widely used as a selective tool to release lysosomal Ca^{2+} (Berg *et al.*, 1994; Haller *et al.*, 1996; Churchill *et al.*, 2002; Morgan & Galione, 2007; Dionisio *et al.*, 2011; Coen *et al.*, 2012; Davis *et al.*, 2012; Kilpatrick *et al.*, 2013; Ruas *et al.*, 2015; Melchionda *et al.*, 2016). However, GPN has also been used to disrupt lysosomes during autophagy (Thurston *et al.*, 2012; Berezhnov *et al.*, 2016), nutrient sensing (Sbano *et al.*, 2017), lysosomal ionic balance (Steinberg *et al.*, 2010; Chakraborty & Leung, 2017) and other lysosomal functions (Liu *et al.*, 2012; Sbano *et al.*, 2017). GPN is a substrate of the lysosomal enzyme, cathepsin C, and it has long been believed to cause selective and transient permeabilization of lysosomes in cells (Berg *et al.*, 1994; Haller *et al.*, 1996; Churchill *et al.*, 2002; Morgan & Galione, 2007; Dionisio *et al.*, 2011; Coen *et al.*, 2012; Davis *et al.*, 2012; Kilpatrick *et al.*, 2013; Ruas *et al.*, 2015; Melchionda *et al.*, 2016).

Cathepsin C, also called dipeptidyl peptidase 1 or CTSC, is one of over 50 identified hydrolases in lysosomes. Eleven cysteine cathepsins have been identified, including cathepsins B, C, F, H, K, L, O, S, V and X (Repnik *et al.*, 2012). Cathepsin C was first discovered in the 1940s (Gutmann & Fruton, 1948), and its cDNA was sequenced in the 1990s (Paris *et al.*, 1995). Cathepsin C is a tetramer, with four identical subunits, Each subunit comprises an N-terminal fragment, also known as the residual propart domain, a heavy chain and a light chain (Dolenc *et al.*, 1995; Cigic *et al.*, 1998). Cathepsin C primarily acts as a non-specific amino dipeptidase that cleaves two-residue units from the N-terminus of polypeptides (Turk *et al.*, 1998). However, at high pH, cathepsin C has been reported to also act as a transferase to drive the reaction in the opposite direction (Planta *et al.*, 1964; McGuire *et al.*, 1992). Cathepsin C cleaves 2-residue units until the C-terminus is reached or an arginine or lysine residue is encountered at the N-terminus (McGuire *et al.*, 1992). Cathepsin C is also thought not to cleave when proline is present on either side of the peptide

bond of a substrate (McGuire *et al.*, 1992). The targeting of cathepsin B, D and L to lysosomes is dependent on the M6P receptor, which is specifically involved in the targeting of proteins to the lysosomal lumen (Pohlmann *et al.*, 1995; Probst *et al.*, 2006). Furthermore, immunofluorescent labelling of other cathepsins, particularly cathepsin D, shows a punctate structure that colocalises with lysosomal markers (Probst *et al.*, 2006; Jin & Mills, 2014). Cathepsin C colocalises with LAMP1 in hippocampal pyramidal neurons (Koike *et al.*, 2013). Although some cathepsins have been reported to be present in the nucleus (Goulet *et al.*, 2004; Duncan *et al.*, 2008), most of the identified functions of cathepsins are related to their proteolytic activity in lysosomes.

Studies using pharmacological inhibitors have been very important in elucidating the functions of cathepsin C. Cystatin F (Hamilton *et al.*, 2008) and E-64 (Towatari *et al.*, 1991) are naturally occurring non-selective cysteine proteases that have been shown to inhibit cathepsin C activity at high concentrations. However, their lack of specificity limits their use in the selective characterisation of cathepsin C functions. Other cathepsin C inhibitors include diazomethylketones (Kam *et al.*, 2004), vinyl sulfones (Korver *et al.*, 2001) and semi-carbazides (Bondebjerg *et al.*, 2005). Of these, Gly-Phe-diazomethylketone (Gly-Phe-DMK) is widely used to selectively inhibit cathepsin C, with no significant effect on other proteases (Thiele & Lipsky, 1990; McGuire *et al.*, 1993; Repnik *et al.*, 2017). Previous work has shown that inhibition of other cathepsins such as cathepsins B, L and S (but not C) does not prevent the effects of GPN (Gerasimenko *et al.*, 2006; Lopez-Sanjurjo *et al.*, 2013). However, the effect of cathepsin C inhibition on GPN-mediated effects on lysosomes remains largely unexplored.

4.1.2 Lysosomotropic agents

Lysosomes are susceptible to the trapping of basic compounds due to their very acidic luminal pH. Lysosomotropic agents are basic lipophilic compounds that can freely permeate the PM and accumulate in lysosomes where they become protonated. The now charged molecule is trapped in the lysosomal lumen and cannot freely diffuse back into the cytosol (de Duve *et al.*, 1974; Villamil Giraldo *et al.*, 2014). This pH partitioning drives the accumulation of these compounds to concentrations up to 100 fold higher in lysosomes compared to the cytosol (Oda *et al.*, 1986). This accumulation is widely referred to as lysosomotropism. A previous screen to identify lysosomotropic drugs found this property across structurally and functionally diverse classes of pharmacological agents such as

antimalarial drugs, antidepressants and anticancer drugs (Nadanaciva *et al.*, 2011). However, the physiochemical properties of these drugs were similar, with all of the lysosomotropic agents having a Clog*P* (Clog*P* refers to the logarithm of the partition coefficient between n-octanol and water, a measure of hydrophilicity) greater than 2, and a basic pKa above 6.5 (Nadanaciva *et al.*, 2011). This observation agrees with a previous suggestion that the lipophilicity and basic property of a compound could make it prone to lysosomal accumulation (de Duve *et al.*, 1974). Lysosomotropism is also linked to drug-induced toxicity. A screen of currently licenced pharmaceuticals found that compounds with lysosomotropic profiles increase lysosomal volume, induce DNA fragmentation and alter the size of the nucleus (Lu *et al.*, 2012). GPN has been reported to be a weak base and slightly hydrophobic (Jadot *et al.*, 1984). However, the lysosomotropic tendency of GPN, as well as the interplay between the lysosomotropic effects of GPN and its reported effects on lysosomal Ca^{2+} and pH, have been largely unexplored.

4.1.3 Lysosomal membrane permeabilization

Lysosomotropism has been linked to lysosomal membrane permeabilization (LMP) and cytotoxicity (Lu *et al.*, 2012; Villamil Giraldo *et al.*, 2014). The unusually harsh proteolytic and acidic lumen of lysosomes is encapsulated by a single membrane, protecting the cytosol and the rest of the cell from lysosomal contents. Substantial damage to the lysosomal membrane could, therefore, breach this protection and lead to the release of lysosomal contents, potentially introducing hydrolytic enzymes into the cytosol as well as leading to cytosolic acidification (Guicciardi *et al.*, 2004; Terman *et al.*, 2006). Complete or partial permeabilization of the lysosomal membrane has been reported to induce necrosis (Kagedal *et al.*, 2001) or apoptosis (Li *et al.*, 2000), respectively. Compounds reported to induce LMP include detergents such as O-methyl-serine dodecylamine hydrochloride (MSDH) (Dubowchik *et al.*, 1995) and L-leucyl-L-leucine methyl ester (LeuLeuOMe) (Uchimoto *et al.*, 1999). Sphingosine, a naturally occurring phospholipid precursor, has also been reported to induce LMP through a cathepsin-mediated mechanism (Kagedal *et al.*, 2001; Werneburg *et al.*, 2002; Ullio *et al.*, 2012). Examples of lysosomotropic agents reported to induce LMP include chloroquine (Geng *et al.*, 2010), chlorpromazine (Ch'Ng *et al.*, 2011), thioridazine (Ashoor *et al.*, 2013), desipramine (Honegger *et al.*, 1983) and imipramine (Lu *et al.*, 2017). LMP has also been reported to occur following non-pharmacological stimuli such as following oxidative stress (Terman *et al.*, 2006) and DNA damage (Emert-Sedlak *et al.*, 2005; Paquet *et al.*, 2005). It is also not clear if all or only a subset of lysosomes are

susceptible to LMP (Guicciardi *et al.*, 2004). The mechanism of LMP are poorly understood however, LeuLeuOMe is believed to polymerise in a cathepsin C-dependent manner (Repnik *et al.*, 2017). The polymer is membranolytic and leads to damage of lysosomal membranes. Damaged lysosomes are reported to rapidly recruit endosomal sorting complex required for transport (ESCRT) machinery which promotes membrane repair (Skowyra *et al.*, 2018).

The major techniques used in detect LMP include the use of antibodies to show redistribution of lysosomal proteins such as cathepsins into the cytosol following damage to the lysosomal membrane. For example, immunofluorescent labelling of cathepsin B in healthy cells usually shows punctate structures in regions of the cells that co-localise with lysosomal markers. However, following LMP, cathepsin B appears diffusely in the cytosol (Boya *et al.*, 2003). Furthermore, subcellular fractionation has revealed the translocation of lysosomal proteases following LMP (Michallet *et al.*, 2004). Similar results have been reported using optical microscopy techniques visualising LMP through fluorescently labelled lysosomal proteases (Werneburg *et al.*, 2002; Werneburg *et al.*, 2007). Another means of detecting LMP is the use of fluorescent molecules that can be directed to the lysosomal lumen. Lysosomotropic probes are fluorophores conjugated to basic moieties allowing their accumulation in lysosomes via pH partitioning. The LysoTracker dyes are examples of lysosomotropic probes, and have been widely used in studies of lysosomes (Akazawa *et al.*, 2009; Brailoiu *et al.*, 2009; Demaegd *et al.*, 2013; Lopez-Sanjurjo *et al.*, 2013). The reduction in LysoTracker fluorescence is commonly claimed to report LMP (Kilpatrick *et al.*, 2013; Repnik *et al.*, 2017). However, it is important to consider that this reduction could also be an indication of the increase in the pH_{ly} and is therefore not an exclusive reporter of LMP. Acridine orange (AO) is another marker of LMP. It is also lysosomotropic and emits red fluorescence when accumulated in lysosomes, and green florescence when in the cytosol and nucleus (Antunes *et al.*, 2001; Boya *et al.*, 2003; Michallet *et al.*, 2004; Trincheri *et al.*, 2007). However, due to its lysosomotropic property, attributing its change in fluorescence to LMP may be erroneous as any change in the pH of the compartment could alter AO distribution. A third means of detecting LMP is using Dx-conjugated fluorophores of different sizes, which can be directed to the lysosomal lumen by hijacking the endocytic machinery. The dextrans are taken up via endocytosis and then allowed to travel along the pathway until they reach the terminal parts of the endo/lysosomal pathway. Staurosporine, an LMP-inducing agent, was shown to result in the loss of dextran lower than 40 kDa from lysosomes into the cytosol, and retention of 70-kDa and 250-kDa dextrans (Bidere *et al.*, 2003).

The conventional explanation for the mechanism of action of GPN suggests that cathepsin C cleaves GPN into the dipeptide and naphthylamide group (Figure 4.1). The dipeptides are unable to diffuse across the lysosomal membrane due to their polarity, and this leads to an osmotic build up in lysosomes and an eventual bursting of their membrane. However, the evidence for this is not clear. Furthermore, following a disruptive fractionation protocol, GPN was shown to result in loss of an endocytosed ligand from the lysosomes in cell-free preparations (Berg *et al.*, 1994). This work has largely provided the basis for the widely accepted view that the activity of GPN is due to the osmotic permeabilization of lysosomes in a cathepsin C-dependent manner. However, considering this work was carried out in isolated liver fractions, it is important to carefully evaluate the mechanism of action of GPN in intact cells. GPN has also been shown to result in the loss of lysosomotropic dyes such as LysoTracker in MCDK cells (Haller *et al.*, 1996). The effects of short-term treatments with GPN are thought to be reversible. It has been reported that removal of GPN allows the re-accumulation of lysosomotropic dyes by an unknown mechanism; membrane resealing has been suggested (Steinberg *et al.*, 2010). Studies utilising dextran targeted to lysosomes have suggested a size cut-off of the pores at >10 kDa, as dextrans of 10 kDa and above were retained in lysosomes (Steinberg *et al.*, 2010; Penny *et al.*, 2014). In summary, the evidence for the widely accepted view that GPN induces permeabilization of the lysosomal membrane is not well substantiated by the literature.

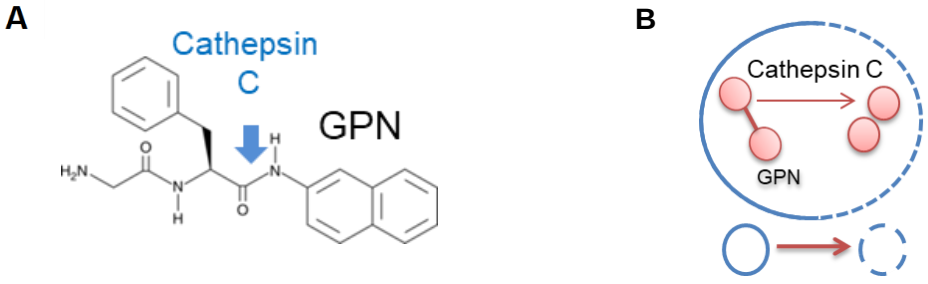

Figure 4.1 **GPN is a cathepsin C substrate.** (A) GPN is cleaved by cathepsin C (blue arrow) to release the naphthylamine group. (B) The cleavage of GPN by cathepsin C is proposed to lead to an acute osmotic swelling and permeabilization of the lysosomal membrane to allow the release of lysosomal luminal contents.

4.1.4 GPN and lysosomal Ca^{2+}

GPN has been used as a means of selectively releasing lysosomal Ca^{2+}. Inhibition of cathepsins, other than cathepsin C, does not affect GPN-mediated effects on $[Ca^{2+}]_c$ (Gerasimenko, 2006; Steen *et al.*, 2007; Lopez Sanjurjo *et al.*, 2013). However, the contribution of ER and lysosomes to GPN-mediated Ca^{2+} signals is not clear. Especially as GPN-induced Ca^{2+} release from lysosomes is believed to diffuse towards the ER and activate ER CICR channels, amplifying the initial Ca^{2+} signal (Kilpatrick *et al.*, 2013; Morgan *et al.*, 2015) in a similar way to physiological stimuli such as NAADP (Morgan, 2011b). GPN-mediated increase in $[Ca^{2+}]_c$ is massively attenuated following emptying of the ER in monocytes (Sivaramakrishnan *et al.*, 2012), fibroblasts (Kilpatrick *et al.*, 2013), lymphocytes (Steen *et al.*, 2007) and in epithelial cells (Haller *et al.*, 1996). However, in human lymphoblasts, GPN remains able to induce Ca^{2+} signals following treatment with thapsigargin or ionomycin (Lloyd-Evans *et al.*, 2008).

The work presented in this chapter investigates the mechanism of action of GPN and its selectivity for lysosomes.

4.2 Materials and Methods

All materials and methods have been described in chapter 2.

4.3 Results and Discussion

4.3.1 GPN evokes pH changes and Ca^{2+} signals without rupturing lysosomes

The mechanism of action of GPN is largely thought to be due to the osmotic permeabilization of lysosomes following its cleavage by cathepsin C (Figure 4.1).

Oregon Green-Dx, fluorescein-Dx and LysoTracker Red were used to assess pH_{ly}. The pKa of Oregon Green-Dx (4.7) is optimal for measurements of pH_{ly} (Sabnis, 2015). Fluorescein is also pH-sensitive with a higher pKa of 6.3 (Canton & Grinstein, 2015). Oregon Green-Dx (10 kDa) (Christensen *et al.*, 2002; Haggie & Verkman, 2007; Weinert *et al.*, 2010) and fluorescein-Dx (Christensen *et al.*, 2002; Weinert *et al.*, 2010; Lelouvier & Puertollano, 2011; Voronov *et al.*, 2013; Penny *et al.*, 2014; Johnson *et al.*, 2016) have been routinely used in the study of lysosomal biology.

The fluorescence intensity of Oregon Green (Lopez-Sanjurjo *et al.*, 2013) and fluorescein (Aits *et al.*, 2015) is greatly reduced at very low pH, such as found in lysosomes. A shift to a more alkaline pH causes an increase in fluorescence. GPN acutely caused fluorescence to decrease for LysoTracker Red and increase for Oregon Green-Dx (10 kDa) and fluorescein-Dx (3 kDa) (Figure 4.2, Table 4.1). pH_{ly} did not recover following prolonged treatment with GPN in HEK cells (Figure 4.3). Therefore, GPN causes a sustained increase in pH_{ly}.

GPN induced a transient increase in $[Ca^{2+}]_c$ in cells bathed in Ca^{2+}-free HBS, showing that this Ca^{2+} is mobilised from intracellular stores (Figure 4.4A). The Ca^{2+} signals evoked by GPN were slower than those evoked by carbachol, which stimulates IP_3 formation and Ca^{2+} release through IP_3Rs, but faster than those evoked by inhibiting the ER Ca^{2+} pump (SERCA) with thapsigargin (Figure 4.4B, C). While these results are consistent with the reported actions of GPN, additional observations are not consistent with its presumed mode of action (Figure 4.1B).

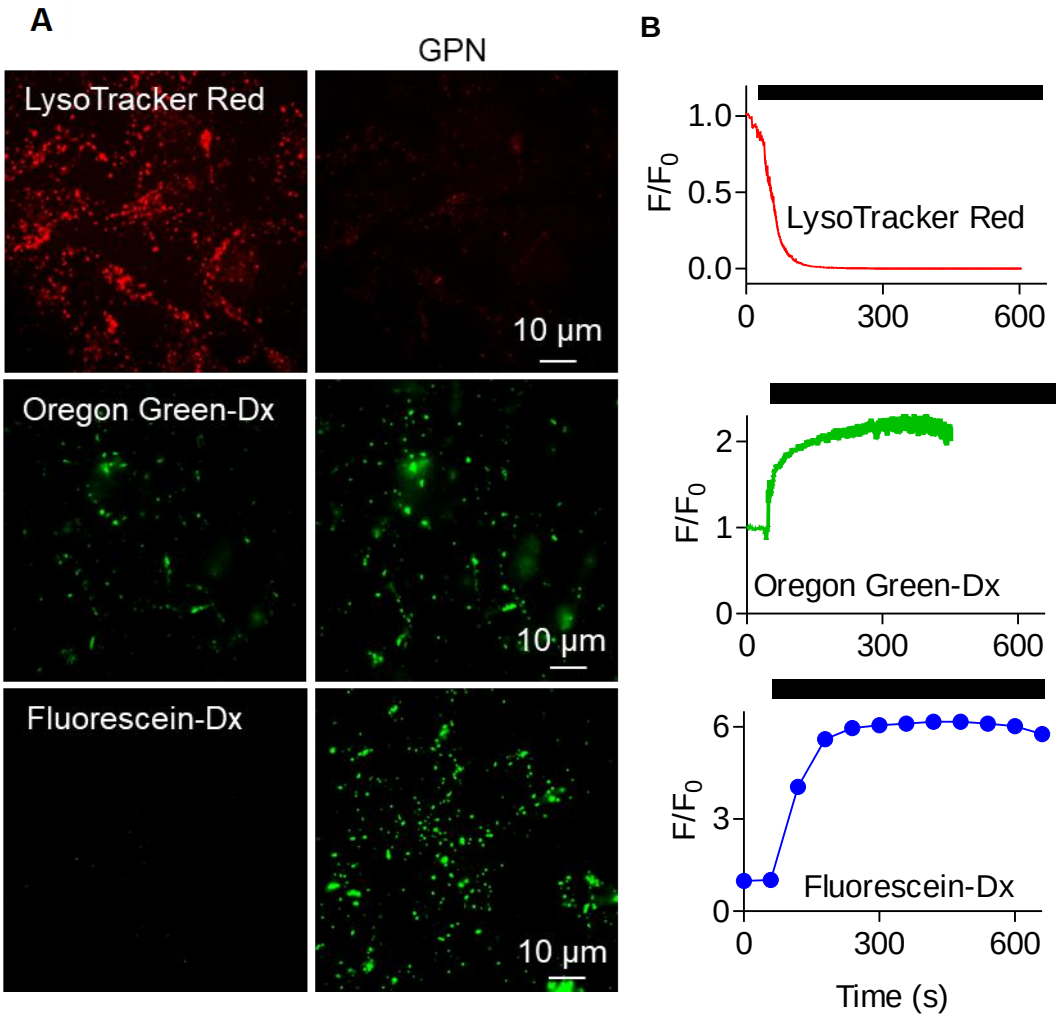

Figure 4.2 **GPN increases pH_{ly} in HEK cells.** (A) Wide-field images of HEK cells loaded with LysoTracker Red or Dx conjugates of Oregon Green-Dx (10 kDa) or fluorescein-Dx (3 kDa) show an increase in pH_{ly} after addition of GPN (200 µM, 200 s). (B) Time courses of GPN-evoked pH_{ly} changes. Each trace shows mean ± SD from 3-4 ROIs in a single cell.

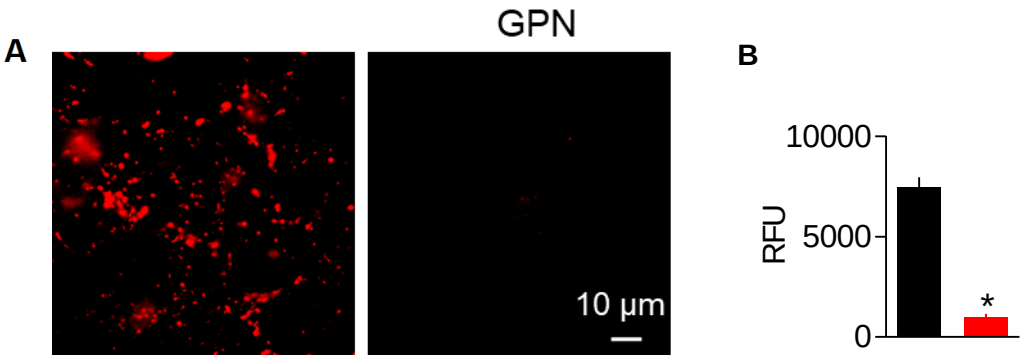

Figure 4.3 **pH_{ly} does not recover after prolonged treatment with GPN** (A) Wide-field images show LysoTracker Red staining (100 nM, 20 min) of HEK cells with and without GPN (200 µM, 30 min). (B) Summary results (mean ± SEM, n = 4 coverslips) show the intensity of LysoTracker Red staining. $^{*}P < 0.05$, Student's t-test. RFU, Relative fluorescence unit.

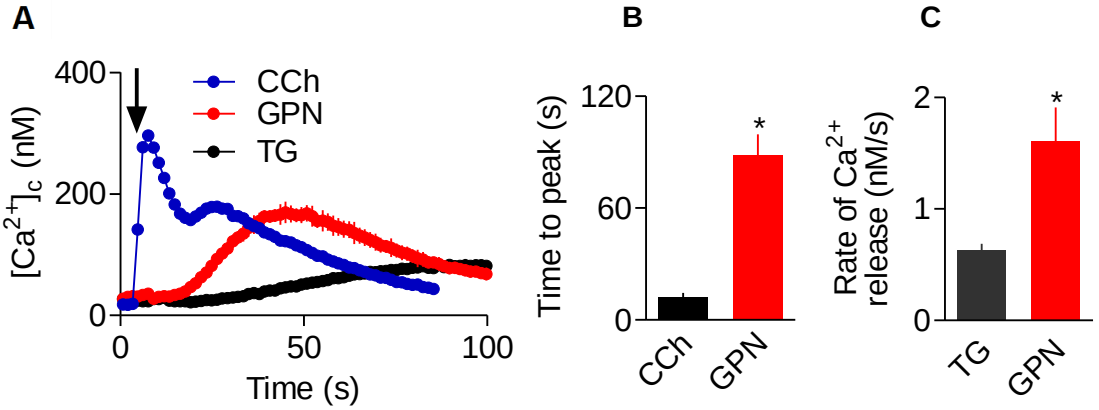

Figure 4.4 **GPN-induced increase in $[Ca^{2+}]_c$ is faster than that evoked by CCh, but slower than that evoked by thapsigargin.** (A) Initial responses of HEK cells to carbachol (CCh, 1 mM), GPN (200 µM) or thapsigargin (TG, 1 µM) in Ca^{2+}-free HBS (mean ± SD of 3 replicates). Arrow shows point of addition. (B) From experiments similar to those in A, times to peak increase in $[Ca^{2+}]_c$ are shown (mean ± SEM, n = 4, with 3 replicates). $^{*}P < 0.05$, Student's t-test. (C) Similar analysis shows rates of rise of $[Ca^{2+}]_c$ after addition of GPN (200 µM) or thapsigargin (1 µM) in Ca^{2+}-free HBS, each measured over the same range of $[Ca^{2+}]_c$. Results show means ± SEM, n = 5, with 3 replicates. $^{*}P < 0.05$, Student's t-test.

The suggested disruptive mechanism of action of GPN, in which the formation of pores in the lysosomal membrane is believed to result in the loss of low-molecular weight lysosomal components including H^+, is expected to induce intracellular acidification (Guicciardi *et al.*, 2004; Terman *et al.*, 2006). This occurs, for example, when TNFα triggers loss of H^+ and cathepsin D from lysosomes during the early stages of apoptosis (Nilsson et al., 2006). However, the direct effect of GPN on cytosolic pH (pH_{cyt}) has hitherto not been explored. To investigate this, SNARF-5F, a ratiometric pH-sensitive dye was used to measure pH_{cyt}, because it allows for a reliable measurement minimising artefacts due to photobleaching, the variability of cell thickness, dye leakage and non-uniform loading of the indicator (Liu *et al.*, 2001). To allow direct comparison with GPN-mediated Ca^{2+} signals, all experiments were performed 30 s after addition of BAPTA (2.5 mM) to chelate extracellular Ca^{2+}. Under these conditions, GPN induced an increase in pH_{cyt} in HEK cells. GPN was obtained from Bachem (Lopez-Sanjurjo *et al.*, 2013) and from Santa Cruz (Kilpatrick *et al.*, 2013), two reliable and widely used sources of GPN. Following addition of GPN, there was a rapid increase in pH_{cyt} with a peak at approximately 50 s. The pH_{cyt} then returned to baseline after 10 min. (Figure 4.5A). The maximum change in pH_{cyt} following GPN in HEK cells was 0.35 ± 0.03 pH units following 400 µM GPN (Bachem) and 0.30 ± 0.03 following 400 µM GPN (Santa Cruz) (Figure 4.5B). Similar results were obtained in HeLa cells (Figure 4.5B).

As there was no difference in the kinetics of cytosolic alkalinization between the two sources of GPN, the rest of the experiments described were performed with GPN from Bachem. These results establish that GPN from two different sources induces an increase in pH_{cyt} in HEK and HeLa cells.

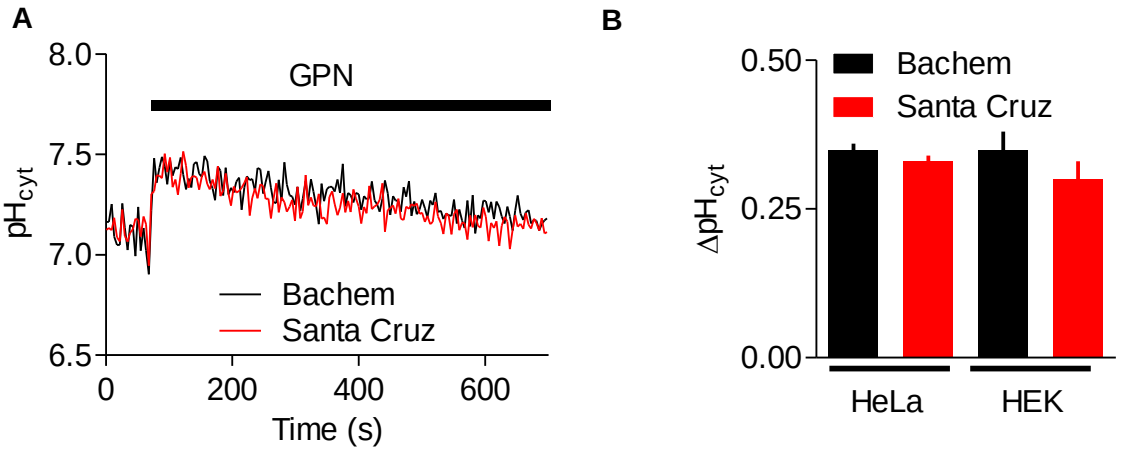

Figure 4.5 **GPN induces an acute cytosolic alkalinization in HEK cells.** (A) Populations of HEK cells loaded with SNARF-5F were stimulated in Ca^{2+}-free HBS with GPN (200 µM). 2.5 mM BAPTA was added to cells 30 s prior to GPN stimulation. (B) Summary results show the effects of GPN (200 µM) from the indicated suppliers on pH_{cyt} in HEK and HeLa cells. Results are mean ± SEM, n = 5.

The regulation of pH_{cyt} and pH_{ly} is intricately entangled. One possibility was that the effect of GPN on pH_{cyt} was intertwined with a permeabilization of lysosomes and consequent loss of the H^+ gradient. Therefore, the effect of the pH_{ly} gradient on the GPN-induced increase in pH_{cyt} was tested. Bafilomycin A_1 has been previously shown to abrogate the lysosomal H^+ gradient (**Chapter 3**). There was no significant difference between the basal pH_{cyt} in control cells and cells pre-treated with bafilomycin A_1 (Figure 4.6B). Furthermore, pre-treatment with bafilomycin A_1 did not affect the peak change in pH_{cyt} following treatment with GPN (Figure 4.6A, C). This establishes that the ability of GPN to increase pH_{cyt} is independent of the lysosomal H^+ gradient.

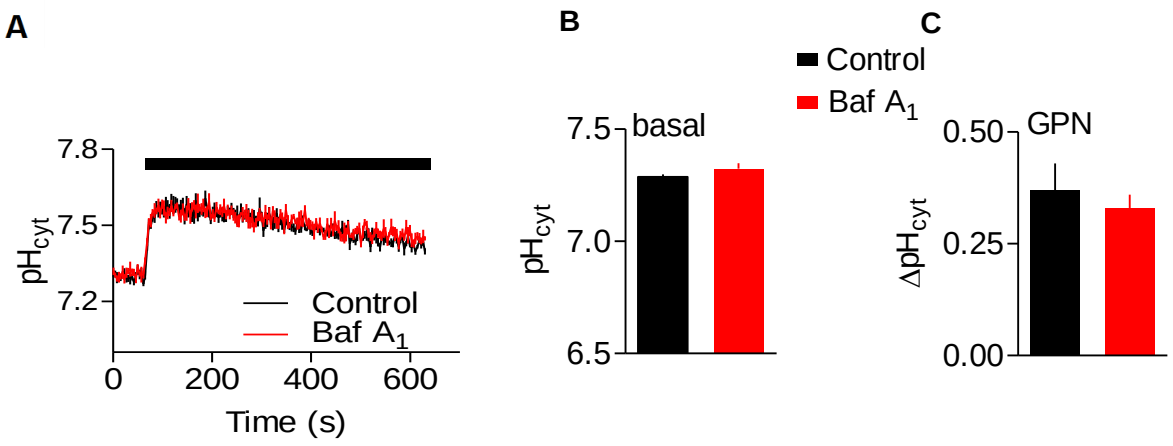

Figure 4.6 **GPN-induced increase in pH_{cyt} is independent of the lysosomal H^+ gradient.** (A) HEK cells loaded with SNARF-5F were stimulated in Ca^{2+}-free HBS with GPN (200 µM) with or without pre-treatment with bafilomycin A_1 (1 µM, 1 h). Results are mean ± SD for one experiment with triplicate determinations (B) Summary data shows the basal pH_{cyt} with or without bafilomycin A_1 pre-treatment (1 µM, 1 h). Results are mean ± SEM from 5 independent experiments. $P = 0.30$. (C) Summary data shows the peak change in pH_{cyt} with or without bafilomycin A_1 pre-treatment (1 µM, 1 h). Results are mean ± SEM from 5 independent experiments. $P = 0.37$, paired Student's *t*-test.

Overwhelmingly, the evidence for lysosomal membrane permeabilization arises from loss of acidotropic dyes such as LysoTracker Red (Kilpatrick *et al.*, 2013; Repnik *et al.*, 2017) and Acridine Orange (Antunes *et al.*, 2001; Boya *et al.*, 2003; Michallet *et al.*, 2004; Trincheri *et al.*, 2007), which will redistribute when pH_{ly} increases. GPN has been previously reported to result in the loss of low molecular weight dextran (< 10 kDa), purportedly due to a cathepsin C-dependent permeabilization (Penny *et al.*, 2014; Penny *et al.*, 2015).

In cells where LysoTracker accumulation was abolished by GPN, it did not acutely affect the number of lysosomes assessed by Alexa Fluor 488-Dx (10 kDa) (Figure 4.7). This is consistent with previous reports using rhodamine-Dx (10 kDa) (Penny *et al.*, 2014) and Oregon Green-Dx (Steinberg *et al.*, 2010; Penny *et al.*, 2014), that large-molecular weight components are not lost from lysosomes following treatment with GPN.

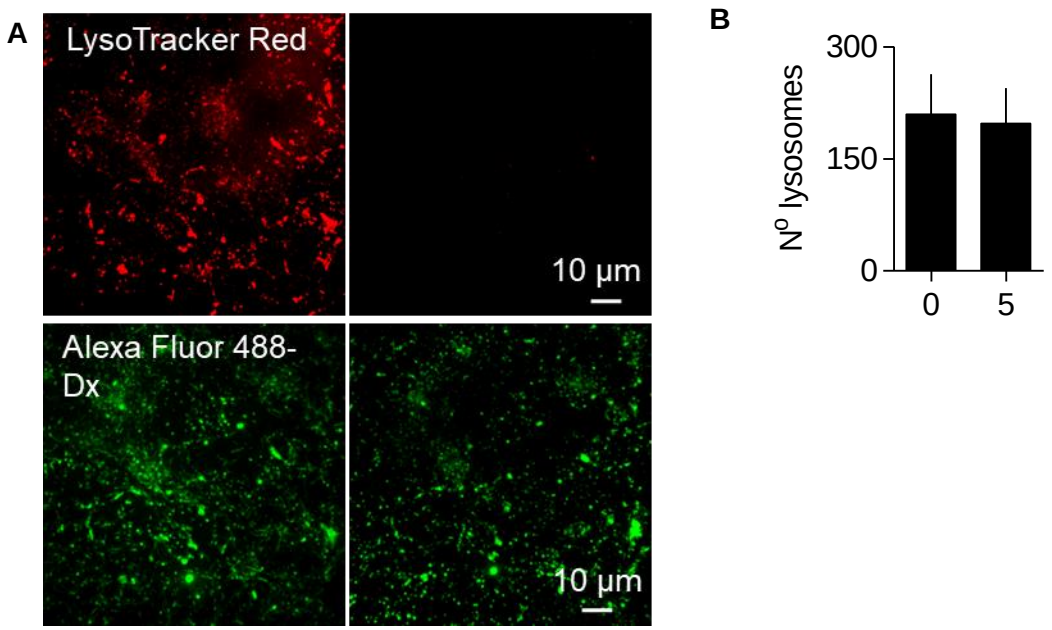

Figure 4.7 **GPN does not affect the distribution of Alexa Fluor 488-Dx.** (A) Simultaneous recording of LysoTracker Red and Alexa Fluor 488-Dx (M_r ~10,000) from HEK cells treated with GPN (300 µM) showing that an increase in pH_{ly} is not accompanied by loss of large molecules from lysosomes. (B) Summary results (mean ± SEM, *n* = 3 show the number of lysosomes identified by Alexa Fluor 488-Dx before and 5 mins after addition of GPN.

Lysosomes were also loaded with Lucifer Yellow (M_r 457). This low-molecular weight marker accumulates in lysosomes when loaded via the endocytic machinery (Yang *et al.*, 1998; Chaurra *et al.*, 2011; Bright *et al.*, 2016). In cells where lysosomes were loaded with Lucifer Yellow, GPN did not acutely affect the number lysosomes (Figure 4.8). Addition of GPN has been previously reported to result in a partial dissipation of Lucifer Yellow only in a sub-population of lysosomes in NRK cells (Bright *et al.*, 2016). However, at times matching GPN-evoked Ca^{2+} signals, there was no evidence of GPN-mediated loss of Lucifer Yellow accumulation.

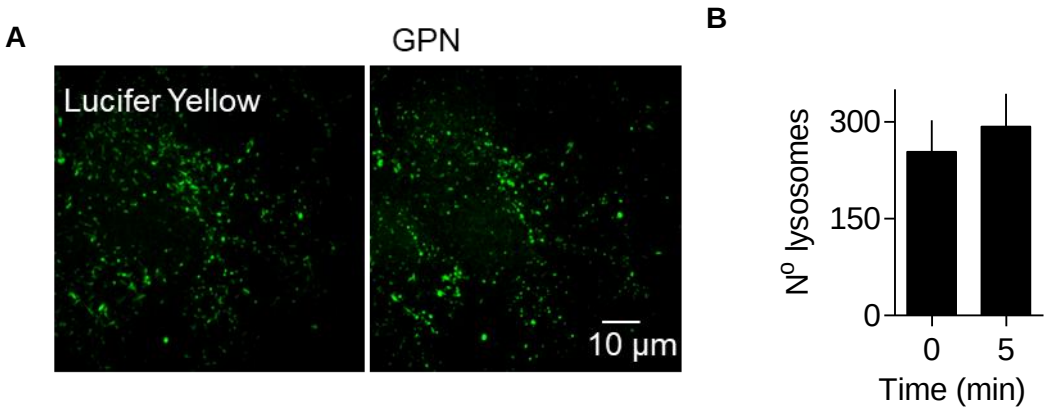

Figure 4.8 **GPN does not affect the distribution of Lucifer Yellow.** (A) Lack of effect of GPN (200 µM, 10 min) on the punctate fluorescence from endocytosed Lucifer Yellow (M_r 447). (B) Summary results (mean ± SEM, *n* = 5 show the number of lysosomes identified (per field of view) by Lucifer Yellow before and 5 mins after addition of GPN.

More prolonged incubations with GPN (>10 min) caused some loss of lysosomal Alexa Fluor 488-Dx, but even after 25 min most was retained by lysosomes (Atakpa et al 2018). Altogether, these results are not consistent with the acute effects of GPN on pH_{cyt} or $[Ca^{2+}]_c$ arising from rupture of lysosomes.

Since Ca^{2+} indicators are pH-sensitive (see Speake and Elliott, 1998), one possibility is that the change in fluorescence observed in fluo 8 following GPN is due to a shift in the affinity of the indicator for Ca^{2+} due to pH changes. However, I determined that the K_D of fluo 8 for Ca^{2+} did not change between pH 7 and 8. K_D = 434 ± 51 nM at pH 7, 374 ± 43 nM at pH 7.3, 355 ± 39 nM at pH 7.6 and 401 ± 29 nM at pH 8 (Figure 4.9). This establishes that the GPN-evoked increases in fluo 8 fluorescence are due an increase in $[Ca^{2+}]_c$.

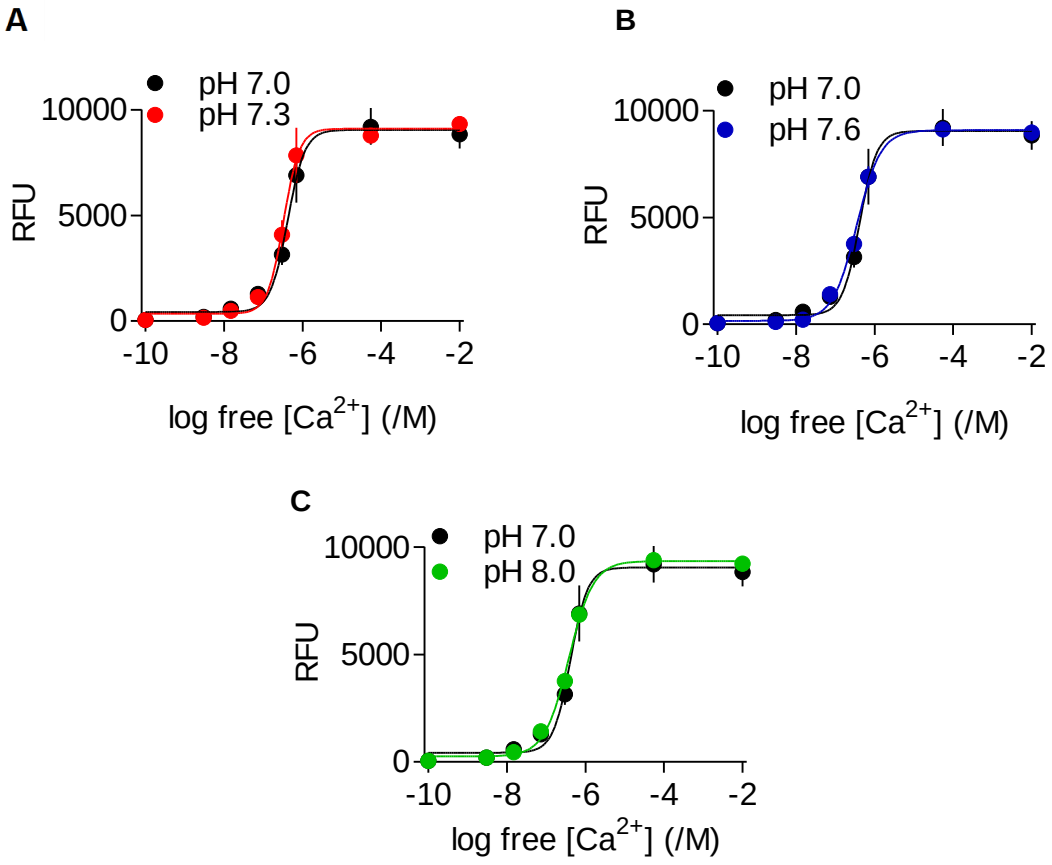

Figure 4.9 **The affinity of fluo 8 for Ca^{2+} is unaffected by changing pH between 7 and 8.** (A-C) Fluorescence of fluo 8 in BAPTA-buffered modified cytosol-like medium (MCLM) at the indicated pH. Since the K_D of BAPTA for Ca^{2+} (160 nM in the absence of Mg^{2+}) (Pethig *et al.*, 1989) is unaffected by pH changes between 7 and 8 (Tsien, 1980), the free [Ca^{2+}] of MCLM containing 10 mM BAPTA, but without Mg^{2+}, was computed at the indicated pH using the same K_D for Ca^{2+} for each pH. Results are mean ± SEM, *n* = 3, each with 3 determinations. RFU, relative fluorescent unit.

4.3.2 GPN-evoked increase in $[Ca^{2+}]_c$ requires Ca^{2+} in the ER

The increase in $[Ca^{2+}]_c$ evoked by GPN was abolished by depleting the ER of Ca^{2+} using CPA to inhibit SERCA (Figure 4.10). Similar results was obtained in HAP1 cells, where treatment with thapsigargin significantly attenuated GPN-induced Ca^{2+} signals (see Figure 4.13B).

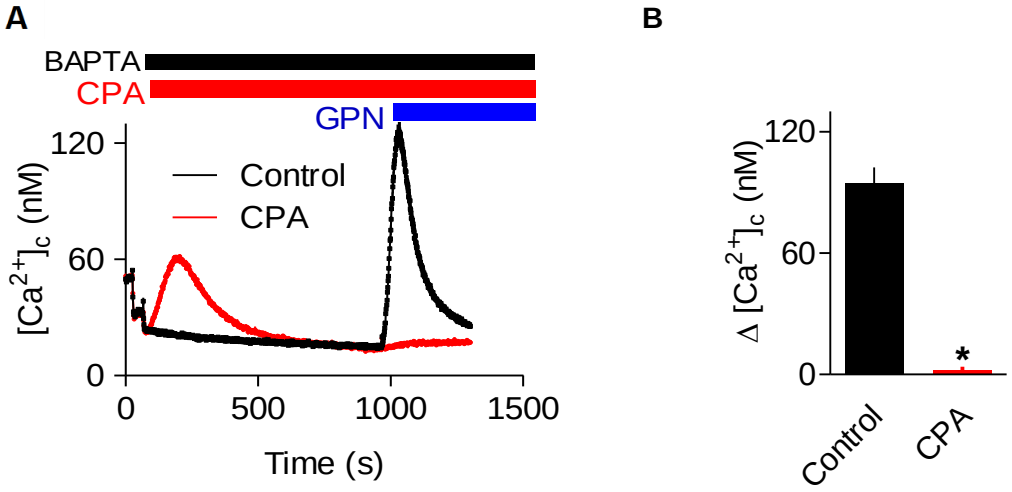

Figure 4.10 **GPN-induced increase in $[Ca^{2+}]_c$ is blocked by inhibition of SERCA in HEK cells.** (A) HEK cells in Ca^{2+}-free HBS were stimulated with GPN (200 μM) alone or after addition of CPA (20 μM). Results show mean ± SD for 3 wells from a typical experiment. (B) Summary results show peak increases in $[Ca^{2+}]_c$ evoked by GPN ($\Delta[Ca^{2+}]_c$) with or without pre-incubation with CPA (20 μM, 15 min). Results are means ± SEM, $n = 3$. $^*P < 0.05$, Student's *t*-test.

Although no SERCA was detected in the proteome of lysosomal membranes (Bagshaw et al., 2005; Chapel et al., 2013), it has been suggested that a SERCA with reduced Ca^{2+} affinity (SERCA3) may contribute to Ca^{2+} uptake by acidic stores (Lopez *et al.*, 2005). Therefore, it was important to investigate whether inhibition of GPN-evoked cytosolic Ca^{2+} signals by thapsigargin and CPA might be due to direct inhibition of lysosomal Ca^{2+} sequestration. When activated by carbachol (CCh), M_3Rs stimulate phospholipase C and thereby Ca^{2+} release from ER through IP_3Rs. However, endogenous expression of M_3Rs is insufficient to fully deplete the ER of Ca^{2+} in HEK cells (Konieczny *et al.*, 2017). Therefore, a viral vector, BacMam, was used to over-express M_3Rs in HEK cells. Overexpression of M_3R increased the Ca^{2+} mobilised from the ER (Figure 4.11A, B). Under these conditions, IP_3-evoked Ca^{2+} release from the ER also massively and rapidly attenuated the cytosolic Ca^{2+} signals evoked

by GPN (Figure 4.11C, D). This confirms that loss of Ca^{2+} from the ER, rather than SERCA inhibition itself, rapidly inhibits GPN-evoked increases in $[Ca^{2+}]_c$.

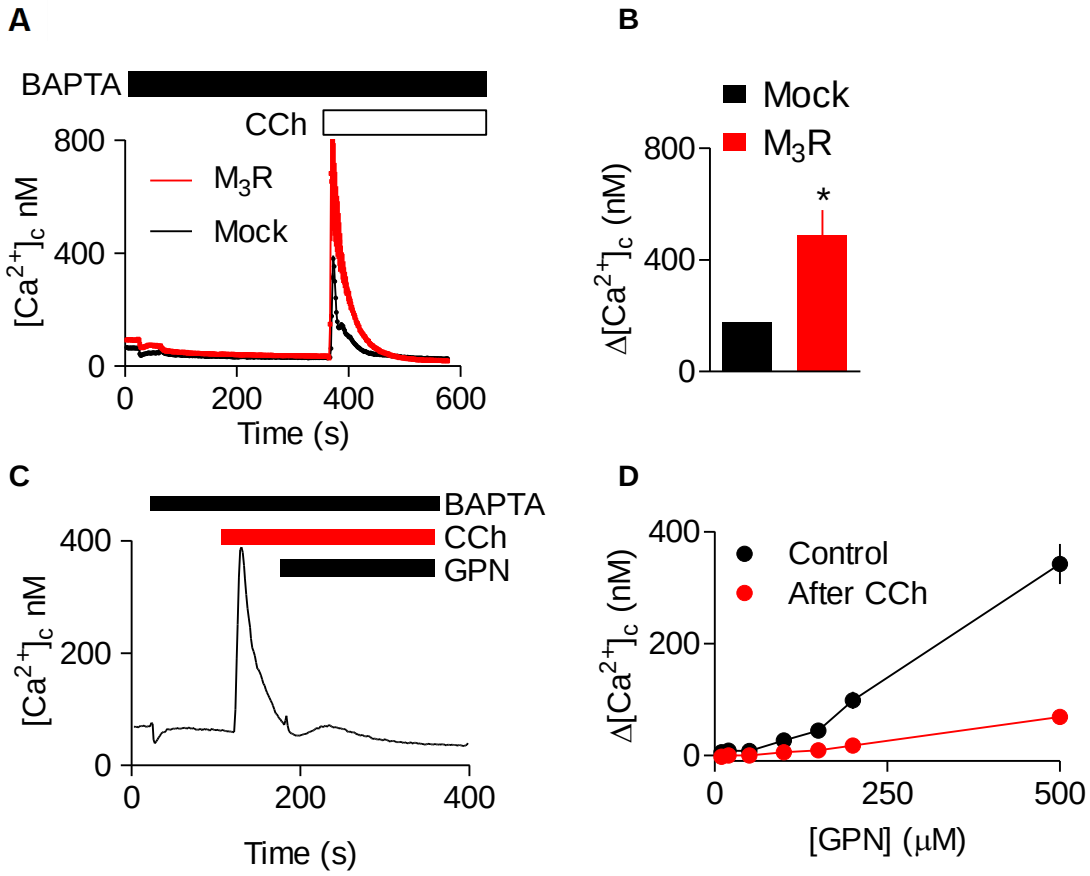

Figure 4.11 **Depleting ER Ca^{2+} stores by activating IP_3Rs rapidly attenuates GPN-evoked increases in $[Ca^{2+}]_c$.** (A) The results show $[Ca^{2+}]_c$ recorded from a population of fluo 8-loaded HEK cells with or without (mock-infected) over-expressed M_3Rs, and stimulated with a maximally effective concentration of CCh (1 mM). BAPTA (2.5 mM) was added before CCh to chelate extracellular Ca^{2+}. (B) Summary results (mean ± SEM, n = 3) show the peak increase in $[Ca^{2+}]_c$ ($\Delta[Ca^{2+}]_c$). $^*P < 0.05$, Student's t-test. Responses to CCh were abolished in cells pre-treated with thapsigargin (1 μM, 15 min) to inhibit SERCA (results not shown). (C) HEK cells over-expressing M_3Rs were stimulated with CCh (1 mM) in Ca^{2+}-free HBS and then with GPN (200 μM). Results show mean of 3 replicates. (D) Summary results (mean ± SEM, n = 3) show responses to the indicated concentrations of GPN alone or after stimulation with CCh. The results demonstrate that depleting the ER of Ca^{2+} by stimulating IP_3Rs rapidly attenuates the increase in $[Ca^{2+}]_c$ evoked by GPN.

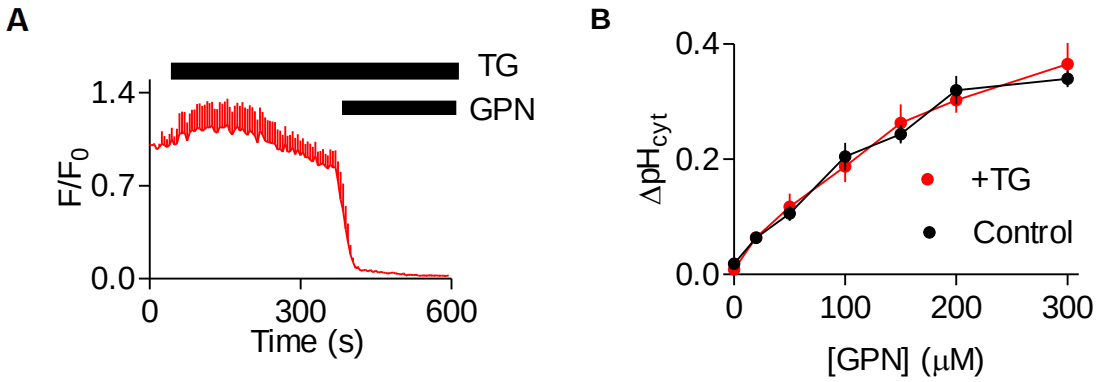

Figure 4.12 **GPN-induced increases in pH_{ly} and pH_{cyt} are unaffected by pre-treatment with thapsigargin.** (A) Typical time course showing effect of GPN (200 μM) on LysoTracker Red fluorescence in HEK cells after treatment with thapsigargin (TG, 1 μM, 5 min). (B) Similar analyses of the effects of the indicated concentrations of GPN in Ca^{2+}-free HBS alone or after treatment with thapsigargin (TG, 1 μM, 15 min) on ΔpH_{cyt} (mean ± SEM, n = 3, each with duplicate determinations).

The effect of thapsigargin on the GPN-induced increase in pH_{ly} and pH_{cyt} was also assessed. A previous study showed that thapsigargin does not affect pH_{ly}, as LysoTracker accumulation was unaffected (Ganley *et al.*, 2011). Here, pre-treatment with thapsigargin did not affect the GPN-induced increase in pH_{ly} or pH_{cyt} (Figure 4.12).

4.3.3 GPN-induced increase in $[Ca^{2+}]_c$ is not mediated by canonical CICR channels

Why should loss of Ca^{2+} from the ER abolish the response to GPN? Hitherto, it has been supposed that any contribution of the ER to lysosomal Ca^{2+} signals arises from an amplification of the initial Ca^{2+} release from lysosomes by Ca^{2+}-induced Ca^{2+} release (CICR) through either IP_3Rs or ryanodine receptors (RyRs) (Zhu *et al.*, 2010; Morgan, 2011a; Kilpatrick *et al.*, 2013) in the ER. Both IP_3Rs and RyRs are stimulated by cytosolic Ca^{2+} (Endo *et al.*, 1970; Iino, 1990; Taylor & Tovey, 2010). In HEK-IP_3RKO cells, the Ca^{2+} signals evoked by 200 μM GPN were similar to those in normal HEK cells, and they were again blocked by pre-treatment with thapsigargin (Figure 4.13A). Similarly, the Ca^{2+} signals evoked by GPN were unchanged in HAP1-IP_3RKO cells (Figure 4.13B).

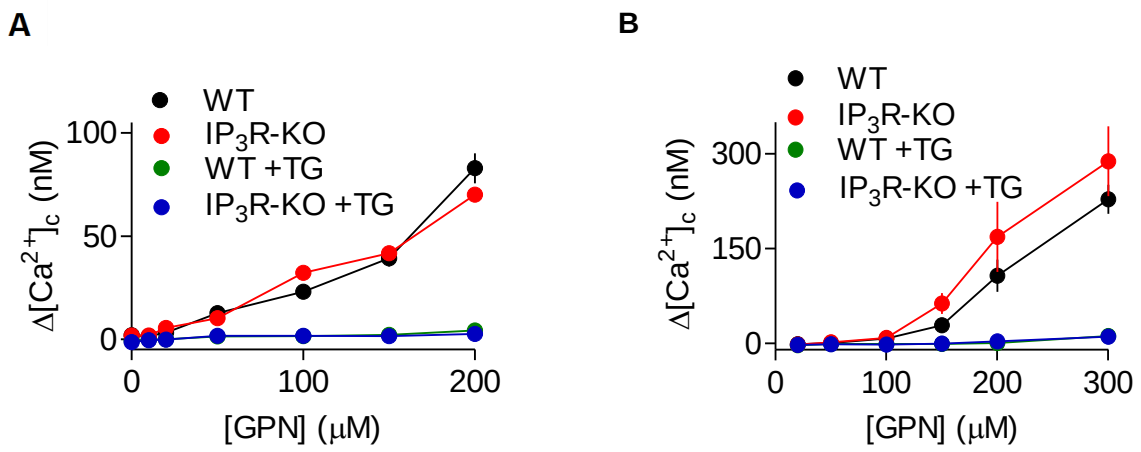

Figure 4.13 **GPN-induced increase in $[Ca^{2+}]_c$ is unaffected by knock-out of IP_3R.** (A) HEK cells with (wild-type, WT) or without IP_3Rs (IP_3R-KO) were stimulated in Ca^{2+}-free HBS with GPN (200 μM) alone or after treatment with thapsigargin (TG, 1 μM, 15 min). Results (mean ± SEM, *n* = 4, with 3 replicates) show $\Delta[Ca^{2+}]_c$. (B) Effects of GPN (200 μM) in Ca^{2+}-free HBS on HAP1 cells with (wild-type, WT) or without IP_3Rs (IP_3R-KO), alone or after treatment with thapsigargin (TG, 1 μM, 15 min). Results show mean ± SEM, *n* = 3, each with 3 replicates.

Some HEK cells have been reported to express RyR (Kurian *et al.*, 2009). However, caffeine, which stimulates RyRs, did not evoke Ca^{2+} release in the HEK or HAP1 cells used here (Figure 4.14A, C). Furthermore, prolonged incubation with a high concentration of ryanodine to block RyR did not affect the Ca^{2+} signals evoked by GPN in the HEK cells used here (Figure 4.14B). Similarly, prolonged incubation with ryanodine did not affect the Ca^{2+} signals evoked by GPN in HAP1 cells (Figure 4.14 D).

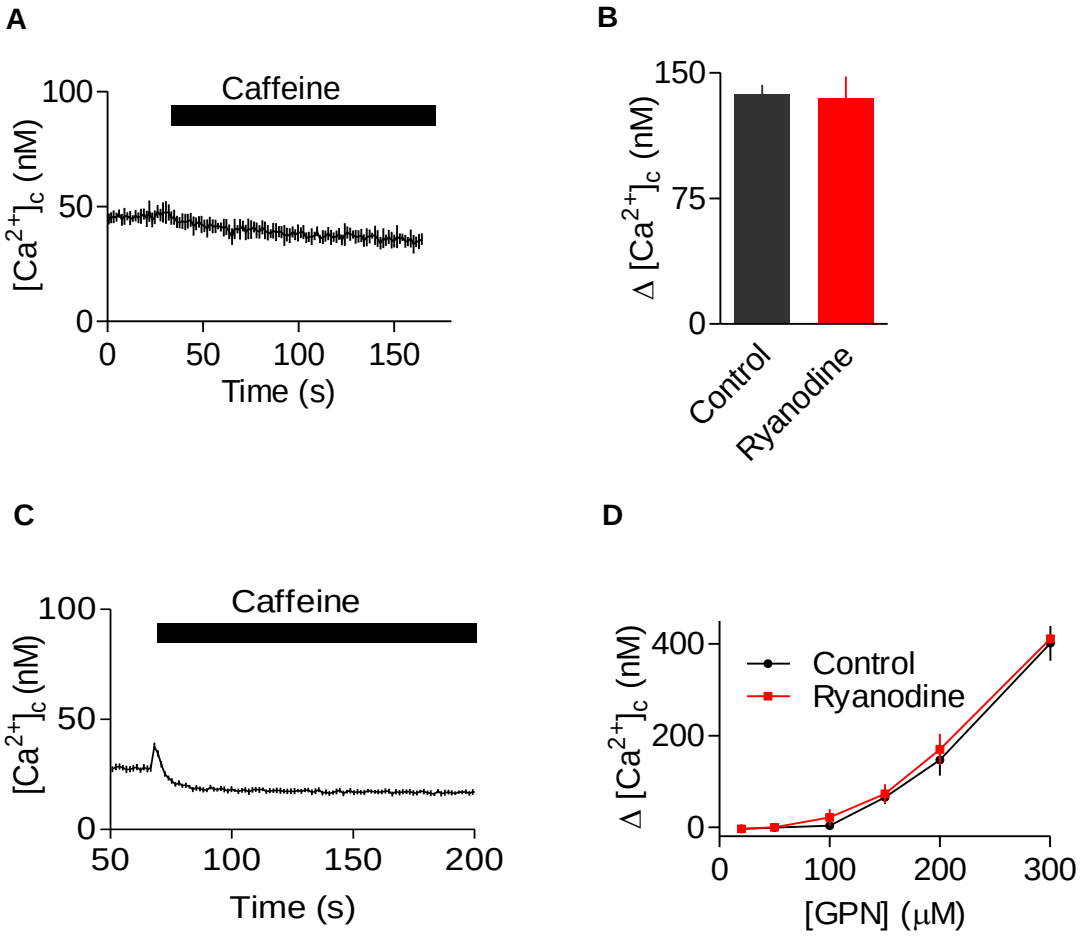

Figure 4.14 **RyRs do not contribute to cytosolic Ca^{2+} signals evoked by GPN.** (A) Effects of caffeine (1 mM) in Ca^{2+}-free HBS on $[Ca^{2+}]_c$ in HEK cells. Traces show mean ± SD from 3 replicates. Similar results were obtained in 3 independent analyses. (B) Effects of GPN in Ca^{2+}-free HBS on the peak increase in $[Ca^{2+}]_c$ ($\Delta[Ca^{2+}]_c$) alone or after treatment with ryanodine (20 µM, 15 min) to inhibit RyRs. Results (mean ± SEM, *n* = 3, each with 3 replicates) are from HEK cells stimulated with 200 µM GPN. (C) Effects of caffeine (1 mM) in Ca^{2+}-free HBS on $[Ca^{2+}]_c$ in HAP1 cells. Traces show mean ± SD from 3 replicates. Similar results were obtained in 3 independent analyses. (D) Effects of GPN (200 µM) in Ca^{2+}-free HBS on HAP1 cells alone or after treatment with ryanodine (20 µM, 15 min). Results show mean ± SEM, *n* = 3, each with 3 replicates.

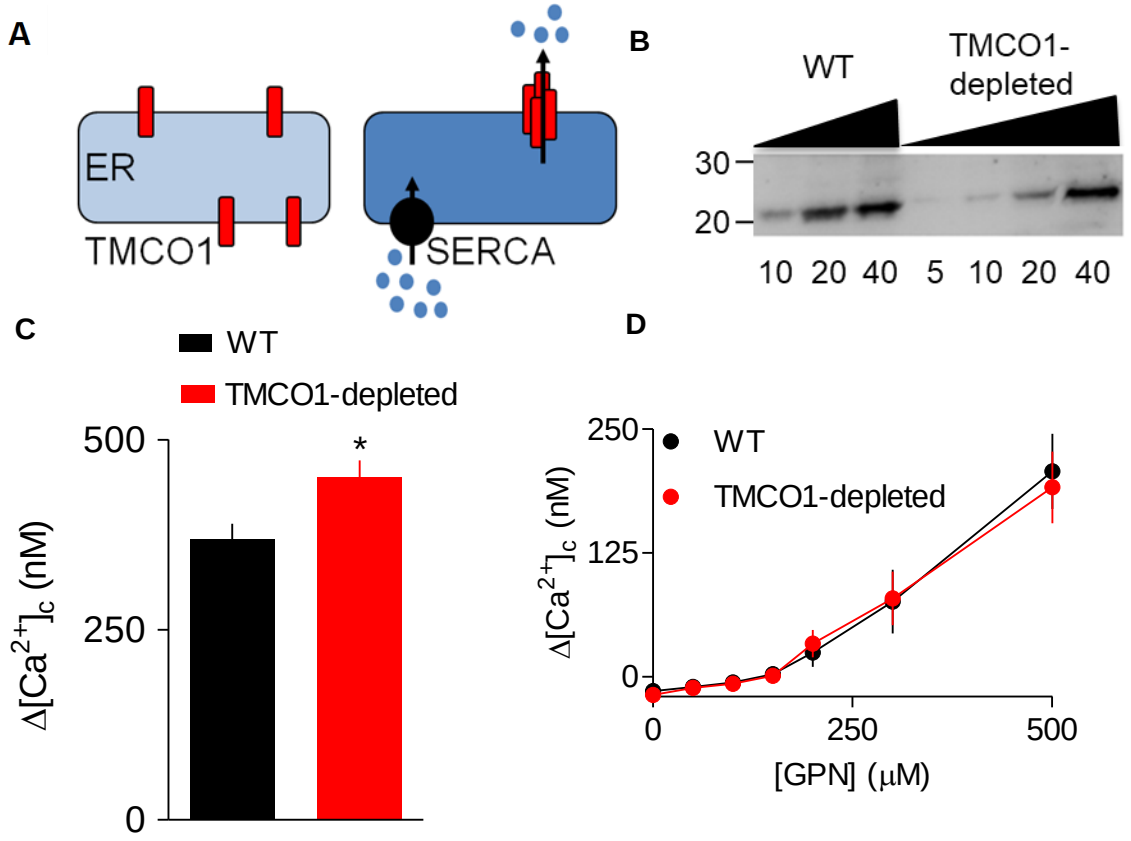

Figure 4.15 **CICR mediated by TMCO1 does not contribute to GPN-evoked increases in $[Ca^{2+}]_c$.** (A) TMCO1 is proposed to oligomerize into a functional Ca^{2+}-permeable channel as the ER loads with Ca^{2+}. Hence, TMCO1 may be able to mediate CICR as Ca^{2+} released by other intracellular channels fuels ER Ca^{2+} uptake by SERCA leading to Ca^{2+} overload and the opening of TMCO1. (B) Typical Western blot showing expression of β-actin and TMCO1 in HEK cells in which CRISPR/Cas9 was used to achieve a partial knock-down of TMCO1 (67 ± 14 %, n = 4, mean ± SD). M_r markers (kDa) and protein loadings (μg) are shown. (C, D) Peak Ca^{2+} signals evoked by a maximally effective concentration of carbachol (C) or the indicated concentrations of GPN (D) in Ca^{2+}-free HBS (mean ± SEM, n = 3). $^*P < 0.05$, Student's t-test.

Another possible CICR channel in the ER is TMCO1 (transmembrane coiled-coil domain 1). TMCO1 is an ER membrane protein that oligomerizes to form a Ca^{2+} pore as the ER overloads with Ca^{2+} (Figure 4.15A) (Wang *et al.*, 2016). TMCO1 might thereby allow GPN-evoked Ca^{2+} release from lysosomes to be amplified. Multiple rounds of CRISPR/Cas9 failed to achieve a complete knockout of TMCO1 in HEK cells, but with TMCO1 expression reduced by 67 ± 14% (Figure 4.15B), there was the expected increase in carbachol-evoked Ca^{2+} signals (Figure 4.15C) (Wang *et al.*, 2016), but there was no effect on the increase in $[Ca^{2+}]_c$ evoked by GPN (Figure 4.15D).

These results establish that none of the known mechanisms (RyR, IP_3R and TMCO1) that might mediate CICR from the ER contribute to the increase in $[Ca^{2+}]_c$ evoked by GPN. The results so far demonstrate that GPN increases pH_{ly} and $[Ca^{2+}]_c$, but they challenge the conventional explanations for these phenomena (Figure 4.1B).

4.3.4 Effects of GPN on pH_{ly}, pH_{cyt} and $[Ca^{2+}]_c$ do not require cathepsin C

The effects of GPN are thought to require its proteolysis by cathepsin C (Figure 4.1), an enzyme that is widely assumed to be expressed mainly in lysosomes (Rao *et al.*, 1997; Wolters & Chapman, 2000). This distribution of cathepsin C is invoked to suggest that GPN selectively targets lysosomes.

Various approaches were adopted to assess the contribution of cathepsin C to the effects of GPN. CRISPR/Cas9 was used to generate HEK cells devoid of cathepsin C activity (HEK-CTSC-KO) (Figure 4.16A-C). Gly-Phe-DMK was used to inhibit cathepsin C activity (Methot *et al.*, 2007; Repnik *et al.*, 2017). Gly-Phe-DMK binds covalently to Cys-234 on the active site of cathepsin C and blocks its ability to cleave its substrates (Molgaard *et al.*, 2007). The proteolytic activity of cathepsin C measured using the fluorogenic substrate, Gly-Arg-AMC in whole HEK cell lysates, was completely inhibited by the cathepsin C inhibitor Gly-Phe-DMK (Figure 4.16B, C). Gly-Arg-AMC is cleaved by cathepsin C to release the fluorogenic AMC. There was no detected AMC following prolonged inhibition of cathepsin C with Gly-Phe-DMK. In all conditions, a buffer control, containing no cell lysates was included to control for any basal fluorescence from the substrate. There was no significant difference between the buffer conditions and cells pre-treated with the cathepsin C inhibitor. (Figure 4.16B, C). There was no detectable AMC in HEK-CTSCKO cells (Figure 4.16B, C).

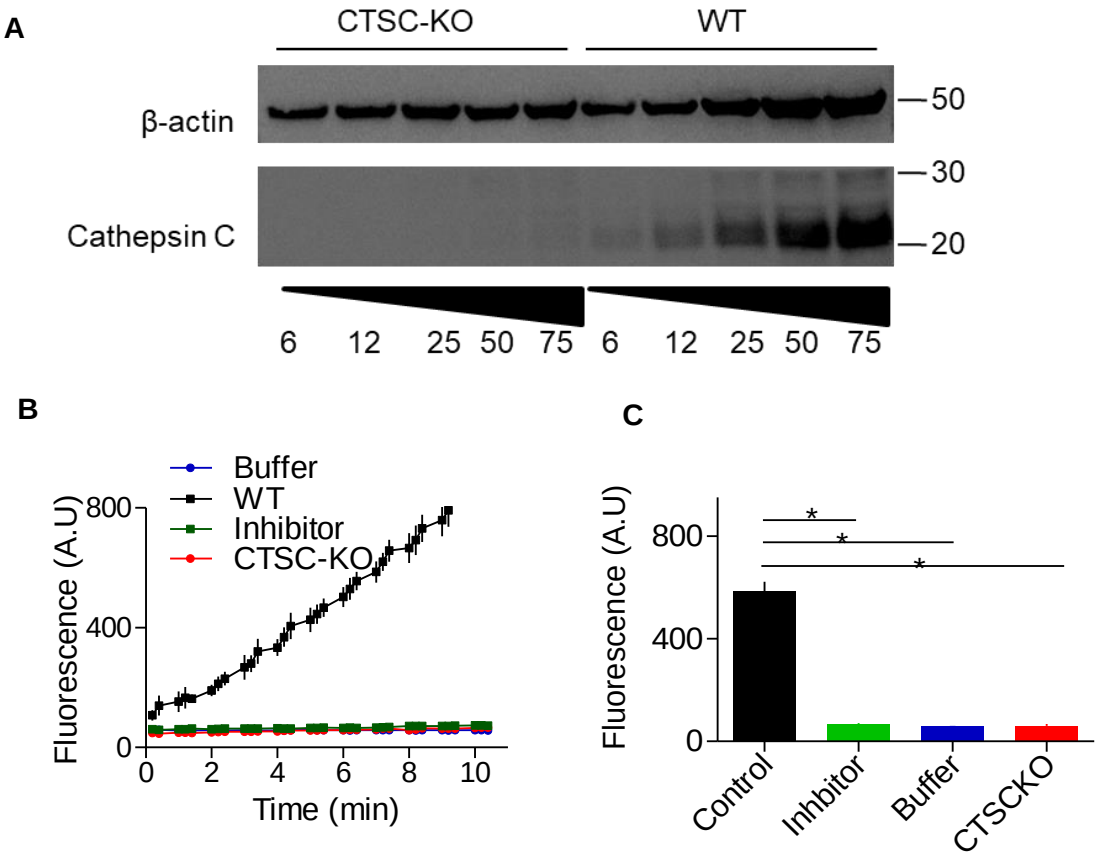

Figure 4.16 **Cathepsin C is not detected following CRISPR/Cas9-mediated gene-editing in HEK-CTSCKO cells.** (A)Western blot probing expression of cathepsin C and actin in HEK WT and HEK-CTSCKO. Lysates were serially diluted; the amount of total protein loaded in each lane is indicated. (B) Cleavage of the fluorogenic cathepsin C substrate Gly-Arg-AMC (50 µM) was assessed in whole cell lysates obtained from HEK WT or HEK-CTSCKO. Buffer control was included to correct for any basal change in fluorescence. Results are mean ± SD for 1 experiment with triplicate determinations, typical of 3 independent experiments. (C) Summary results from experiments described in B, shows the relative fluorescence of AMC detected in the conditions shown after 7 min. Results are mean ± SEM for 3 experiments. $^{*}P < 0.05$, one-way ANOVA, Tukey's test.

In HEK WT cells, GPN induced a significant increase in the OG fluorescence (Figure 4.17A, C). Furthermore, GPN resulted in a 74 ± 5% increase in the fluorescence of fluorescein-Dx (3-kDa) in HEK WT cells (Figure 4.17B, D, Table 4.1).

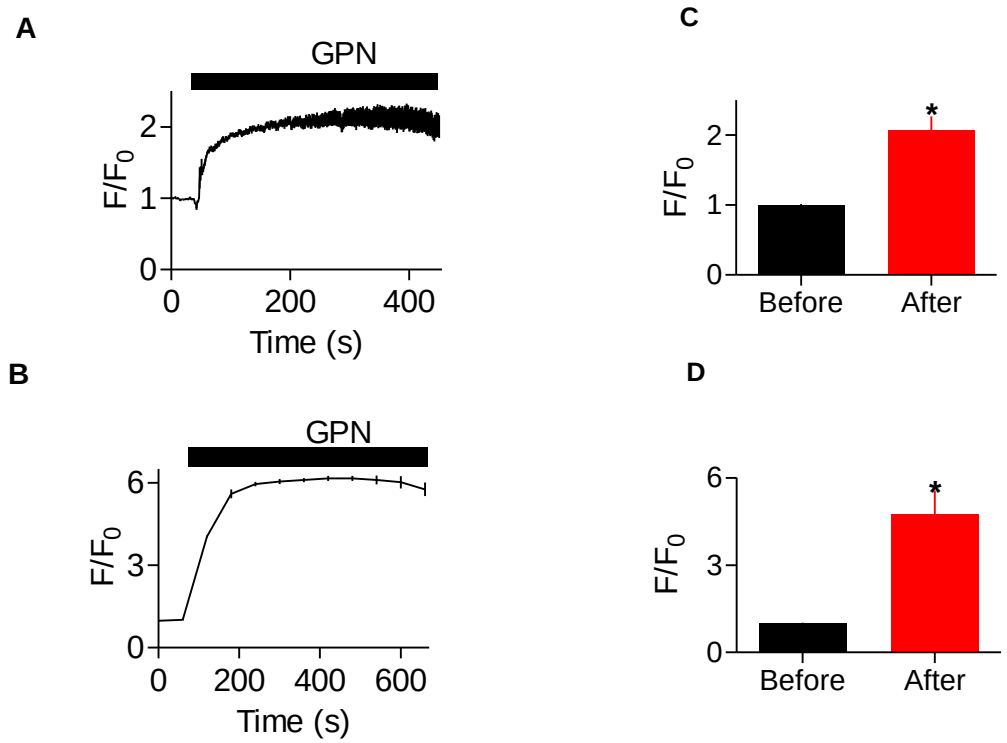

Figure 4.17 **GPN induces an increase in pH_{ly}.** (A-B) Representative traces show the effect of GPN (300 µM) on Oregon Green-Dx (A) or fluorescein-Dx (B) fluorescence in HEK WT cells. (C-D) Summary results shows the effect of GPN on Oregon Green-Dx (C) or fluorescein-Dx (D) fluorescence in HEK WT cells before or 200 s after addition of GPN. Results shown are means ± SEM from 5 experiments. $^{*}P < 0.05$, paired Student's *t*-test.

In the next experiment, the role of cathepsin C in the GPN-mediated increase in pH_{ly} was assessed. In HEK-CTSCKO cells, GPN induced a 45 ± 5% increase in the Oregon Green-Dx fluorescence (Figure 4.18A, C). Furthermore, GPN resulted in a 68 ± 8% increase in the fluorescence of fluorescein-Dx (3-kDa) in HEK-CTSC KO cells (Figure 4.18B, D, Table 4.1). These results suggest that the GPN-evoked increase in pH_{ly} is independent of cathepsin C activity.

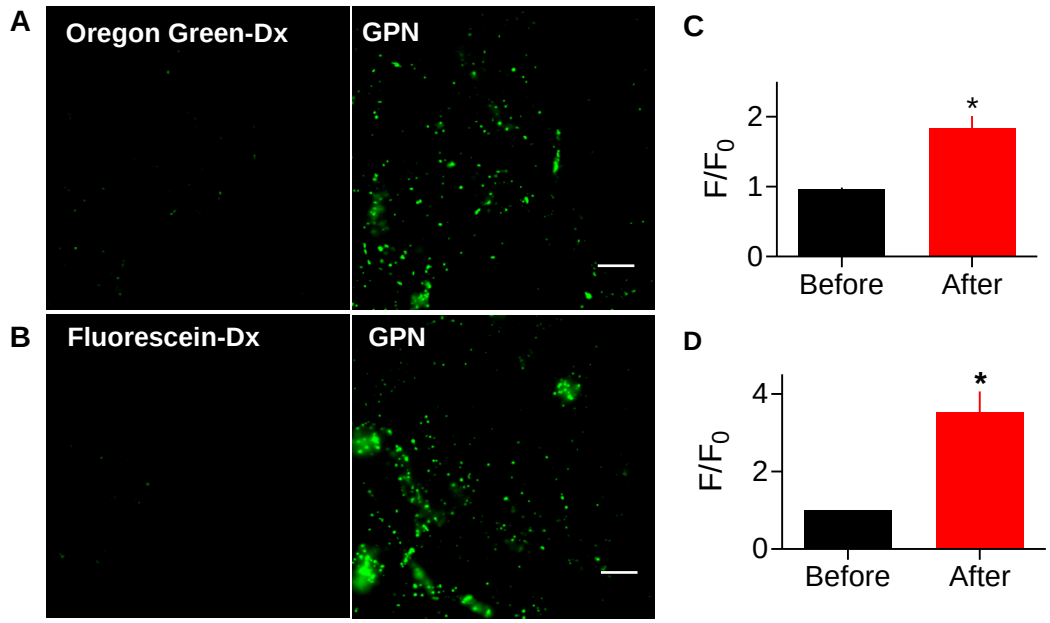

Figure 4.18 **GPN induces an increase in pH_{ly} in cells lacking cathepsin C.** (A-B) Wide-field fluorescence images of HEK CTSCKO cells loaded with Oregon Green-Dx (A) or fluorescein-Dx (B). Images are shown before and 200 s after GPN (300 µM). Each image is representative of at least 3 independent experiments. Scale bar = 10 µm and applies to all images. (C-D) Summary results show the effect of GPN on Oregon Green-Dx (C) or fluorescein-Dx (D) fluorescence in HEK CTSCKO cells before or 200 s after addition of GPN. Results shown are means ± SEM from 5 experiments. $^{*}P < 0.05$, paired Student's *t*-test.

D-GPN, in which the L-Phe of L-GPN (hitherto described as GPN) is replaced by D-Phe; was also used to assess the role of cathepsin C is mediating the effect of GPN. Unlike L-GPN, D-GPN is not a substrate for cathepsin C (Jadot *et al.*, 1990). In HEK WT cells, D-caused an increase in Oregon Green-Dx fluorescence (44 ± 8%) (Figure 4.19A, C, Table 4.1) and a 65 ± 8 % increase in the fluorescence of fluorescein-Dx (Figure 4.19B, D, Table 4.1).

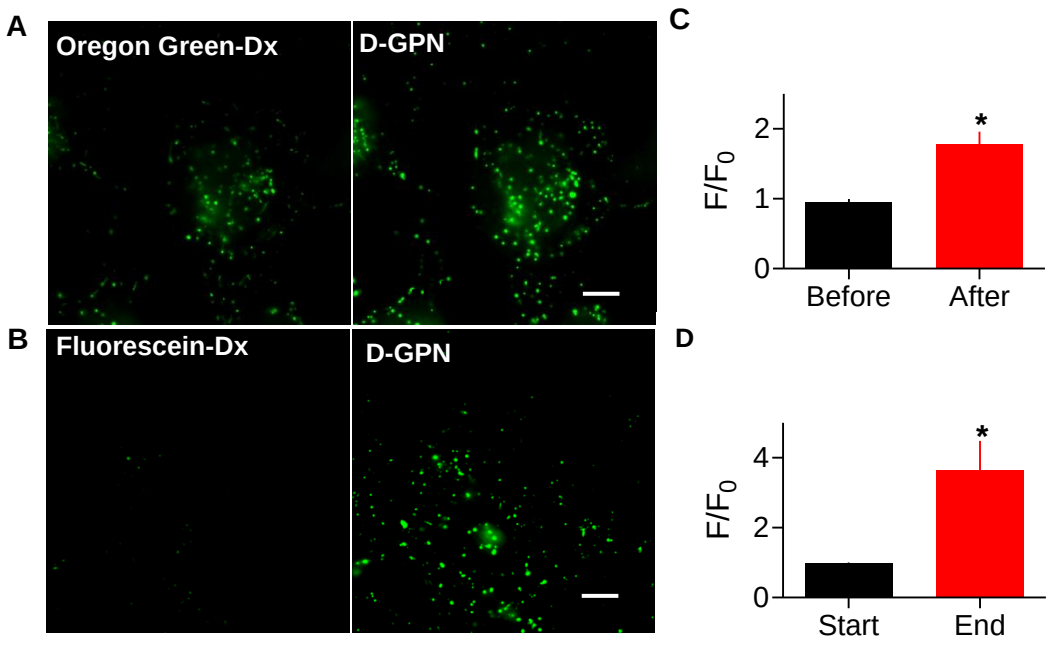

Figure 4.19 **D-GPN induces an increase in pH_{ly}.** (A-B) Wide-field fluorescence images of HEK WT cells loaded with Oregon Green-Dx (A) or fluorescein-Dx (B). Images are shown before and 200 s after addition of D-GPN (300 µM). Each image is representative of at least three independent experiments. Scale bar = 10 µm and applies to all images. (C-D) Summary results show the effect of D-GPN on Oregon Green-Dx (C) or fluorescein-Dx (D) fluorescence in HEK WT cells before or 200 s after addition of GPN. Results shown are means ± SEM from 5 experiments. $^{*}P < 0.05$, paired Student's *t*-test.

GPN-induced loss of LysoTracker accumulation from lysosomes was unaffected by loss of cathepsin C (Figure 4.20). D-GPN also rapidly dissipated LysoTracker staining in HEK cells (Figure 4.20, Table 4.1). GPN caused the usual sustained increase in pH_{ly} in HEK cells without cathepsin C; and in normal HEK cells, GPN and D-GPN caused indistinguishable increases in pH_{ly}.

These results establish that the effects of GPN on pH_{ly} do not require cathepsin C, since the effects of GPN are unperturbed in cells with no demonstrable cathepsin C activity.

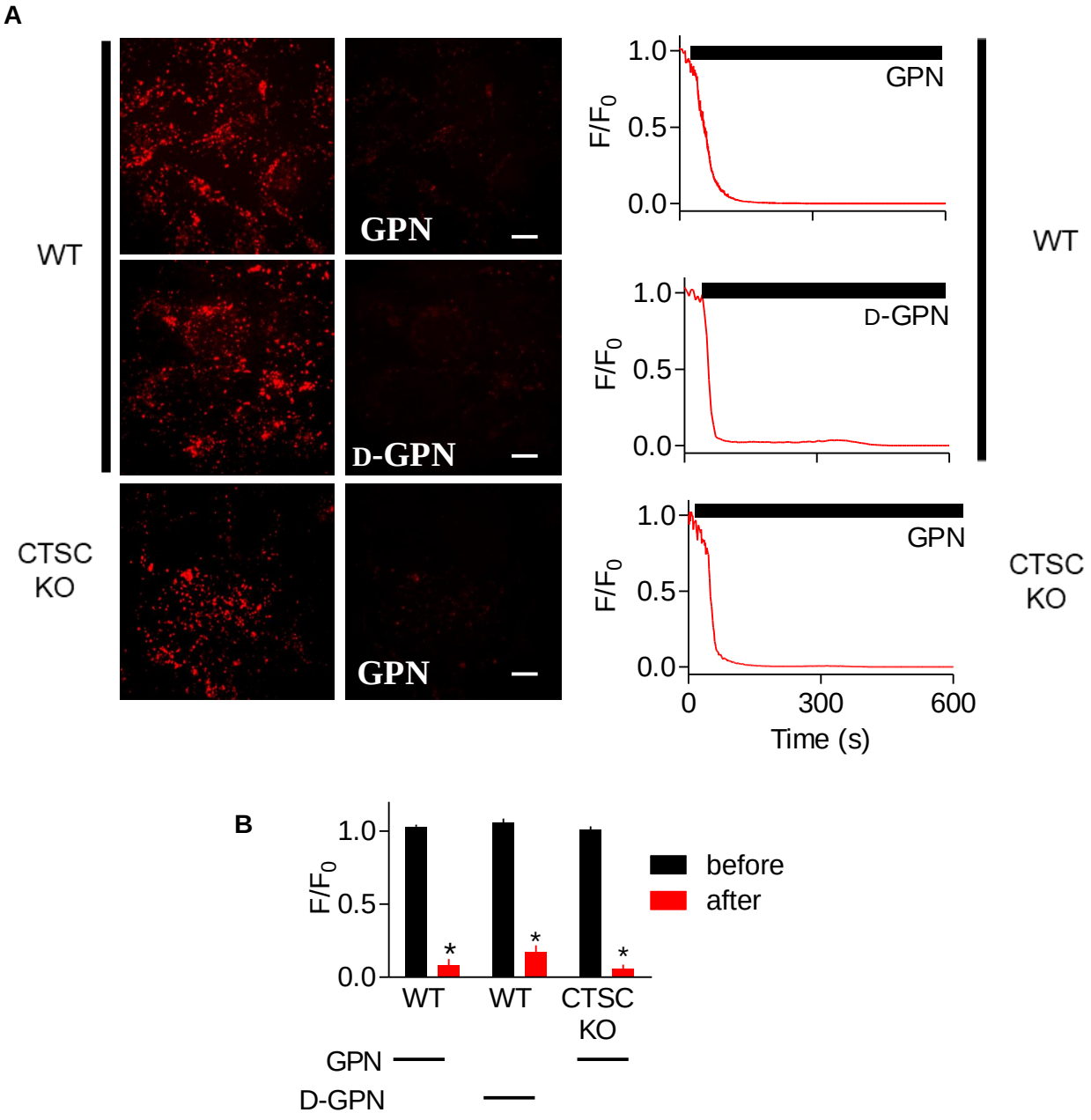

Figure 4.20 **GPN induces release of LysoTracker from lysosomes.** (A) Wide-field fluorescence images of HEK cells loaded with LysoTracker Red (100 nM, 20 min) before and 200 s after addition of GPN or D-GPN. Scale bar = 10 µm, and applies to all images. Representative traces next to the images show time course of LysoTracker Red following addition of GPN or D-GPN. (B) Summary results show the effect of GPN or D-GPN on LysoTracker Red fluorescence as means ± SEM from 6 independent experiments. $^{*}P < 0.05$, 2-way ANOVA, Bonferroni post hoc tests.

Table 4.1 **GPN-induced increase in pH_{ly}.** Changes in fluorescence of Oregon Green-Dx, fluorescein-Dx and LysoTracker Red induced by GPN (300 µM, 200s) in HEK cells. Results are means ± range from at least 4 independent experiments. A percentage decrease is shown for LysoTracker Red.

Fluorophore	**Loading**	**WT (GPN) (%)**	**CTSCKO (GPN) (%)**	**WT (D-GPN) (%)**
Oregon Green	Dx conjugate	50 ± 5	45 ± 5	44 ± 8
Fluorescein	Dx conjugate	74 ± 7	68 ± 8	65 ± 8
LysoTracker	Acidotropic dye	92 ± 5	94 ± 3	83 ± 4

The role of cathepsin C in the GPN-induced effect on pH_{cyt} was also assessed. In HEK WT cells, inhibition of cathepsin C activity did not affect the basal pH_{cyt} (Figure 4.21A, Table 4.2). The GPN-induced cytosolic alkalinization was also unaffected by cathepsin C inhibition. The maximum change in pH_{cyt} was 0.31 ± 0.06 in control cells and 0.28 ± 0.04 in cells treated with Gly-Phe-DMK (Figure 4.21B, Table 4.2).

Similarly, in HeLa cells, inhibition of cathepsin C activity did not affect the basal pH_{cyt} (Figure 4.21C, Table 4.2). GPN-induced cytosolic alkalinization was also unaffected by cathepsin C inhibition. The maximum change in pH_{cyt} was 0.41 ± 0.02 in control cells and 0.40 ± 0.04 in cells, treated with the inhibitor (Figure 4.21D, Table 4.2).

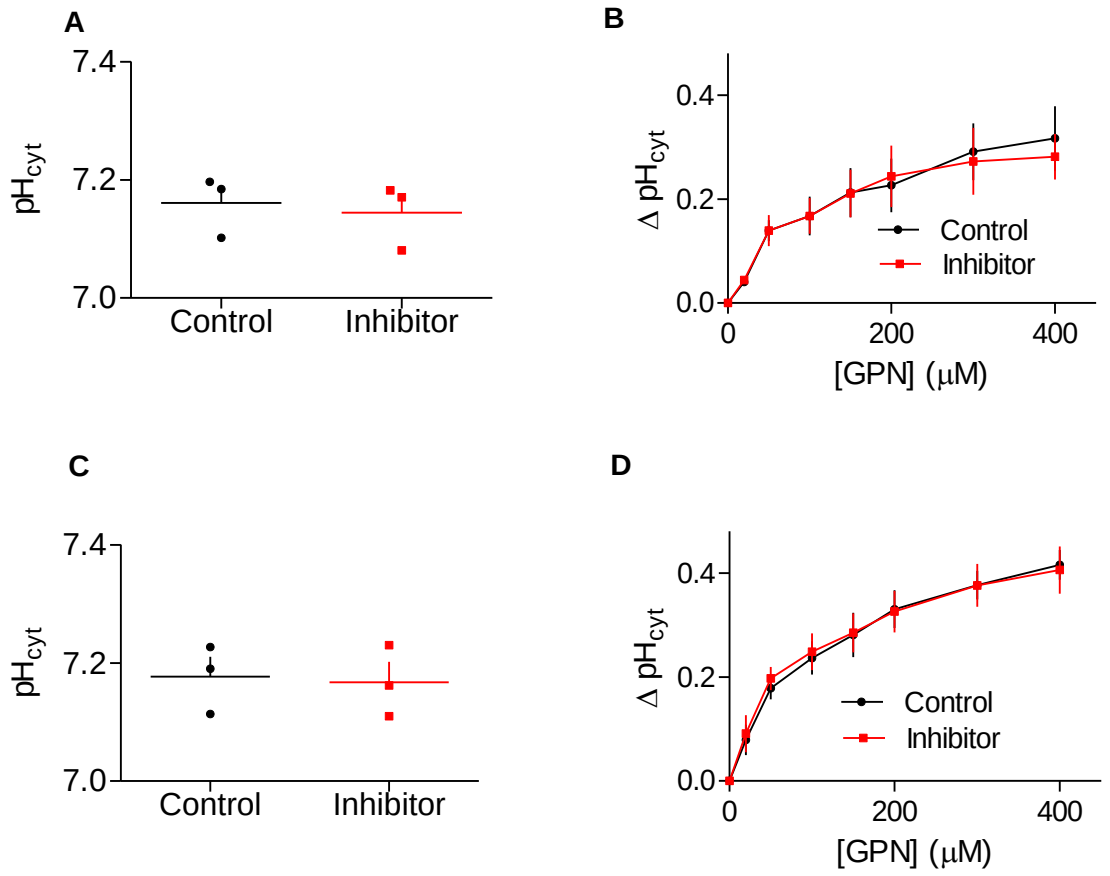

Figure 4.21 **GPN-mediated increase in pH_{cyt} is unaffected by inhibition of cathepsin C.** (A, B) Effects of the cathepsin C inhibitor (Gly-Phe-DMK, 10 µM, 72 h) on basal pH_{cyt} measured using SNARF-5F (A) and peak ΔpH_{cyt} (B), measured 30 s after GPN addition in HEK cells. Results are mean ± SEM from 3 independent experiments. (C, D) Effects of the cathepsin C inhibitor (Gly-Phe-DMK, 10 µM, 72 h) on basal pH_{cyt} (C) and peak ΔpH_{cyt} (D), measured 30 s after GPN addition in HeLa cells. Results are mean ± SEM from 3 independent experiments.

KO of cathepsin C also did not affect the basal pH_{cyt} (Figure 4.22A). There was also no significant difference between GPN-induced cytosolic alkalinization in HEK WT compared to cathepsin C KO cells (Figure 4.22B).

In HEK WT cells, treatment with D-GPN rapidly increased pH_{cyt} with a peak increase after approximately 50 s. It then returned to baseline after about 10 min. The maximum change in pH_{cyt} following treatment with 400 µM D-GPN was 0.34 ± 0.04 (Figure 4.23A, B).

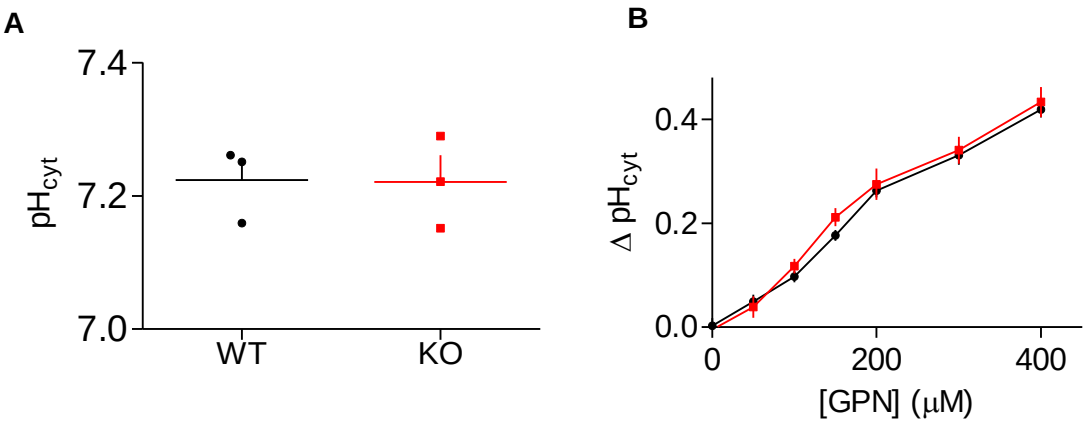

Figure 4.22 **GPN-mediated increase in pH_{cyt} is unaffected by knock-out of cathepsin C.** (A) Basal pH_{cyt} was measured in HEK WT cells and HEK-CTSCKO cells using SNARF-5F. Results are mean ± SEM. $n = 3$, $P = 0.10$, paired Student's *t*-test. (B) GPN-mediated increase in pH_{cyt} is shown in HEK WT cells (black) and HEK-CTSCKO cells (red). Results are mean ± SEM from 3 independent experiments.

Table 4.2 **Inhibition of cathepsin C does not affect the GPN-induced increase in pH_{cyt}.** Effect of cathepsin C inhibitor (Gly-Phe-DMK) on basal and peak changes in pH_{cyt} evoked by GPN (300 μM) in populations of HEK and HeLa cells loaded with SNARF-5F. Results are means ± SEM from 3 experiments

Cell type	Treatment	Basal pH_{cyt}	Peak ΔpH_{cyt}
HEK WT	Control	7.16 ± 0.02	0.31 ± 0.06
	Gly-Phe-DMK	7.14 ± 0.03	0.28 ± 0.04
HeLa	Control	7.17 ± 0.03	0.41 ± 0.02
	Gly-Phe-DMK	7.16 ± 0.03	0.40 ± 0.04

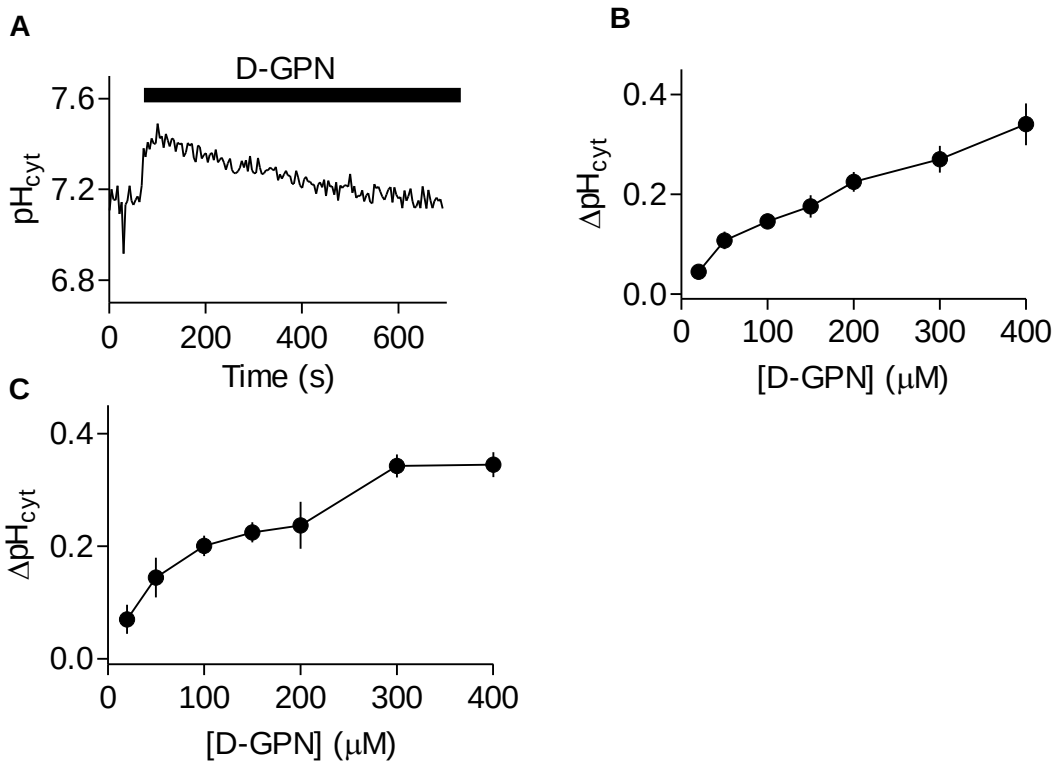

Figure 4.23 **D-GPN increases pH_{cyt} in mammalian cells.** Populations of HEK cells loaded with SNARF-5F were stimulated in Ca^{2+}-free HBS with D-GPN (300 μM). Results are mean ± SD for 1 experiment with triplicate determinations, typical of 3 independent experiments. (B) Summary results show that D-GPN increases pH_{cyt} in a concentration-dependent manner in HEK cells. Results are mean ± SEM, *n* = 3. (C) Summary results show D-GPN increases pH_{cyt} in a concentration-dependent manner in HeLa cells. Results are mean ± SEM, *n* = 3.

Similar results were obtained in HeLa cells, where treatment with D-GPN also increased pH_{cyt} in a concentration-dependent manner (Figure 4.23C).

These results establish that GPN-mediated effects on pH_{cyt} are not consistent with its proposed mode of action (Figure 4.1B), as GPN acutely increases pH_{cyt} in a cathepsin C-independent manner.

The role of cathepsin C on the GPN-evoked increase in $[Ca^{2+}]_c$ was next assessed. Inhibition of cathepsin C with Gly-Phe-DMK did not affect the basal $[Ca^{2+}]_c$ in HEK cells. Basal $[Ca^{2+}]_c$ was 20 ± 3 nM in control cells and 20 ± 4 nM in cells treated with the inhibitor (P = 0.19, paired Student's t test, n = 4). Furthermore, the concentration-dependent effects of GPN on $[Ca^{2+}]_c$ were indistinguishable in control HEK cells and in HEK cells treated with Gly-Phe-DMK (Figure 4.24A, B).

Similar analyses showed that there was no difference in basal $[Ca^{2+}]_c$ between HEK WT cells and HEK-CTSCKO cells (29 ± 8 nM in HEK WT cells and 23 ± 5 nM in HEK-CTSCKO cells) (P = 0.30, paired Student's t test, n = 4). There was no difference in the GPN-induced increase in $[Ca^{2+}]_c$ between HEK WT cells and HEK-CTSCKO cells (Figure 4.25).

Finally, D-GPN caused the same concentration-dependent increases in $[Ca^{2+}]_c$ as GPN (Figure 4.26). These results demonstrate that the effects of GPN on pH_{ly}, pH_{cyt} and $[Ca^{2+}]_c$ do not require cathepsin C

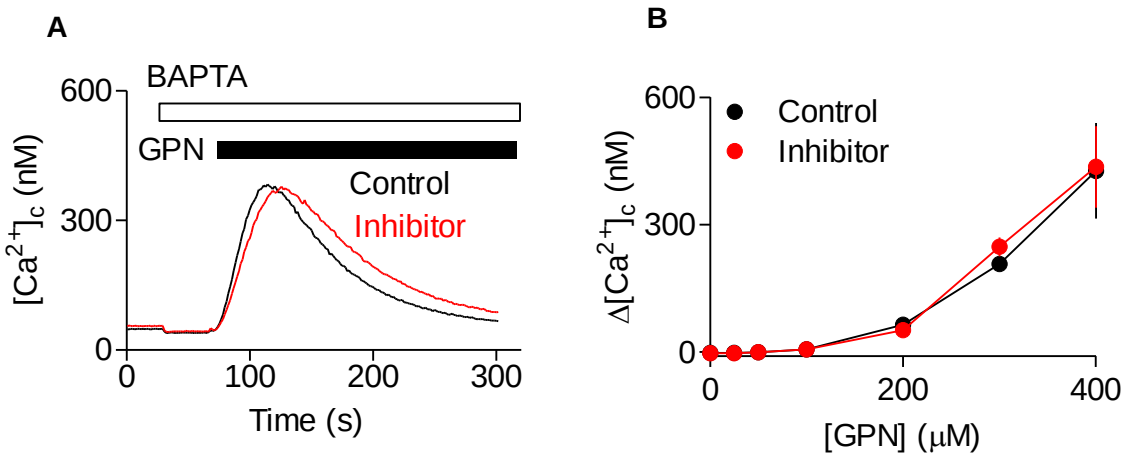

Figure 4.24 **GPN-mediated increase in $[Ca^{2+}]_c$ is unaffected by inhibition of cathepsin C.** (A) Populations of HEK cells in Ca^{2+}-free HBS were stimulated with GPN (200 μM), with or without pre-incubation with cathepsin C inhibitor (10 μM, 72 h). Results are means ± SD for three wells from a single experiment (B) Summary results from experiments described in A shows the effects of cathepsin C inhibitor on $\Delta[Ca^{2+}]_c$. Results are means ± SEM for 4 independent experiments.

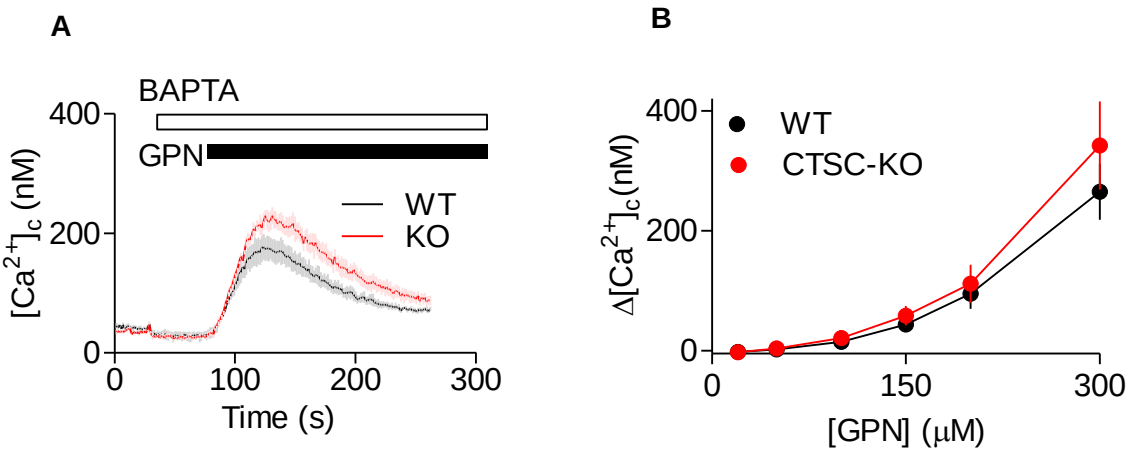

Figure 4.25 **GPN-mediated increase in $[Ca^{2+}]_c$ is unaffected by knock-out of cathepsin C.** (A) Populations of HEK WT (WT) cells or HEK-CTSCKO (KO) cells were stimulated with GPN (300 μM), in Ca^{2+}-free HBS. Results are means ± SD for three wells from a single experiment. (B) Summary results show the concentration-dependent effect of GPN on $\Delta[Ca^{2+}]_c$. Results are means ± SEM for 6 independent experiments.

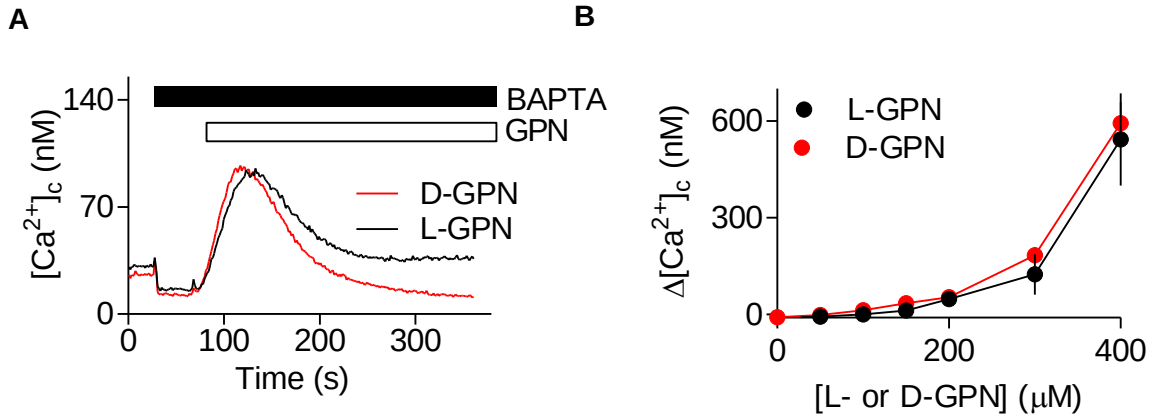

Figure 4.26 **D-GPN increases $[Ca^{2+}]_c$ in HEK cells**. (A) Populations of HEK WT cells in Ca^{2+}-free HBS were stimulated with D-GPN or GPN (200 μM). Results are means ± SD for three wells from a single experiment. (B) Concentration-dependent effects of GPN and D-GPN on $\Delta[Ca^{2+}]_c$. Results are means ± SEM for 3 independent experiments.

4.3.5 Other weak bases evoke ER-dependent Ca^{2+} signals

GPN, but not D-GPN, is a substrate for cathepsin C, but both are amphipathic weak bases (Table 4.3), which, in common with other lysosomotropic agents, accumulate within lysosomes (Figure 4.27A) (Nadanaciva *et al*., 2011; Villamil Giraldo *et al*., 2014). Therefore, the actions of GPN were compared with NH_4Cl, another lysosomotropic agent that is often used to increase pH_{ly} (e.g., Johnson *et al*., 2016), and with an unrelated structure, fluoxetine (the antidepressant, Prozac), which also has lysosomotropic properties (Lu *et al.*, 2017). As expected NH_4Cl and fluoxetine caused transient increases in pH_{cyt}, similar to those evoked by GPN (Figure 4.27B, C).

Table 4.3 Properties of GPN, fluoxetine and established lysosomotropic agents.

	[a]Estimated pK_a	[a]Estimated ACD/logP	[d]Estimated *C*logP
NH_3	8.86	-0.98	ND
LysoTracker Red	[b]7.5	ND	[b]2.10
[c]GPN	7.84	2.40	3.01
Fluoxetine	9.8	4.17	4.57

Basic pK_a refers to the pK_a of the most basic moiety within the molecule. logP is the log of the partition coefficient of the neutral species between n-octanol and water. ACD/logP and *C*log*P* are derived from different algorithms used to estimate logP values (reviewed in Mannhold *et al.*, 2009). [a]From Chemicalize (2018) calculation module: https://chemicalize.com/ developed by ChemAxon (http://www.chemaxon.com); except for [b](Duvvuri *et al.*, 2004). [c]For GPN, the most extremely basic moieties were disregarded, since their pK_a values (13.6 and 15.3) lie too far beyond the physiological pH range; pK_a values determined using the ACD/PhysChem Suite, version 12.0, Advanced Chemistry Development Inc, Toronto, Canada (http://ilab.cds.rsc.org/?cdsrdr=1). [d]From http://ilab.cds.rsc.org/?cdsrdr=1, except for [b](Duvvuri *et al.*, 2004). Most lysosomotropic compounds have basic pK_a values >6.5 and *C*log*P* values >2 (McCarl *et al.*, 2009). ND, not determined.

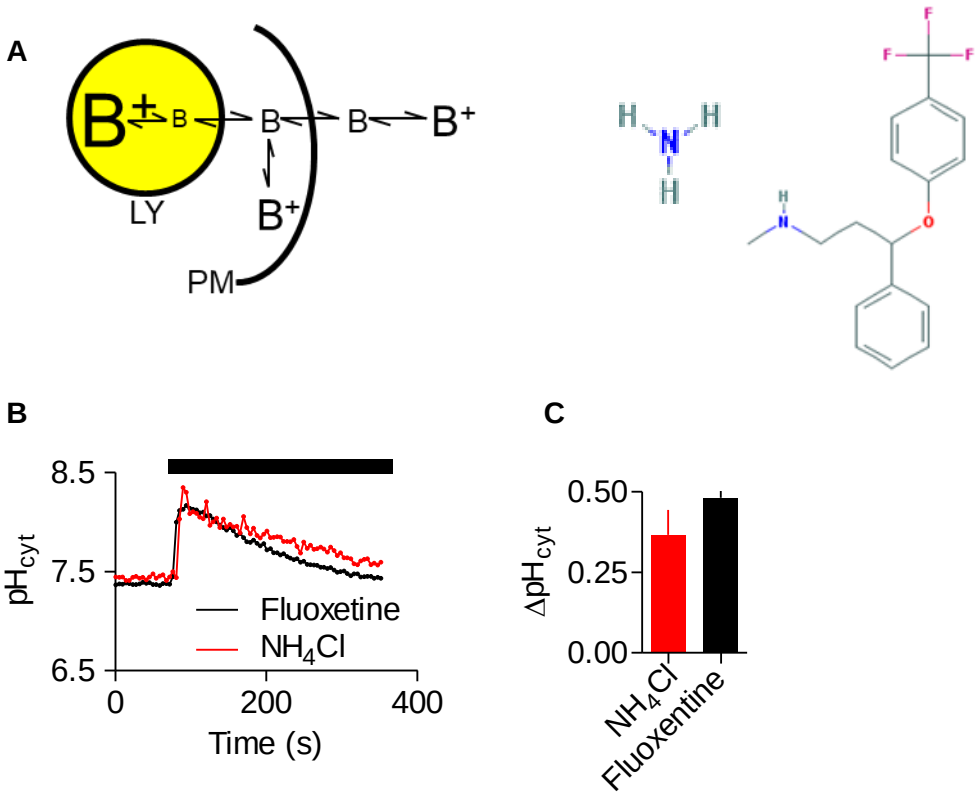

Figure 4.27 **Other compounds that increase pH_{cyt}.** (A) Structures and mechanisms of action of some lysosomotropic drugs. B and B^+ is the unprotonated and protonated form of a weakly basic compound respectively (B) A population of HEK cells loaded with SNARF-5F were stimulated with fluoxetine (300 μM) and NH_4Cl (20 mM). Results are mean ± SD from 3 wells in one experiment. (C) Summary results show the peak increase in pH_{cyt} (ΔpH_{cyt}). Results are means ± SEM from 3 independent experiments.

NH_4Cl and fluoxetine also caused a rapid increase in pH_{ly}, revealed by the loss of LysoTracker accumulation in HEK cells (Figure 4.28A-C). This is in agreement with previous reports of weak bases, such as fluoxetine, resulting in loss of LysoTracker accumulation in lysosomes (Kazmi *et al.*, 2013; Lu *et al.*, 2017).

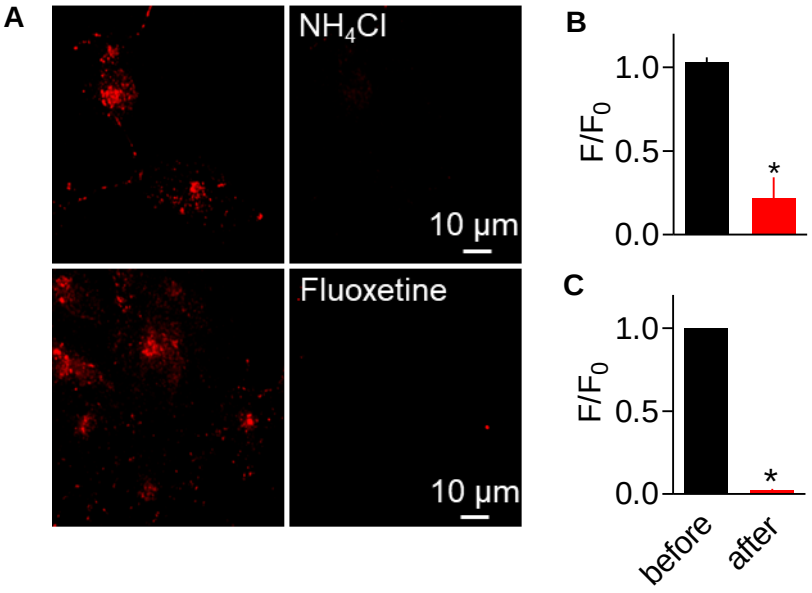

Figure 4.28 **Fluoxetine and NH_4Cl acutely increase pH_{ly}.** (A) Confocal images of HEK cells loaded with LysoTracker Red (100 nM, 20 min) and then treated (200 s) with NH_4Cl (20 mM) or fluoxetine (300 µM). (B-C) Summary results (mean ± SEM, n = 3-4) show fluorescence as F/F_0, where F_0 and F are fluorescence recorded before and 200 s after the addition of NH_4Cl (B) or fluoxetine (C). $^*P < 0.05$, paired Student's t-test.

D-GPN, the form of GPN that is not a substrate for cathepsin C, also increased $[Ca^{2+}]_c$ and this was abolished by thapsigargin (Figure 4.29). Similarly, NH_4Cl and fluoxetine caused increases in $[Ca^{2+}]_c$, like those evoked by GPN, which were also abolished by thapsigargin (Figure 4.29).

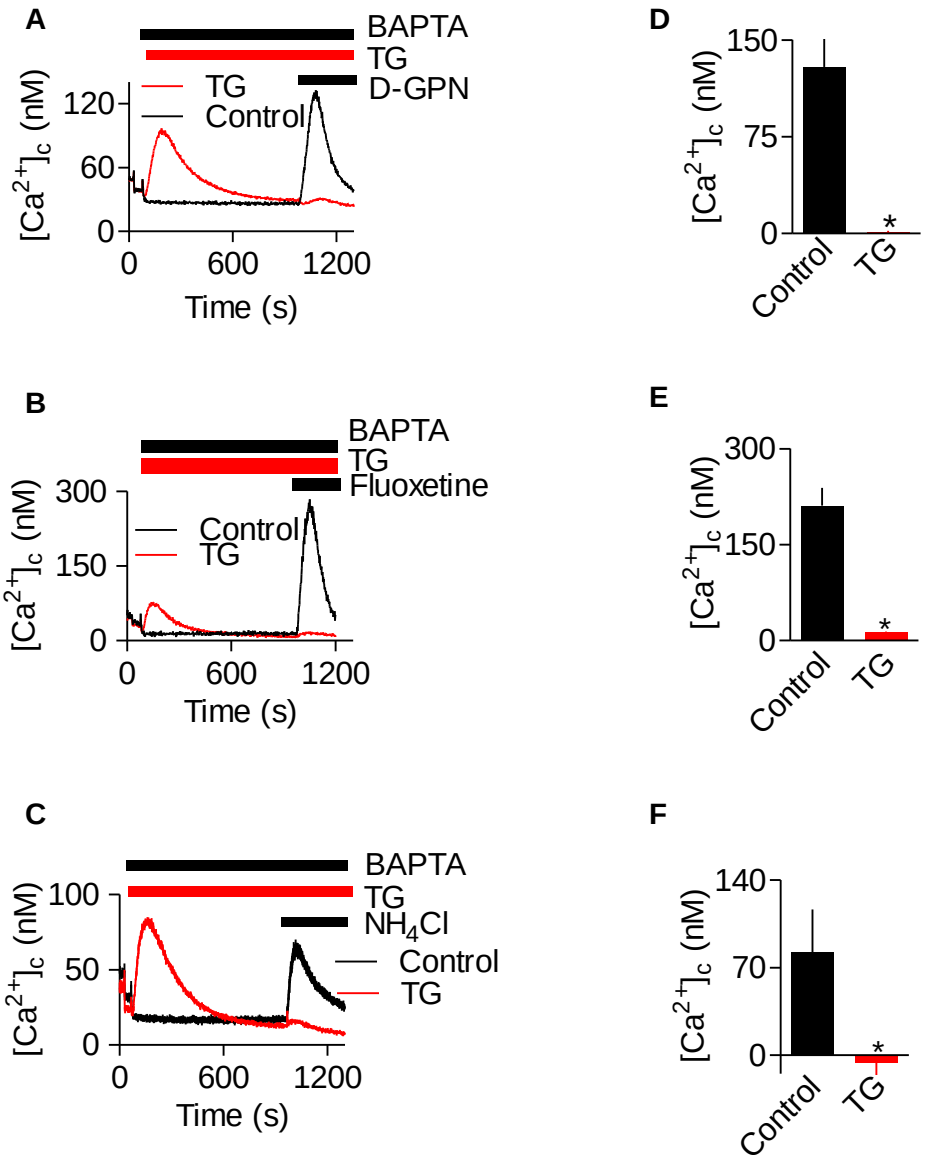

Figure 4.29 **Other weak bases cause increases in $[Ca^{2+}]_c$ that are dependent on Ca^{2+} within the ER**. (A-C) Effects of thapsigargin (TG, 1 μM, 15 min) in Ca^{2+}-free HBS on the Ca^{2+} signals evoked by D-GPN (200 μM) (A), fluoxetine (300 μM) (B), or NH_4Cl (20 mM) (C). Results show mean ± SD with 3 determinations. (D-F) Summary results show peak increases in $[Ca^{2+}]_c$ following D-GPN (200 μM) (D), fluoxetine (300 μM) (E), or NH_4Cl (20 mM) (F), with or without thapsigargin. Mean ± SEM, n = 3, each with 3 replicates. $^*P < 0.05$, Student's t-test.

Using carbachol or thapsigargin to estimate the residual Ca^{2+} content of the ER (by stimulating IP_3 formation or inhibiting SERCA, respectively), both GPN and NH_4Cl were observed to cause a concentration-dependent decrease in the ER Ca^{2+} content (Figure 4.30). Since CCh, through IP_3, stimulates Ca^{2+} release, while TG, by inhibiting SERCA, unmasks a basal leak, the peak amplitudes of the Ca^{2+} signals are different for the two stimuli. Both, however, reveal a similar concentration-dependent decrease in ER Ca^{2+} content after GPN treatment

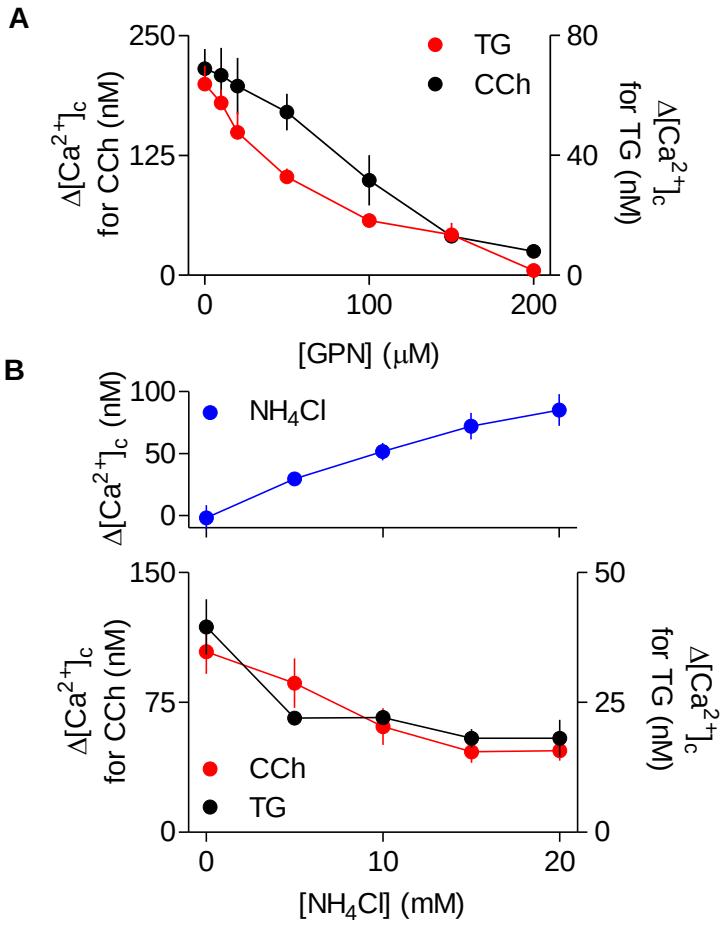

Figure 4.30 **GPN and NH_4Cl deplete the ER of Ca^{2+}.** (A) HEK cells were stimulated with the indicated concentrations of GPN (15 min) in Ca^{2+}-free HBS before addition of carbachol (CCh, 1 mM) or thapsigargin (TG, 1 μM) to estimate the amount of Ca^{2+} remaining within the ER. Results (mean ± SEM, n = 3) show the $\Delta[Ca^{2+}]_c$ for CCh or TG. (B) Similar analyses (mean ± SEM, n = 4-6) show the effects of pre-treatment with NH_4Cl (15 min) on the subsequent $\Delta[Ca^{2+}]_c$ evoked by CCh or TG. The upper panel shows $\Delta[Ca^{2+}]_c$ evoked by NH_4Cl.

These results establish that four different weak bases (GPN, D-GPN, NH_4Cl and fluoxetine) have similar effects. Each causes a sustained increase in pH_{ly}, and transient increases in pH_{cyt} and $[Ca^{2+}]_c$. The latter invariably requires Ca^{2+} within the ER.

4.3.6 GPN stimulates Ca^{2+} release from the ER by increasing pH_{cyt}.

Since no known CICR mechanism contributes to the Ca^{2+} signals evoked by GPN (**Section 4.3.3)**, the requirement for ER Ca^{2+} cannot arise from it amplifying an initial GPN-evoked Ca^{2+} release from lysosomes. However. as discussed in **Chapter 3**, the ER is important for lysosomal Ca^{2+} uptake. Therefore, a plausible possibility was that the primary action of GPN might be to trigger Ca^{2+} release from lysosomes, which might then be attenuated when lysosomes can no longer acquire Ca^{2+} from ER. Evidence that IP_3-evoked Ca^{2+} release from the ER immediately attenuates responses to GPN (Figure 4.11) argues against this proposal, and subsequent experiments confirm that it is untenable.

After dissipation of the pH_{ly} gradient by sustained treatment with bafilomycin A_1, the GPN-evoked increase in $[Ca^{2+}]_c$ was exaggerated (Figure 4.31A, B), just as responses to Ca^{2+} release from the ER through IP_3Rs or inhibition of SERCA are exaggerated after bafilomycin A_1 treatment (**Chapter 3**). Hence, under conditions where GPN cannot cause an increase in pH_{ly} and when lysosomes are thought to be unable to accumulate Ca^{2+} (**Chapter 3**), GPN evokes larger increases in $[Ca^{2+}]_c$. Therefore, it was important to consider whether the GPN-evoked increases in pH_{cyt} might directly stimulate Ca^{2+} release from the ER.

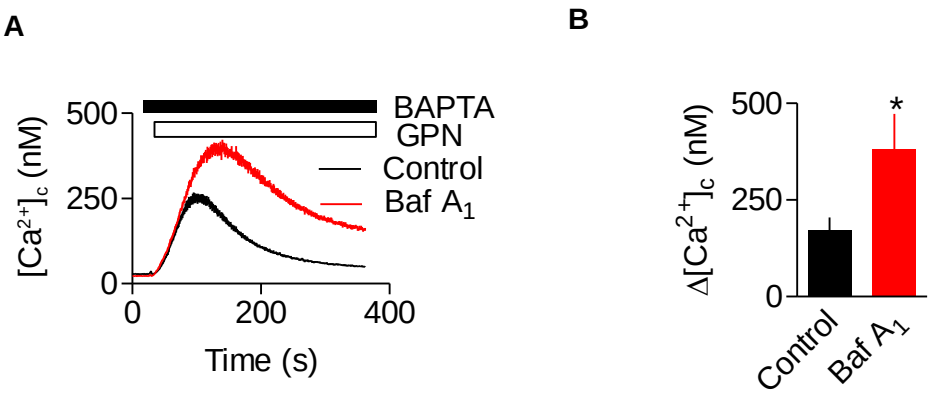

Figure 4.31 **GPN-induced increase in $[Ca^{2+}]_c$ is not prevented by loss of the lysosomal H^+ gradient**. (A) Effects of bafilomycin A_1 (Baf A_1, 1 μM, 1 h) on the Ca^{2+} signals evoked by GPN (200 μM) in HEK cells in Ca^{2+}-free HBS. Mean ± SD of 3 replicates. (B) Summary (mean ± SEM, n = 4, with 3 replicates). $^*P < 0.05$, Student's t-test.

HEK cells were loaded with sodium propionate (NaP), a weak acid, to buffer the pH_{cyt} changes evoked by GPN. NaP caused an initial drop in pH_{cyt}, but it slowly recovered. Subsequent addition of GPN then caused an attenuated increase in pH_{cyt} (Figure 4.32A, B). The immediate effect of GPN on pH_{cyt} was only modestly attenuated by NaP, but by 2 min the response was reduced by more than 60% (Figure 4.32).

Pre-treatment with NaP did not affect LysoTracker accumulation in HEK cells, and GPN rapidly dissipated this accumulation (Figure 4.33). Therefore, treatment with NaP does not affect the GPN-mediated increase in pH_{ly}.

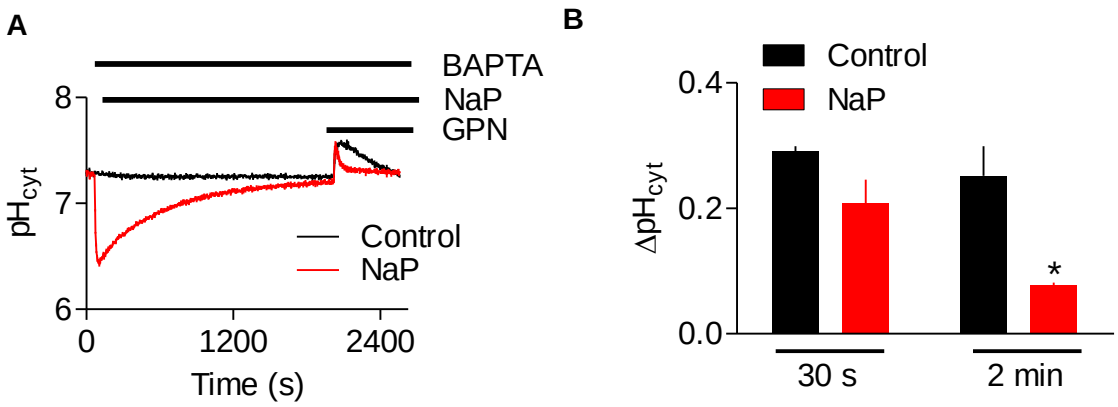

Figure 4.32 **Sodium propionate attenuates the prolonged increase in pH_{cyt} evoked by GPN.** (A) Population of HEK cells loaded with SNARF-5F in Ca^{2+}-free HBS were treated with sodium proprionate (NaP, 30 mM) before addition of GPN (200 µM). Results show pH_{cyt} (mean of 3 replicates). (B) Summary (mean ± SEM, *n* = 3, each with 3 replicates) show ΔpH_{cyt} measured 30 s or 2 min after GPN addition.

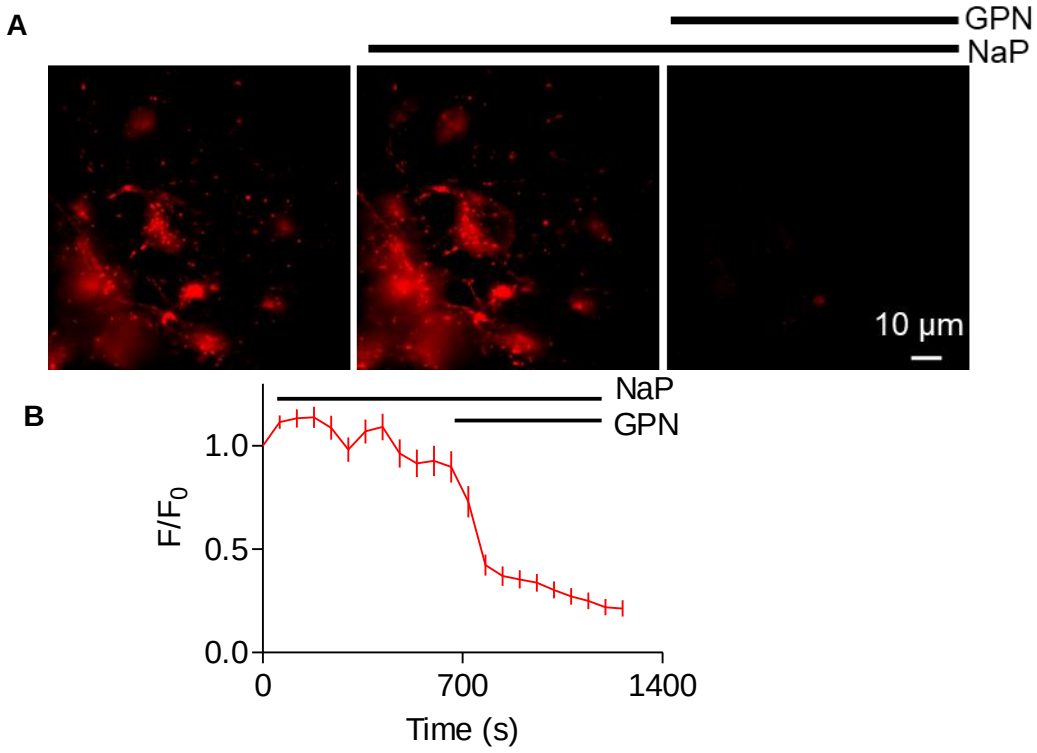

Figure 4.33 **GPN increases pH_{ly} in the presence of sodium propionate of HEK cells.** (A) Typical images of the effects of NaP (30 mM, 30 min) and then GPN (200 µM, 30 s) on LysoTracker Red staining. (B) Time-course shows the effect of of NaP (30 mM, 10 min) and then GPN (200 µM, 30 s) on LysoTracker Red staining. Mean ± SD, from 3 cells.

The GPN-evoked increase in $[Ca^{2+}]_c$, which takes 106 ± 2 s to reach its peak (Figure 4.4), was almost abolished by NaP (Figure 4.34A, B). NaP had no effect on the increase in $[Ca^{2+}]_c$ evoked by carbachol or the Ca^{2+} content of the intracellular stores assessed by addition of ionomycin (Figure 4.34C, D).

These results demonstrate that an increase in pH_{cyt} is required for GPN to increase $[Ca^{2+}]_c$, while an increase in pH_{ly} is ineffective.

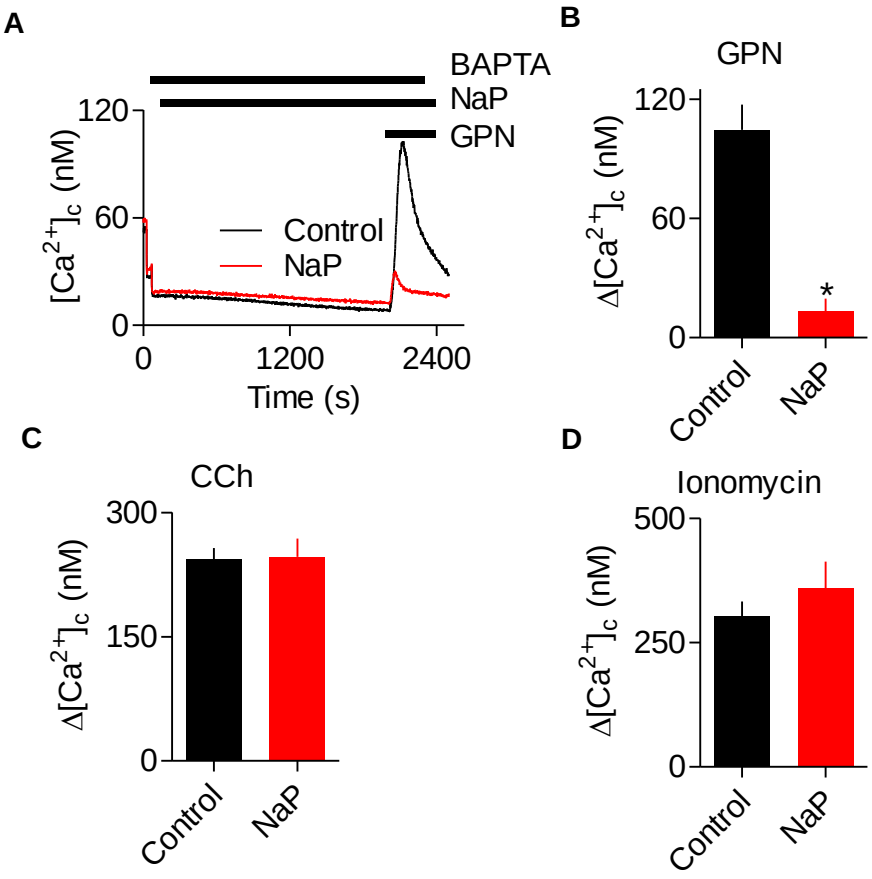

Figure 4.34 **Pre-incubation with sodium propionate selectively attenuates the GPN-induced increase in $[Ca^{2+}]_c$.** (A) Populations of HEK cells loaded with fluo 8 in Ca^{2+}-free HBS were treated with sodium proprionate (NaP, 30 mM) before addition of GPN (200 µM). Results show $[Ca^{2+}]_c$ (mean of 3 replicates). (B-D) Summary results (mean ± SEM, n = 4 (B) or 3 (C, D), each with 3 replicates) show peak Ca^{2+} signals ($\Delta[Ca^{2+}]_c$) evoked by GPN (200 µM, B), carbachol (CCh, 1 mM, C) or ionomycin (5 µM, D) in Ca^{2+}-free HBS following treatment with NaP (30 mM). $^*P < 0.05$, Student's t-test.

4.4 Conclusions

GPN is used extensively to perturb lysosomes and, as interest in the contributions of lysosomes to Ca^{2+} signalling has grown, GPN has been widely used to release Ca^{2+} from lysosomes (**Section 4.1**). It has been universally assumed that GPN achieves selectivity for lysosomes because its cleavage by a lysosomal enzyme, cathepsin C, causes an osmotic stress that ruptures lysosomal membranes (Figure 4.1). My results challenge these assumptions and demonstrate that GPN does not selectively target lysosomes.

GPN does not acutely rupture lysosomes (Figure 4.2, 4.7, 4.8) and it causes a transient increase in pH_{cyt} (Figure 4.5). GPN also increases pH_{ly} and $[Ca^{2+}]_c$. None of these effects of GPN requires cathepsin C (**Section 4.3.4**). The GPN-evoked increase in $[Ca^{2+}]_c$ is mediated by Ca^{2+} release from the ER, with no evident involvement of lysosomes: the Ca^{2+} signals are abolished by depleting the ER of Ca^{2+} (Figure 4.10, 4.13, 4.29), amplified when lysosomes are no longer acidified (Figure 4.31), and they show no requirement for CICR from the ER (Figure 4.13).

Several lines of evidence show that the GPN-evoked increase in pH_{cyt} stimulates Ca^{2+} release from the ER. Other membrane-permeant weak bases mimic GPN (**Section 4.3.5**), depleting the ER of Ca^{2+} abolishes the GPN-evoked increase in $[Ca^{2+}]_c$ (Figure 4.10, 4.13, 4.29) without affecting the pH_{cyt} increase (Figure 4.12), and an increase in pH_{ly} is not required for GPN to release Ca^{2+} (Figure 4.31). Finally, GPN-evoked Ca^{2+} release is almost abolished by buffering the pH_{cyt} changes under conditions where GPN still causes an increase in pH_{ly} (**Section 4.3.6**). This suggests that GPN, and other membrane-permeant weak bases, cause an increase in pH_{cyt}, which then stimulates Ca^{2+} release from the ER (Figure 4.35).

Cells tightly control their pH_{cyt} passively with buffers, and actively by means of ion transporters (Casey *et al.*, 2010), but many stimuli cause acute increases in pH_{cyt} at least as large as those evoked by GPN ($\Delta pH = 0.37 \pm 0.06$, Figure 4.5). The stimuli include those that activate the plasma membrane Na^+-H^+ exchanger (NHE) through protein kinase C (Wakabayashi *et al.*, 2006) and signals that prepare sperm for fertilization (Babcock *et al.*, 1983).

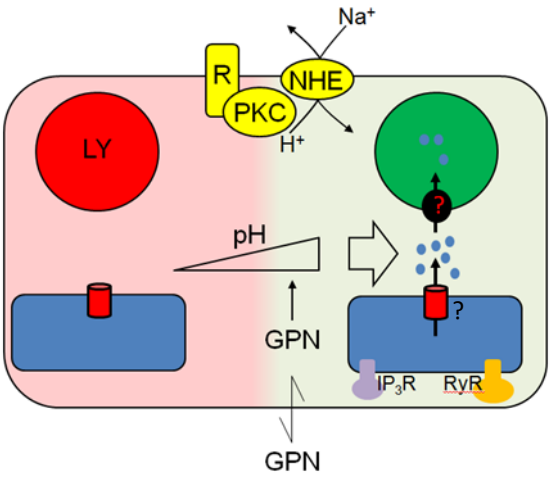

Figure 4.35 **GPN evokes Ca^{2+} release from the ER via an increase in pH_{cyt}.** GPN, a weak membrane-permeant base, causes pH_{cyt} to transiently increase and this directly stimulates Ca^{2+} release from the ER by a mechanism that requires neither IP_3Rs nor RyRs. Some of the Ca^{2+} released by this pH-regulated mechanism, in common with that released by IP_3Rs, is then accumulated by lysosomes (LY). Many physiological stimuli that increase pH_{cyt}, including those that stimulate NHE through protein kinase C (PKC), may evoke increases in $[Ca^{2+}]_c$ through the same pathway.

Furthermore, in tumours, pH_{cyt} is often increased (Schreiber, 2005). In many cell types, an increase in pH_{cyt} increases $[Ca^{2+}]_c$. In some cells, the response requires Ca^{2+} entry (Grinstein & Goetz, 1985; Wakabayashi *et al.*, 2006), but in many others it is due to Ca^{2+} release from intracellular stores, most likely the ER (Siskind *et al.*, 1989; Shorte *et al.*, 1991; Batlle *et al.*, 1993; Yodozawa *et al.*, 1997; Speake & Elliott, 1998; Willoughby *et al.*, 2001). The mechanisms are unknown, and since the pH of the ER lumen (pH_{ER}) is assumed to equilibrate rapidly with pH_{cyt} (Casey *et al.*, 2010), the effect might be exercised from the cytosol or ER lumen. Because increased pH_{ER} would be expected to increase Ca^{2+} buffering and so decrease ER luminal free $[Ca^{2+}]$, the Ca^{2+} release evoked by increased pH_{cyt} is probably due to the opening of a Ca^{2+}-permeable ER channel. At increased pH_{cyt}, phospholipase C may be stimulated (Yodozawa *et al.*, 1997) and IP_3 also binds more tightly to IP_3Rs (Joseph *et al.*, 1989), but GPN-evoked Ca^{2+} release does not require IP_3Rs (Figure 4.13). SERCA, which transports Ca^{2+} in exchange for H^+, is inhibited by increased pH (Lytton *et al.*, 1992; Li *et al.*, 2012). Inhibition of SERCA cannot explain my results because the Ca^{2+} release evoked by GPN was both faster and more substantial than that evoked by inhibition of SERCA by CPA

or thapsigargin (Figure 4.4, 4.13). Hence, modest increases in pH_{cyt}, similar to those evoked by many physiological stimuli, trigger a substantial Ca^{2+} release from the ER that requires neither RyRs nor IP_3Rs.

The evidence that GPN induces lysosomal rupture is not well substantiated in the literature. Multiple studies rely on acidotropic dyes such as lysotracker red and acridine orange as a measure of LMP (Haller *et al.*, 1996; Penny *et al.*, 2014; Ruas *et al.*, 2015) . However, this is problematic as the distribution of these dyes is pH-dependent. GPN was shown to cause a partial loss of lucifer yellow in normal Rat Kidney Epithelial Cells (Bright *et al.*, 2016). Furthermore, GPN was also shown to acutely reduce the fluorescence of MagicRed in lysosomes, reporting LMP (Skowyra *et al.*, 2018). However, NH_4Cl which has been shown not to induce LMP (Skowyra *et al.*, 2018), has also been shown to markedly reduce MagicRed fluorescence in mammalian cells (Johnson *et al.*, 2016). Nevertheless, GPN was shown to mediate ESCRT-recruitment to lysosomes to a lesser degree than following LeuLeuOMe, in a Ca^{2+}-dependent manner (Skowyra *et al.*, 2018). Whereas GPN-induced LMP was assessed via a pH-sensitive molecule (MagicRed), LeuLeuOMe -induced LMP was more robustly assessed using pH independent markers such as Gal3 and endocytosed dextrans. Nevertheless, there remains gaps and inconsistencies between the evidence of the effect of GPN on lysosomal membranes and previously reported effects of GPN on Ca^{2+} signals. Careful reconsideration of the preceding literature on the use of GPN as a Ca^{2+} release tool selective to lysosome is required in light of this new evidence showing the effects of GPN on cytosolic pH and Ca^{2+}.

In conclusion the results presented here show that, GPN does not, as hitherto supposed, evoke Ca^{2+} release from lysosomes through its cathepsin C-mediated proteolysis. Instead, GPN, in common with other membrane-permeant weak bases and many physiological stimuli, transiently increases pH_{cyt}, and that directly stimulates Ca^{2+} release from the ER by a mechanism that is independent of known ER Ca^{2+} release channels.

5. Conclusions

Lysosomes have been reported to contain substantial amounts of Ca^{2+} (Christensen *et al.*, 2002), and they are increasingly regarded as a Ca^{2+} store. Lysosomes express Ca^{2+} release channels, including TRPML, TPC2 and ATP-regulated P2X4 receptors, that allow Ca^{2+} release by specific stimulus (Morgan *et al.*, 2011). Ca^{2+} uptake by lysosomes has been proposed to be facilitated by MCS between lysosomes and ER, stabilized by scaffold proteins (Taylor, 1998; Probst *et al.*, 2006; Alpy *et al.*, 2013; Friedman *et al.*, 2013; Phillips & Voeltz, 2016). The cytosolic Ca^{2+} signals evoked by TRPML or TPC2 can be amplified by CICR through IP_3Rs or RyRs in closely apposed ER (Nakade *et al.*, 1994; Patel *et al.*, 2010; Morgan *et al.*, 2011). Conversely, Ca^{2+} released by ER channels can be rapidly sequestered by lysosomes. This sequestration can both attenuate cytosolic Ca^{2+} signals evoked by IP_3Rs (Lopez Sanjurjo *et al.*, 2013) and, by loading lysosomes with Ca^{2+}, prime TPC2 to respond (Morgan *et al.*, 2013), control fusion and fission within endolysosomal pathways (Ruas *et al.*, 2010), and regulate autophagy and lysosomal biogenesis through calcineurin activated by TRMPL-mediated Ca^{2+} release (Medina *et al.*, 2015). A major limitation in the field is the lack of tools both to measure luminal lysosomal $[Ca^{2+}]$ and to selectively release Ca^{2+} from lysosomes.

In the first part of this project (**Chapter 3**), I investigated the role of IP_3R in regulating lysosomal Ca^{2+} homeostasis. Previous work from this laboratory showed that lysosomes selectively sequester Ca^{2+} released from IP_3Rs and not Ca^{2+} entering via SOCE assessed via global $[Ca^{2+}]_c$ measurements (Lopez-Sanjurjo *et al.*, 2013). But the mechanisms underlying this selectivity were not clear. In this project, I investigated mechanisms regulating the transfer of Ca^{2+} from the ER to lysosomes. From the results presented, I draw the following conclusions:

1. The ER through its SERCA and IP_3Rs, provides a route through which Ca^{2+} can be accumulated from the low $[Ca^{2+}]_c$ of resting cells by a high-affinity uptake system (SERCA) and then delivered locally through large-conductance channels (IP_3Rs and perhaps others) at a high local concentration to a low-affinity uptake system in lysosomes. The ER, with its high-affinity SERCA and large-conductance Ca^{2+} channels, behaves like a compressor or piston linking a low $[Ca^{2+}]_c$ to the low-affinity

uptake systems of lysosomes. This provides a close analogy with the relationship between ER and MCU in mitochondria.

2. Increasing pH_{ly} does not immediately prevent Ca^{2+} uptake, but it slowly causes lysosomes to enlarge, redistribute, reduce their affiliation with IP_3Rs and lose their ability to selectively sequester Ca^{2+} released by IP_3Rs. I suggest that abrogating the lysosomal H^+ gradient disrupts the contacts between ER and lysosomes, and thereby the ability of IP_3R to selectively deliver Ca^{2+} to lysosomes.

In the second part of this project (**Chapter 4**), I investigated the mechanism of action of GPN. GPN has been widely used to elucidate mechanisms of lysosomal Ca^{2+} uptake and release. GPN is proposed to be cleaved by cathepsin C, which I investigated further in **Chapter 4**. From the results presented in **Chapter 4**, I conclude that GPN does not, as hitherto supposed, evoke Ca^{2+} release from lysosomes through its cathepsin C-mediated proteolysis. Instead, GPN, in common with other membrane-permeant weak bases and many physiological stimuli, transiently increases pH_{cyt}, and that directly stimulates Ca^{2+} release from the ER by a mechanism that is independent of known ER Ca^{2+} release channels.

In summary, the coupling of lysosomes to the ER at MCS is critical for lysosome Ca^{2+} uptake. Although IP_3R are not essential for the formation of these MCS, they deliver their Ca^{2+} to the lysosomes at these junctions. It is still not clear if all lysosomal Ca^{2+} uptake occurs at the MCS between ER and lysosomes. This issue will be effectively resolved only when it becomes possible to measure the luminal $[Ca^{2+}]$ in individual lysosomes in contact with the ER. It has been suggested that IP_3R provide the only means by which Ca^{2+} exchange occurs from the ER to lysosomes (Garrity *et al.*, 2016). My results are consistent with ER-lysosome MCS being required for lysosomal Ca^{2+} uptake after Ca^{2+} release through IP_3R. This would provide a link between receptor-regulated IP_3 formation and Ca^{2+} handling by lysosomes. It remains to be determined whether the same contact sites are required for all Ca^{2+} uptake by lysosomes.

References

Abu-Remaileh M, Wyant GA, Kim C, Laqtom NN, Abbasi M, Chan SH, Freinkman E, Sabatini DM (2017). Lysosomal metabolomics reveals V-ATPase- and mTOR-dependent regulation of amino acid efflux from lysosomes. *Science* **358:** 807-813.

Aharon-Peretz J, Rosenbaum H, Gershoni-Baruch R (2004). Mutations in the glucocerebrosidase gene and Parkinson's Disease in Ashkenazi Jews. *New Engl J Med* **351:** 1972–1977.

Aits S, Jaattela M, Nylandsted J (2015). Methods for the quantification of lysosomal membrane permeabilization: a hallmark of lysosomal cell death. *Methods Cell Biol* **126:** 261-285.

Akazawa Y, Mott JL, Bronk SF, Werneburg NW, Kahraman A, Guicciardi ME, Meng XW, Kohno S, Shah VH, Kaufmann SH, McNiven MA, Gores GJ (2009). Death receptor 5 internalization is required for lysosomal permeabilization by TRAIL in malignant liver cell lines. *Gastroenterol* **136:** 2365-2376.

Albarran L, Lopez JJ, Woodard GE, Salido GM, Rosado JA (2016). Store-operated Ca^{2+} entry-associated regulatory factor (SARAF) plays an important role in the regulation of arachidonate-regulated Ca^{2+} (ARC) channels. *J Biol Chem* **291:** 6982-6988.

Albrieux M, Lee HC, Villaz M (1998). Calcium signaling by cyclic ADP-ribose, NAADP, and inositol trisphosphate are involved in distinct functions in ascidian oocytes. *J Biochem* **273:** 14566–14574.

Aley PK, Mikolajczyk AM, Munz B, Churchill GC, Galione A, Berger F (2010). Nicotinic acid adenine dinucleotide phosphate regulates skeletal muscle differentiation via action at two-pore channels. *Proc Natl Acad Sci* **107:** 19927–19932.

Allbritton NL, Meyer T, Stryer L (1992). Range of messenger action of calcium ion and inositol 1,4,5-trisphosphate. *Science* **258:** 1812-1815.

Alpy F, Rousseau A, Schwab Y, Legueux F, Stoll I, Wendling C, Spiegelhalter C, Kessler P, Mathelin C, Rio MC, Levine TP, Tomasetto C (2013). STARD3/STARD3NL and VAP make a novel molecular tether between late endosomes and the ER. *J Cell Sci* **126:** 5500-5512.

Alzayady KJ, Wang L, Chandrasekhar R, Wagner LE, 2nd, Van Petegem F, Yule DI (2016). Defining the stoichiometry of inositol 1,4,5-trisphosphate binding required to initiate Ca^{2+} release. *Sci Signal* **9:** ra35.

Ando H, Kawaai K, Mikoshiba K (2014). IRBIT: A regulator of ion channels and ion transporters. *Biochim Biophys Acta* **1843:** 2195-2204.

Ando H, Mizutani A, Matsu-ura T, Mikoshiba K (2003). IRBIT, a novel inositol 1,4,5-trisphosphate (IP_3) receptor-binding protein, is released from the IP_3 receptor upon IP_3 binding to the receptor. *J Biol Chem* **278:** 10602-10612.

Aniento F (1993). Cytoplasmic dynein-dependent vesicular transport from early to late endosomes *J Cell Biol* **123:** 1373–1387.

Aniento F, Gu F, Parton RG, Gruenberg J (1996). An endosomal β COP is involved in the pH-dependent formation of transport vesicles destined for late endosomes. *J Cell Biol* **133:** 29-41.

Antunes F, Cadenas E, Brunk UT (2001). Apoptosis induced by exposure to a low steady-state concentration of H_2O_2 is a consequence of lysosomal rupture. *Biochem J* **356:** 549-555.

Araiza-Casillas R, Cardenas F, Morales Y, Cardiel MH (2004). Factors associated with chloroquine-induced retinopathy in rheumatic diseases. *LUPUS* **13:** 119-124.

Ashoor R, Yafawi R, Jessen B, Lu S (2013). The contribution of lysosomotropism to autophagy perturbation. *PLoS One* **8:** e82481.

Aston D, Capel RA, Ford KL, Christian HC, Mirams GR, Rog-Zielinska EA, Kohl P, Galione A, Burton RA, Terrar DA (2017). High resolution structural evidence suggests the sarcoplasmic reticulum forms microdomains with acidic stores (lysosomes) in the heart. *Sci Rep* **7:** 40620.

Baars TL, Petri S, Peters C, Mayer A (2007). Role of the V-ATPase in regulation of the vacuolar fission-fusion equilibrium. *Mol Biol Cell* **18:** 3873-3882.

Babcock DF, Rufo GA, Jr., Lardy HA (1983). Potassium-dependent increases in cytosolic pH stimulate metabolism and motility of mammalian sperm. *Proc Natl Acad Sci* **80:** 1327-1331.

Bargal R, Avidan N, Ben-Asher E, Olender Z, Zeigler M, Frumkin A, Raas-Rothschild A, Glusman G, Lancet D, Bach G (2000). Identification of the gene causing mucolipidosis type IV. *Nat Genet* **26:** 118–123.

Basu SK, Goldstein JL, Anderson RG, Brown MS (1981). Monensin interrupts the recycling of low density lipoprotein receptors in human fibroblasts. *Cell* **24:** 493-502.

Batlle DC, Peces R, LaPointe MS, Ye M, Daugirdas JT (1993). Cytosolic free calcium regulation in response to acute changes in intracellular pH in vascular smooth muscle. *Am J Physiol* **264:** 932-943.

Baughman JM, Perocchi F, Girgis HS, Plovanich M, Belcher-Timme CA, Sancak Y, Bao XR, Strittmatter L, Goldberger O, Bogorad RL, Koteliansky V, Mootha VK (2011). Integrative genomics identifies MCU as an essential component of the mitochondrial calcium uniporter. *Nature* **476:** 341–345.

Bautista DM, Siemens J, Glazer JM, Tsuruda PR, Basbaum AI, Stucky CL, Jordt SE, Julius D (2007). The menthol receptor TRPM8 is the principal detector of environmental cold. *Nature* **448:** 204-208.

Berezhnov AV, Soutar MP, Fedotova EI, Frolova MS, Plun-Favreau H, Zinchenko VP, Abramov AY (2016). Intracellular pH modulates autophagy and mitophagy. *J Biol Chem* **291:** 8701-8708.

Berg TO, Stromhaug E, Lovdal T, Seglen O, Berg T (1994). Use of glycyl-L-phenylalanine 2-naphthylamide, a lysosome-disrupting cathepsin C substrate, to distinguish between lysosomes and prelysosomal endocytic vacuoles. *Biochem J* **300:** 229-236.

Bernstein HN, Ginsberg J (1964). The pathology of chloroquine retinopathy. *Arch ophthal* **71:** 238-245.

Berridge MJ (1997). Elementary and global aspects of calcium signalling. *J Physiol* **499:** 291-306.

Berridge MJ (2006). Calcium microdomains: organization and function. *Cell Calcium* **40:** 405-412.

Berridge MJ (2007). Inositol trisphosphate and calcium oscillations. *Biochem Soc Symp* **74:** 1-7.

Berridge MJ, Dawson RM, Downes CP, Heslop JP, Irvine RF (1983). Changes in the levels of inositol phosphates after agonist-dependent hydrolysis of membrane phosphoinositides. *Biochem J* **212:** 473-482.

Berridge MJ, Lipp P, Bootman MD (2000). The versatility and universality of calcium signalling. *Nat Rev Mol Cell Biol* **1:** 11-21.

Bers DM (2000). Calcium fluxes involved in control of cardiac myocyte contraction. *Circ Res* **87:** 275-281.

Bers DM (2002). Cardiac excitation-contraction coupling. *Nature* **415:** 198-205.

Bertram R, Sherman A, Satin LS (2010). Electrical bursting, calcium oscillations, and synchronization of pancreatic islets. *Adv Exp Med Biol* **654:** 261-279.

Bidere N, Lorenzo HK, Carmona S, Laforge M, Harper F, Dumont C, Senik A (2003). Cathepsin D triggers Bax activation, resulting in selective apoptosis-inducing factor (AIF) relocation in T lymphocytes entering the early commitment phase to apoptosis. *J Biol Chem* **278:** 31401-31411.

Biel M, Michalakis S (2009). Cyclic nucleotide-gated channels. *Hand Exp Pharmacol* **191:** 111-136.

Birnbaumer L (2009). The TRPC class of ion channels: a critical review of their roles in slow, sustained increases in intracellular Ca^{2+} concentrations. *Annu Rev Pharmacol Toxicol* **49:** 395-426.

Blaustein MP, Lederer WJ (1999). Sodium/calcium exchange: its physiological implications. *Physiol Rev* **79:** 763-854.

Bleasdale JE, Thakur NR, Gremban RS, Bundy GL, Fitzpatrick FA, Smith RJ, Bunting S (1990). Selective inhibition of receptor-coupled phospholipase C-dependent processes in human platelets and polymorphonuclear neutrophils. *J Pharmacol Exp Ther* **255:** 756-768.

Blondel O, Bell GI, Moody M, Miller RJ, Gibbons SJ (1994). Creation of an inositol 1,4,5-trisphosphate-sensitive Ca^{2+} store in secretory granules of insulin-producing cells. *J Biol Chem* **269:** 27167-27170.

Bodzeta A, Kahms M, Klingauf J (2017). The presynaptic v-ATPase reversibly disassembles and thereby modulates exocytosis but is not part of the fusion machinery. *Cell Rep* **20:** 1348-1359.

Bondebjerg J, Fuglsang H, Valeur KR, Kaznelson DW, Hansen JA, Pedersen RO, Krogh BO, Jensen BS, Lauritzen C, Petersen G, Pedersen J, Naerum L (2005). Novel semicarbazide-derived inhibitors of human dipeptidyl peptidase I (hDPPI). *Bioorg Med Chem* **13:** 4408-4424.

Bootman MD, Berridge MJ (1995). The elemental principles of calcium signaling. *Cell* **83:** 675-678.

Bootman MD, Collins TJ, Peppiatt CM, Prothero LS, MacKenzie L, De Smet P, Travers M, Tovey SC, Seo JT, Berridge MJ, Ciccolini F, Lipp P (2001). Calcium signalling-an overview. *Semin Cell Dev Biol* **12:** 3-10.

Bosanac I, Alattia J-R, Mal TK, Chan J, Talarico S, Tong FK, Tong KI, Yoshikawa F, Furuichi T, Iwai M, Michikawa T, Mikoshiba K, Ikura M (2002). Structure of the inositol 1,4,5-trisphosphate receptor binding core in complex with its ligand. *Nature* **420:** 696-700.

Boya P, Andreau K, Poncet D, Zamzami N, Perfettini JL, Metivier D, Ojcius DM, Jaattela M, Kroemer G (2003). Lysosomal membrane permeabilization induces cell death in a mitochondrion-dependent fashion. *J Exp Med* **197:** 1323-1334.

Brailoiu E, Churamani D, Cai X, Schrlau MG, Brailoiu GC, Gao X, Hooper R, Boulware MJ, Dun NJ, Marchant JS, Patel S (2009). Essential requirement for two-pore channel 1 in NAADP-mediated calcium signaling. *J Cell Biol* **186:** 201-219.

Brailoiu E, Hooper R, Cai X, Brailoiu GC, Keebler MV, Dun NJ, Marchant JS, Patel S (2010). An ancestral deuterostome family of two-pore channels mediates nicotinic acid adenine dinucleotide phosphate-dependent calcium release from acidic organelles. *J Biol Chem* **285:** 2897-2901.

Brandman O, Liou J, Park WS, Meyer T (2007). STIM2 is a feedback regulator that stabilizes basal cytosolic and endoplasmic reticulum Ca^{2+} levels. *Cell* **131:** 1327-1339.

Braulke T, Bonifacino JS (2009). Sorting of lysosomal proteins. *Biochim Biophys Acta* **1793:** 605–614.

Bright NA, Davis LJ, Luzio JP (2016). Endolysosomes are the principal intracellular sites of acid hydrolase activity. *Curr Biol* **26:** 2233-2245.

Bright NA, Gratian MJ, Luzio JP (2005). Endocytic delivery to lysosomes mediated by concurrent fusion and kissing events in living cells. *Curr Biol* **15:** 360–365.

Brini M, Carafoli E (2009). Calcium pumps in health and disease. *Physiol Rev* **89:** 1341-1378.

Brini M, Carafoli E (2011). The plasma membrane Ca^{2+} ATPase and the plasma membrane sodium calcium exchanger cooperate in the regulation of cell calcium. *Cold Spring Harb Persp Biol* **3:** a004168.

Bruce JIE, Shuttleworth TJ, Giovannucci DR, Yule DI (2002). Phosphorylation of inositol 1,4,5-trisphosphate receptors in parotid acinar cells. A mechanism for the synergistic effects of cAMP on Ca^{2+} signaling. *J Biol Chem* **277:** 1340-1348.

Buck E, Zimanyi I, Abramson JJ, Pessah IN (1992). Ryanodine stabilizes multiple conformational states of the skeletal muscle calcium release channel. *J Biol Chem* **267:** 23560-23567.

Burnashev N (1998). Calcium permeability of ligand-gated channels. *Cell Calcium* **24:** 325-332.

Burnashev N, Zhou Z, Neher E, Sakmann B (1995). Fractional calcium currents through recombinant GluR channels of the NMDA, AMPA and kainate receptor subtypes. *J Physiol* **485:** 403-418.

Cahalan MD (2009). STIMulating store-operated Ca^{2+} entry. *Nat Cell Biol* **11:** 669-677.

Cai X, Patel S (2010). Degeneration of an intracellular ion channel in the primate lineage by relaxation of selective constraints. *Mol Biol Evol* **27:** 2352-2359.

Calcraft PJ, Ruas M, Pan Z, Cheng X, Arredouani A, Hao X, Tang J, Rietdorf K, Teboul L, Chuang KT, Lin P, Xiao R, Wang C, Zhu Y, Lin Y, Wyatt CN, Parrington J, Ma J, Evans AM, Galione A, Zhu MX (2009). NAADP mobilizes calcium from acidic organelles through two-pore channels. *Nature* **459:** 596-600.

Cancela JM, Churchill GC, Galione A (1999). Coordination of agonist-induced Ca^{2+}-signalling patterns by NAADP in pancreatic acinar cells. *Nature* **398:** 74–76.

Cang C, Zhou Y, Navarro B, Seo YJ, Aranda K, Shi L, Battaglia-Hsu S, Nissim I, Clapham DE, Ren D (2013). mTOR regulates lysosomal ATP-sensitive two-pore Na^+ channels to adapt to metabolic state. *Cell* **152:** 778-790.

Canton J, Grinstein S (2015). Measuring lysosomal pH by fluorescence microscopy. *Methods Cell Biol* **126:** 85-99.

Cao Q, Yang Y, Zhong XZ, Dong XP (2017). The lysosomal Ca^{2+} release channel TRPML1 regulates lysosome size by activating calmodulin. *J Biol Chem* **292:** 8424-8435.

Cao Q, Zhong XZ, Zou Y, Murrell-Lagnado R, Zhu MX, Dong X-P (2015). Calcium release through P2X4 activates calmodulin to promote endolysosomal membrane fusion. *J Cell Bio* **209:** 879.

Carafoli E (1991). Calcium pump of the plasma membrane. *Physiol Rev* **71:** 129-153.

Cárcel-Trullols J, Kovács AD, Pearce DA (2015). Cell biology of the NCL proteins: What they do and don't do. *Biochim Biophys Acta* **1852:** 2242–2255.

Cardenas C, Miller RA, Smith I, Bui T, Molgo J, Muller M, Vais H, Cheung KH, Yang J, Parker I, Thompson CB, Birnbaum MJ, Hallows KR, Foskett JK (2010). Essential regulation of cell bioenergetics by constitutive $InsP_3$ receptor Ca^{2+} transfer to mitochondria. *Cell* **142:** 270-283.

Carpenter AE, Jones TR, Lamprecht MR, Clarke C, Kang IH, Friman O, Guertin DA, Chang JH, Lindquist RA, Moffat J, Golland P, Sabatini DM (2006). CellProfiler: image analysis software for identifying and quantifying cell phenotypes. *Genome biol* **7:** R100.

Casey JR, Grinstein S, Orlowski J (2010). Sensors and regulators of intracellular pH. *Nat Rev Mol Cell Biol* **11:** 50-61.

Catterall WA (1991). Excitation-contraction coupling in vertebrate skeletal muscle: a tale of two calcium channels. *Cell* **64:** 871-874.

Catterall WA (2000). From ionic currents to molecular mechanisms: the structure and function of voltage-gated sodium channels. *Neuron* **26:** 13-25.

Cerny J, Feng Y, Yu A, Miyake K, Borgonovo B, Klumperman J, Meldolesi J, McNeil PL, Kirchhausen T (2004). The small chemical vacuolin-1 inhibits Ca^{2+}-dependent lysosomal exocytosis but not cell resealing. *EMBO Rep* **5:** 883-888.

Ch'Ng JH, Liew K, Goh ASP, Sidhartha E, Tan KSW (2011). Drug-induced permeabilization of parasite's digestive vacuole is a key trigger of programmed cell death in Plasmodium falciparum. *Cell Death Dis* **2:** e216.

Chakraborty K, Leung K (2017). High lumenal chloride in the lysosome is critical for lysosome function. *Elife* **6:** e28862.

Chakraborty S, Deb BK, Chorna T, Konieczny V, Taylor CW, Hasan G (2016). Mutant IP_3 receptors attenuate store-operated Ca^{2+} entry by destabilizing STIM-Orai interactions in *Drosophila* neurons. *J Cell Sci* **129:** 3903-3910.

Chaloux B, Caron AZ, Guillemette G (2007). Protein kinase A increases the binding affinity and the Ca^{2+} release activity of the inositol 1,4,5-trisphosphate receptor type 3 in RINm5F cells. *Biol Cell* **99:** 379-388.

Chang CL, Chen YJ, Quintanilla CG, Hsieh TS (2018). EB1 binding restricts STIM1 translocation to ER-PM junctions and regulates store-operated Ca^{2+} entry. *J Cell Biol* **217:** 2047-2058.

Chang J, Lee S, Blackstone C (2013). Protrudin binds atlastins and endoplasmic reticulum-shaping proteins and regulates network formation. *Proc Natl Acad Sci* **110:** 14954-14959.

Chaurra A, Gutzman BM, Taylor E, Ackroyd PC, Christensen KA (2011). Lucifer Yellow as a live cell fluorescent probe for imaging water transport in subcellular organelles. *Appl spectro* **65:** 20-25.

Chini EN, Beers KW, Dousa TP (1995). Nicotinate adenine dinucleotide phosphate (NAADP) triggers a specific calcium release system in sea urchin eggs. *J Biol Chem* **270:** 3216-3223.

Christensen KA, Myers JT, Swanson JA (2002). pH-dependent regulation of lysosomal calcium in macrophages. *J Cell Sci* **115:** 599-607.

Churchill GC, Okada Y, Thomas JM, Genazzani AA, Patel S, Galione A (2002). NAADP mobilizes Ca^{2+} from reserve granules, lysosome-related organelles, in sea urchin eggs. *Cell* **111:** 703-708.

Cigic B, Krizaj I, Kralj B, Turk V, Pain RH (1998). Stoichiometry and heterogeneity of the pro-region chain in tetrameric human cathepsin C. *Biochim Biophys Acta* **1382:** 143-150.

Clague MJ, Urbe S, Aniento F, Gruenberg J (1994). Vacuolar ATPase activity is required for endosomal carrier vesicle formation. *J Biol Chem* **269:** 21-24.

Clapper DL, Walseth TF, Dargie PJ, Lee HC (1987). Pyridine nucleotide metabolites stimulate calcium release from sea urchin egg microsomes desensitized to inositol trisphosphate. *J Biol Chem* **262:** 9561-9568.

Coen K, Flannagan RS, Baron S, Carraro-Lacroix LR, Wang D, Vermeire W, Michiels C, Munck S, Baert V, Sugita S, Wuytack F, Hiesinger PR, Grinstein S, Annaert W (2012).

Lysosomal calcium homeostasis defects, not proton pump defects, cause endo-lysosomal dysfunction in PSEN-deficient cells. *J Cell Biol* **198:** 23-35.

Collins TJ, Lipp P, Berridge MJ, Bootman MD (2001). Mitochondrial Ca^{2+} uptake depends on the spatial and temporal profile of cytosolic Ca^{2+} signals. *J Biol Chem* **276:** 26411-26420.

Collins TP, Bayliss R, Churchill GC, Galione A, Terrar DA (2011). NAADP influences excitation-contraction coupling by releasing calcium from lysosomes in atrial myocytes. *Cell Calcium* **50:** 449-458.

Cooper GM, Hausman RE (2000). *The Cell*. edn, vol. 85. Sinauer Associates, Sunderland.

Cosker F, Cheviron N, Yamasaki M, Menteyne A, Lund FE, Moutin MJ, Galione A, Cancela JM (2010). The ecto-enzyme CD38 is a nicotinic acid adenine dinucleotide phosphate (NAADP) synthase that couples receptor activation to Ca^{2+} mobilization from lysosomes in pancreatic acinar cells. *J Biol Chem* **285:** 38251-38259.

Cosson P, Marchetti A, Ravazzola M, Orci L (2012). Mitofusin-2 independent juxtaposition of endoplasmic reticulum and mitochondria: an ultrastructural study. *PLoS One* **7:** e46293.

Costes SV, Daelemans D, Cho EH, Dobbin Z, Pavlakis G, Lockett S (2004). Automatic and quantitative measurement of protein-protein colocalization in live cells. *Biophys J* **86:** 3993-4003.

Csordas G, Renken C, Varnai P, Walter L, Weaver D, Buttle KF, Balla T, Mannella CA, Hajnoczky G (2006). Structural and functional features and significance of the physical linkage between ER and mitochondria. *J Cell Biol* **174:** 915-921.

Csordas G, Varnai P, Golenar T, Roy S, Purkins G, Schneider TG, Balla T, Hajnoczky G (2010). Imaging interorganelle contacts and local calcium dynamics at the ER-mitochondrial interface. *Mol Cell* **39:** 121-132.

Cullen PJ, Lockyer PJ (2002). Integration of calcium and ras signalling. *Nat rev mol Cell Biol* **3:** 339-348.

Dakin K, Li WH (2007). Cell membrane permeable esters of D-*myo*-inositol 1,4,5-trisphosphate. *Cell Calcium* **42:** 291-301.

Davis LC, Morgan AJ, Chen JL, Snead CM, Bloor-Young D, Shenderov E, Stanton-Humphreys MN, Conway SJ, Churchill GC, Parrington J, Cerundolo V, Galione A (2012). NAADP activates two-pore channels on T cell cytolytic granules to stimulate exocytosis and killing. *Curr Biol* **22:** 2331-2337.

de Brito OM, Scorrano L (2008). Mitofusin 2 tethers endoplasmic reticulum to mitochondria. *Nature* **456:** 605-610.

de Duve C, de Barsy T, Poole B, Trouet A, Tulkens P, Van Hoof F (1974). Commentary. Lysosomotropic agents. *Biochem Pharmacol* **23:** 2495-2531.

De Stefani D, Raffaello A, Teardo E, Szabo I, Rizzuto R (2011). A forty-kilodalton protein of the inner membrane is the mitochondrial calcium uniporter. *Nature* **476:** 336-340.

De vos KJ, Mórotz GM, Stoica R, Tudor EL, Lau K, Ackerley S, Warley A, Shaw CE, Miller CC (2012). VAPB interacts with the mitochondrial protein PTPIP51 to regulate calcium homeostasis. *Hum Mol Genet.* **21:** 1299-1311.

Dellis O, Dedos S, Tovey SC, Rahman T-U-, Dubel SJ, Taylor CW (2006). Ca^{2+} entry through plasma membrane IP_3 receptors. *Science* **313:** 229-233.

Demaegd D, Foulquier F, Colinet AS, Gremillon L, Legrand D, Mariot P, Peiter E, Van Schaftingen E, Matthijs G, Morsomme P (2013). Newly characterized Golgi-localized family of proteins is involved in calcium and pH homeostasis in yeast and human cells. *Proc Natl Acad Sci* **110:** 6859-6864.

Denton RM (2009). Regulation of mitochondrial dehydrogenases by calcium ions. *Biochim Biophys Acta* **1787:** 1309-1316.

des Georges A, Clarke OB, Zalk R, Yuan Q, Condon KJ, Grassucci RA, Hendrickson WA, Marks AR, Frank J (2016). Structural basis for gating and activation of RyR1. *Cell* **167:** 145-157.

Dickinson GD, Churchill GC, Brailoiu E, Patel S (2010). Deviant NAADP-mediated Ca^{2+}-signalling upon lysosome proliferation. *J Biol Chem* **285:** 13321-13325.

Dickinson GD, Swaminathan D, Parker I (2012). The probability of triggering calcium puffs is linearly related to the number of inositol trisphosphate receptors in a cluster. *Biophys J* **102:** 1826-1836.

Dickson EJ, Jensen JB, Vivas O, Kruse M, Traynor-Kaplan AE, Hille B (2016). Dynamic formation of ER-PM junctions presents a lipid phosphatase to regulate phosphoinositides. *J Cell Biol* **213:** 33-48.

Dionisio N, Albarran L, Lopez JJ, Berna-Erro A, Salido GM, Bobe R, Rosado JA (2011). Acidic NAADP-releasable Ca^{2+} compartments in the megakaryoblastic cell line MEG01. *Biochim Biophys Acta* **1813:** 1483-1494.

Dolenc I, Turk B, Pungercic G, Ritonja A, Turk V (1995). Oligomeric structure and substrate induced inhibition of human cathepsin C. *J Biol Chem* **270:** 21626-21631.

Dolman NJ, Tepikin AV (2006). Calcium gradients and the Golgi. *Cell Calcium* **40:** 505–512.

Dong XP, Shen D, Wang X, Dawson T, Li X, Zhang Q, Cheng X, Zhang Y, Weisman LS, Delling M, Xu H (2010). PI(3,5)P_2 controls membrane traffic by direct activation of mucolipin Ca^{2+} release channels in the endolysosome. *Nat Commun* **1:** 38.

Drose S, Altendorf K (1997). Bafilomycins and concanamycins as inhibitors of V-ATPases and P-ATPases. *J Exp Biol* **200:** 1-8.

Dubowchik GM, Gawlak SL, Firestone RA (1995). The in vitro effects of three lysosomotropic detergents against three human tumor cell lines. *Bioorg Med Chem* **5:** 893-898.

Duncan EM, Muratore-Schroeder TL, Cook RG, Garcia BA, Shabanowitz J, Hunt DF, Allis CD (2008). Cathepsin L proteolytically processes histone H3 during mouse embryonic stem cell differentiation. *Cell* **135:** 284-294.

Durchfort N, Verhoef S, Vaughn MB, Shrestha R, Adam D, Kaplan J, Ward DM (2012). The enlarged lysosomes in beige J cells result from decreased lysosome fission and not increased lysosome fusion. *Traffic* **13:** 108-119.

Duvvuri M, Gong Y, Chatterji D, Krise JP (2004). Weak base permeability characteristics influence the intracellular sequestration site in the multidrug-resistant human leukemic cell line HL-60. *J Biol Chem* **279:** 32367-32372.

Eden ER, White IJ, Tsapara A, Futter CE (2010). Membrane contacts between endosomes and ER provide sites for PTP1B-epidermal growth factor receptor interaction. *Nat Cell Biol* **12:** 267-272.

Eick S, Puklo M, Adamowicz K, Kantyka T, Hiemstra P, Stennicke H, Guentsch A, Schacher B, Eickholz P, Potempa J (2014). Lack of cathelicidin processing in Papillon-Lefevre syndrome patients reveals essential role of LL-37 in periodontal homeostasis. *Orphanet J rare dis* **9:** 148.

Emert-Sedlak L, Shangary S, Rabinovitz A, Miranda MB, Delach SM, Johnson DE (2005). Involvement of cathepsin D in chemotherapy-induced cytochrome c release, caspase activation, and cell death. *Mol Cancer Ther* **4:** 733-742.

Emmanouilidou E, Teschemacher AG, Pouli AE, Nicholls LI, Seward EP, Rutter GA (1999). Imaging Ca^{2+} concentration changes at the secretory vesicle surface with a recombinant targeted cameleon. *Curr Biol* **9:** 915-918.

Endo M, Tanaka M, Ogawa Y (1970). Calcium induced release of calcium from the sarcoplasmic reticulum of skinned skeletal muscle fibres. *Nature* **228:** 34-36.

Esposito B, Gambara G, Lewis AM, Palombi F, D'Alessio A, Taylor LX, Genazzani AA, Ziparo E, Galione A, Churchill GC, Filippini A (2011). NAADP links histamine H1 receptors to secretion of von Willebrand factor in human endothelial cells. *Blood* **117:** 4968-4977.

Essletzbichler P, Konopka T, Santoro F, Chen D, Gapp BV, Kralovics R, Brummelkamp TR, Nijman SM, Burckstummer T (2014). Megabase-scale deletion using CRISPR/Cas9 to generate a fully haploid human cell line. *Genome Res* **24:** 2059-2065.

Fabiato A (1983). Calcium-induced release of calcium from cardiac sarcoplasmic reticulum. *Am J Physiol* **245:** C1-C14.

Fagan KA, Graf RA, Tolman S, Schaak J, Cooper DMF (2000). Regulation of a Ca^{2+}-sensitive adenylyl cyclase in an excitable cell. Role of voltage-gated versus capacitative Ca^{2+} entry. *J Biol Chem* **275:** 40187-40194.

Fan G, Baker ML, Wang Z, Baker MR, Sinyagovskiy PA, Chiu W, Ludtke SJ, Serysheva, II (2015). Gating machinery of $InsP_3R$ channels revealed by electron cryomicroscopy. *Nature* **527:** 336-341.

Favia A, Desideri M, Gambara G, D'Alessio A, Ruas M, Esposito B, Del Bufalo D, Parrington J, Ziparo E, Palombi F, Galione A, Filippini A (2014). VEGF-induced neoangiogenesis is mediated by NAADP and two-pore channel-2-dependent Ca^{2+} signaling. *Proc Natl Acad Sci* **111:** E4706-E4715.

Feske S, Gwack Y, Prakriya M, Srikanth S, Puppel SH, Tanasa B, Hogan PG, Lewis RS, Daly M, Rao A (2006). A mutation in Orai1 causes immune deficiency by abrogating CRAC channel function. *Nature* **441:** 179-185.

Filadi R, Greotti E, Turacchio G, Luini A, Pozzan T, Pizzo P (2015). Mitofusin 2 ablation increases endoplasmic reticulum-mitochondria coupling. *Proc Natl Acad Sci* **112** E2174-E2181.

Fill M, Copello JA (2002). Ryanodine receptor calcium release channels. *Physiol Rev* **82:** 893-922.

Forgac M (2007). Vacuolar ATPases: rotary proton pumps in physiology and pathophysiology. *Nat Rev Mol Cell Biol* **8:** 917-929.

Foskett JK, White C, Cheung KH, Mak DO (2007). Inositol trisphosphate receptor Ca^{2+} release channels. *Physiol Rev* **87:** 593-658.

Fredriksson S, Gullberg M, Jarvius J, Olsson C, Pietras K, Gustafsdottir SM, Ostman A, Landegren U (2002). Protein detection using proximity-dependent DNA ligation assays. *Nat Biotechnol* **20:** 473-477.

Friedman JR, Dibenedetto JR, West M, Rowland AA, Voeltz GK (2013). Endoplasmic reticulum-endosome contact increases as endosomes traffic and mature. *Mol Biol Cell* **24:** 1030-1040.

Friedman JR, Lackner LL, West M, DiBenedetto JR, Nunnari J, Voeltz GK (2011). ER tubules mark sites of mitochondrial division. *Science* **334:** 358-362.

Frolov A, Zielinski SE, Crowley JR, Dudley-Rucker N, Schaffer JE, Ory DS (2003). NPC1 and NPC2 regulate cellular cholesterol homeostasis through generation of low density lipoprotein cholesterol-derived oxysterols. *J Biol Chem* **278:** 25517-25525.

Furuichi T, Yoshikawa S, Miyawaki A, Wada K, Maeda M, Mikoshiba K (1989). Primary structure and functional expression of the inositol 1,4,5-trisphosphate-binding protein P_{400}. *Nature* **342:** 32-38.

Futter CE (1996). Multivesicular endosomes containing internalized EGF-EGF receptor complexes mature and then fuse directly with lysosomes. *J Cell Bio* **132:** 1011–1023.

Ganley IG, Wong PM, Gammoh N, Jiang X (2011). Distinct autophagosomal-lysosomal fusion mechanism revealed by thapsigargin-induced autophagy arrest. *Mol Cell* **42:** 731-743.

Gao Y, Chen Y, Zhan S, Zhang W, Xiong F, Ge W (2017). Comprehensive proteome analysis of lysosomes reveals the diverse function of macrophages in immune responses. *Oncotarget* **8:** 7420-7440.

Garrity AG, Wang W, Collier CM, Levey SA, Gao Q, Xu H (2016). The endoplasmic reticulum, not the pH gradient, drives calcium refilling of lysosomes. *Elife* **5**.

Geng Y, Kohli L, Klocke BJ, Roth KA (2010). Chloroquine-induced autophagic vacuole accumulation and cell death in glioma cells is p53 independent. *Neuro-Oncol* **12:** 473-481.

Gerasimenko JV (2006). NAADP, cADPR and IP_3 all release Ca^{2+} from the endoplasmic reticulum and an acidic store in the secretory granule area. *J Cell Sci* **119:** 226-238.

Gerasimenko JV, Maruyama Y, Yano K, Dolman NJ, Tepikin AV, Petersen OH, Gerasimenko OV (2003). NAADP mobilizes Ca^{2+} from a thapsigargin-sensitive store in the nuclear envelope by activating ryanodine receptors. *J Cell Biol* **163:** 271-282.

Gerasimenko JV, Sherwood M, Tepikin AV, Petersen OH, Gerasimenko OV (2006). NAADP, cADPR and IP_3 all release Ca^{2+} from the endoplasmic reticulum and an acidic store in the secretory granule area. *J Cell Sci* **119:** 226-238.

Gerasimenko JV, Tepikin AV, Petersen OH, Gerasimenko OV (1998). Calcium uptake via endocytosis with rapid release from acidifying endosomes. *Curr Biol* **8:** 1335-1338.

Giorgi C, Ito K, Lin HK, Santangelo C, Wieckowski MR, Lebiedzinska M, Bononi A, Bonora M, Duszynski J, Bernardi R, Rizzuto R, Tacchetti C, Pinton P, Pandolfi PP (2010). PML regulates apoptosis at endoplasmic reticulum by modulating calcium release. *Science* **330:** 1247-1251.

Giovannucci DR, Groblewski GE, Sneyd J, Yule DI (2000). Targeted phosphorylation of inositol 1,4,5-trisphosphate receptors selectively inhibits localized Ca^{2+} release and shapes oscillatory Ca^{2+} signals. *J Biol Chem* **275:** 33704-33711.

Golabek AA, Kaczmarski W, Kida E, Kaczmarski A, Michalewski MP, Wisniewski KE (1999). Expression studies of CLN3 protein (battenin) in fusion with the green fluorescent protein in mammalian cells in vitro. *Mol Genet Metab* **66:** 277-282.

Gonzalez-Noriega A, Grubb JH, Talkad V, Sly WS (1980). Chloroquine inhibits lysosomal enzyme pinocytosis and enhances lysosomal enzyme secretion by impairing receptor recycling. *J Cell Biol* **85:** 839-852.

Goulet B, Baruch A, Moon NS, Poirier M, Sansregret LL, Erickson A, Bogyo M, Nepveu A (2004). A cathepsin L isoform that is devoid of a signal peptide localizes to the nucleus in S phase and processes the CDP/Cux transcription factor. *Mol Cell* **14:** 207-219.

Grimm C, Holdt LM, Chen C-C, Hassan S, Müller C, Jörs S, Cuny H, Kissing S, Schröder B, Butz E, Northoff B, Castonguay J, Luber CA, Moser M, Spahn S, Lüllmann-Rauch R, Fendel C, Klugbauer N, Griesbeck O, Haas A, Mann M, Bracher F, Teupser D, Saftig P, Biel M, Wahl-Schott C (2014). High susceptibility to fatty liver disease in two-pore channel 2-deficient mice. *Nat Commun* **5:** 4699.

Grinstein S, Goetz JD (1985). Control of free cytoplasmic calcium by intracellular pH in rat lymphocytes. *Biochim Biophys Acta* **819:** 267-270.

Grosche J, Matyash V, Moller T, Verkhratsky A, Reichenbach A, Kettenmann H (1999). Microdomains for neuron-glia interaction: parallel fiber signaling to Bergmann glial cells. *Nat Neurosci* **2:** 139-143.

Guha S, Baltazar GC, Tu LA, Liu J, Lim JC, Lu W, Argall A, Boesze-Battaglia K, Laties AM, Mitchell CH (2012). Stimulation of the D5 dopamine receptor acidifies the lysosomal pH of retinal pigmented epithelial cells and decreases accumulation of autofluorescent photoreceptor debris. *J Neurochem* **122:** 823-833.

Guha S, Coffey EE, Lu W, Lim JC, Beckel JM, Laties AM, Boesze-Battaglia K, Mitchell CH (2014). Approaches for detecting lysosomal alkalinization and impaired degradation in fresh and cultured RPE cells: evidence for a role in retinal degenerations. *Experimental eye research* **126:** 68-76.

Guicciardi ME, Leist M, Gores GJ (2004). Lysosomes in cell death. *Oncogene* **23:** 2881-2890.

Gutmann HR, Fruton JS (1948). On the proteolytic enzymes of animal tissues; an intracellular enzyme related to chymotrypsin. *J Biol Chem* **174:** 851-858.

Gwack Y, Srikanth S, Oh-Hora M, Hogan PG, Lamperti ED, Yamashita M, Gelinas C, Neems DS, Sasaki Y, Feske S, Prakriya M, Rajewsky K, Rao A (2008). Hair loss and defective T- and B-cell function in mice lacking ORAI1. *Mol Cell Biol* **28:** 5209-5222.

Haggie PM, Verkman AS (2007). Cystic fibrosis transmembrane conductance regulator-independent phagosomal acidification in macrophages. *J Biol Chem* **282:** 31422-31428.

Haller T, Dietl P, Deetjen P, Volkl H (1996). The lysosomal compartment as intracellular calcium store in MDCK cells: a possible involvement in $InsP_3$-mediated Ca^{2+} release. *Cell Calcium* **19:** 157-165.

Hamilton G, Colbert JD, Schuettelkopf AW, Watts C (2008). Cystatin F is a cathepsin C-directed protease inhibitor regulated by proteolysis. *EMBO J* **27:** 499-508.

Hamilton SL, Reid MB (2000). RyR1 modulation by oxidation and calmodulin. *Antioxid Redox Signal* **2:** 41-45.

Heigwer F, Kerr G, Boutros M (2014). E-CRISP: fast CRISPR target site identification. *Nat Methods* **11:** 122-123.

Helle SC, Kanfer G, Kolar K, Lang A, Michel AH, Kornmann B (2013). Organization and function of membrane contact sites. *Biochim Biophys Acta* **1833:** 2526-2541.

Hilge M (2012). Ca^{2+} regulation of ion transport in the Na^{+}/Ca^{2+} exchanger. *J Biol Chem* **287:** 31641–31649.

Hirata Y, Brotto M, Weisleder N, Chu Y, Lin P, Zhao X, Thornton A, Komazaki S, Takeshima H, Ma J, Pan Z (2006). Uncoupling store-operated Ca^{2+} entry and altered Ca^{2+} release from sarcoplasmic reticulum through silencing of junctophilin genes. *Biophys J* **90:** 4418-4427.

Hofmann T, Obukhov AG, Schaefer M, Harteneck C, Gudermann T, Schultz G (1999). Direct activation of human TRPC6 and TRPC3 channels by diacylglycerol. *Nature* **397:** 259–263.

Hogan PG, Chen L, Nardone J, Rao A (2003). Transcriptional regulation by calcium, calcineurin, and NFAT. *Genes Dev* **17:** 2205-2232.

Hogan PG, Rao A (2007). Dissecting I_{CRAC}, a store-operated calcium current. *Trends Biochem Sci* **32:** 235-245.

Hogan PG, Rao A (2015). Store-operated calcium entry: Mechanisms and modulation. *Biochem Biophys Res Commun* **460:** 40-49.

Hohenegger M, Suko J, Gscheidlinger R, Drobny H, Zidar A (2002). Nicotinic acid-adenine dinucleotide phosphate activates the skeletal muscle ryanodine receptor. *Biochem J* **367:** 423-431.

Holtta-Vuori M, Alpy F, Tanhuanpaa K, Jokitalo E, Mutka AL, Ikonen E (2005). MLN64 is involved in actin-mediated dynamics of late endocytic organelles. *Mol Biol Cell* **16:** 3873-3886.

Honegger UE, Roscher AA, Wiesmann UN (1983). Evidence for lysosomotropic action of desipramine in cultured human fibroblasts. *J Pharmacol Exp Ther* **225:** 436-441.

Honrath B, Metz I, Bendridi N, Rieusset J, Culmsee C (2017). Glucose-regulated protein 75 determines ER-mitochondrial coupling and sensitivity to oxidative stress in neuronal cells. *Cell death disc* **3:** 17076.

Hou X, Pedi L, Diver MM, Long SB (2012). Crystal structure of the calcium release-activated calcium channel Orai. *Science* **338:** 1308-1313.

Huotari J, Helenius A (2011). Endosome maturation. *EMBO J* **30:** 3481-3500.

Huss M, Helmut W (2009). Inhibitors of V-ATPases: old and new players. *J Exp Biol* **212:** 341-346.

Huynh C, Andrews NW (2005). The small chemical vacuolin-1 alters the morphology of lysosomes without inhibiting Ca^{2+}-regulated exocytosis. *EMBO Rep* **6:** 843-847.

Ihrke G, Kyttälä A, Russell MRG, Rous BA, Luzio JP (2004). Differential use of two AP-3-mediated pathways by lysosomal membrane proteins. *Traffic* **5:** 946–962.

Iino M (1990). Biphasic Ca^{2+} dependence of inositol 1,4,5-trisphosphate-induced Ca^{2+} release in smooth muscle cells of the guinea pig taenia caeci. *J Gen Physiol* **95:** 1103-1122.

Inesi G, Tadini-Buoninsegni F (2014). Ca^{2+}/H^{+} exchange, lumenal Ca^{2+} release and Ca^{2+}/ATP coupling ratios in the sarcoplasmic reticulum ATPase. *J Cell Commun Signal* **8:** 5-11.

Ingerman E, Perkins EM, Marino M, Mears JA, McCaffery JM, Hinshaw JE, Nunnari J (2005). Dnm1 forms spirals that are structurally tailored to fit mitochondria. *J Cell Biol* **170:** 1021-1027.

Irvine R (2007). Cell signaling. The art of the soluble. *Science* **316:** 845–846.

Irvine RF (1990). "Quantal" Ca^{2+} release and the control of Ca^{2+} entry by inositol phosphates - a possible mechanism. *FEBS Lett* **263:** 5-9.

Iwai M, Tateishi Y, Hattori M, Mizutani A, Nakamura T, Futatsugi A, Inoue T, Furuichi T, Michikawa T, Mikoshiba K (2005). Molecular cloning of mouse type 2 and type 3 inositol 1,4,5-trisphosphate receptors and identification of a novel type 2 receptor splice variant. *J Biol Chem* **280:** 10305-10317.

Jadot M, Bielande V, Beauloye V, Wattiaux-De Coninck S, Wattiaux R (1990). Cytotoxicity and effect of glycyl-D-phenylalanine-2-naphthylamide on lysosomes. *Biochim Biophys Acta* **1027:** 205-209.

Jadot M, Colmant C, Wattiaux-De Coninck S, Wattiaux R (1984). Intralysosomal hydrolysis of glycyl-L-phenylalanine 2-naphthylamide. *Biochem J* **219:** 965-970.

Jaiswal JK, Andrews NW, Simon SM (2002). Membrane proximal lysosomes are the major vesicles responsible for calcium-dependent exocytosis in nonsecretory cells. *J Cell Biol* **159:** 625-635.

Jin RU, Mills JC (2014). RAB26 coordinates lysosome traffic and mitochondrial localization. *J Cell Sci* **127:** 1018-1032.

Jing J, He L, Sun A, Quintana A, Ding Y, Ma G, Tan P, Liang X, Zheng X, Chen L, Shi X, Zhang SL, Zhong L, Huang Y, Dong MQ, Walker CL, Hogan PG, Wang Y, Zhou Y (2015). Proteomic mapping of ER-PM junctions identifies STIMATE as a regulator of Ca^{2+} influx. *Nat Cell Biol* **17:** 1339-1347.

Johnson DE, Ostrowski P, Jaumouille V, Grinstein S (2016). The position of lysosomes within the cell determines their luminal pH. *J Cell Biol* **212:** 677-692.

Jones L, Ma L, Castro J, Litjens T, Barritt GJ, Rychkov GY (2011). The predominant role of IP_3 type 1 receptors in activation of store-operated Ca^{2+} entry in liver cells. *Biochim Biophys Acta* **1808:** 745–751.

Jongsma ML, Berlin I, Wijdeven RH, Janssen L, Janssen GM, Garstka MA, Janssen H, Mensink M, van Veelen PA, Spaapen RM, Neefjes J (2016). An ER-associated pathway defines endosomal architecture for controlled cargo transport. *Cell* **166:** 152-166.

Joseph SK, Rice HL, Williamson JR (1989). The effect of external calcium and pH on inositol trisphosphate-mediated calcium release from cerebellum microsomal fractions. *Biochem J* **258:** 261-265.

Kaftan EJ, Ehrlich BE, Watras J (1997). Inositol 1,4,5-trisphosphate ($InsP_3$) and calcium interact to increase the dynamic range of $InsP_3$ receptor-dependent calcium signaling. *J Gen Physiol* **110:** 529-538.

Kagedal K, Zhao M, Svensson I, Brunk UT (2001). Sphingosine-induced apoptosis is dependent on lysosomal proteases. *Biochem J* **359:** 335-343.

Kam CM, Gotz MG, Koot G, McGuire M, Thiele D, Hudig D, Powers JC (2004). Design and evaluation of inhibitors for dipeptidyl peptidase I (Cathepsin C). *Arch Biochem Biophys* **427:** 123-134.

Kar P, Nelson C, Parekh AB (2011). Selective activation of the transcription factor NFAT1 by calcium microdomains near Ca^{2+} release-activated Ca^{2+} (CRAC) channels. *J Biol Chem* **286:** 14795-14803.

Kazmi F, Hensley T, Pope C, Funk RS, Loewen GJ, Buckley DB, Parkinson A (2013). Lysosomal sequestration (trapping) of lipophilic amine (cationic amphiphilic) drugs in immortalized human hepatocytes (Fa2N-4 cells). *Drug metab dispos* **41:** 897-905.

Kerschbaum HH, Cahalan MD (1999). Single-channel recording of a store-operated Ca^{2+} channel in Jurkat T lymphocytes. *Science* **283:** 836-839.

Kilpatrick BS, Eden ER, Schapira AH, Futter CE, Patel S (2013). Direct mobilisation of lysosomal Ca^{2+} triggers complex Ca^{2+} signals. *J Cell Sci* **126:** 60-66.

Kilpatrick BS, Yates E, Grimm C, Schapira AH, Patel S (2016). Endo-lysosomal TRP mucolipin-1 channels trigger global ER Ca^{2+} release and Ca^{2+} influx. *J Cell Sci* **129:** 3859-3867.

Kiselyov K, Yamaguchi S, Lyons CW, Muallem S (2010). Aberrant Ca^{2+} handling in lysosomal storage disorders. *Cell Calcium* **47:** 103-111.

Klemper MS (1985). An adenosine triphosphate-dependent calcium uptake pump in human neutrophil lysosomes. *J Clin Invest* **76:** 303-310.

Koike M, Shibata M, Ezaki J, Peters C, Saftig P, Kominami E, Uchiyama Y (2013). Differences in expression patterns of cathepsin C/dipeptidyl peptidase I in normal, pathological and aged mouse central nervous system. *Eur J Neurosci* **37:** 816-830.

Konieczny V, Tovey SC, Mataragka S, Prole DL, Taylor CW (2017). Cyclic AMP recruits a discrete Intracellular Ca^{2+} store by unmasking hypersensitive IP_3 receptors. *Cell Rep* **18:** 711-722.

Koos B, Andersson L, Clausson CM, Grannas K, Klaesson A, Cane G, Soderberg O (2013). Analysis of protein interactions in situ by proximity ligation assays. *Curr Topic Microbiol Immunol* **377:** 111-126.

Korver GE, Kam CM, Powers JC, Hudig D (2001). Dipeptide vinyl sulfones suitable for intracellular inhibition of dipeptidyl peptidase I. *Int Immunopharmacol* **1:** 21-32.

Korzeniowski MK, Szanda G, Balla T, Spat A (2009). Store-operated Ca^{2+} influx and subplasmalemmal mitochondria. *Cell Calcium* **46:** 49-55.

Krause KH, Lew PD (1987). Subcellular distribution of Ca^{2+} pumping sites in human neutrophils. *J Clin Invest* **80:** 107-116.

Kupzig S, Walker SA, Cullen PJ (2005). The frequencies of calcium oscillations are optimized for efficient calcium-mediated activation of Ras and the ERK/MAPK cascade. *Proc Natl Acad Sci* **102:** 7577-7582.

Kurian N, Hall CJ, Wilkinson GF, Sullivan M, Tobin AB, Willars GB (2009). Full and partial agonists of muscarinic M_3 receptors reveal single and oscillatory Ca^{2+} responses by β_2-adrenoceptors. *J Pharmacol Exp Ther* **330:** 502-512.

Kushmerick MJ, Moerland TS, Wiseman RW (1992). Mammalian skeletal muscle fibers distinguished by contents of phosphocreatine, ATP, and Pi. *Proc Natl Acad Sci* **89:** 7521-7525.

Lacinova L (2005). Voltage-dependent calcium channels. *Gen physiol bioph* **24:** 1-78.

Lai FA, Erickson HP, Rousseau E, Liu QY, Meissner G (1988). Purification and reconstitution of the calcium release channel from skeletal muscle. *Nature* **331:** 315-319.

Lange I, Yamamoto S, Partida-Sanchez S, Mori Y, Fleig A, Penner R (2009). TRPM2 functions as a lysosomal Ca^{2+}-release channel in beta cells. *Sci Signal* **2:** ra23.

Lee HC (1997). Mechanisms of calcium signaling by cyclic ADP-ribose and NAADP. *Physiol Rev* **1997:** 1133-1164.

Lee HC (1999). A unified mechanism of enzymatic synthesis of two calcium messengers: cyclic ADP-ribose and NAADP. *Biol Chem* **380:** 785-793.

Lee HC, Aarhus R, Graeff RM (1995). Sensitization of calcium-induced calcium release by cyclic ADP-ribose and calmodulin. *J Biol Chem* **270:** 9060-9066.

Lee KP, Yuan JP, Hong JH, So I, Worley PF, Muallem S (2010). An endoplasmic reticulum/plasma membrane junction: STIM1/Orai1/TRPCs. *FEBS J* **584:** 2022-2027.

Lelouvier B, Puertollano R (2011). Mucolipin-3 regulates luminal calcium, acidification, and membrane fusion in the endosomal pathway. *J Biol Chem* **286:** 9826-9832.

Lewis RS (2007). The molecular choreography of a store-operated calcium channel. *Nature* **446:** 284-287.

Li S, Hao B, Lu Y, Yu P, Lee HC, Yue J (2012). Intracellular alkalinization induces cytosolic Ca^{2+} increases by inhibiting sarco/endoplasmic reticulum Ca^{2+}-ATPase (SERCA). *PLoS One* **7:** e31905.

Li W, Yuan X, Nordgren G, Dalen H, Dubowchik GM, Firestone RA, Brunk UT (2000). Induction of cell death by the lysosomotropic detergent MSDH. *FEBS Lett* **470:** 35-39.

Liao Y, Erxleben C, Abramowitz J, Flockerzi V, Zhu MX, Armstrong DL, Birnbaumer L (2008). Functional interactions among Orai1, TRPCs, and STIM1 suggest a STIM-regulated heteromeric Orai/TRPC model for SOCE/Icrac channels. *Proc Natl Acad Sci* **105:** 2895-2900.

Lin-Moshier Y, Walseth TF, Churamani D, Davidson SM, Slama JT, Hooper R, Brailoiu E, Patel S, Marchant JS (2012). Photoaffinity labeling of nicotinic acid adenine dinucleotide phosphate (NAADP) targets in mammalian cells. *J Biol Chem* **287:** 2296-2307.

Liou J, Fivaz M, Inoue T, Meyer T (2007). Live-cell imaging reveals sequential oligomerization and local plasma membrane targeting of stromal interaction molecule 1 after Ca^{2+} store depletion. *Proc Natl Acad Sci* **104:** 9301-9306.

Liou J, Kim ML, Heo WD, Jones JT, Myers JW, Ferrell JE, Jr., Meyer T (2005). STIM is a Ca^{2+} sensor essential for Ca^{2+}-store-depletion-triggered Ca^{2+} influx. *Curr Biol* **15:** 1235-1241.

Lippincott-Schwartz J, Yuan L, Tipper C, Amherdt M, Orci L, Klausner RD (1991). Brefeldin A's effects on endosomes, lysosomes, and the TGN suggest a general mechanism for regulating organelle structure and membrane traffic. *Cell* **67:** 601-616.

Liu J, Diwu Z, Leung WY (2001). Synthesis and photophysical properties of new fluorinated benzo[c]xanthene dyes as intracellular pH indicators. *Bioorg Med Chem Lett* **11:** 2903-2905.

Liu J, Lu W, Reigada D, Nguyen J, Laties AM, Mitchell CH (2008). Restoration of lysosomal pH in RPE cells from cultured human and ABCA4(-/-) mice: pharmacologic approaches and functional recovery. *Invest Ophthalmol Vis Sci* **49:** 772-780.

Liu X, Singh BB, Ambudkar IS (2003). TRPC1 is required for functional store-operated Ca^{2+} channels. Role of acidic amino acid residues in the S5-S6 region. *J Biol Chem* **278:** 11337-11343.

Liu Y, Zhou Y, Zhu K (2012). Inhibition of glioma cell lysosome exocytosis inhibits glioma invasion. *PLoS One* **7:** e45910.

Lloyd-Evans E, Morgan AJ, He X, Smith DA, Elliot-Smith E, Sillence DJ, Churchill GC, Schuchman EH, Galione A, Platt FM (2008). Niemann-Pick disease type C1 is a sphingosine storage disease that causes deregulation of lysosomal calcium. *Nat Med* **14:** 1247-1255.

Lopez-Sanjurjo CI, Tovey SC, Prole DL, Taylor CW (2013). Lysosomes shape Ins(1,4,5)P_3-evoked Ca^{2+} signals by selectively sequestering Ca^{2+} released from the endoplasmic reticulum. *J Cell Sci* **126:** 289-300.

Lopez JJ, Albarran L, Gomez LJ, Smani T, Salido GM, Rosado JA (2016). Molecular modulators of store-operated calcium entry. *Biochim Biophys Acta* **1863:** 2037-2043.

Lopez JJ, Camello-Almaraz C, Pariente JA, Salido GM, Rosado JA (2005). Ca^{2+} accumulation into acidic organelles mediated by Ca^{2+}- and vacuolar H^+-ATPases in human platelets. *Biochem J* **390:** 243-252.

Lopez Sanjurjo CI, Tovey SC, Prole DL, Taylor CW (2013). Lysosomes shape Ins(1,4,5)P_3-evoked Ca^{2+} signals by selectively sequestering Ca^{2+} released from the endoplasmic reticulum. *J Cell Sci* **126:** 289-300.

Lu S, Jessen B, Strock C, Will Y (2012). The contribution of physicochemical properties to multiple in vitro cytotoxicity endpoints. *Toxicol In Vitro* **26:** 613-620.

Lu S, Sung T, Lin N, Abraham RT, Jessen BA (2017). Lysosomal adaptation: How cells respond to lysosomotropic compounds. *PLoS One* **12:** e0173771.

Lu W, Wang J, Peng G, Shimoda LA, Sylvester JT (2009). Knockdown of stromal interaction molecule 1 attenuates store-operated Ca^{2+} entry and Ca^{2+} responses to acute hypoxia in pulmonary arterial smooth muscle. *Am J Physiol* **297:** L17-25.

Lu Y, Hao B, Graeff R, Yue J (2013). NAADP/TPC2/Ca^{2+} signaling inhibits autophagy. *Comm Integr biol* **6:** e27595.

Luzio JP, Hackmann Y, Dieckmann NM, Griffiths GM (2014). The biogenesis of lysosomes and lysosome-related organelles. *Cold Spring Harb Persp Biol* **6:** a016840.

Lytton J, Westlin M, Burk SE, Shull GE, MacLennan DH (1992). Functional comparisons between isoforms of the sarcoplasmic or endoplasmic reticulum family of calcium pumps. *J Biol Chem* **267:** 14483-14489.

Maeda N, Niinobe M, Inoue Y, Mikoshiba K (1989). Developmental expression and intracellular location of P400 protein characteristic of Purkinje cells in the mouse cerebellum. *Dev Biol* **133:** 67-76.

Mak DO, Foskett JK (1998). Effects of divalent cations on single-channel conduction properties of *Xenopus* IP_3 receptor. *Am J Physiol* **275:** C179-C188.

Malviya AN, Rogue P, Vincendon G (1990). Stereospecific inositol 1,4,5-[^{32}P]trisphosphate binding to isolated rat liver nuclei: Evidence for inositol trisphosphate receptor-mediated calcium release from the nucleus. *Proc Natl Acad Sci* **87:** 9270-9274.

Mangieri LR, Mader BJ, Thomas CE, Taylor CA, Luker AM, Tse TE, Huisingh C, Shacka JJ (2014). ATP6V0C knockdown in neuroblastoma cells alters autophagy-lysosome pathway

function and metabolism of proteins that accumulate in neurodegenerative disease. *PLoS One* **9:** e93257.

Mannhold R, Poda GI, Ostermann C, Tetko IV (2009). Calculation of molecular lipophilicity: State-of-the-art and comparison of log P methods on more than 96,000 compounds. *J Pharm Sci* **98:** 861-893.

Marchi S, Pinton P (2014). The mitochondrial calcium uniporter complex: molecular components, structure and physiopathological implications. *J Physiol* **592:** 829-839.

Marx SO, Ondrias K, Marks AR (1998). Coupled gating between individual skeletal muscle Ca^{2+} release channels (ryanodine receptors). *Science* **281:** 818-821.

Mataragka S, Taylor CW (2018). All three IP_3 receptor subtypes generate Ca^{2+} puffs, the universal building blocks of IP_3-evoked Ca^{2+} signals. *J Cell Sci***:** In Press.

Mauvezin C, Nagy P, Juhasz G, Neufeld TP (2015). Autophagosome-lysosome fusion is independent of V-ATPase-mediated acidification. *Nat Commun* **6:** 7007.

Maxson ME, Grinstein S (2014). The vacuolar-type H^+-ATPase at a glance - more than a proton pump. *J Cell Sci* **127:** 4987-4993.

McCarl CA, Picard C, Khalil S, Kawasaki T, Rother J, Papolos A, Kutok J, Hivroz C, Ledeist F, Plogmann K, Ehl S, Notheis G, Albert MH, Belohradsky BH, Kirschner J, Rao A, Fischer A, Feske S (2009). ORAI1 deficiency and lack of store-operated Ca^{2+} entry cause immunodeficiency, myopathy, and ectodermal dysplasia. *J Allergy Clin Immunol* **124:** 1311-1318.

McCue HV, Wardyn JD, Burgoyne RD, Haynes LP (2013). Generation and characterization of a lysosomally targeted, genetically encoded Ca^{2+}-sensor. *Biochem J* **449:** 449-457.

McGuire MJ, Lipsky PE, Thiele DL (1992). Purification and characterization of dipeptidyl peptidase I from human spleen. *Arch Biochem Biophys* **295:** 280-288.

McGuire MJ, Lipsky PE, Thiele DL (1993). Generation of active myeloid and lymphoid granule serine proteases requires processing by the granule thiol protease dipeptidyl peptidase I. *J Biol Chem* **268:** 2458-2467.

McNally BA, Somasundaram A, Yamashita M, Prakriya M (2012). Gated regulation of CRAC channel ion selectivity by STIM1. *Nature* **482:** 241-245.

Mears JA, Lackner LL, Fang S, Ingerman E, Nunnari J, Hinshaw JE (2011). Conformational changes in Dnm1 support a contractile mechanism for mitochondrial fission. *Nat Struct Mol Biol* **18:** 20-26.

Medina DL, Di Paola S, Peluso I, Armani A, De Stefani D, Venditti R, Montefusco S, Scotto-Rosato A, Prezioso C, Forrester A, Settembre C, Wang W, Gao Q, Xu H, Sandri M, Rizzuto R, De Matteis MA, Ballabio A (2015). Lysosomal calcium signalling regulates autophagy through calcineurin and TFEB. *Nat Cell Biol* **17:** 288-299.

Mehta D, Ahmmed GU, Paria BC, Holinstat M, Voyno-Yasenetskaya T, Tiruppathi C, Minshall RD, Malik AB (2003). RhoA interaction with inositol 1,4,5-trisphosphate receptor and transient receptor potential channel-1 regulates Ca^{2+} entry. Role in signaling increased endothelial permeability. *J Biol Chem* **278:** 33492-33500.

Meier-Ruge W (1965). Experimental investigation of the morphogenesis of chloroquine retinopathy. *Arch ophthal* **73:** 540-544.

Meijering E, Dzyubachyk O, Smal I (2012). Methods for cell and particle tracking. *Methods Enzymol* **504:** 183-200.

Melchionda M, Pittman JK, Mayor R, Patel S (2016). Ca^{2+}/H^{+} exchange by acidic organelles regulates cell migration in vivo. *J Cell Biol* **212:** 803-813.

Mellman I, Fuchs R, Helenius A (1986). Acidification of the endocytic and exocytic pathways. *Annu Rev Biochem* **55:** 663-700.

Mendes CCP, Gomes DA, Thompson M, Souto NC, Goes TS, Goes AM, Rodrigues MA, Gomez MV, Nathanson MH, Leite MF (2005). The Type III Inositol 1,4,5-Trisphosphate Receptor Preferentially Transmits Apoptotic Ca 2+ Signals into Mitochondria. *J Biol Chem* **280:** 40892–40900.

Methot N, Rubin J, Guay D, Beaulieu C, Ethier D, Reddy TJ, Riendeau D, Percival MD (2007). Inhibition of the activation of multiple serine proteases with a cathepsin C inhibitor requires sustained exposure to prevent pro-enzyme processing. *J Biol Chem* **282:** 20836-20846.

Michallet MC, Saltel F, Flacher M, Revillard JP, Genestier L (2004). Cathepsin-dependent apoptosis triggered by supraoptimal activation of T lymphocytes: a possible mechanism of high dose tolerance. *J Immunol* **172:** 5405-5414.

Michikawa T, Hirota J, Kawano S, Hiraoka M, Yamada M, Furuichi T, Mikoshiba K (1999). Calmodulin mediates calcium-dependent inactivation of the cerebellar type 1 inositol 1,4,5-trisphosphate receptor. *Neuron* **23:** 799-808.

Miederer AM, Alansary D, Schwar G, Lee PH, Jung M, Helms V, Niemeyer BA (2015). A STIM2 splice variant negatively regulates store-operated calcium entry. *Nat Commun* **6:** 6899.

Mignery GA, Sudhof TC, Takei K, De Camilli P (1989). Putative receptor for inositol 1,4,5-trisphosphate similar to ryanodine receptor. *Nature* **342:** 192-195.

Milani G, Schereiber AZ, Vercesi AE (2001). Ca^{2+} transport into an intracellular acidic compartment of Candida parapsilosis. *FEBS Lett* **500:** 80-84.

Miller AT, Sandberg M, Huang YH, Young M, Sutton S, Sauer K, Cooke MP (2007). Production of Ins(1,3,4,5)P4 mediated by the kinase Itpkb inhibits store-operated calcium channels and regulates B cell selection and activation. *Nat Immunol* **8:** 514–521.

Mirnikjoo B, Balasubramanian K, Schroit AJ (2009). Mobilization of lysosomal calcium regulates the externalization of phosphatidylserine during apoptosis. *J Biol Chem* **284:** 6918-6923.

Mojzisová A, Krizanová O, Záciková L, Komínková V, Ondrias K (2001). Effect of nicotinic acid adenine dinucleotide phosphate on ryanodine calcium release channel in heart. *Pflugers Archiv : Euro J physiol* **441:** 674–677.

Molgaard A, Arnau J, Lauritzen C, Larsen S, Petersen G, Pedersen J (2007). The crystal structure of human dipeptidyl peptidase I (cathepsin C) in complex with the inhibitor Gly-Phe-CHN_2. *Biochem J* **401:** 645-650.

Montero M, Alonso MT, Carnicero E, Cuchillo-Ibanez I, Albillos A, Garcia AG, Garcia-Sancho J, Alvarez J (2000). Chromaffin-cell stimulation triggers fast millimolar mitochondrial Ca^{2+} transients that modulate secretion. *Nat Cell Biol* **2:** 57-61.

Morgan AJ (2011a). Molecular mechanisms of endolysosomal Ca^{2+} signalling in health and disease. *Biochem J* **439:** 349-374.

Morgan AJ (2011b). Sea urchin eggs in the acid reign. *Cell Calcium* **50:** 147–156.

Morgan AJ (2014). Two-pore channels (TPCs): current controversies. *Bioessays* **36:** 173-183.

Morgan AJ, Davis LC, Galione A (2015). Imaging approaches to measuring lysosomal calcium. *Methods Cell Biol* **126:** 159-195.

Morgan AJ, Davis LC, Wagner SK, Lewis AM, Parrington J, Churchill GC, Galione A (2013). Bidirectional Ca^{2+} signaling occurs between the endoplasmic reticulum and acidic organelles. *J Cell Biol* **18:** 789-805.

Morgan AJ, Galione A (2007). NAADP induces pH changes in the lumen of acidic Ca^{2+} stores. *Biochem J* **402:** 301-310.

Morgan AJ, Platt FM, Lloyd-Evans E, Galione A (2011). Molecular mechanisms of endolysosomal Ca^{2+} signalling in health and disease. *Biochem J* **439:** 349-374.

Mukherjee S, Maxfield FR (2004). Lipid and cholesterol trafficking in NPC. *Biochim Biophys Acta* **1685:** 28-37.

Mullock BM, Bright NA, Fearon CW, Gray SR, Luzio JP (1998). Fusion of lysosomes with late endosomes produces a hybrid organelle of intermediate density and is NSF dependent. *J Cell Bio* **140:** 591–601.

Murley A, Lackner LL, Osman C, West M, Voeltz GK, Walter P, Nunnari J (2013). ER-associated mitochondrial division links the distribution of mitochondria and mitochondrial DNA in yeast. *Elife* **2:** e00422.

Nadanaciva S, Lu S, Gebhard DF, Jessen BA, Pennie WD, Will Y (2011). A high content screening assay for identifying lysosomotropic compounds. *Toxicol In Vitro* **25:** 715-723.

Nagai T, Yamada S, Tominaga T, Ichikawa M, Miyawaki A (2004). Expanded dynamic range of fluorescent indicators for Ca^{2+} by circularly permuted yellow fluorescent proteins. *Proc Natl Acad Sci* **101:** 10554-10559.

Nakade S, Rhee SK, Hamanaka H, Mikoshiba K (1994). Cyclic AMP-dependent phosphorylation of an immunoaffinity-purified homotetrameric inositol 1,4,5-trisphosphate receptor (type I) increases Ca^{2+} flux in reconstituted lipid vesicles. *J Biol Chem* **269:** 6735-6742.

Nakanishi S, Maeda N, Mikoshiba K (1991). Immunohistochemical localization of an inositol 1,4,5-trisphosphate receptor, P400, in neural tissue: studies in developing and adult mouse brain. *J Neurosci* **11:** 2075-2086.

Nanou E, Catterall WA (2018). Calcium channels, synaptic plasticity, and neuropsychiatric disease. *Neuron* **98:** 466-481.

Navazio L, Bewell MA, Siddiqua A, Dickinson GD, Galione A, Sanders D (2000). Calcium release from the endoplasmic reticulum of higher plants elicited by the NADP metabolite nicotinic acid adenine dinucleotide phosphate. *Proc Natl Acad Sci* **97:** 8693–8698.

Neudorfer O, Giladi N, Elstein D, Abrahamov A, Turezkite T, Aghai E, Reches A, Bembi B, Zimran A (1996). Occurrence of Parkinson's syndrome in type 1 Gaucher disease. *QJM* **89:** 691–694.

Neufeld EB, Stonik JA, Demosky SJ, Jr., Knapper CL, Combs CA, Cooney A, Comly M, Dwyer N, Blanchette-Mackie J, Remaley AT, Santamarina-Fojo S, Brewer HB, Jr. (2004). The ABCA1 transporter modulates late endocytic trafficking: insights from the correction of the genetic defect in Tangier disease. *J Biol Chem* **279:** 15571-15578.

Nunez MT, Gaete V, Escobar A (1990). Endocytic vesicles contain a calmodulin-activated Ca^{2+} pump that mediates the inhibition of acidification by calcium. *Biochim Biophys Acta* **1028:** 21-24.

O-Uchi J, Pan S, Sheu S-S (2012). Molecular identities of mitochondrial Ca^{2+} influx mechanism: Updated passwords for accessing mitochondrial Ca^{2+}-linked health and disease. *J Gen Physiol* **139:** 435–443.

Oda K, Koriyama Y, Yamada E, Ikehara Y (1986). Effects of weakly basic amines on proteolytic processing and terminal glycosylation of secretory proteins in cultured rat hepatocytes. *Biochem J* **240:** 739.

Ogunbayo OA, Zhu Y, Rossi D, Sorrentino V, Ma J, Zhu MX, Evans AM (2011). Cyclic adenosine diphosphate ribose activates ryanodine receptors, whereas NAADP activates two-pore domain channels. *J Biol Chem* **286:** 9136–9140.

Oh-Hora M, Yamashita M, Hogan PG, Sharma S, Lamperti E, Chung W, Prakriya M, Feske S, Rao A (2008). Dual functions for the endoplasmic reticulum calcium sensors STIM1 and STIM2 in T cell activation and tolerance. *Nat Immunol* **9:** 432-443.

Okada T, Inoue R, Yamazaki K, Maeda A, Kurosaki T, Yamakuni T, Tanaka I, Shimizu S, Ikenaka K, Imoto K, Mori Y (1999). Molecular and functional characterization of a novel mouse transient receptor potential protein homologue TRP7. Ca^{2+}-permeable cation channel that is constitutively activated and enhanced by stimulation of G protein-coupled receptor. *J Biol Chem* **274:** 27359-27370.

Orrenius S, Zhivotovsky B, Nicotera P (2003). Calcium: Regulation of cell death: the calcium–apoptosis link. *Nat Rev Mol Cell Biol* **4:** 552–565.

Paknejad N, Hite RK (2018). Structural basis for the regulation of inositol trisphosphate receptors by Ca^{2+} and IP_3. *Nat Struct Mol Biol* **25:** 660-668.

Palty R, Raveh A, Kaminsky I, Meller R, Reuveny E (2012). SARAF inactivates the store operated calcium entry machinery to prevent excess calcium refilling. *Cell* **149:** 425-438.

Palty R, Silverman WF, Hershfinkel M, Caporale T, Sensi SL, Parnis J, Nolte C, Fishman D, Shoshan-Barmatz V, Herrmann S, Khananshvili D, Sekler I (2010). NCLX is an essential component of mitochondrial Na^+/Ca^{2+} exchange. *Proc Natl Acad Sci* **107:** 436-441.

Paquet C, Sane AT, Beauchemin M, Bertrand R (2005). Caspase- and mitochondrial dysfunction-dependent mechanisms of lysosomal leakage and cathepsin B activation in DNA damage-induced apoptosis. *Leukemia* **19:** 784-791.

Parekh AB, Putney JW (2005). Store-operated calcium channels. *Physiol Rev* **85:** 757-810.

Paris A, Strukelj B, Pungercar J, Renko M, Dolenc I, Turk V (1995). Molecular cloning and sequence analysis of human preprocathepsin C. *FEBS Lett* **369:** 326-330.

Park CY, Hoover PJ, Mullins FM, Bachhawat P, Covington ED, Raunser S, Walz T, Garcia KC, Dolmetsch RE, Lewis RS (2009). STIM1 clusters and activates CRAC channels via direct binding of a cytosolic domain to Orai1. *Cell* **136:** 876-890

Patel S, Docampo R (2010). Acidic calcium stores open for business: expanding the potential for intracellular Ca^{2+} signaling. *Trends Cell Biol* **20:** 277-286.

Patel S, Marchant JS, Brailoiu E (2010). Two-pore channels: regulation by NAADP and customized roles in triggering calcium signals. *Cell Calcium* **47:** 480-490.

Peden AA, Oorschot V, Hesser BA, Austin CD, Scheller RH, Klumperman J (2004). Localization of the AP-3 adaptor complex defines a novel endosomal exit site for lysosomal membrane proteins. *J Cell Bio* **164:** 1065–1076.

Penny CJ, Kilpatrick BS, Eden ER, Patel S (2015). Coupling acidic organelles with the ER through Ca^{2+} microdomains at membrane contact sites. *Cell Calcium* **58:** 387-396.

Penny CJ, Kilpatrick BS, Han JM, Sneyd J, Patel S (2014). A computational model of lysosome-ER Ca^{2+} microdomains. *J Cell Sci* **127:** 2934-2943.

Peri F, Nusslein-Volhard C (2008). Live imaging of neuronal degradation by microglia reveals a role for V_0-ATPase A1 in phagosomal fusion in vivo. *Cell* **133:** 916-927.

Periasamy M, Kalyanasundaram A (2007). SERCA pump isoforms: their role in calcium transport and disease. *Muscle Nerve* **35:** 430-442.

Petersen OH (2004). Local and global Ca^{2+} signals: physiology and pathophysiology. *Biol Res* **37:** 661-664.

Pethig R, Kuhn M, Payne R, Adler E, Chen TH, Jaffe LF (1989). On the dissociation constants of BAPTA-type calcium buffers. *Cell Calcium* **10:** 491-498.

Philipp S, Trost C, Warnat J, Rautmann J, Himmerkus N, Schroth G, Kretz O, Nastainczyk W, Cavalie A, Hoth M, Flockerzi V (2000). TRP4 (CCE1) protein is part of native calcium release-activated Ca^{2+}-like channels in adrenal cells. *J Biol Chem* **275:** 23965-23972.

Phillips MJ, Voeltz GK (2016). Structure and function of ER membrane contact sites with other organelles. *Nat Rev Mol Cell Biol* **17:** 69-82.

Pinton P, Giorgi C, Siviero R, Zecchini E, Rizzuto R (2008). Calcium and apoptosis: ER-mitochondria Ca^{2+} transfer in the control of apoptosis. *Oncogene* **27:** 6407-6418.

Pinton P, Pozzan T, Rizzuto R (1998). The Golgi apparatus is an inositol 1,4,5-trisphosphate-sensitive Ca^{2+} store, with functional properties distinct from those of the endoplasmic reticulum. *EMBO J* **17:** 5298-5308.

Pitt SJ, Funnell T, Sitsapesan M, Venturi E, Rietdorf K, Ruas M, Ganesan A, Gosain R, Churchill GC, Zhu MX, Parrington J, Galione A, Sitsapesan R (2010). TPC2 is a novel NAADP-sensitive Ca^{2+}-release channel, operating as a dual sensor of luminal pH and Ca^{2+}. *J Biol Chem* **285:** 35039-35046.

Pitt SJ, Lam AK, Rietdorf K, Galione A, Sitsapesan R (2014). Reconstituted human TPC1 is a proton-permeable ion channel and is activated by NAADP or Ca^{2+}. *Sci Signal* **7:** ra46.

Plant TD, Schaefer M (2005). Receptor-operated cation channels formed by TRPC4 and TRPC5. *Arch Pharmacol* **371:** 266-276.

Planta RJ, Gorter J, Gruber M (1964). The catalytic properties of cathepsin C. *Biochim Biophys Acta* **89:** 511-519.

Pohlmann R, Boeker MW, von Figura K (1995). The two mannose 6-phosphate receptors transport distinct complements of lysosomal proteins. *J Biol Chem* **270:** 27311-27318.

Pouli AE, Karagenc N, Wasmeier C, Hutton JC, Bright N, Arden S, Schofield JG, Rutter GA (1998). A phogrin-aequorin chimaera to image free Ca^{2+} in the vicinity of secretory granules. *Biochem J* **330:** 1399-1404.

Pozzan T, Rizzuto R, Volpe P, Meldolesi J (1994). Molecular and cellular physiology of intracellular calcium stores. *Physiol Rev* **74:** 595-636.

Prakriya M, Lewis RS (2015). Store-operated calcium channels. *Physiol Rev* **95:** 1383-1436.

Prasad V, Okunade GW, Miller ML, Shull GE (2004). Phenotypes of SERCA and PMCA knockout mice. *Biochem Biophys Res Commun* **322:** 1192-1203.

Presley JF, Mayor S, McGraw TE, Dunn KW, Maxfield FR (1997). Bafilomycin A_1 treatment retards transferrin receptor recycling more than bulk membrane recycling. *J Biol Chem* **272:** 13929-13936.

Prins D, Michalak M (2011). Organellar calcium buffers. *Cold Spring Harb Perspect Biol* **3:** a004069.

Prinz WA (2014). Bridging the gap: Membrane contact sites in signaling, metabolism, and organelle dynamics. *J Cell Biol* **205:** 759-769.

Probst OC, Ton P, Svoboda B, Gannon A, Schuhmann W, Wieser J, Pohlmann R, Mach L (2006). The 46-kDa mannose 6-phosphate receptor does not depend on endosomal acidification for delivery of hydrolases to lysosomes. *J Cell Sci* **119:** 4935-4943.

Prole DL, Taylor CW (2011). Identification of intracellular and plasma membrane calcium channel homologues in pathogenic parasites. *PLoS One* **6:** e26218.

Prole DL, Taylor CW (2012). Identification and analysis of cation channel homologues in human pathogenic fungi. *PLoS One* **7:** e42404.

Prole DL, Taylor CW (2016). Inositol 1,4,5-trisphosphate receptors and their protein partners as signalling hubs. *J Physiol* **594:** 2849-2866.

Pryor PR, Luzio JP (2009). Delivery of endocytosed membrane proteins to the lysosome. *Biochim Biophys Acta* **1793:** 615-624.

Pryor PR, Mullock BM, Bright NA, Gray SR, Luzio JP (2000). The role of intraorganellar Ca^{2+} in late endosome-lysosome heterotypic fusion and in the reformation of lysosomes from hybrid organelles. *J Cell Biol* **149:** 1053-1062.

Putney JW (2004). Store-operated calcium channels: how do we measure them and do we care? *Science STKE* **pe37**.

Putney JW, Jr. (1986). A model for receptor-regulated calcium entry. *Cell Calcium* **7:** 1-12.

Quon E, Beh CT (2015). Membrane contact sites: Complex zones for membrane association and lipid exchange. *Lipid insights* **8:** 55-63.

Qureshi OS, Paramasivam A, Yu JC, Murrell-Lagnado RD (2007). Regulation of P2X4 receptors by lysosomal targeting, glycan protection and exocytosis. *J Cell Sci* **120:** 3838-3849.

Raiborg C, Wenzel EM, Pedersen NM, Olsvik H, Schink KO, Schultz SW, Vietri M, Nisi V, Bucci C, Brech A, Johansen T, Stenmark H (2015). Repeated ER-endosome contacts promote endosome translocation and neurite outgrowth. *Nature* **520:** 234-238.

Rao NV, Rao GV, Hoidal JR (1997). Human dipeptidyl-peptidase I. Gene characterization, localization, and expression. *J Biol Chem* **272:** 10260-10265.

Reaves B, Banting G (1994). Vacuolar ATPase inactivation blocks recycling to the trans-Golgi network from the plasma membrane. *FEBS Lett* **345:** 61-66.

Rebbeck RT, Karunasekara Y, Gallant EM, Board PG, Beard NA, Casarotto MG, Dulhunty AF (2011). The β1a subunit of the skeletal DHPR binds to skeletal RyR1 and activates the channel via its 35-residue C-terminal tail. *Biophys J* **100:** 922-930.

Reczek D, Schwake M, Schroder J, Hughes H, Blanz J, Jin X, Brondyk W, Van Patten S, Edmunds T, Saftig P (2007). LIMP-2 is a receptor for lysosomal mannose-6-phosphate-independent targeting of beta-glucocerebrosidase. *Cell* **131:** 770-783.

Redmann M, Benavides GA, Berryhill TF, Wani WY, Ouyang X, Johnson MS, Ravi S, Barnes S, Darley-Usmar VM, Zhang J (2017). Inhibition of autophagy with bafilomycin and chloroquine decreases mitochondrial quality and bioenergetic function in primary neurons. *Redox biology* **11:** 73-81.

Repnik U, Distefano MB, Speth MT, Ng MYW, Progida C, Hoflack B, Gruenberg J, Griffiths G (2017). LLOMe does not release cysteine cathepsins to the cytosol but inactivates them in transiently permeabilized lysosomes. *J Cell Sci* **130:** 3124-3140.

Repnik U, Stoka V, Turk V, Turk B (2012). Lysosomes and lysosomal cathepsins in cell death. *Biochim Biophys Acta* **1824:** 22-33.

Rizzuto R, Brini M, Murgia M, Pozzan T (1993). Microdomains with high Ca^{2+} close to IP_3-sensitive channels that are sensed by neighbouring mitochondria. *Science* **262:** 744-747.

Rizzuto R, De Stefani D, Raffaello A, Mammucari C (2012). Mitochondria as sensors and regulators of calcium signalling. *Nat Rev Mol Cell Biol* **13:** 566-578.

Rizzuto R, Duchen MR, Pozzan T (2004). Flirting in little spce: the ER/mitochondria Ca^{2+} liaison. *Science STKE* **re1**.

Rizzuto R, Pinton P, Carrington W, Fay FS, Fogarty KE, Lifshitz LM, Tuft RA, Pozzan T (1998). Close contacts with the endoplasmic reticulum as determinants of mitochondrial Ca^{2+} responses. *Science* **280:** 1763-1766.

Rocha N, Kuijl C, van der Kant R, Janssen L, Houben D, Janssen H, Zwart W, Neefjes J (2009). Cholesterol sensor ORP1L contacts the ER protein VAP to control Rab7-RILP-p150 Glued and late endosome positioning. *J Cell Biol* **185:** 1209-1225.

Roczniak-Ferguson A, Petit CS, Froehlich F, Qian S, Ky J, Angarola B, Walther TC, Ferguson SM (2012). The transcription factor TFEB links mTORC1 signaling to transcriptional control of lysosome homeostasis. *Sci Signal* **5:** ra42.

Ronco V, Potenza DM, Denti F, Vullo S, Gagliano G, Tognolina M, Guerra G, Pinton P, Genazzani AA, Mapelli L, Lim D, Moccia F (2015). A novel Ca^{2+}-mediated cross-talk between endoplasmic reticulum and acidic organelles: implications for NAADP-dependent Ca^{2+} signalling. *Cell Calcium* **57:** 89-100.

Rooney EK, Gross JD (1992). ATP-driven Ca^{2+}/H^{+} antiport in acid vesicles from Dictyostelium. *Proc Natl Acad Sci* **89:** 8025-8029.

Rooney EK, Gross JD, Satre M (1994). Characterisation of an intracellular Ca^{2+} pump in Dictyostelium. *Cell Calcium* **16:** 509-522.

Roos J, DiGregorio PJ, Yeromin AV, Ohlsen K, Lioudyno M, Zhang S, Safrina O, Kozak JA, Wagner SL, Cahalan MD, Velicelebi G, Stauderman KA (2005). STIM1, an essential and conserved component of store-operated Ca^{2+} channel function. *J Cell Biol* **169:** 435-445.

Rowland AA, Chitwood PJ, Phillips MJ, Voeltz GK (2014). ER contact sites define the position and timing of endosome fission. *Cell* **159:** 1027-1041.

Ruas M, LC D, CC C, AJ M, KT C, TF W, C G, Garnham C, Powell T, Platt N, Platt FM, Biel M, Wahl-Schott C, Parrington J, A. G (2015). Expression of Ca^{2+} permeable two-pore channels rescues NAADP signalling in TPC-deficient cells. *EMBO J* **34:** 1743-1758.

Ruas M, Rietdorf K, Arredouani A, Davis LC, Lloyd-Evans E, Koegel H, Funnell TM, Morgan AJ, Ward JA, Watanabe K, Cheng X, Churchill GC, Zhu MX, Platt FM, Wessel GM, Parrington J, Galione A (2010). Purified TPC isoforms form NAADP receptors with distinct roles for Ca^{2+} signaling and endolysosomal trafficking. *Curr Biol* **20:** 703-709.

Ruckl M, Parker I, Marchant JS, Nagaiah C, Johenning FW, Rudiger S (2015). Modulation of elementary calcium release mediates a transition from puffs to waves in an IP_3R cluster model. *PLoS Comput Biol* **11:** e1003965.

Rybalchenko V, Ahuja M, Coblentz J, Churamani D, Patel S, Kiselyov K, Muallem S (2012). Membrane potential regulates nicotinic acid adenine dinucleotide phosphate (NAADP) dependence of the pH- and Ca^{2+}-sensitive organellar two-pore channel TPC1. *J Biol Chem* **287:** 20407-20416.

Sabnis RW (2015). Oregon Green 488 carboxylic acid succinimidyl ester. In. *Handbook of Fluorescent Dyes and Probes*. 308-309.

Saftig P, Klumperman J (2009). Lysosome biogenesis and lysosomal membrane proteins: trafficking meets function. *Nat Rev Mol Cell Biol* **10:** 623-635.

Sakurai Y (2015). Ebola virus. Two-pore channels control Ebola virus host cell entry and are drug targets for disease treatment. *Science* **347:** 995-998.

Saleem H, Tovey SC, Rahman T, Riley AM, Potter BV, Taylor CW (2013). Stimulation of inositol 1,4,5-trisphosphate (IP_3) receptor subtypes by analogues of IP_3. *PLoS One* **8:** e54877.

Sancak Y, Bar-Peled L, Zoncu R, Markhard AL, Nada S, Sabatini DM (2010). Ragulator-Rag complex targets mTORC1 to the lysosomal surface and is necessary for its activation by amino acids. *Cell* **141:** 290-303.

Sander JD, Maeder ML, Reyon D, Voytas DF, Joung JK, Dobbs D (2010). ZiFiT (Zinc Finger Targeter): an updated zinc finger engineering tool. *Nucleic Acids Res* **38:** W462-468.

Sardi SP, Cheng SH, Shihabuddin LS (2015). Gaucher-related synucleinopathies: the examination of sporadic neurodegeneration from a rare (disease) angle. *Prog Neurobiol* **125:** 47-62.

Saucedo LJ, Gao X, Chiarelli DA, Li L, Pan D, Edgar BA (2003). Rheb promotes cell growth as a component of the insulin/TOR signalling network. *Nat Cell Biol* **5:** 566-571.

Sbano L, Bonora M, Marchi S, Baldassari F, Medina DL, Ballabio A, Giorgi C, Pinton P (2017). TFEB-mediated increase in peripheral lysosomes regulates store-operated calcium entry. *Sci Rep* **7:** 40797.

Schieder M, Rotzer K, Bruggemann A, Biel M, Wahl-Schott C (2010a). Planar patch clamp approach to characterize ionic currents from intact lysosomes. *Sci Signal* **3:** pl3.

Schieder M, Rotzer K, Bruggemann A, Biel M, Wahl-Schott CA (2010b). Characterization of two-pore channel 2 (TPCN2)-mediated Ca^{2+} currents in isolated lysosomes. *J Biol Chem* **285:** 21219-21222.

Schönknecht G (2013). Calcium signals from the vacuole. *Plants* **2:** 589-614.

Schreiber R (2005). Ca^{2+} signaling, intracellular pH and cell volume in cell proliferation. *J Membr Biol* **205:** 129-137.

Schroder BA, Wrocklage C, Hasilik A, Saftig P (2010). The proteome of lysosomes. *Proteomics* **10:** 4053-4076.

Schwaller B (2010). Cytosolic Ca^{2+} buffers. *Cold Spring Harb Perspect Biol* **2:** a004051.

Scott CC, Gruenberg J (2011). Ion flux and the function of endosomes and lysosomes: pH is just the start: the flux of ions across endosomal membranes influences endosome function not only through regulation of the luminal pH. *Bioessays* **33:** 103-110.

Seo MD, Velamakanni S, Ishiyama N, Stathopulos PB, Rossi AM, Khan SA, Dale P, Li C, Ames JB, Ikura M, Taylor CW (2012). Structural and functional conservation of key domains in $InsP_3$ and ryanodine receptors. *Nature* **483:** 108-112.

Settembre C, Di Malta C, Polito VA, Garcia Arencibia M, Vetrini F, Erdin S, Erdin SU, Huynh T, Medina D, Colella P, Sardiello M, Rubinsztein DC, Ballabio A (2011). TFEB links autophagy to lysosomal biogenesis. *Science* **332:** 1429-1433.

Settembre C, Fraldi A, Medina DL, Ballabio A (2013). Signals from the lysosome: a control centre for cellular clearance and energy metabolism. *Nat Rev Mol Cell Biol* **14:** 283-296.

Shah PK, Sawhamini R (2001). Structural understanding of the transmembrane domains of inositol triphosphate receptors (*sic*) and ryanodine receptors towards calcium channeling. *Protein Eng* **14:** 867-874.

Sharma S, Quintana A, Findlay GM, Mettlen M, Baust B, Jain M, Nilsson R, Rao A, Hogan PG (2013). An siRNA screen for NFAT activation identifies septins as coordinators of store-operated Ca^{2+} entry. *Nature* **499:** 238-242.

Shen D, Wang X, Li X, Zhang X, Yao Z, Dibble S, Dong XP, Yu T, Lieberman AP, Showalter HD, Xu H (2012). Lipid storage disorders block lysosomal trafficking by inhibiting a TRP channel and lysosomal calcium release. *Nat Commun* **3:** 731.

Short AD, Taylor CW (2000). Parathyroid hormone controls the size of the intracellular Ca^{2+} stores available to receptors linked to inositol trisphosphate formation. *J Biol Chem* **275:** 1807-1813.

Shorte SL, Collingridge GL, Randall AD, Chappell JB, Schofield JG (1991). Ammonium ions mobilize calcium from an internal pool which is insensitive to TRH and ionomycin in bovine anterior pituitary cells. *Cell Calcium* **12:** 301-312.

Shuttleworth TJ (1996). Arachidonic acid activates the noncapacitative entry of Ca^{2+} during $[Ca^{2+}]_i$ oscillations. *J Biol Chem* **271:** 21720-21725.

Siskind MS, McCoy CE, Chobanian A, Schwartz JH (1989). Regulation of intracellular calcium by cell pH in vascular smooth muscle cells. *Am J Physiol* **256:** C234-240.

Sivaramakrishnan V, Bidula S, Campwala H, Katikaneni D, Fountain SJ (2012). Constitutive lysosome exocytosis releases ATP and engages P2Y receptors in human monocytes. *J Cell Sci* **125:** 4567-4575.

Skowyra ML, Schlesinger PH, Naismith TV, Hanson PI (2018). Triggered recruitment of ESCRT machinery promotes endolysosomal repair. *Science* **360**.

Slavov N, Carey J, Linse S (2013). Calmodulin transduces Ca^{2+} oscillations into differential regulation of its target proteins. *ACS chem neuro* **4:** 601-612.

Smith IF, Swaminathan D, Dickinson GD, Parker I (2014). Single-molecule tracking of inositol trisphosphate receptors reveals different motilities and distributions. *Biophys J* **107:** 834-845.

Smyth JT, Dehaven WI, Bird GS, Putney JW, Jr. (2008). Ca^{2+}-store-dependent and independent reversal of Stim1 localization and function. *J Cell Sci* **121:** 762-772.

Soboloff J, Spassova MA, Tang XD, Hewavitharana T, Xu W, Gill DL (2006). Orai1 and STIM reconstitute store-operated calcium channel function. *J Biol Chem* **30:** 20661-20665.

Solovyova N, Fernyhough P, Glazner G, Verkhratsky A (2002). Xestospongin C empties the ER calcium store but does not inhibit $InsP_3$-induced Ca^{2+} release in cultured dorsal root ganglia neurones. *Cell Calcium* **32:** 49-52.

Speake T, Elliott AC (1998). Modulation of calcium signals by intracellular pH in isolated rat pancreatic acinar cells. *J Physiol* **506:** 415-430.

Srikanth S, Jung HJ, Kim KD, Souda P, Whitelegge J, Gwack Y (2010). A novel EF-hand protein, CRACR2A, is a cytosolic Ca^{2+} sensor that stabilizes CRAC channels in T cells. *Nat Cell Biol* **12:** 436-446.

Stathopulos PB, Zheng L, Li GY, Plevin MJ, Ikura M (2008). Structural and mechanistic insights into STIM1-mediated initiation of store-operated calcium entry. *Cell* **135:** 110-122.

Steen M, Kirchberger T, Guse AH (2007). NAADP mobilizes calcium from the endoplasmic reticular Ca^{2+} store in T-lymphocytes. *J Biol Chem* **282:** 18864-18871.

Steinberg BE, Huynh KK, Brodovitch A, Jabs S, Stauber T, Jentsch TJ, Grinstein S (2010). A cation counterflux supports lysosomal acidification. *J Cell Biol* **189:** 1171-1186.

Stephens GJ, Morris NP, Fyffe RE, Robertson B (2001). The $Ca_v2.1/\alpha1A$ (P/Q-type) voltage-dependent calcium channel mediates inhibitory neurotransmission onto mouse cerebellar Purkinje cells. *Eur J Neurosci* **13:** 1902-1912.

Stoorvogel W, Strous GJ, Geuze HJ, Oorschot V, Schwartz AL (1991). Late endosomes derive from early endosomes by maturation. *Cell* **65:** 417-427.

Storrie B, Desjardins M (1996). The biogenesis of lysosomes: is it a kiss and run, continuous fusion and fission process? *Bioessays* **18:** 895-903.

Stransky LA, Forgac M (2015). Amino acid availability modulates vacuolar H^+-atpase assembly. *J Biol Chem* **290:** 27360-27369.

Strasser B, Iwaszkiewicz J, Michielin O, Mayer A (2011). The V-ATPase proteolipid cylinder promotes the lipid-mixing stage of SNARE-dependent fusion of yeast vacuoles. *Embo J* **30:** 4126-4141.

Sundivakkam PC, Freichel M, Singh V, Yuan JP, Vogel SM, Flockerzi V, Malik AB, Tiruppathi C (2012). The Ca^{2+} sensor stromal interaction molecule 1 (STIM1) is necessary and sufficient for the store-operated Ca^{2+} entry function of transient receptor potential canonical (TRPC) 1 and 4 channels in endothelial cells. *Mol Pharmacol* **81:** 510-526.

Szabadkai G, Bianchi K, Varnai P, De Stefani D, Wieckowski MR, Cavagna D, Nagy AI, Balla T, Rizzuto R (2006). Chaperone-mediated coupling of endoplasmic reticulum and mitochondrial Ca^{2+} channels. *J Cell Biol* **175:** 901-911.

Tabary O, Boncoeur E, de Martin R, Pepperkok R, Clement A, Schultz C, Jacquot J (2006). Calcium-dependent regulation of NF-(kappa)B activation in cystic fibrosis airway epithelial cells. *Cell Signal* **18:** 652-660.

Takeda K, Cabrera M, Rohde J, Bausch D, Jensen ON, Ungermann C (2008). The vacuolar V1/V0-ATPase is involved in the release of the HOPS subunit Vps41 from vacuoles, vacuole fragmentation and fusion. *FEBS Lett* **582:** 1558-1563.

Takeshima H, Komazaki S, Nishi M, Iino M, Kangawa K (2000). Junctophilins: a novel family of junctional membrane complex proteins. *Mol Cell* **6:** 11-22.

Tamarina NA, Kuznetsov A, Philipson LH (2008). Reversible translocation of EYFP-tagged STIM1 is coupled to calcium influx in insulin secreting beta-cells. *Cell Calcium* **44:** 533-544.

Taufiq R, Skupin A, Falcke M, Taylor CW (2009). Clustering of $InsP_3$ receptors by $InsP_3$ retunes their regulation by $InsP_3$ and Ca^{2+}. *Nature* **458:** 655-659.

Taylor CW (1998). Inositol trisphosphate receptors: Ca^{2+}-modulated intracellular Ca^{2+} channels. *Biochim Biophys Acta* **1436:** 19-33.

Taylor CW, Dale P (2012). Intracellular Ca^{2+} channels - a growing community. *Mol Cell Endocrinol* **353:** 21-28.

Taylor CW, Genazzani AA, Morris SA (1999). Expression of inositol trisphosphate receptors. *Cell Calcium* **26:** 237-251.

Taylor CW, Konieczny V (2016). IP_3 receptors: Take four IP_3 to open. *Sci Signal* **9:** pe1.

Taylor CW, Tovey SC (2010). IP_3 receptors: toward understanding their activation. *Cold Spring Harb Perspect Biol* **2:** a004010.

Terman A, Kurz T, Gustafsson B, Brunk UT (2006). Lysosomal labilization. *IUBMB Life* **58:** 531-539.

Thiele DL, Lipsky PE (1990). Mechanism of L-leucyl-L-leucine methyl ester-mediated killing of cytotoxic lymphocytes: dependence on a lysosomal thiol protease, dipeptidyl peptidase I, that is enriched in these cells. *Proc Natl Acad Sci* **87:** 83-87.

Thillaiappan NB, Chavda AP, Tovey SC, Prole DL, Taylor CW (2017). Ca^{2+} signals initiate at immobile IP_3 receptors adjacent to ER-plasma membrane junctions. *Nat Commun* **8:** 1505.

Thivolet C, Vial G, Cassel R, Rieusset J, Madec AM (2017). Reduction of endoplasmic reticulum- mitochondria interactions in beta cells from patients with type 2 diabetes. *PLoS One* **12:** e0182027.

Thomas D, Lipp P, Tovey SC, Berridge MJ, Li W, Tsien RY, Bootman MD (2000). Microscopic properties of elementary Ca^{2+} release sites in non-excitable cells. *Curr Biol* **10:** 8-15.

Thrower EC, Choe CU, So SH, Jeon SH, Ehrlich BE, Yoo SH (2003). A functional interaction between chromogranin B and inositol 1,4,5-trisphosphate receptor/Ca^{2+} channel. *J Biol Chem* **278:** 49699-49708.

Thurley K, Tovey SC, Moenke G, Prince VL, Meena A, Thomas AP, Skupin A, Taylor CW, Falcke M (2014). Reliable encoding of stimulus intensities within random sequences of intracellular Ca^{2+} spikes. *Sci Signal* **7:** ra59.

Thurston TL, Wandel MP, von Muhlinen N, Foeglein A, Randow F (2012). Galectin 8 targets damaged vesicles for autophagy to defend cells against bacterial invasion. *Nature* **482:** 414-418.

Thwaites DT, Anderson CM (2011). The SLC36 family of proton-coupled amino acid transporters and their potential role in drug transport. *Br J Pharmacol* **164:** 1802-1816.

Tiruppathi C, Ahmmed GU, Vogel SM, Malik AB (2006). Ca^{2+} signaling, TRP channels, and endothelial permeability. *Microcirculation* **13:** 693-708.

Togashi K, Hara Y, Tominaga T, Higashi T, Konishi Y, Mori Y, Tominaga M (2006). TRPM2 activation by cyclic ADP-ribose at body temperature is involved in insulin secretion. *EMBO J* **25:** 1804-1815.

Tovey SC, de Smet P, Lipp P, Thomas D, Young KW, Missiaen L, De Smedt H, Parys JB, Berridge MJ, Thuring J, Holmes A, Bootman MD (2001). Calcium puffs are generic $InsP_3$-activated elementary calcium signals and are downregulated by prolonged hormonal stimulation to inhibit cellular calcium responses. *J Cell Sci* **114:** 3979-3989.

Tovey SC, Dedos SG, Taylor EJ, Church JE, Taylor CW (2008). Selective coupling of type 6 adenylyl cyclase with type 2 IP_3 receptors mediates direct sensitization of IP_3 receptors by cAMP. *J Cell Biol* **183:** 297-311.

Tovey SC, Goraya TA, Taylor CW (2003). Parathyroid hormone increases the sensitivity of inositol trisphosphate receptors by a mechanism that is independent of cyclic AMP. *Br. J Pharmacol* **138:** 81-90.

Tovey SC, Taylor CW (2013). Cyclic AMP directs inositol (1,4,5)-trisphosphate-evoked Ca^{2+} signalling to different intracellular Ca^{2+} stores. *J Cell Sci* **126:** 2305-2313.

Towatari T, Nikawa T, Murata M, Yokoo C, Tamai M, Hanada K, Katunuma N (1991). Novel epoxysuccinyl peptides. A selective inhibitor of cathepsin B, in vivo. *FEBS Lett* **280:** 311-315.

Trincheri NF, Nicotra G, Follo C, Castino R, Isidoro C (2007). Resveratrol induces cell death in colorectal cancer cells by a novel pathway involving lysosomal cathepsin D. *Carcinogenesis* **28:** 922-931.

Trollinger DR, Cascio WE, Lemasters JJ (1997). Selective loading of Rhod 2 into mitochondria shows mitochondrial Ca^{2+} transients during the contractile cycle in adult rabbit cardiac myocytes. *Biochem Biophys Res Commun* **236:** 738-742.

Tsien RY (1980). New calcium indicators and buffers with high selectivity against magnesium and protons: design, synthesis, and properties of prototype structures. *Biochemistry* **19:** 2396-2404.

Tsujishita Y, Hurley JH (2000). Structure and lipid transport mechanism of a StAR-related domain. *Nat Struct Biol* **7:** 408-414.

Tu H, Miyakawa T, Wang Z, Glouchankova L, Iino M, Bezprozvanny I (2002). Functional characterization of the type 1 inositol 1,4,5-trisphosphate receptor coupling doamain SII(±) splice variants and the *Opisthotonos* mutant form. *Biophys J* **82:** 1995-2004.

Tu H, Wang Z, Bezprozvanny I (2005). Modulation of mammalian inositol 1,4,5-trisphosphate receptor isoforms by calcium: a role of calcium sensor region. *Biophys J* **88:** 1056-1069.

Tu JC, Xiao B, Yuan JP, Lanahan AA, Leoffert K, Li M, Linden DJ, Worley PF (1998). Homer binds a novel proline-rich motif and links group 1 metabotropic glutamate receptors with IP_3 receptors. *Neuron* **21:** 717-726.

Tugba Durlu-Kandilci N (2010). TPC2 proteins mediate nicotinic acid adenine dinucleotide phosphate (NAADP)- and agonist-evoked contractions of smooth muscle. *J Biol Chem* **285:** 24925-24932.

Turk D, Guncar G, Podobnik M, Turk B (1998). Revised definition of substrate binding sites of papain-like cysteine proteases. *Biol Chem* **379:** 137-147.

Turk V, Turk B, Turk D (2001). Lysosomal cysteine proteases: facts and opportunities. *EMBO J* **20:** 4629-4633.

Uchimoto T, Nohara H, Kamehara R, Iwamura M, Watanabe N, Kobayashi Y (1999). Mechanism of apoptosis induced by a lysosomotropic agent, L-Leucyl-L-Leucine methyl ester. *Apoptosis* **4:** 357-362.

Ullio C, Casas J, Brunk UT, Sala G, Fabrias G, Ghidoni R, Bonelli G, Baccino FM, Autelli R (2012). Sphingosine mediates TNFalpha-induced lysosomal membrane permeabilization and ensuing programmed cell death in hepatoma cells. *J Lipid Res* **53:** 1134-1143.

Valm AM, Cohen S, Legant WR, Melunis J, Hershberg U, Wait E, Cohen AR, Davidson MW, Betzig E, Lippincott-Schwartz J (2017). Applying systems-level spectral imaging and analysis to reveal the organelle interactome. *Nature* **546:** 162-167.

van Weert AW, Dunn KW, Geuze HJ, Maxfield FR, Stoorvogel W (1995). Transport from late endosomes to lysosomes, but not sorting of integral membrane proteins in endosomes, depends on the vacuolar proton pump. *J Cell Biol* **130:** 821-834.

Vanderheyden V, Devogelaere B, Missiaen L, De Smedt H, Bultynck G, Parys JB (2009). Regulation of inositol 1,4,5-trisphosphate-induced Ca^{2+} release by reversible phosphorylation and dephosphorylation. *Biochim Biophys Acta* **1793:** 959-970.

Vazquez G, Wedel BJ, Aziz O, Trebak M, Putney JW, Jr. (2004). The mammalian TRPC cation channels. *Biochim Biophys Acta* **1742:** 21-36.

Vercesi AE, Moreno SN, Docampo R (1994). Ca^{2+}/H^{+} exchange in acidic vacuoles of Trypanosoma brucei. *Biochem J* **304:** 227-233.

Vervloessem T, Yule DI, Bultynck G, Parys JB (2015). The type 2 inositol 1,4,5-trisphosphate receptor, emerging functions for an intriguing Ca^{2+}-release channel. *Biochim Biophys Acta* **1853:** 1992-2005.

Villamil Giraldo AM, Appelqvist H, Ederth T, Ollinger K (2014). Lysosomotropic agents: impact on lysosomal membrane permeabilization and cell death. *Biochem Soc Trans* **42:** 1460-1464.

Virginio C, North RA, Surprenant A (1998). Calcium permeability and block at homomeric and heteromeric $P2X_2$ and $P2X_3$ receptors, and P2X receptors in rat nodose neurones. *J Physiol* **510:** 27-35.

Volterra A, Meldolesi J (2005). Astrocytes, from brain glue to communication elements: the revolution continues. *Nat Rev Neurosci* **6:** 626-640.

Voronov I, Ochotny N, Jaumouille V, Owen C, Manolson MF, Aubin JE (2013). The R740S mutation in the V-ATPase a3 subunit increases lysosomal pH, impairs NFATc1 translocation, and decreases in vitro osteoclastogenesis. *J Bone Miner Res* **28:** 108-118.

Wagner LE, 2nd, Li WH, Joseph SK, Yule DI (2004). Functional consequences of phosphomimetic mutations at key cAMP-dependent protein kinase phosphorylation sites in the type 1 inositol 1,4,5-trisphosphate receptor. *J Biol Chem* **279:** 46242-46252.

Wagner LE, Li W-H, Yule DL (2003). Phosphorylation of type 1 inositol 1,4,5-trisphosphate receptors by cyclic nucleotide-dependent protein kinases. *J Biol Chem* **278:** 45811-45817.

Wakabayashi I, Poteser M, Groschner K (2006). Intracellular pH as a determinant of vascular smooth muscle function. *J Vasc Res* **43:** 238-250.

Walseth TF, Lin-Moshier Y, Jain P, Ruas M, Parrington J, Galione A, Marchant JS, Slama JT (2011). Photoaffinity labeling of high affinity nicotinic acid adenine dinucleotide phosphate (NAADP)-binding proteins in sea urchin egg. *J Biol Chem* **287:** 2308-2315.

Walseth TF, Lin-Moshier Y, Weber K, Marchant JS, Slama JT, Guse AH (2012). Nicotinic acid adenine dinucleotide 2'-phosphate (NAADP) binding proteins in T-lymphocytes. *Messenger* **1:** 86-94.

Wang QC, Zheng Q, Tan H, Zhang B, Li X, Yang Y, Yu J, Liu Y, Chai H, Wang X, Sun Z, Wang JQ, Zhu S, Wang F, Yang M, Guo C, Wang H, Li Y, Chen Q, Zhou A, Tang TS (2016). TMCO1 Is an ER Ca^{2+} load-activated Ca^{2+} channel. *Cell* **165:** 1454-1466.

Wang W, Zhang X, Gao Q, Lawas M, Yu L, Cheng X, Gu M, Sahoo N, Li X, Li P, Ireland S, Meredith A, Xu H (2017). A voltage-dependent K^+ channel in the lysosome is required for refilling lysosomal Ca^{2+} stores. *J Cell Biol* **216:** 1715-1730.

Wang X, Zhang X, Dong XP, Samie M, Li X, Cheng X, Goschka A, Shen D, Zhou Y, Harlow J, Zhu MX, Clapham DE, Ren D, Xu H (2012). TPC proteins are phosphoinositide-activated sodium-selective ion channels in endosomes and lysosomes. *Cell* **151:** 372-383.

Weinert S, Jabs S, Supanchart C, Schweizer M, Gimber N, Richter M, Rademann J, Stauber T, Kornak U, Jentsch TJ (2010). Lysosomal pathology and osteopetrosis upon loss of H^+-driven lysosomal Cl^- accumulation. *Science* **328:** 1401-1403.

Welsh DG, Morielli AD, Nelson MT, Brayden JE (2002). Transient receptor potential channels regulate myogenic tone of resistance arteries. *Circ Res* **90:** 248-250.

Werneburg NW, Guicciardi ME, Bronk SF, Gores GJ (2002). Tumor necrosis factor-alpha-associated lysosomal permeabilization is cathepsin B dependent. *Am J Physiol* **283:** G947-956.

Werneburg NW, Guicciardi ME, Bronk SF, Kaufmann SH, Gores GJ (2007). Tumor necrosis factor-related apoptosis-inducing ligand activates a lysosomal pathway of apoptosis that is regulated by Bcl-2 proteins. *J Biol Chem* **282:** 28960-28970.

Wheeler GL, Brownlee C (2008). Ca^{2+} signalling in plants and green algae - changing channels. *Trends Plant Sci* **13:** 506-514.

Whitaker M (2006). Calcium at fertilization and in early development. *Physiol Rev* **86:** 25-88.

Willoughby D, Thomas R, Schwiening C (2001). The effects of intracellular pH changes on resting cytosolic calcium in voltage-clamped snail neurones. *J Physiol* **530:** 405-416.

Wolters PJ, Chapman HA (2000). Importance of lysosomal cysteine proteases in lung disease. *Respir Res* **1:** 170-177.

Wood SA, Brown WJ (1992). The morphology but not the function of endosomes and lysosomes is altered by brefeldin A. *J Cell Biol* **119:** 273-285.

Yamaguchi S, Jha A, Li Q, Soyombo AA, Dickinson GD, Churamani D, Brailoiu E, Patel S, Muallem S (2011). Transient receptor potential mucolipin 1 (TRPML1) and two-pore channels are functionally independent organellar ion channels. *J Biol Chem* **286:** 22934-22942.

Yamasaki M, Masgrau R, Morgan AJ, Churchill GC, Patel S, Ashcroft SJ, Galione A (2004). Organelle selection determines agonist-specific Ca^{2+} signals in pancreatic acinar and beta cells. *J Biol Chem* **279:** 7234-7240.

Yang AJ, Chandswangbhuvana D, Margol L, Glabe CG (1998). Loss of endosomal/lysosomal membrane impermeability is an early event in amyloid Abeta1-42 pathogenesis. *J Neurosci Res* **52:** 691-698.

Yang H, Mergler S, Sun X, Wang Z, Lu L, Bonanno JA, Pleyer U, Reinach PS (2005). TRPC4 knockdown suppresses epidermal growth factor-induced store-operated channel activation and growth in human corneal epithelial cells. *J Biol Chem* **280:** 32230-32237.

Yeromin AV, Zhang SL, Jiang W, Yu Y, Safrina O, Cahalan MD (2006). Molecular identification of the CRAC channel by altered ion selectivity in a mutant of Orai. *Nature* **443:** 226-229.

Yin J, Kuebler WM (2010). Mechanotransduction by TRP channels: general concepts and specific role in the vasculature. *Cell Biochem Biophys* **56:** 1-18.

Yodozawa S, Speake T, Elliott A (1997). Intracellular alkalinization mobilizes calcium from agonist-sensitive pools in rat lacrimal acinar cells. *J Physiol* **499:** 601-611.

Yoo SH, Albanesi JP (1990). Inositol 1,4,5-trisphosphate-triggered Ca^{2+} release from bovine adrenal medullary secretory vesicles. *J Biol Chem.* **265:** 13446-13448.

Yoon YH, Cho KS, Hwang JJ, Lee SJ, Choi JA, Koh JY (2010). Induction of lysosomal dilatation, arrested autophagy, and cell death by chloroquine in cultured ARPE-19 cells. *Invest Ophthalmol Vis Sci* **51:** 6030-6037.

Yoshimori T, Yamamoto A, Moriyama Y, Futai M, Tashiro Y (1991). Bafilomycin A_1, a specific inhibitor of vacuolar-type H^+-ATPase, inhibits acidification and protein degradation in lysosomes of cultured cells. *J Biol Chem* **266:** 17707-17712.

Yuan JP, Zeng W, Dorwart MR, Choi YJ, Worley PF, Muallem S (2009). SOAR and the polybasic STIM1 domains gate and regulate Orai channels. *Nat Cell Biol* **11:** 337-343.

Zhang CS, Jiang B, Li M, Zhu M, Peng Y, Zhang YL, Wu YQ, Li TY, Liang Y, Lu Z, Lian G, Liu Q, Guo H, Yin Z, Ye Z, Han J, Wu JW, Yin H, Lin SY, Lin SC (2014). The lysosomal v-ATPase-Ragulator complex is a common activator for AMPK and mTORC1, acting as a switch between catabolism and anabolism. *Cell Metab* **20:** 526-540.

Zhang F, Li PL (2007). Reconstitution and characterization of a nicotinic acid adenine dinucleotide phosphate (NAADP)-sensitive Ca^{2+} release channel from liver lysosomes of rats. *J Biol Chem* **282:** 25259-25269.

Zhang S, Fritz N, Ibarra C, Uhlen P (2011). Inositol 1,4,5-trisphosphate receptor subtype-specific regulation of calcium oscillations. *Neurochem Res* **36:** 1175-1185.

Zhang S, Remillard CV, Fantozzi I, Yuan JX (2004). ATP-induced mitogenesis is mediated by cyclic AMP response element-binding protein-enhanced TRPC4 expression and activity in human pulmonary artery smooth muscle cells. *Am J Physiol Cell Physiol* **287:** C1192-1201.

Zhao Y, Araki S, Wu J, Teramoto T, Chang YF, Nakano M, Abdelfattah AS, Fujiwara M, Ishihara T, Nagai T, Campbell RE (2011). An expanded palette of genetically encoded Ca^{2+} indicators. *Science* **333:** 1888-1891.

Zheng S, Zhou L, Ma G, Zhang T, Liu J, Li J, Nguyen NT, Zhang X, Li W, Nwokonko R, Zhou Y, Zhao F, Liu J, Huang Y, Gill DL, Wang Y (2018). Calcium store refilling and STIM activation in STIM- and Orai-deficient cell lines. *Pflugers Arch* **In press**

Zhu MX, Ma J, Parrington J, Calcraft PJ, Galione A, Evans AM (2010). Calcium signaling via two-pore channels: local or global, that is the question. *Am J Physiol* **298:** C430-C441.

Zimanyi I, Buck E, Abramson JJ, Mack MM, Pessah IN (1992). Ryanodine induces persistent inactivation of the Ca^{2+} release channel from skeletal muscle sarcoplasmic reticulum. *Mol Pharmacol* **42:** 1049-1057.

Zoncu R, Bar-Peled L, Efeyan A, Wang S, Sancak Y, Sabatini DM (2011). mTORC1 senses lysosomal amino acids through an inside-out mechanism that requires the vacuolar H^+-ATPase. *Science* **334:** 678-683.